This is to certify that the

dissertation entitled

THE IMPROVEMENT OF THE HYGROTHERMAL AND MECHANICAL PROPERTIES OF BISMALEIMIDE AND K3B/IM7 CARBON FIBER COMPOSITES THROUGH A SYSTEMATIC STUDY OF THE INTERPHASE

presented by

Mark S. Wilenski

has been accepted towards fulfillment
of the requirements for

Ph.D. degree in Material Science and Mechanics

Lawrence T. Drzal, Ph.D.
Major professor

Date November 11, 1993 Lawrence T. Drzal

THE IMPROVEMENT OF THE HYGROTHERMAL AND MECHANICAL PROPERTIES OF BISMALEIMIDE AND K3B/IM7 CARBON FIBER COMPOSITES THROUGH A SYSTEMATIC STUDY OF THE INTERPHASE

By

Mark S. Wilenski

A DISSERTATION

Submitted to
Michigan State University
in partial fulfillment of the requirements
for the degree of

DOCTOR OF PHILOSOPHY

Department of Materials Science and Mechanics

1997

ABSTRACT

THE IMPROVEMENT OF THE HYGROTHERMAL AND MECHANICAL PROPERTIES OF BISMALEIMIDE AND K3B/IM7 CARBON FIBER COMPOSITES THROUGH A SYSTEMATIC STUDY OF THE INTERPHASE

By

Mark S. Wilenski

Advanced aircraft travel at speeds in excess of mach 2 result in external skin temperatures ranging from -60°C to +190°C with extreme heating and cooling rates in the presence of moisture. This combination of environments presents a challenge to current materials. IM7 carbon fiber composites made with either bismaleimide (a thermoset) or K3B (a thermoplastic polyimide) resin are being considered for this use. The overall objective of this research was to develop a greater understanding of both the macroscopic response of these materials to hygrothermal and thermal spike environments, as well as the molecular level interactions which affect the ability of the resins to bond to the fiber.

Hygrothermal testing of BMI/IM7 composites showed that resin properties are reduced by the presence of moisture while composite properties are virtually unaffected. Exposure of composites to a relatively small number of thermal spikes between room temperature and 250°C was shown to have little effect on BMI/IM7 composites, but causes excessive blistering of wet K3B/IM7 composites.

A macroscopic microcracking phenomenon is observed in cross-ply laminates of the BMI/IM7 system. This was shown to be due to the generation of thermal residual stresses formed during cool down from a "stress-free temperature." Both finite element and analytical models were utilized to analyze the causes of this microcracking with a focus on methods for minimizing the resultant stresses. Several methods with potential were identified and suggestions for future work are made.

Microscopically, tests of the bond strength between both the BMI and K3B resins with the unsized IM7 fiber indicated that the adhesion was low. Experimentation on the BMI/IM7 system was able to identify that the only active adhesion promoting mechanism was mechanical interlocking and not chemical bonds between functionalities on the fiber surface and the resin. Various methods for improving the adhesion in the BMI/IM7 system were attempted and some encouraging results were found.

Finally, a set of methodologies for designing an interphase material which will provide an optimum bond between a fiber and resin is presented. These methodologies have been incorporated into an artificial intelligence framework and can be used to tailor composite properties through the addition of an interphase with specific properties.

ACKNOWLEDGMENTS

This dissertation represents three years of contemplation, sweat, and toil. While I will happily take the blame for everything herein which deserves blame, I must drag a few others into the picture to accept the proverbial award of gratitude (in whatever shape manifests itself).

Throughout my encounter with life, I have been encouraged along the paths of my choosing by my loving family. I have happily ridden along being propelled by their unique forms of support (wavelike wouldn't you know) and have found that the summer dive trips, motor-home sized graduation cards, Christmas Key's trips, and infinite other Wilenski things are both who and why I am. I must thank 'Doc' Nelson for he was the one who told me in high school that not only *could* I get a PhD, but that I *would* get one whether I knew it or not.

Then there are the folks more directly related to the pages which follow. To my advisor Dr. Lawrence Drzal I owe many thanks for the freedom with which he allowed me to work and the many times he helped pull my befuddled brain out of the depths of foolish misconception. Thanks to Dr. E. Eugene Shin and Dr. Roger Morgan for organizing the project of which this was but a part, and for all of the help and discussions along the way. I am very grateful to the other members of my committee who each was chosen for a

particular skill which I knew I would require. Sincere gratitude to: Dr. Ron Averill for mechanics help and providing me with the MicMec program which saved me from tons of finite element frustrations; Dr. Greg Baker for doing his best to teach me the many aspects of chemistry which elude me (I must state that I am personally to blame for any chemistry related shortcomings herein); and finally Dr. Jim Lucas for providing insight into moisture related effects. Thanks to Lei Chen and Dr. Gilliland for the statistical derivation in Appendix C. I am indebted to the Air Force Office of Scientific Research and people of the United States of America for funding this research.

There were also many people who helped deflect my general Brownian motion toward appropriate targets. They were Dr. Andre Lee, Mike Rich, Brian Rook, Bob Jurek, Dr. Cara Weitzsacker, Jason Lincoln, Dr. Sanjay Padaki, Dr. Murty Vyakarnam, Dr. Rik ter Veen, and soon to be Drs JinKyu Choi, and Ed. Drown (Note there is absolutely no order to this list!!!). Also, to the wonderful students who endured working with/for me: Dave Knop (who certainly did more than his fair share of this research), Amanda Centeck, Mark Niesen, and Shawn Corbin.

Finally great thanks to Brett Wilson (for the liquid beverages, volleyball, and general traipsing); Michelle Hignite (for Europe, 'real' conversations-whatever they may be, and similar traipsing); Wendy Reffeor (for plays, wine, beaches - well ... traipsing); and finally Cara (see above) for the many meals on short notice, hours of being a concept bored (sounding board), and all other forms of the mental and physical traipsing and tripping that were done.

TABLE OF CONTENTS

LIST OF TABLES

LIST OF FIGURES

Chapter 1

INTRODUCTION

The High Speed Civil Transport (HSCT) is being designed to have a cruise speed of mach 2.4 and will require materials which can survive exposure to extreme temperatures, moisture, and thermal shock for lifetimes of 60,000 hours under structural loadings. Anticipated flight cycles include rapid thermal excursions between temperatures of -60°C and +190°C. Cooling rates during these excursions are quoted at up to ~500°C/min. A thermoset, bismaleimide (BMI), and a thermoplastic, Avimid® K3B, with IM7 carbon fibers are candidate systems for advanced military and commercial aircraft. These systems have been chosen for their excellent mechanical properties and high temperature capability.

There are currently several limitations associated with the hygrothermal performance of these materials. BMI composites experience significant transverse microcracking during their initial cure cycle which presents a path for moisture diffusion, and causes a reduction in properties [1]. Because BMI composites do not get fully crosslinked during standard cure and post-cure cycles [2], they continue to cure during service at the high use temperatures. This increased cure causes a mechanical property reduction of up to 50% [2]. Prior to this work, a variety of studies were performed to determine the overall effect of moisture and cure progression on BMI composite properties [2-5]. Few people

have, however, studied methods for improving the performance of these systems. Those methods which have been studied usually cause a reduction in the desirable properties of the BMI resin (Tg, modulus, processability, and solvent susceptibility) [2]. If these materials are to be used for these advanced applications, their response to these environmental conditions must be fully understood, and, if possible, significantly improved.

The objective of the research presented here is to generate an understanding of the interactions between the effects of moisture and temperature on the physical properties of the BMI/IM7 system. Specifically, the research was aimed at relating the macroscopic response of the material to the microscopic properties at the interface between the fiber and matrix. The interfacial properties of both the BMI/IM7 and K3B/IM7 systems are shown to be very poor. By testing the nature of the bond which exists between the fiber and matrix, methods for improving the performance of the system were found and investigated. The BMI specimens used in this study were fabricated from initial components allowing strict control of the processing method and variation of processing parameters and cure cycles. The K3B specimens were provided in final form by the Boeing Commercial Airplane Company, and thus less testing flexibility was available. For this reason, the majority of the study was focused on the BMI system, but when possible studies of the K3B system are included.

The research has been organized into seven major sections which are represented by Chapters 2 through 7 in this dissertation. Chapter 2 begins with a review of the materials

used in the study and investigations into the nature of the cure of the BMI resin. The experimental details for the testing portions of Chapters 4-6 are given in Chapter 3.

An investigation into the cause of the microcracking phenomenon is presented in Chapter 4. A theory for the mechanism which causes this microcracking is introduced, and modeling based upon this was performed to show the effects of the various controllable parameters. The modeling was also used to suggest a method for the relief of the microcracking. This method entails the addition of an appropriate interphase between the fiber and matrix. Finally, experimental studies of the microcracking phenomenon were performed and support the conclusions of the modeling efforts. These studies also revealed that poor bonding exists between the fiber and matrix in these systems.

A study of the hygrothermal response of the BMI resin and composites is presented in Chapter 5. The cure is related to the physical properties of the resin, and a study of the moisture diffusion behavior of both the resins and their composites was performed. The effects of moisture and extent of cure were studied using a variety of tests on both the macroscopic and microscopic scale. Composites of varied fiber content were used to intensify the response of the resin, and to help define the phenomenon encountered. Testing was organized using a factorial design based on these three factors, and results are presented in terms of both the main effects: extent of cure, moisture presence, and volume fraction, as well as an interaction effect between extent of cure and moisture presence. It was found that both increased cure and moisture have a detrimental effect on resin properties, but moisture was seen to have little effect on composites.

This is followed by a study on the effect of the interaction between moisture and rapid temperature spikes in Chapter 6. In this study, only macroscopic composite specimens were used, so the K3B composites were included. Very few effects were seen in this testing with the exception of the wet, thermal spiked K3B specimens which showed a blistering phenomenon after conditioning. The blisters were of sufficient size to cause a doubling of the composite thickness.

With all of the knowledge gained from the studies in the previous chapters, methods for improving the interfacial adhesion of the BMI/IM7 system were investigated. Methods investigated include surface treatment of the IM7 fiber through additional commercial treatment, or air plasma treatment, and sizing of the fibers. Four different materials were used as sizings on the fiber and their effect on the adhesion was determined. It was found that strong surface treatments such as 400% of the commercial treatment caused an increase in adhesion, and this is attributed to an increase in surface roughness. The addition of a PES sizing to the fibers was also shown to increase adhesion, and offers some very promising direction for future research.

As a result of this project, a methodology for designing interphase materials for specific fiber and matrix combinations was developed based upon surface energetics, miscibility parameters, and functional group chemistry. This methodology was implemented within an artificial intelligence framework as an expansion of a currently existing material designer (COMADE) an provides a first attempt at codification of interphase design.

Chapter 2

MATERIAL CHARACTERIZATION

The materials used in this study were: a thermoset bismaleimide resins, Ciba Geigy's Matrimid® 5292; a thermoplastic polyimide resin, DuPont's Avimid® K3B; and Hercules IM7 fibers. The resin systems are quite complex, and thus a variety of analyses were performed to develop a more complete understanding of their processing and performance. This information was used to help explain the phenomenon encountered, and steer improvement efforts. This chapter presents the nature of the IM7 fiber, briefly reviews what is known about the polymerization of the K3B resin, presents detailed experimental data about the cure of the BMI resin and its relation to resin properties, and finally presents the results of a moisture diffusion study performed on all of these materials.

2.1 Hercules IM7 Fiber

Hercules IM7 fiber is a five micron diameter polyacrylonitrile (PAN) based fiber which is produced as 12,000 filament tows. The fibers used in this study were surface treated, but unsized. Two different treatment levels (100% and 400% of the standard commercial treatment) were used to determine the effect of surface treatment level on adhesion levels.

IM7 fibers are usually provided with a proprietary surface treatment which changes the surface chemistry and adhesion properties. There is evidence that this surface treatment increases the adhesion properties of carbon fibers due to the removal of a weak surface layer, and the addition of active chemical groups to the surface [6]. Most of these chemical groups are oxygen and nitrogen containing species with the largest majority being carboxylic [6,7]. Increases in epoxy/carbon fiber interfacial shear strengths of up to 2x have been reported [8], along with the expected increases in matrix dominated composite properties [9-11].

2.2 K3B Resin Description

Avimid® K3B is a melt-fusible polyimide based on pyromellitic dianhydride and 2,2' bis[3,5 dichloro-4-(diaminophenoxy)-phenylpropane] along with other diamines. Dupont classifies it as an amorphous thermoplastic polyimide which has good mechanical properties at temperatures of up to 200°C, and good solvent resistance. Despite requiring 360°C cure temperatures, it can be fabricated in standard autoclaves. Due to its thermoplastic nature, it possesses the additional advantage of allowing the re-processing of poorly manufactured parts [12].

The polymer used in the Avimid® K series is an amorphous linear condensation polyimide produced from monomeric solutions by the reaction of an aromatic diethyl ester with an aromatic diamine in n-methyl pyrollidone (NMP) as a solvent. The reaction

produces water and ethanol as a byproduct as seen in Figure 2-1. Further information concerning the chemistry of K3B resin is not available due to its proprietary nature.

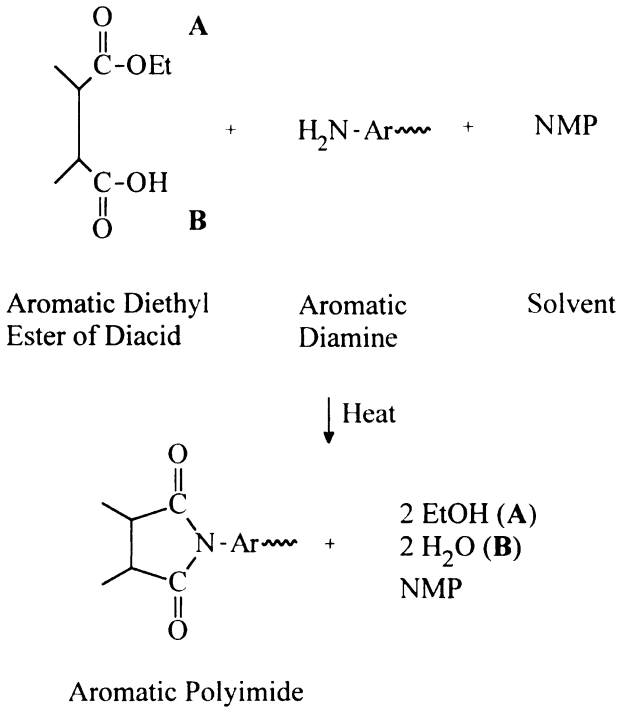

Figure 2-1 - Simplistic Representation of K3B Polymerization Chemistry

2.3 BMI Resin Curing Reaction

Bismaleimide resin is a high temperature thermoset polyimide which possesses good high temperature property retention, processability similar to epoxies, and relatively low cost [13, 14]. Bismaleimide resins are available in five different forms: 1) BMI mixtures; 2) blends of BMIs and BMI-diamine oligomers prepared through a Michael addition

reaction; 3) BMI and olefinic monomeric and/or oligomeric blends; 4) BMI and epoxy blends; and 5) BMI and *O,O'* -dicyanobisphenol A mixtures [14].

The Matrimid 5292 system from Ciba-Geigy belongs to the third class. It is a two part system consisting of 4,4'-bismaleimidodiphenyl methane (BMPM) and *O,O'*-diallyl bisphenol A (DABPA). The chemical structures of these components are shown in Figure 2-2. The BMPM monomer is a crystalline powder which melts at 156°C while the DABPA monomer is a viscous liquid at room temperature [15].

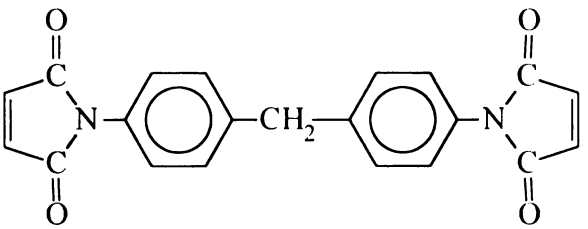

4,4'-bismaleimidodiphenylmethane (BMPM)

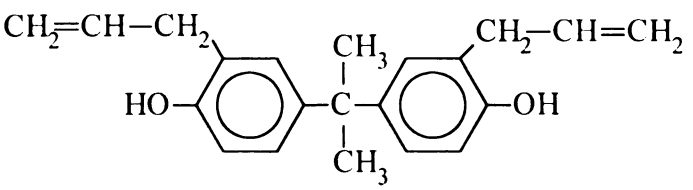

O,O'-diallyl bisphenol A (DABPA)

Figure 2-2 The Chemical Structure of the Matrimid® 5292 Components

2.3.1 Cure Reaction

At temperatures as low as 100°C the allyl bond of the DABPA and the maleimide bond of the BMPM react to form a "prepolymer." This reaction has been termed the "ene" reaction and is shown in Figure 2-3.

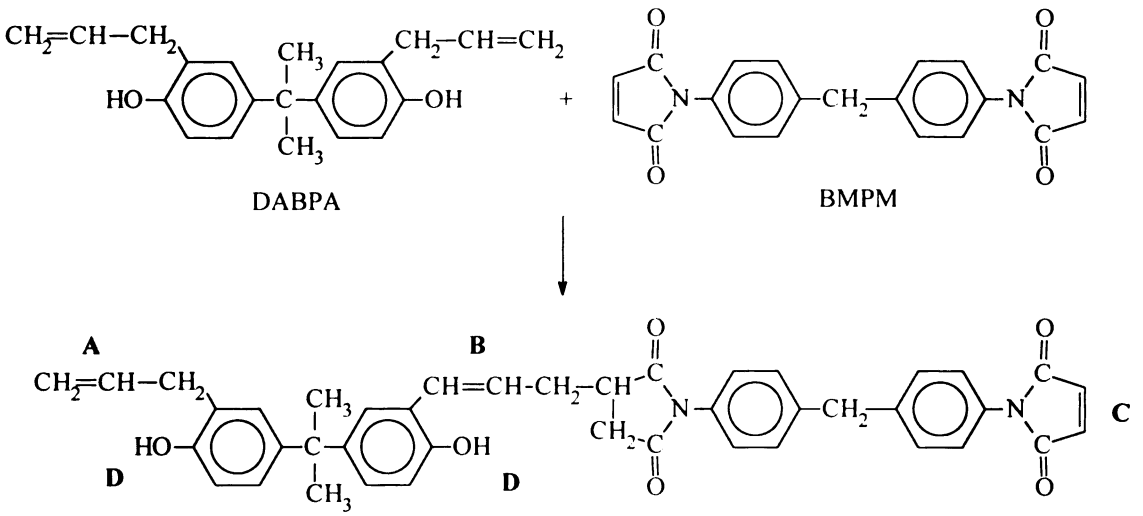

Figure 2-3 The "ene" Reaction

With this prepolymer in the resin mixture during the initial stages of cure, reactions are possible between five active groups. The active groups shown on the prepolymer in Figure 2-3 are the allyl (A), propenyl (B), maleimide (C), and hydroxyl groups (D). The possible reactions include the "ene" reaction shown above, homopolymerization of the allyl groups (Figure 2-4), homopolymerization of the maleimide groups (Figure 2-5), dehydration of the two hydroxyl groups (Figure 2-6), and a cyclization reaction between the allyl and propenyl groups of the prepolymer (Figure 2-7).

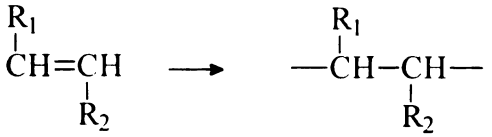

Where R_1 and R_2 are continuations of the 'prepolymer' formed in the "ene" reaction, or the remainder of a DABPA molecule.

Figure 2-4 Homopolymerization of the Allyl Groups

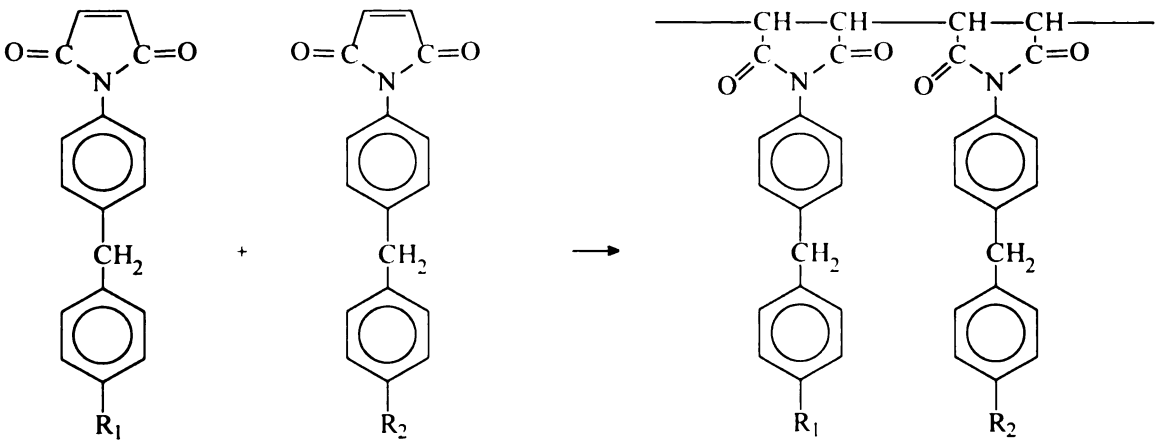

Where R_1 and R_2 are maleimide groups, or continuations of the prepolymer formed in the "ene" reaction.

Figure 2-5 Homopolymerization of the Maleimide Groups

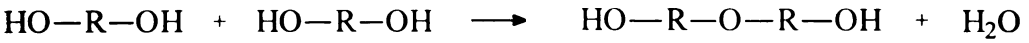

Figure 2-6 Dehydration of the Hydroxyl Groups

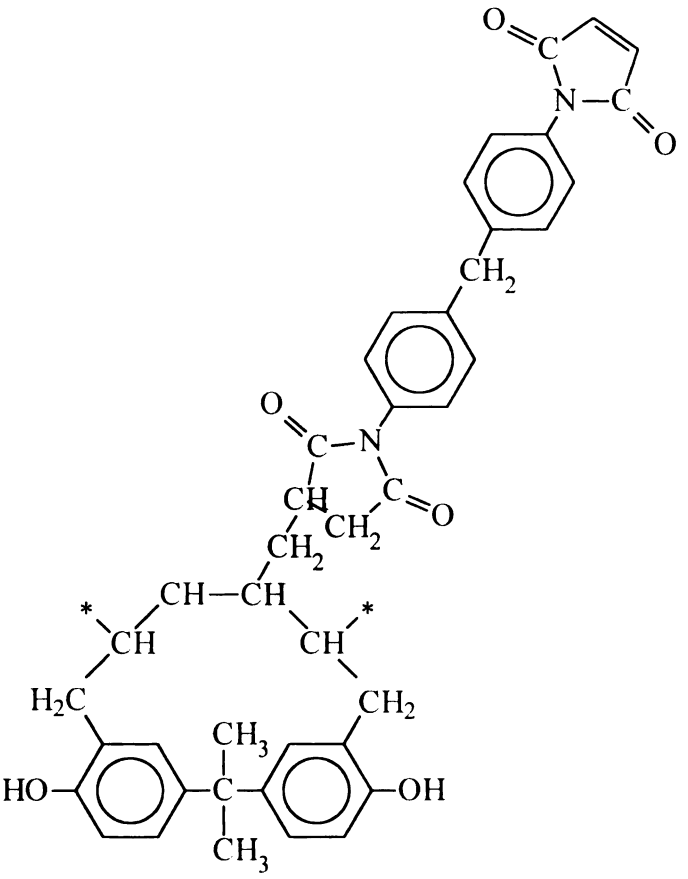

Where * are radicals which react with other molecules.

Figure 2-7 Cyclization of the Prepolymer at High Temperatures

GPC results of resin mixtures aged at low temperatures (100°C) have shown that the "ene" reaction occurs before homopolymerization of either the allyl, or maleimide groups [15, 16]. This is supported by DSC scans of the two separate components (Figure 2-8) which show that for the BMPM, significant reaction doesn't begin until 175°C, and for the DABPA, the reaction requires at least 200°C. A DSC scan of the mixed system (1:1 molar) shows that reaction begins occurring as low as 120°C (Figure 2-9).

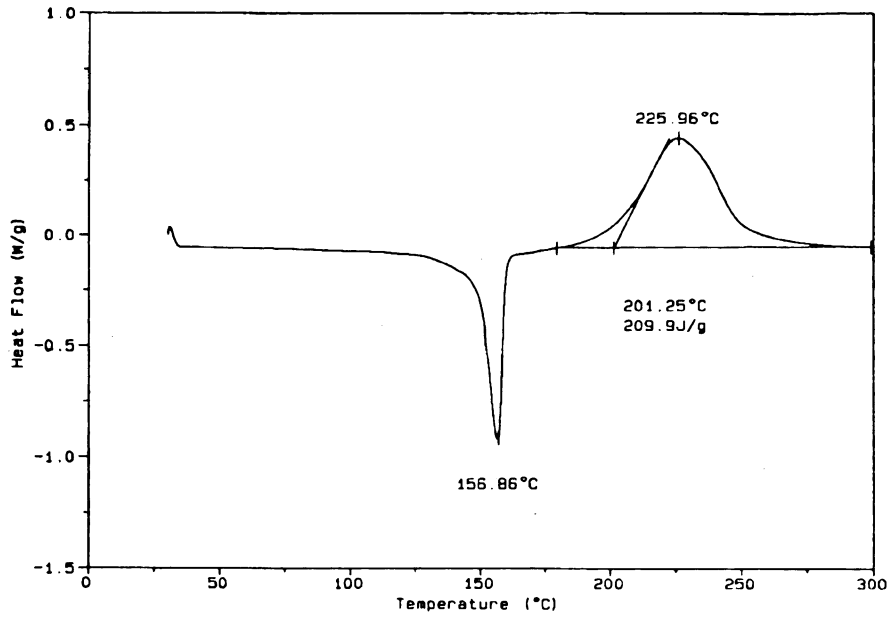

BMPM

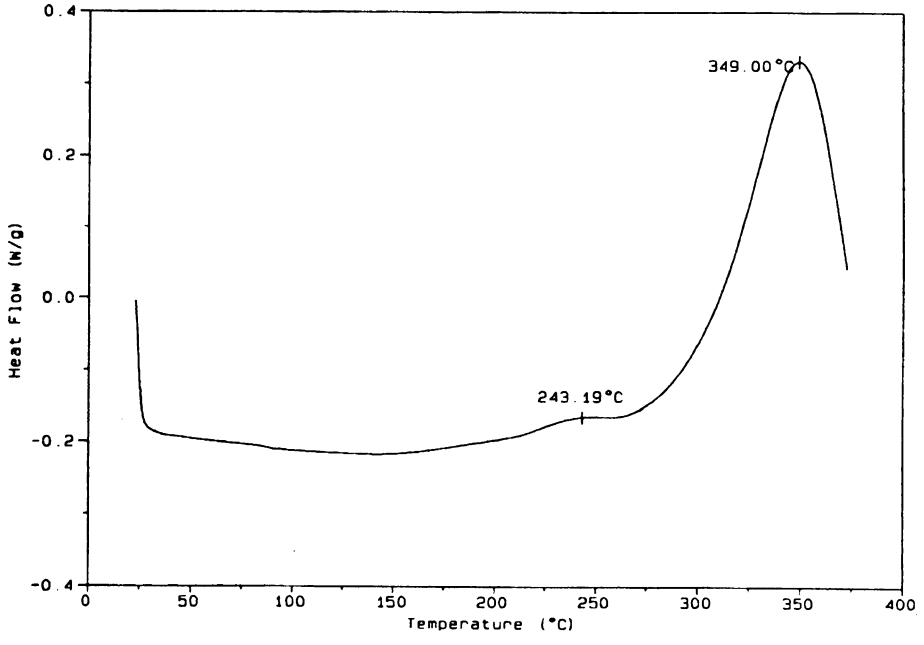

DABPA

Figure 2-8 DSC Scans of BMPM and DABPA at 5°C/min

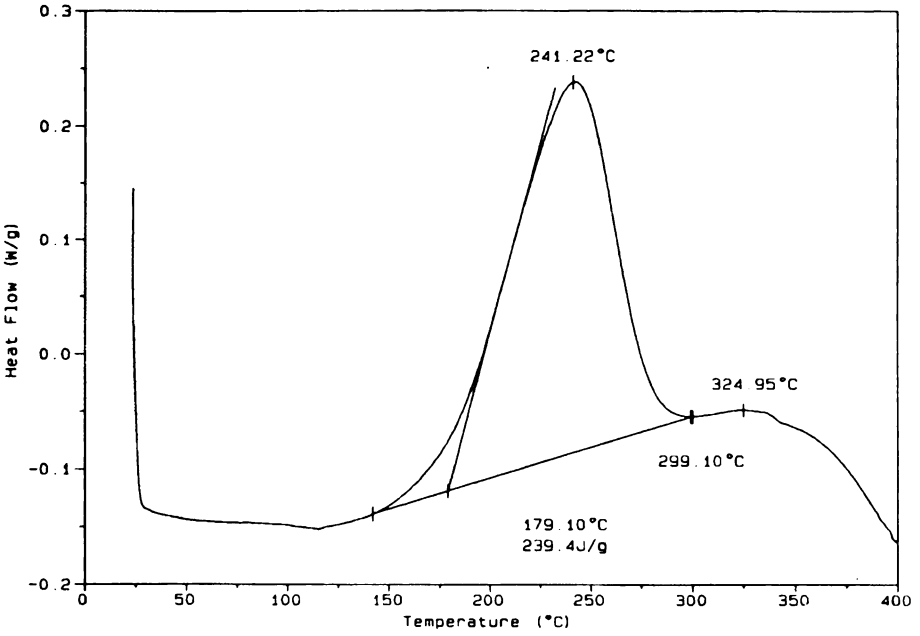

Figure 2-9 DSC Scan of 1:1 molar BMPM/DABPA at 5°C/min

As the cure temperature is increased, the "ene" reaction progresses more rapidly, and the homopolymerization reactions begin. FTIR studies were performed to show the amounts of reacted species during the cure cycle. The actual FTIR curves are provided as Figure 2-10, and the reduced data is shown in Figure 2-11.

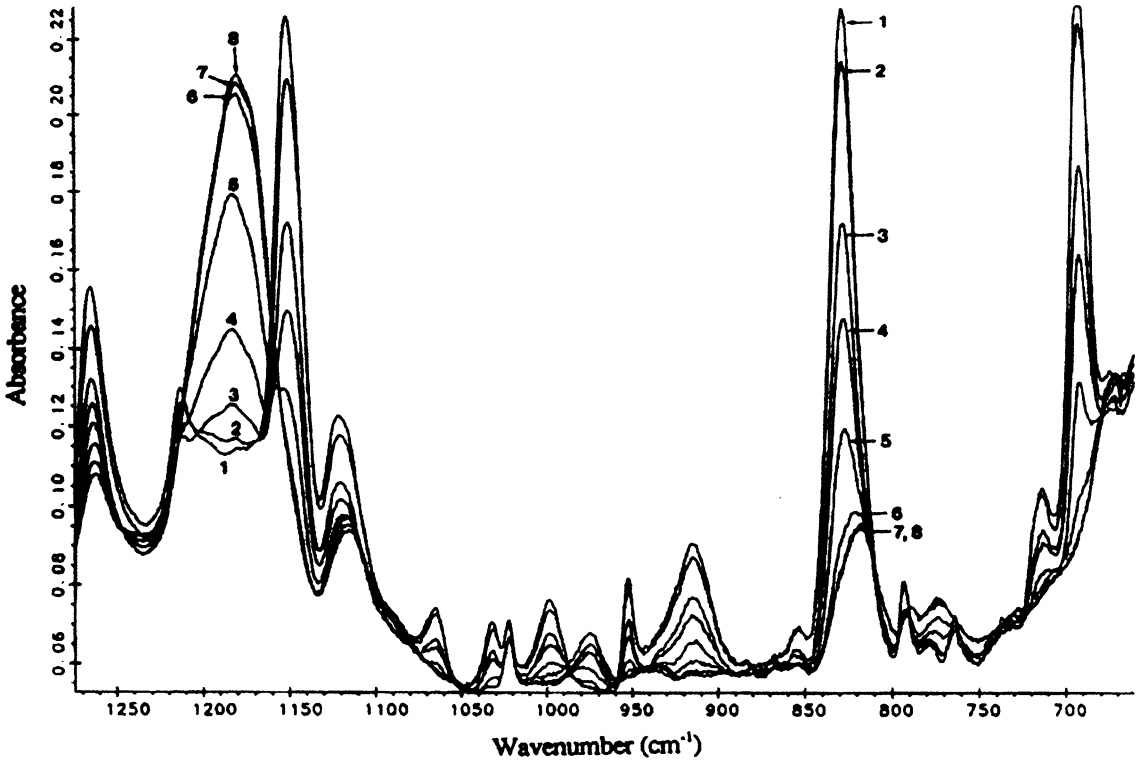

Figure 2-10 FTIR Spectra of 1:1 Molar BMPM/DABPA at the Cure Conditions

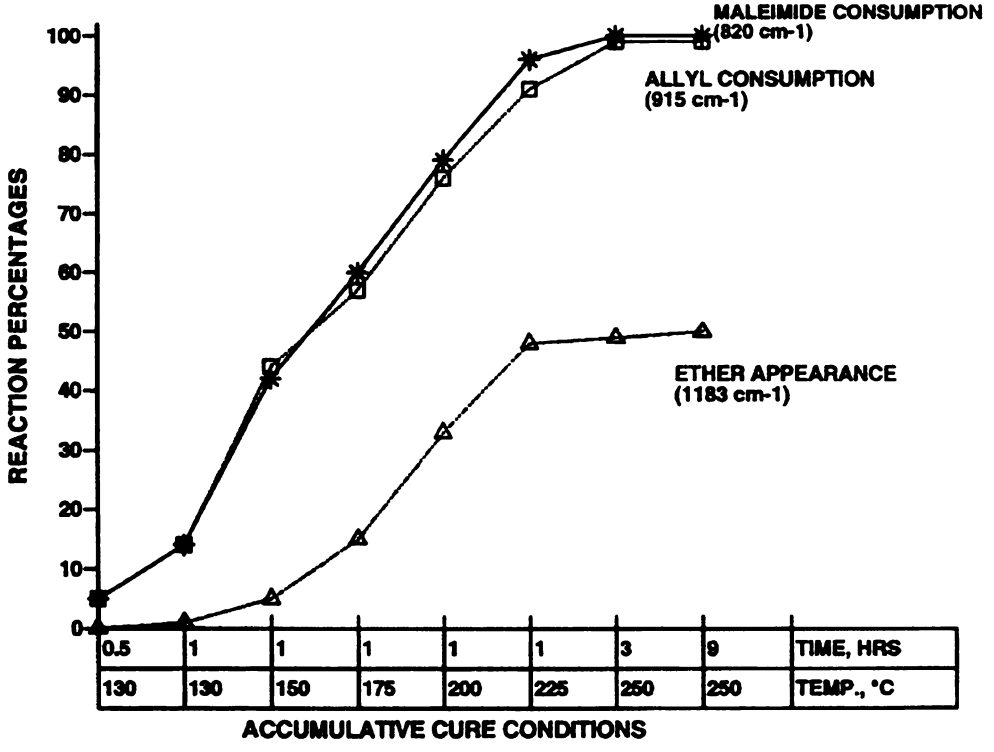

Figure 2-11 Bond Reaction During BMI Curing as a Function of Cure Condition.

The disappearance of the allyl and maleimide groups show a 1:1 correspondence, lending support to the theory that the "ene" reaction continues to be favored over either homopolymerization reaction. The appearance of an ether linkage suggests that the hydroxyl groups react during the cure, but become kinetically hindered by the glassy state. Additional cure at a temperature of 300°C for 9 hours resulted in another 10% reaction of the hydroxyl groups as seen by a decrease in the hydroxyl FTIR band at 3473 cm^{-1}. The concentration of ether linkages, however, did not increase. These ether linkages have been shown to be unstable at 300°C [17]. The presence of the hydroxyl reaction, and instability of the ether linkages is further supported by thermogravimetric analysis (TGA) as shown in Figure 2-12. Rapid weight loss is seen during the initial ramp to 177°C, followed by an increase in weight loss at each step of the cure cycle. Finally a rapid weight loss at 300°C is seen which demonstrates the instability of the ether linkages. Longer TGA experiments showed that the rate of weight loss at 300°C was still increasing after six hours.

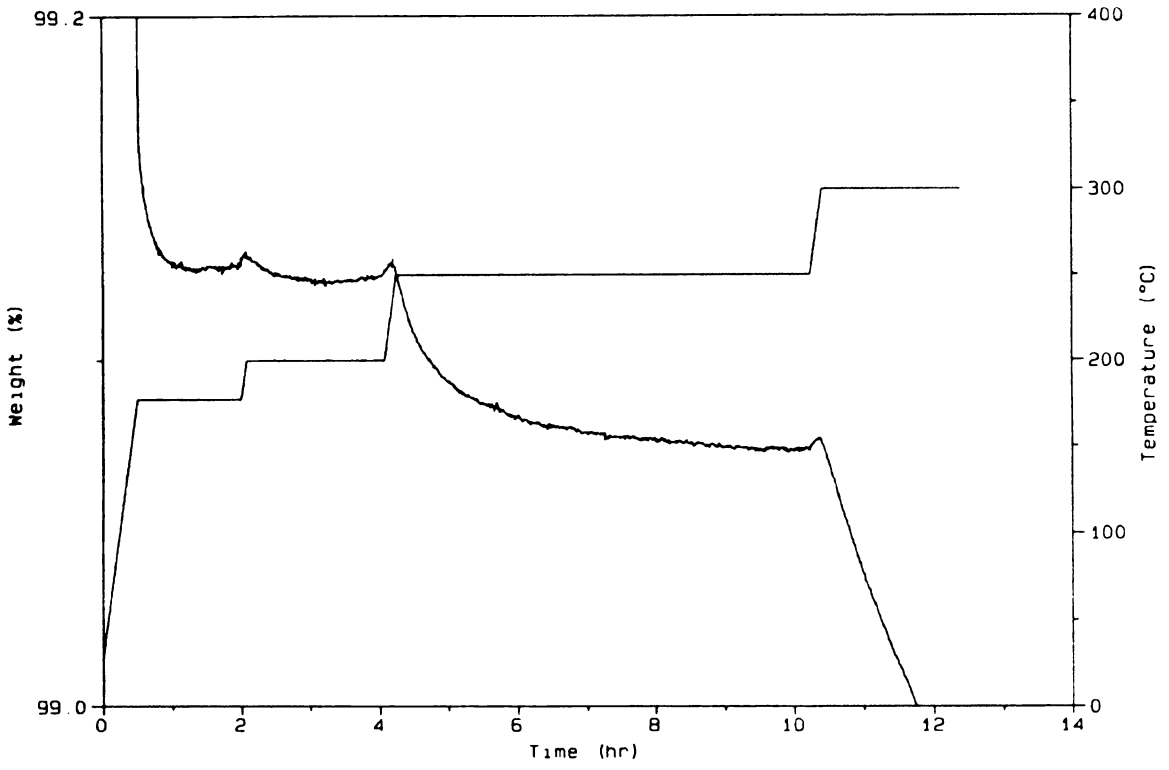

Figure 2-12 Thermogravimetric Analysis Showing Weight Loss Due to the Hydroxyl Reaction and Ether Linkage Instability

Reactions involving the propenyl bond are likely to occur only at relatively high temperatures due to steric hindrance effects. A more complete characterization of the cure reactions of this system has been published [15]. While the exact nature of the ultimate cured network is not known, the reactions suggested here provide insight into the chemical nature and stability of the resin, which is very important when considering long term hygrothermal effects.

2.3.2 Reaction Rate Measurement: Isothermal DSC Profiles

The reaction of this BMI system, as with all polymers, is controlled by both thermodynamics and kinetics. Thermodynamically, all of the reactions presented in the

previous section are viable, but the rates at which they occur varies with temperature in a different manner for each reaction. Kinetically, as the cure progresses, the polymer's chain mobility decreases. This slows the reaction rate by limiting the interaction between active bond sites. Ultimately, the T_g of the resin will exceed the cure temperature and the reactions will slow until they appear to have stopped. The reactions are still occurring, but at a much slower rate.

This presents one of two problems: either additional cure must be provided for increased properties, or the "as-cured" condition is acceptable. If additional cure is desired, the cure temperature must be increased to promote a higher reaction rate. If the "as-cured" system is desired and the use temperature is high (as is generally the case with these materials), increased cure will occur during use, limiting the life of the component.

This discussion illustrates two factors which must be understood before these materials can be safely and economically used. First, the cure kinetics must be understood so that a proper cure cycle can be chosen and the additional cure that takes place in service over time at use temperatures can be predicted. Second, the effect of the extent of cure on the material properties must be understood so that a proper cure cycle can be chosen, and the change in properties over the component lifetime are understood.

To this end, isothermal Differential Scanning Calorimetry (DSC) runs were performed by others associated with this project [15]. For these runs, a small amount of mixed BMI resin was placed in the DSC furnace at the desired temperature, and the amount of heat

evolved was measured as a function of time. The degree of cure, α , was calculated using Eqn. 2-1.

$$\alpha = \frac{\Delta H_t}{\Delta H_\infty} \qquad \text{Eqn. 2-1}$$

Where ΔH_t is the partial heat of reaction at time t and ΔH_∞ is the total heat of reaction. ΔH_∞ was found to have a value of 389 Jg^{-1} via a dynamic DSC scan with a 5°C/min ramp rate. The isothermal percent conversion curves are provided in Figure 2-13. From these curves, the extent of cure for various cure cycles can be approximated.

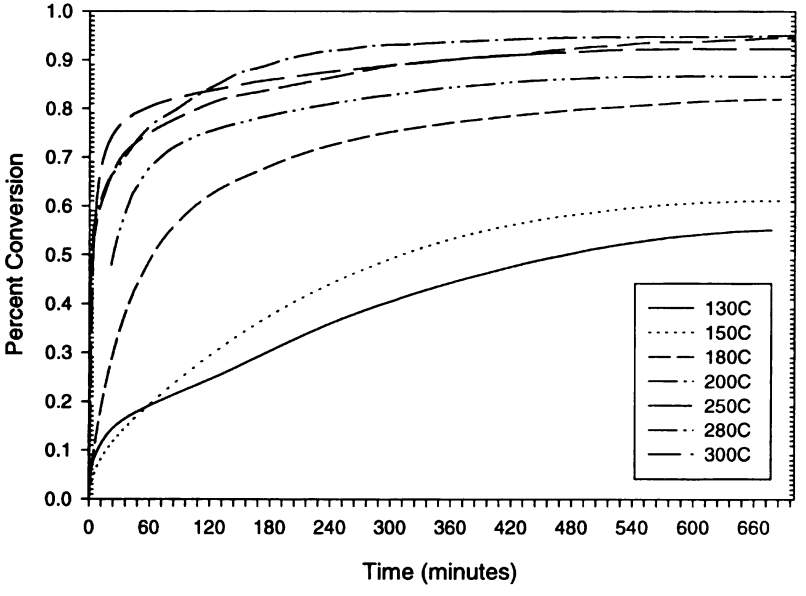

Figure 2-13 DSC Curves Showing Isothermal Cure Profiles of Matrimid® 5292 Bismaleimide Resin

Unfortunately, the extent of cure itself is not a sufficient description of the resin to truly predict material properties because the network structure is a function of the full cure history. Due to competing reactions, different thermal histories will result in different networks which could have significantly different properties. This effect was analyzed by testing resin specimens with a variety of thermal histories and is presented in Chapter 5.

2.3.3 Composite Fabrication Issues

The main use for these high temperature resins is as a matrix for high performance composites. Manufacturing high quality composites with these resins requires an intimate knowledge of the resin's cure mechanism and viscosity profile. The composites used in this research were manufactured by creating pre-impregnated tape (prepreg) of the fibers and resin. This tape is then manually laid-up into a part which is autoclave cured. The full details involved in these processes are provided in Chapter 5. It is absolutely necessary to know the changes in the resin's viscosity through the thermal cycles involved in both the prepregging and autoclave cure cycles. The viscosity of the resin during these cycles was determined and is discussed here.

2.3.3.1 Resin Viscosity During Prepregging

The viscosity of the mixed resin at the prepregging temperature has a great effect on final composite properties. A constant viscosity during prepregging is essential to create uniform prepreg. If the resin viscosity increases too much during the process, the resin content and flow characteristics of the prepreg will change. This in turn can cause

fluctuations in the local volume fraction of the final part which will be shown to have a very significant effect on properties.

A viscosity profile at the prepreg processing temperature of 93°C was performed and is shown in Figure 2-14. A single run of prepreg took approximately 45 minutes of actual run time, and approximately two hours elapsed from the initial resin mixing until completion. It can be seen that the viscosity begins to change significantly toward the end of the time. To counter this, the resin temperature was generally increased by 5-10°C during the final 10 minutes of each prepreg run, and the resin was never reused. Good prepreg quality was achieved with a consistent resin content across the sheet.

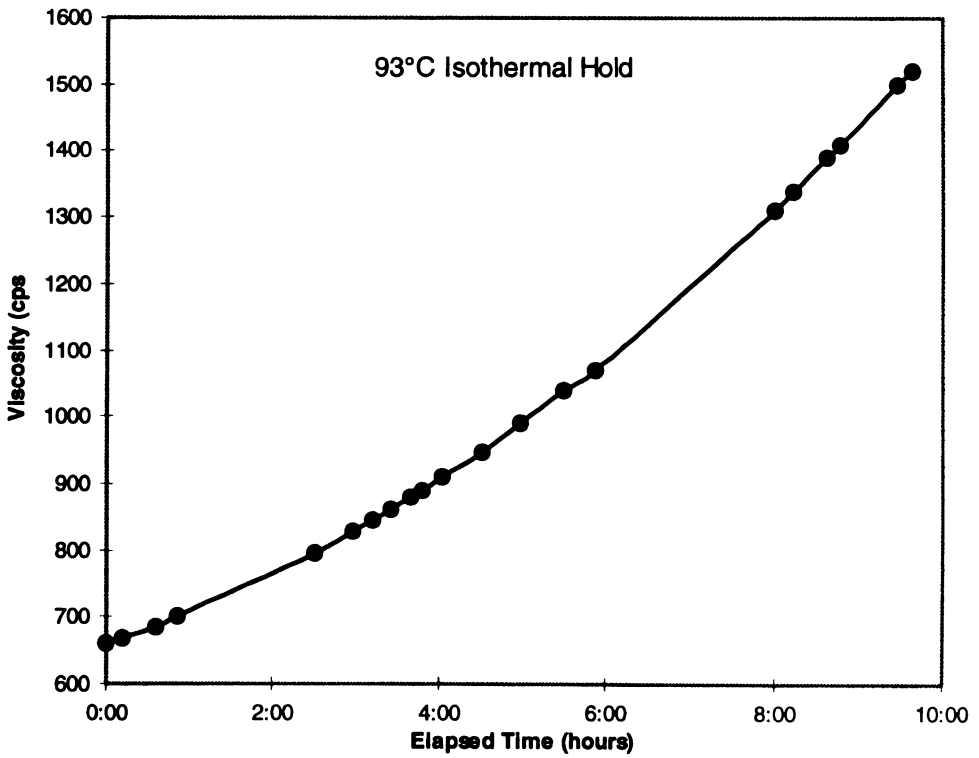

Figure 2-14 Viscosity Profile of BMI Resin at the Prepregging Temperature

2.3.3.2 Resin Viscosity During Autoclave Curing

The uncured part is subjected to a controlled autoclave cure cycle to create a void free composite of high fiber volume fraction. To accomplish this, excess resin and air voids must be removed from the laminate, remaining voids must be minimized, and the resin must become gelled. The cure cycle contains essentially three controllable parameters: temperature, vacuum pressure, and hydrostatic pressure. These parameters must be optimized to achieve the desired laminate quality.

The removal of air voids and excess resin occurs during the initial stages of the cure cycle by applying a vacuum while the resin has a relatively low viscosity. If, however, the viscosity gets too low, the vacuum must be reduced or removed before too much resin is lost which would result in a poor quality laminate. Once the resin has gelled, further resin motion is unlikely and any entrapped voids will remain. The hydrostatic pressure is applied just before gellation to shrink any remaining voids and generally consolidate the laminate.

Obviously, to apply the vacuum and pressure at the proper times, it is very necessary to know the resin viscosity throughout the cure cycle. In thermoset systems such as this one, both the temperature and the extent of reaction control the resin viscosity. Higher temperatures generally reduce the viscosity of fluids, but in this case, the increased temperature also increases the extent of reaction, causing a reduction in viscosity. This competing effect is seen in the viscosity profile shown in Figure 2-15.

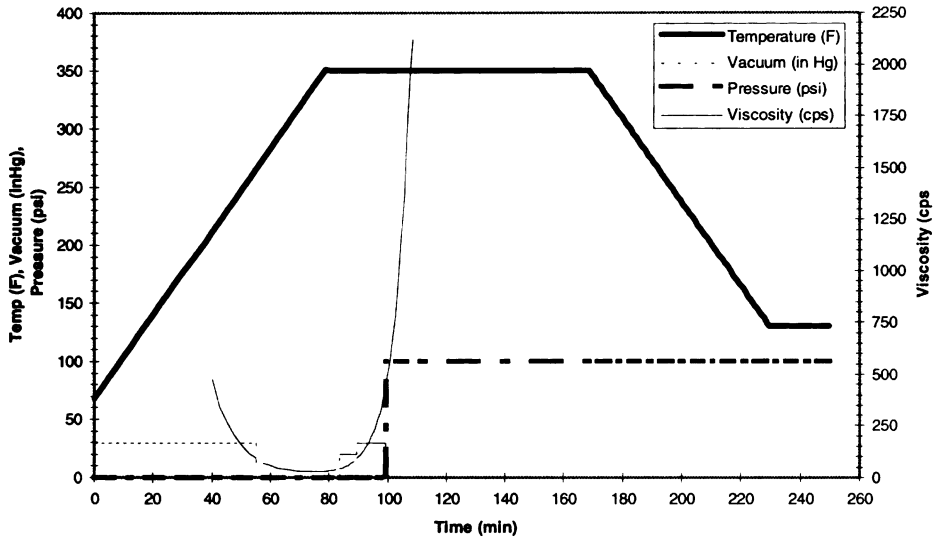

Figure 2-15 Standard Autoclave Cure Cycle for BMI/IM7 Composites

From this profile, it is easily understood that the use of an initial vacuum will help remove excess resin and voids, but the vacuum must be reduced to avoid removing too much resin during the period of extremely low viscosity. The vacuum can then be increased once the viscosity increases, followed by the application of hydrostatic pressure just before complete gellation to shrink the remaining voids.

2.3.3.3 The Effect of Resin Batches on the Viscosity Profile

To further complicate matters, two different batches of resin with significantly different viscosity profiles were used in this study. Their profiles are shown in Figure 2-16. This resulted in prepreg and final panels with different fiber volume fractions, despite identical

processing conditions. The change in the viscosity profile is attributed to a lower activation temperature for the second batch of BMPM resin as seen in Figure 2-17. While this is quite disconcerting for a scientific study, all tests were self-consistent, since specimens made from only one batch of resin were used. In no case did the effect of the two resin batches confound the results.

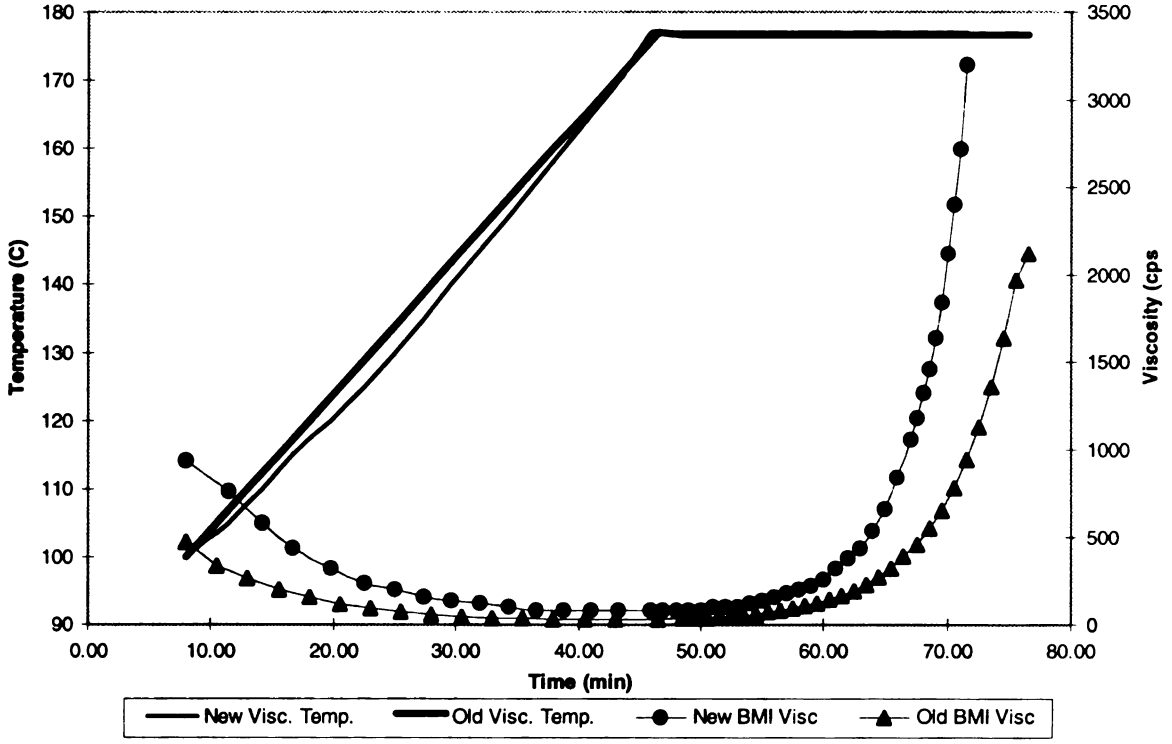

Figure 2-16 Comparison of the Viscosity Profiles of Old and New Batches of BMI Resin Showing the Higher Cure Rate of the New Resin

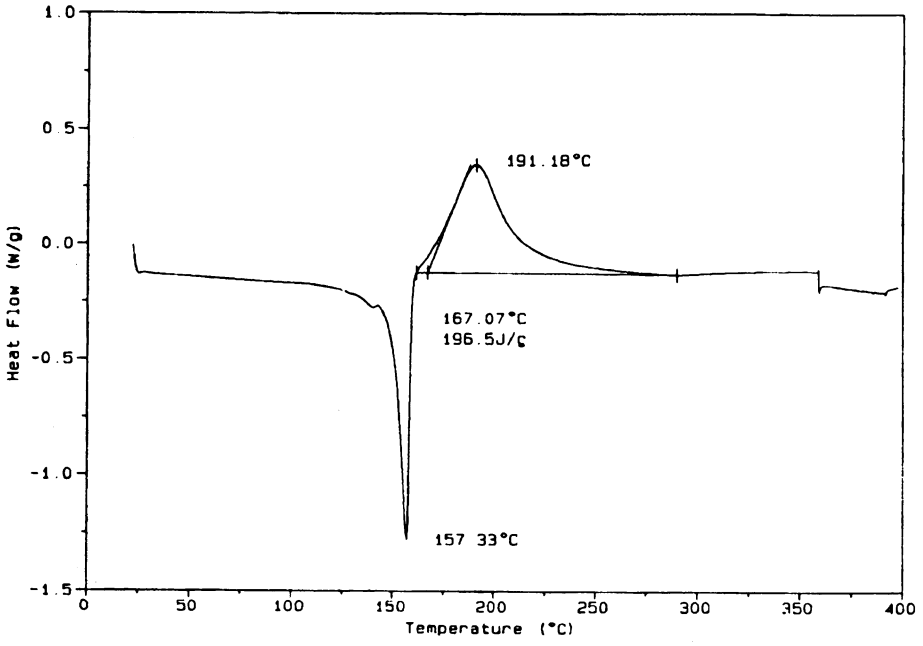

Figure 2-17 DSC Scan of the "New Batch" of BMPM Resin at 5°C/min Showing Lower Activation Temperature

2.4 Material Characterization Conclusions

The materials used in this study were reviewed, and a reaction mechanism for the BMI resin was presented with data supporting the theories presented. Cure reaction rates were presented as a function of temperature and can be used to predict the extent of cure for various cure cycles. The effect of resin viscosity on processing of the BMI was discussed, and an optimized autoclave cure cycle was presented.

A variation in the processing response of the resin was shown to be due to a difference in the activity of the BMPM monomer between two batches used here. This variation will cause no effect on the results of these studies due to a self-consistent use of the resin from each batch.

Chapter 3

EXPERIMENTAL DETAILS

The experimental details for all of the testing associated with this research are provided in this chapter. It is presented in the same order as the data is discussed in the following chapters with the exception of some overlap between the hygrothermal and thermal spike testing which is presented together here, and discussed separately later.

3.1 Overall Specimen Fabrication

Three major types of specimens were manufactured. Resin specimens were created to provide an accurate understanding of the effect of moisture on the resin properties. An extensive study of the effect of cure on resin properties was presented in Chapter 2. Two types of composite panels were created. Sixteen ply, $[0°/90°]_{4S}$, panels were made for macroscopic property testing, and four ply, $[0°/90°]_{S}$, panels were made for tests of the thermal properties of the system. The detailed methods used for manufacturing these specimens is provided here.

3.1.1 BMI Resin

A number of studies on the nature of the pure resin were performed which required macroscopic specimens. For this resin plaques were created. The details of this BMI resin system have been described in detail in Chapter 2.

Ciba-Geigy's Matrimid 5292® resin Part A (BMPM) and Part B (DABPA) were mixed in a stoichiometric ratio (100:85 wt%) at 130°C . The resin was degassed in a 29.5 in. Hg vacuum at 125°C for 30 minutes. The mixed resin was then poured between preheated (93°C) glass plates treated with the Frekote 700NC release agent. The resin plaques were cured in a Blue-M, programmable, nitrogen purged oven. The cure cycles for the resin panels used in these studies are provided in Table 3-1.

Table 3-1 - BMI Resin Panel Post-Cures

Panels	Cure Cycle	Testing Performed
AZ	177°C/1 hr, 200°C/1 hr + 200°C/1 hr, 250°C/6 hrs	Hygrothermal Flexure, and Isothermal and Transient DMA
G	180°C/1 hr, 200°C/2 hrs, 250°C/1 hr	Moisture Diffusion
K	180°C/1 hr, 200°C/2 hrs, 250°C/6 hrs, 300°C/1 hr	Moisture Diffusion
TSR & 2TSR	177°C/1 hr, 200°C/2 hrs, 250°C/6 hrs	Thermal Spike DMA

These plaques were sectioned into the appropriate specimen sizes on a Bennett 5000 Plate Saw, using a 1/8" acrylic underlay and the highest traverse speed setting. The specimens' surfaces were then polished using a Struers Abramin Polisher to remove any possible release agent effects (a minimum of 0.5 mm was removed per side).

3.1.2 BMI/IM7 Composites

The fiber used was Hercules IM7. This is a PAN (polyacrylonitrile) based carbon fiber which was provided in 12,000 filament tows. While normally provided with a sizing which enhances interlaminar shear properties and processability, the fibers used in this study were obtained in an unsized form to avoid unnecessarily confounding the results.

3.1.2.1 BMI/IM7 Prepreg Manufacture

To fabricate the composites, preimpregnated tape (prepreg) was made from the constituent materials using a Research Tool hot melt prepregger. The resin was mixed in a 100:85 wt% ratio (BMPM/DABPA) by heating the liquid to 130°C while stirring and slowly adding the powder. This mixture was then degassed at 130°C in a 29 in. Hg vacuum. It was then cooled to 93°C and poured into the prepregger's resin pot which was preheated to 93°C. IM7 fiber had been threaded through the pot, die, flattening pins (104°C), and guide roller (104°C). The die was 0.22" wide and was shimmed 0.0115" per side. The original gap size is unknown and there was some wear of the die. The fiber was taken up on a 2 ft. diameter drum layered with a teflon release film. A drum speed of

2.1 rpm was used with a traverse rate appropriate to creating gapless tape. Once a complete 12" wide tape was created, it was cut off the drum and sectioned into the desired pieces and stored under refrigeration in nitrogen purged bags until use. Resin content was measured using fiber spool and resin weight losses. The prepreg contained an average of 64 vol% resin and good process control was achieved.

3.1.2.2 BMI Composite Cures

Panels were fabricated using standard hand lay-up technique. Plies were manually oriented as desired. A heat gun and roller were used to press the plies together after application of each ply. The final laminate was then placed on a steel caul plate with bagging material as depicted in Figure 3-1. The number of layers of thin bleeder cloth varied depending upon laminate thickness.

The bagged plate was then placed in a United McGill autoclave and attached to a vacuum line. The cure cycle used is shown in Figure 3-2. The resin viscosity was determined by performing viscometry on neat resin using the cure cycle's temperature profile and was discussed in Chapter 2.

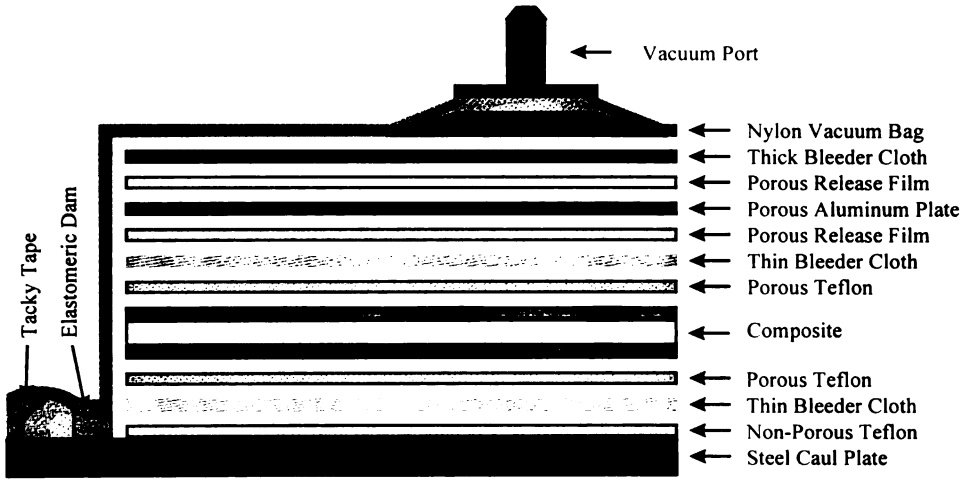

Figure 3-1 Autoclave Vacuum Bagging Scheme

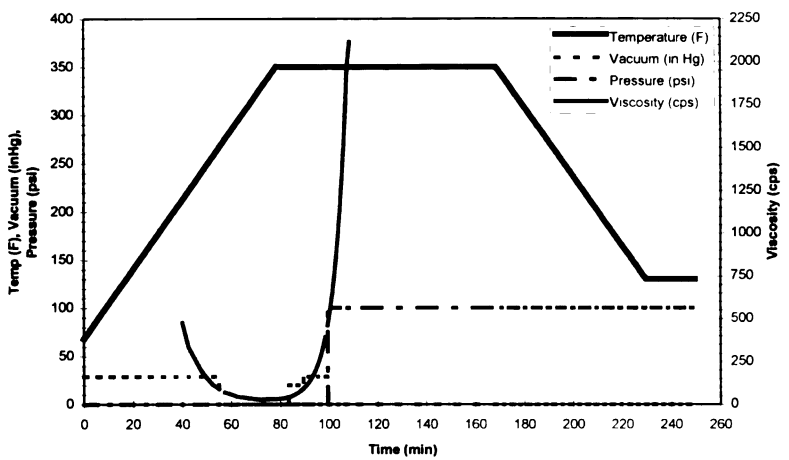

Figure 3-2 Standard Cure Cycle for BMI/IM7 Composites

This cure cycle was varied to create low fiber volume fraction panels. The cycle used to create these panels did not contain a vacuum cycle, and is shown in Figure 3-3. Note that

for panel V, the prepreg was flattened before lay-up using a Carver press at 20 metric tons (over an 11" x 11" area). It was also flattened as a panel once completely laid-up. This helped remove the entrapped air which would have caused voids.

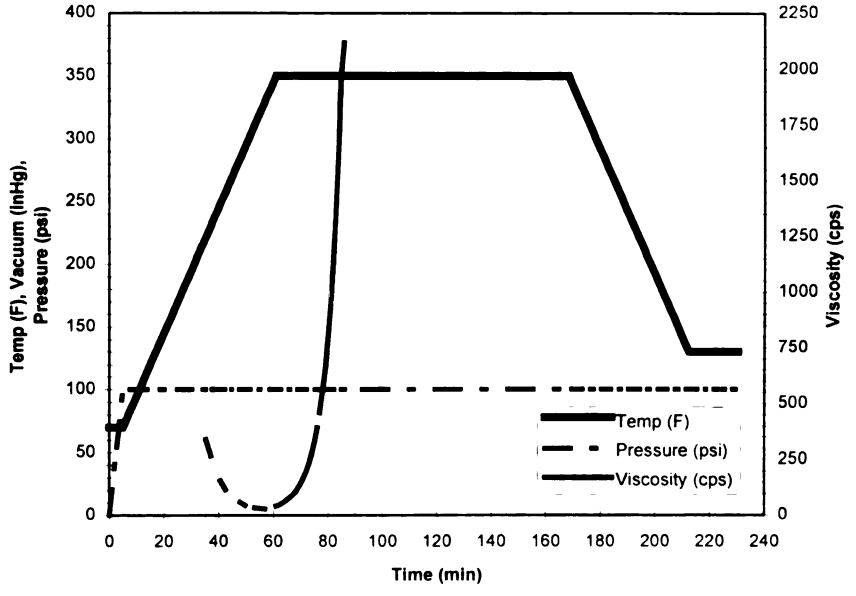

Figure 3-3 Cure Cycle for Low Fiber Volume Fraction BMI/IM7 Composites

The lay-up, cure cycle, and final fiber volume fraction of the composite panels used in this study are summarized in Table 3-2. Panel J was subjected to the cure cycle shown in Figure 3-3, but the vacuum bag was evacuated and sealed off before the thermal cycle.

The shift in resultant fiber volume fraction seen for panels X and Y was due to the new batch of resin which was shown to be reactive at a lower temperature (measured via

DSC), and to have a higher viscosity profile over the thermal cycle (measured via viscometry) as discussed in Chapter 2.

Table 3-2 - BMI Composite Panel Descriptions

Panel	Lay-Up	Cure Cycle	Vf	Comment
H	$[0°/90°]_S$	Standard	62%	
J	$[0°/90°]_S$	Evacuation Only	55%	Dry Outer Ply Surface
W	$[0°/90°]_S$	No Vacuum	47%	
I	$[0°/90°]_{4S}$	Standard	62%	
K	$[0°/90°]_{4S}$	Standard	63%	
V	$[0°/90°]_{4S}$	No Vacuum	35%	
X	$[0°/90°]_{4S}$	Standard	47%	New Batch of Resin
Y	$[0°/90°]_{4S}$	Standard	47%	New Batch of Resin
AA	$[0°]_{16T}$	Standard	55%	New Batch of Resin
AB	$[0°]_{16T}$	Standard	51%	New Batch of Resin

3.1.2.3 BMI Composite Post-Cures

Panels were either directly post-cured after the initial cure, or partially post-cured, sectioned in half, and then one half was post-cured for comparison of cure effects. All post-cures were performed either in a nitrogen purged Kapton® bag, or using a nitrogen purged oven. The panel post-cures are shown in Table 3-3.

3.1.3 K3B/IM7 Panel History

The K3B composite panel used in this study (# 488) was obtained from Boeing Corp. in final form. It was made from DuPont's Avimid® K3B and Hercules IM7 fiber. The panel

had a $[0°/90°]_{4S}$ configuration. All machining was performed on the Bennett 5000 Plate Saw with an acrylic underlay.

Table 3-3 - BMI Composite Panel Post-Cure Cycles

Panels	Post Cure Cycle
HA, JA, WA, IA, KA, VA	200°C/2 hrs
HB, JB, WB, IB, KB, VB	200°C/2 hrs + 280°C/6 hrs
X, Y	200°C/2 hrs + 250°C/6 hrs
AA, AB	200°C/2 hrs + 250°C/6 hrs + 280°C/1 hr

3.1.4 K3B Resin Plaque Manufacture

K3B neat resin specimens were cut from a plaque created at Michigan State University. This plaque was created by taking the K3B monomers, fully imidizing them, and then grinding the resultant polymer into small particles. These particles were then compression molded into a plaque at 350°C.

NOTE: The polymerization cycle for the neat resin and composite K3B specimens is considerably different, allowing for a significant variation in the resultant polymer and thus final properties.

3.2 Microcracking Characterization Experiments

Various experiments were performed which support the modeling work. In particular, 1) the SFT was determined for various cure cycles; 2) unidirectional composites were examined to see if the microscopic mechanism alone is capable of causing matrix failure; and 3) the crack density and width were determined for various SFTs and volume fractions.

3.2.1 Determination of the Stress Free Temperature

The SFT is caused by a combination of the thermal expansion mismatches from both the microscopic and macroscopic mechanisms described in the modeling section, and also by residual stresses due to the shrinkage of the resin. Thus, the SFT itself cannot be simply predicted, or measured by such properties as T_g. To accurately determine an appropriate value for the SFT, unsymmetric laminates were created with the various post-cures. They were then subjected to a thermal ramp and the temperature at which their deflection returned to zero was determined and deemed the stress free state. The procedures used, and results are presented here.

3.2.1.1 Experimental Procedure

Specimens were made at the Composite Materials and Structures Center at Michigan State University from unsized IM7 fiber, and the two component Matrimid 5292® BMI system from Ciba Geigy. Prepreg was made using a Research Tool hot melt prepregger. The resin was mixed at 130°C, degassed at 130°C for 10 minutes under vacuum, and then

brought to 93°C and poured into the resin pot. IM7 fiber tow (12k) was fed through the pot and a shimmed die onto a drum lined with release paper. The final resin content (~62 vol% resin) was determined by fiber spool and resin weight loss.

Panels were created by hand layup of this prepreg. The panel was 10 in^2 with a $[0_2/90_2]_T$ configuration. The cure cycle used is displayed in Figure 3-4. The warped panel was then cut into 20mm wide strips which were approximately 8 inches in length. All panel edges were removed to avoid manufacturing edge defects. Specimens were dried in vacuum at 80°C until their weight loss was no longer accurately measurable. Specimens were post cured in either an inert gas oven, or in a nitrogen purged vacuum bag. Ramp rates were 5°F/min.

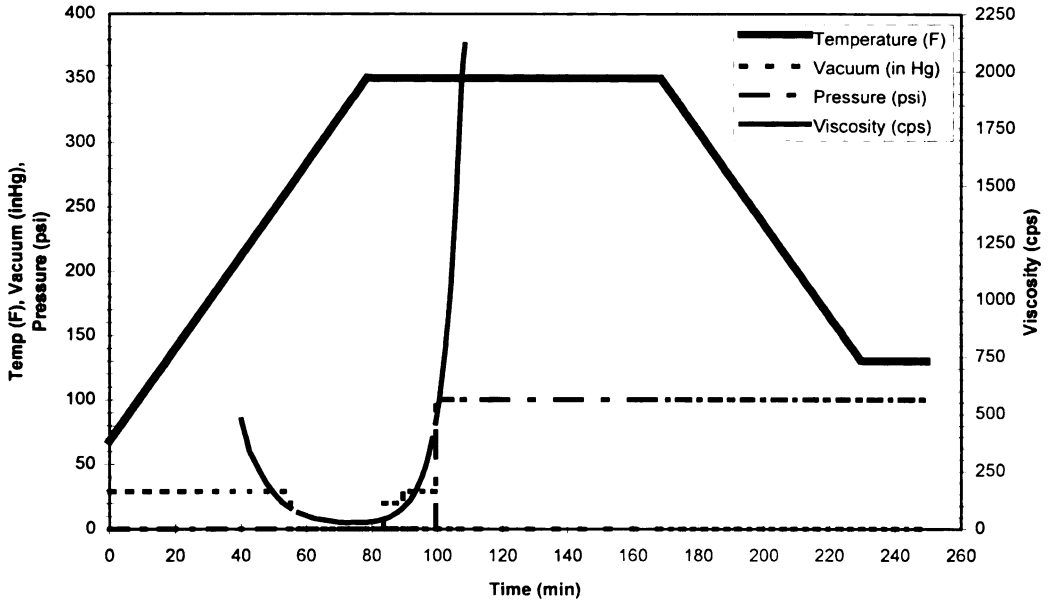

Figure 3-4 Asymmetric Panel Cure Cycle

To determine the SFT, warped $[0_2/90_2]_T$ composite strips were taped in a glass faced oven such that the degree of warp was measurable as seen in Figure 3-5. Temperatures were determined with a thin thermocouple taped directly to the strip. The deflection of the strip was measured as a function of temperature. Extrapolating the deflection vs. temperature curve to zero deflection provided an accurate SFT.

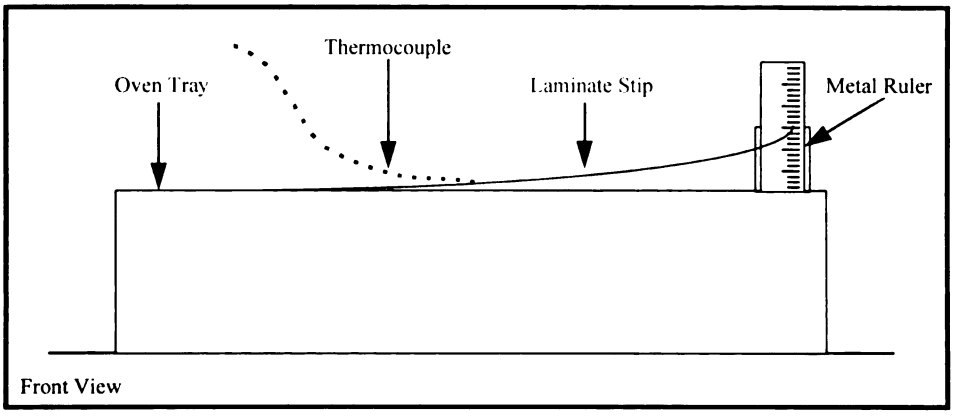

Figure 3-5 Stress Free Temperature Test Set-Up

Two typical deflection vs. temperature curves from the experiments are provided in Figure 3-6. The SFTs associated with various post-cure cycles investigated are provided in Table 3-4.

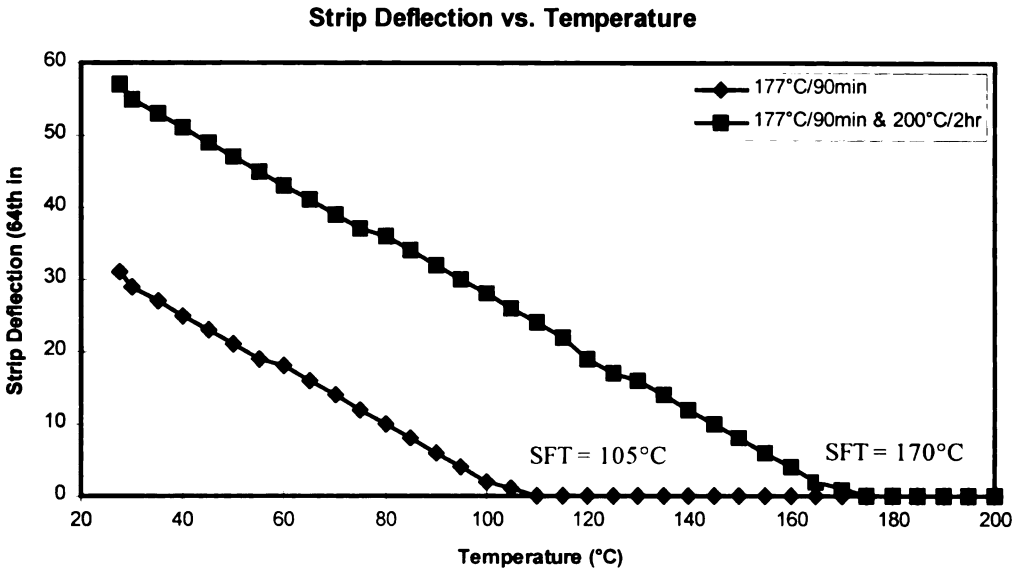

Figure 3-6 Two Typical Strip Deflection Curves Showing the SFT

Table 3-4 Stress Free Temperatures of Various Cure & Post-Cure Cycles

Cure & Post-Cure Cycle	% Cure	Stress Free Temperature
177°C/90 min	.57	100°C
177°C/90 min + 200°C/2hr	.76	170°C
177°C/90 min + 250°C/2hr	.84	230°C
177°C/90 min + 300°C/2hr	.86	245°C
177°C/90 min + 200°C/2hr + 250°C/2hr	.84	210°C
177°C/90 min + 200°C/2hr + 250°C/2hr + 300°C/2hr	.90	240°C

3.2.2 Determination of Microscopic (Fiber Level) Cracking

To determine if the microscopic stresses were sufficient to cause microcracking, unidirectional specimens were created with varied post-cures. These were then sectioned, and polished. Both optical microscopy and ESEM analysis were performed and showed that no cracking existed due to this mechanism.

Unidirectional panels were manufactured using the same procedure outlined in Section 3.2.1.1. The panels were 5 in^2 and had a layup of $[0_4]_T$. The panel was sectioned into approximately 1" squares. These were post-cured in either vacuum, or a nitrogen atmosphere using the post-cure cycles shown in Table 3-5.

Table 3-5 Post-Cure Cycles Used for Microscopic Cracking Experiment

Cure & Post-Cure Cycle
177°C/90 min
177°C/90 min + 200°C/2hr
177°C/90 min + 250°C/2hr
177°C/90 min + 300°C/2hr
177°C/90 min + 200°C/2hr + 250°C/2hr + 300°C/2hr

To determine if there were any microcracks caused by the fiber level expansion mismatch, polished sections of the $[0_4]_T$ panel with varied post-cures were examined. The CMSC's Environmental Scanning Electron Microscope (ESEM) was used to view the specimens at magnifications of up to 10,000x. No microcracking was evident in any of the samples.

3.2.3 Determination of Crack Density and Crack Width

Two separate experiments were performed to measure crack densities and widths. The first was designed to determine the effect of post-cure temperature and stepped post-cures. The second was designed to show the effect of fiber volume fraction (47, 55, and 62% Vf) and cure cycle (Low and High).

3.2.3.1 The Effect of Vf and Post-Cures on Microcracks using Optical Microscopy

Initially, panels were created with varied volume fractions and cure cycles. Crack densities and widths were measured using optical microscopy.

Three cross-ply panels were manufactured using the same procedure outlined in Section 3.1.2. The panels were 5 in^2, had a lay-up of $[0°/90°]_S$, and had volume fractions of 45%, 56%, and 65%. The panels were sectioned into 2" x 1" specimens and dried in a vacuum oven. They were then post-cured in nitrogen atmosphere using the post-cure cycles shown in Table 3-6.

Table 3-6 Post-Cure Cycles Used for Microscopic Cracking Experiment

Cure & Post-Cure Cycle
177°C/90 min
177°C/90 min + 200°C/2hr
177°C/90 min + 250°C/2hr
177°C/90 min + 300°C/2hr
177°C/90 min + 200°C/2hr + 250°C/2hr
177°C/90 min + 200°C/2hr + 250°C/2hr + 300°C/2hr

The post-cured specimens were then sectioned, mounted, and polished. The polished specimens were analyzed using a light microscope. Crack densities were obtained by counting the number of cracks over a measured length of approximately ¾". Crack widths were measured using a video caliper which was calibrated to ±0.01mm before use.

3.2.4 Identification of the Effect of Laminate Features on Crack Propagation

To improve the BMI/IM7 system's toughness, the propagation behavior of cracks must be understood. To determine this, unidirectional composite specimens were incrementally fractured in the ESEM while being monitored.

3.2.4.1 ESEM Vertical Jaw Design

To monitor the fracture of composite specimens in the ESEM, the CMSC's tensile stage was used. This stage fits within the ESEM chamber, and is capable of loading specimens up to 1000 lbs. The original grips for the stage were oriented such that the specimen

"width" is observable. To watch the propagation of cracks in composites, it is necessary to view the "thickness" while under load. To allow this, a set of vertical jaws were designed and fabricated. The designs for these jaws are shown in Figure 3-7, Figure 3-8, and Figure 3-9. They were made from tool steel with tolerances of ±0.010".

Unidirectional ($[0°]_{16T}$) panels were fabricated and cut into notched tensile specimens. They were fabricated according to the procedure outlined earlier in this chapter. The cure cycle was 177°C/90min with both high and low post-cures (280°C/10 hrs, and 200°C/2hrs). Six specimens were fractured in the ESEM and the resulting cracks were observed. Only one specimen's propagation was imaged satisfactorily. This specimen had a high post-cure. A progression of images is provided and discussed in Chapter 4.

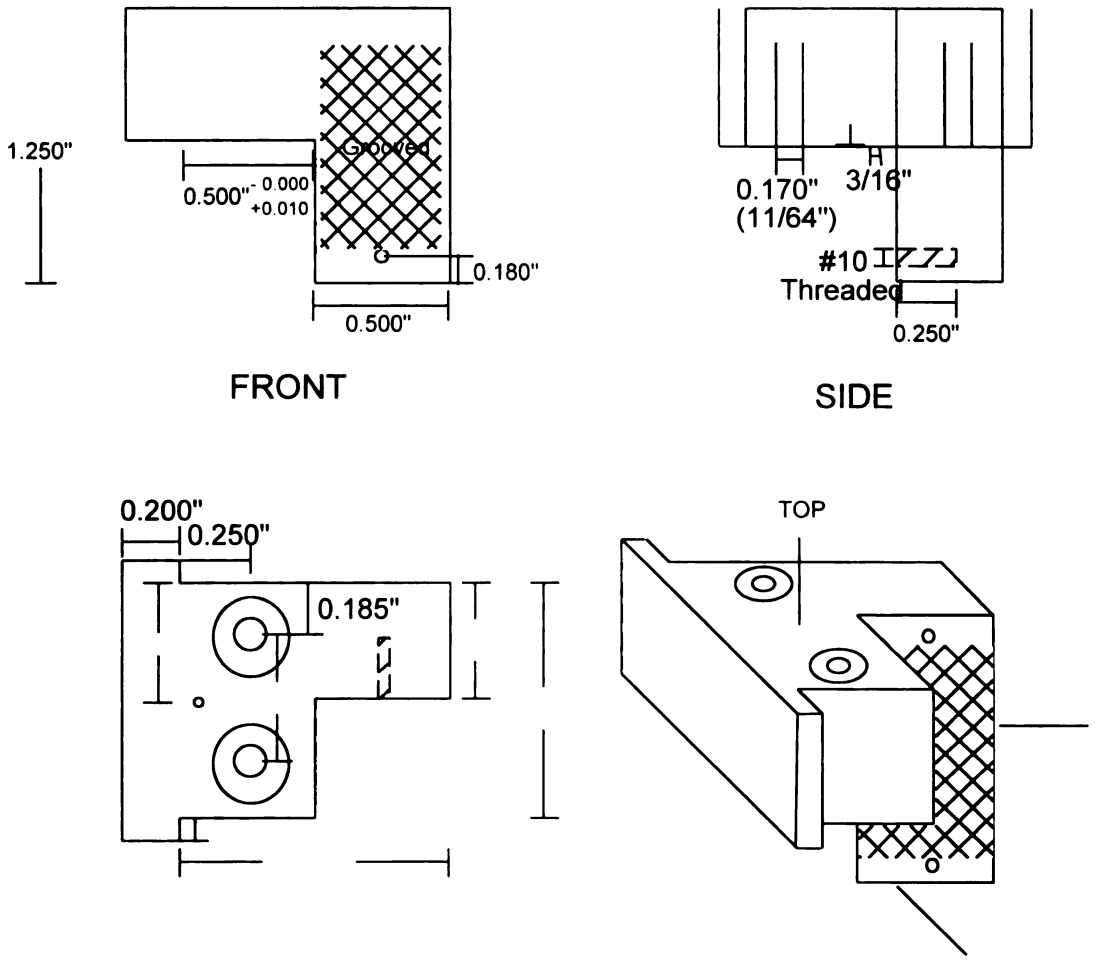

Figure 3-7 ESEM Vertical Jaw - Non-Load Cell End

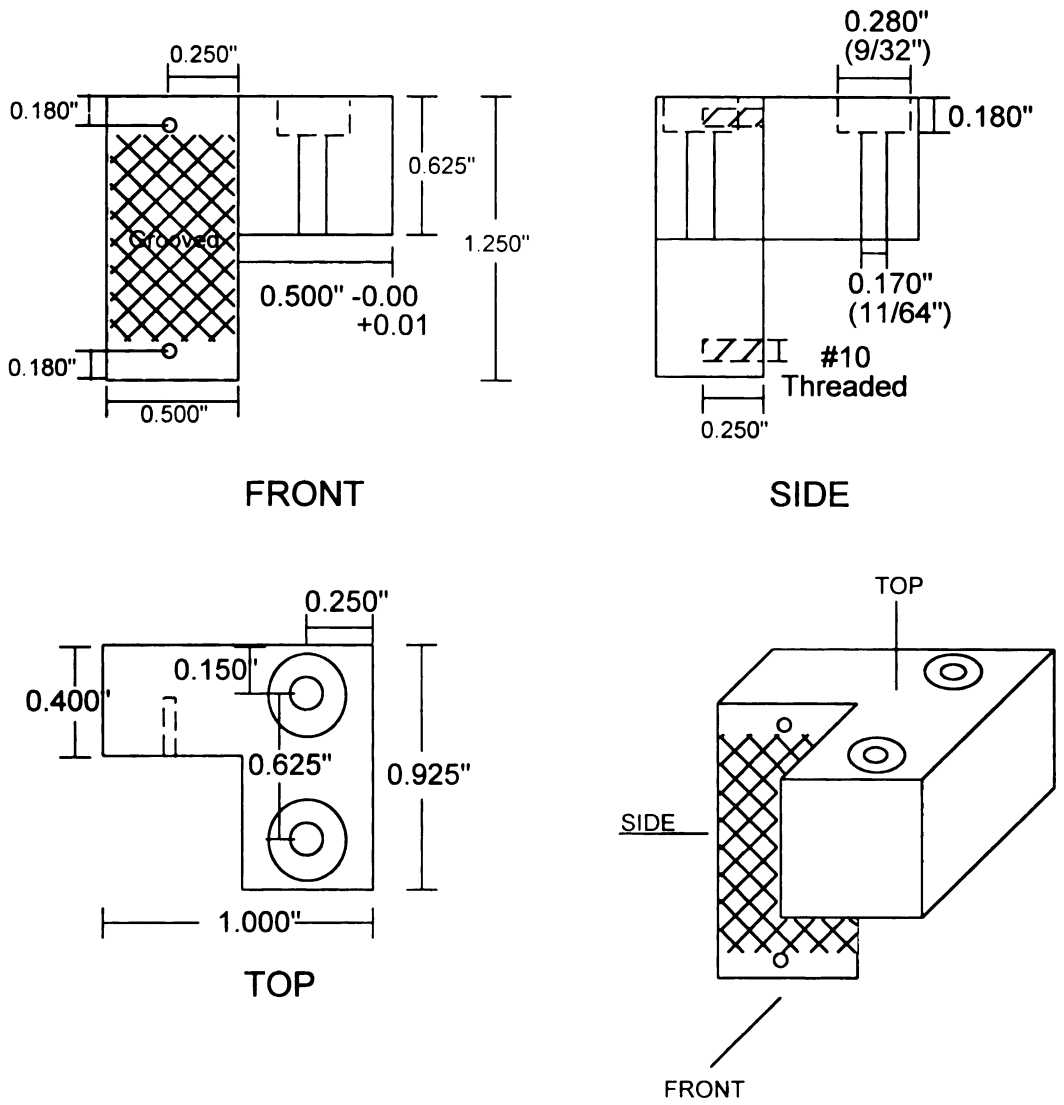

Figure 3-8 ESEM Vertical Jaws - Load Cell End

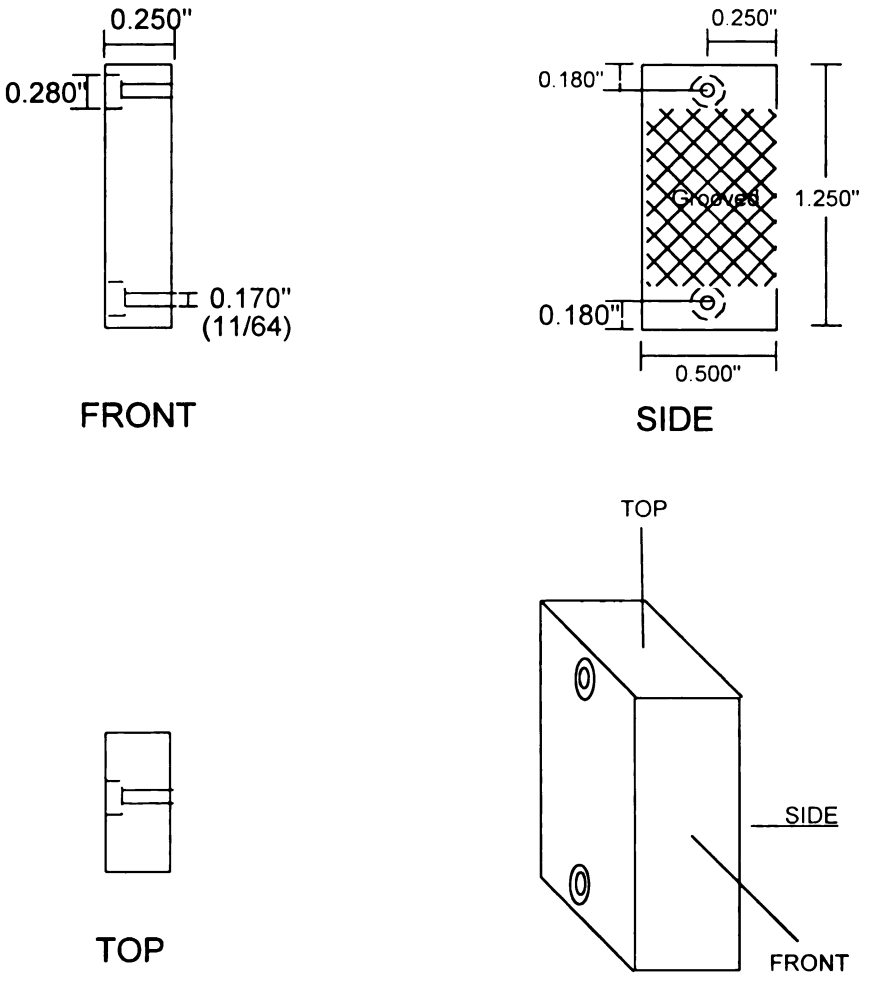

Figure 3-9 ESEM Vertical Jaw Mating Face Plates

3.3 Hygrothermal Study Experiments

The objectives of this hygrothermal study were to identify any effect due to post-cure cycle, moisture, or fiber volume fraction. These factors were chosen for a variety of reasons. Cure may change over the life of the part, and has been shown to reduce mechanical properties over time. Moisture has been shown to be both beneficial and detrimental to composite properties. Volume fraction was chosen because most laminates contain local regions of very high resin content which can have a great effect on composite performance. The properties of these regions can be determined by testing low volume fraction composites. The properties of interest were modulus, strength, failure strain, and T_g. The test scheme used to study these is shown in Table 3-7.

A wide variety of experiments were performed to determine the effect moisture, cure advancement, and volume fraction. The methods used for the fabrication of samples is provided below, followed by the experimental procedures, data reduction schemes, raw tabular results, and failure analysis results for each type of test. The results obtained are analyzed in a method appropriate to the statistical approach taken here and discussed in Chapter 5.

Table 3-7 Hygrothermal Testing Scheme

Test Performed	Materials Studied	Properties Reported
Tensile	BMI Resin	Modulus, Strength, Failure Strain
Flexure	BMI Resin (Three Point. Moisture) BMI Resin (Three Point. Cure Progression) BMI/IM7 (Four Point)	Flexure Modulus Flexure Strength Flexure Failure Strain
Iosipescu Shear	BMI/IM7	Shear Modulus Shear Strength Shear Failure Strain
Isothermal Dynamic Mechanical - Three Point Bend	BMI Resin BMI/IM7	30°C Storage Modulus 30°C Loss Modulus 30°C Tan Delta Tg
Transient Dynamic Mechanical - Single Cantilever	BMI Resin BMI/IM7	155°C Storage Modulus 155°C Loss Modulus 155°C Tan Delta Tg

3.3.1 Hygrothermal Moisture Conditioning

Both BMI resin and composites were tested. Separate conditioning runs were performed for these two specimen types, and are reviewed here.

3.3.1.1 BMI Composite Moisture Conditioning

BMI composite specimens from panels H, J, W, I, K, and V were conditioned for testing. Both saturated ("Wet") and control specimens ("Dry") were tested. The fabrication of these panels was documented in Section 3.1.2.

Specimens were cut from the panels using the Bennett 5000 Plate Saw with a water based coolant, rinsed in clean tap water, and dried with paper towels. All specimens were then dried in a vacuum oven (29 in. Hg vacuum) at 80°C for three weeks. After that time, the specimens were removed and the "Dry" specimens were placed in nitrogen purged zip-lock bags (doubled for insurance against punctures and leaks).

The "Wet" specimens were placed in the Blue-M hygrothermal chamber on glass racks. They received 5 weeks of conditioning at 77°C (72°C wet bulb). The temperature was then dropped to 42°C and the relative humidity was kept at 100% to ensure full saturation. Subsequent moisture diffusion studies of BMI/IM7 cross-ply laminates have shown that BMI cross-ply composites require very little time to reach saturation in 100% humidity (see Chapter 2).

The specimens were removed after approximately 12 months in the chamber. They were quenched into deionized water, weighed, and tested immediately. Specimens were kept saturated between moist towels for the short period between removal and actual testing.

3.3.1.2 BMI Resin Moisture Conditioning

Panel AZ was used for hygrothermal testing of BMI resin. Fabrication of this panel was described earlier. The panel was cut into 3" x 2/5" specimens for flexure testing, and 1" x 2/5" specimens for DMA testing. The Bennett 5000 Plate Saw was used with a water-based coolant. Specimens were subsequently polished to a thickness of 3.6-3.7 mm using

wet polishing techniques. They were then weighed and dried in a vacuum oven for two days. The "dry" specimens were returned to the vacuum oven and received a thermal treatment at 80°C for two days to completely dry them before testing. The "wet" specimens were saturated in a pressure cooker at 98°C and 1 atmosphere for 24 days. They were quenched in a room temperature bath of deionized water, weighed, and tested. During testing, untested specimens were kept saturated between soaked towels.

3.3.2 Resin Flexure Testing

Three point flexure tests of neat resin BMI specimens were performed to determine the change in neat resin properties due to moisture saturation. Specimens measuring 3" x 2/5" were cut from resin plaque AZ. The fabrication of this plaque and conditioning of these specimens were detailed in earlier.

Testing was performed according to ASTM standard D790 for three point flexure testing. The test speed was 0.05 in/min with a span of 2 inches. A two pound preload was used. The moisture content of the specimens was determined both by weight and by Thermal Gravimetric Analysis (TGA). One piece each of a dry and a wet specimen were run in the TGA with a ramp rate of 5°C/min in flowing nitrogen. The resultant weight vs. temperature curves are provided in Figure 3-10 and Figure 3-11. The average weight gain for the wet specimens (by weight measurement) was 4.6 wt% while the dry specimens showed no weight change and negligible evidence of moisture in the TGA curve.

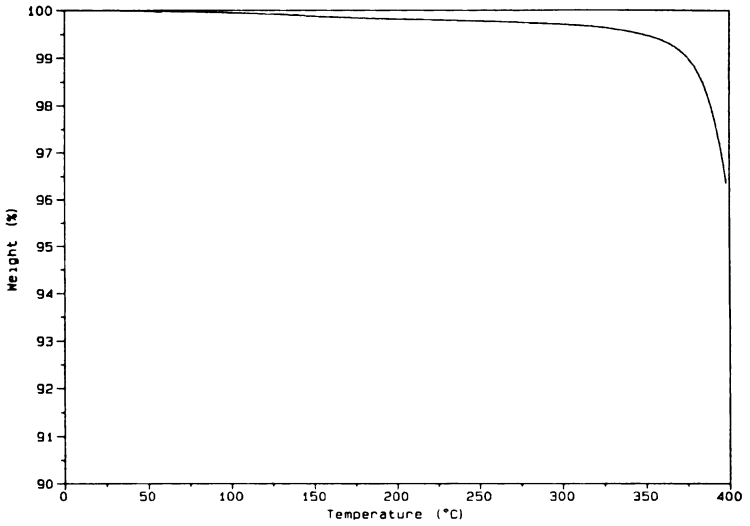

Figure 3-10 TGA of Dry BMI Resin Showing Negligible Moisture

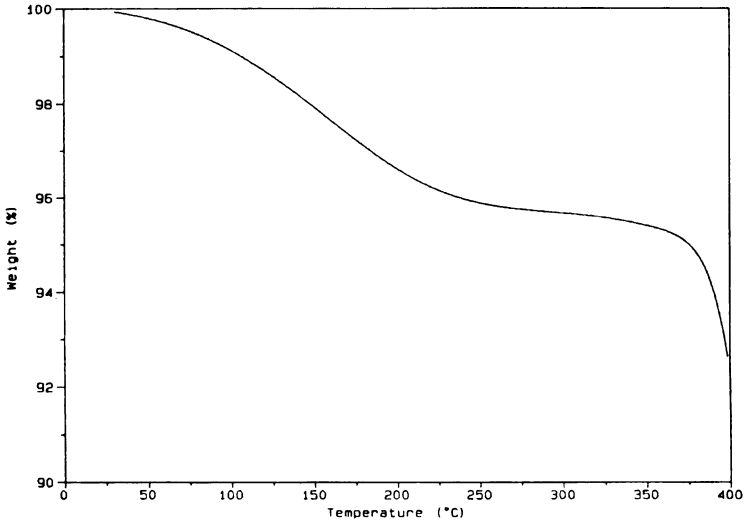

Figure 3-11 TGA of Wet BMI Resin Specimen Showing 4.5% Moisture

The load/displacement data from the tests was logged using the UTS test stand's computer. The file was then analyzed using an Excel macro written expressly for this purpose. The macro performed calculations according to the ASTM standard and plotted the resultant modulus as a straight line shifted from the actual curve with a height corresponding to the failure stress. Table 3-8 summarizes the results of this testing. Summary data for the individual tests has been published elsewhere [18].

Table 3-8 Hygrothermal Resin Flexural Results

Condition	Flex Strength (MPa)	Std. Dev.	Flex Modulus (MPa)	Std. Dev.	Fail Strain (%)	Std. Dev.
Dry Resin	151.0	11.84	3971	40.77	4.238	0.51
Wet Resin	116.9	5.25	3613	57.58	3.311	0.14

Both dry and wet specimens were analyzed in the ESEM. No significant differences in the failure mode was found. Two major morphologies were seen, and are presented in Figure 3-12. The upper images show a rough failure with surface damage evident. The lower images show progression of the crack leaving 'strings' in its path.

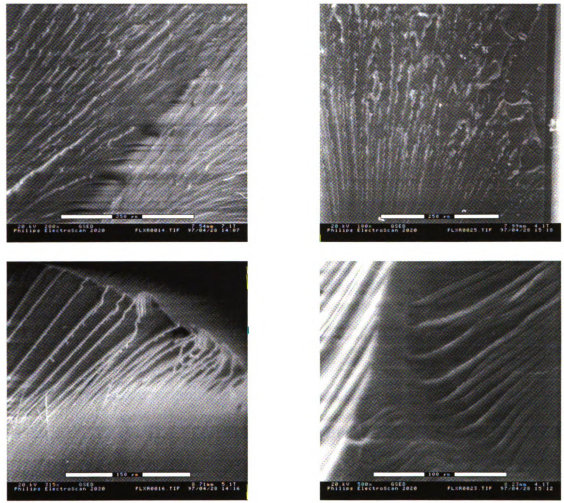

"Dry" Resin "Wet" Resin

Figure 3-12 Failure Micrographs of Dry and Wet Resin Flex Specimens

3.3.3 Hygrothermal Composite Flexure Testing

Four point flexure tests of BMI/IM7 composite specimens were performed to determine the change in composite properties due to moisture saturation, extent of cure, and fiber volume fraction.

Specimens were cut from composite panels I, K, and V. Panels I and K were 62% Vf while V was 35% Vf. All panels had a $[0°/90°]_{4S}$ configuration. Four inch by one inch specimens were cut from these panels using the Bennett 5000 Plate Saw. The fabrication and conditioning of these specimens was described in Sections 3.1.2 and 3.3.1

The average weight gain for the wet specimens (by weight measurement) was 1.5 wt% for low cure 62% Vf specimens, 2.1 wt% for the high cure 62% Vf specimens, 2.1 wt% for low cure 35% Vf specimens, and 3.4 wt% for the high cure 35% Vf specimens. The dry specimens showed no weight change.

Testing was performed according to ASTM standard D790 for four point flexure testing. The test speed for the 62% Vf specimens was 0.15 in/min while the 35% Vf specimens had a test speed of 0.075 in/min. Quarter-point loading was used with a span of 3 inches and a two pound preload.

The load/displacement data for each test was logged using the UTS test stand's computer. The file was then analyzed using an Excel macro written expressly for this purpose. The macro performed calculations according to the ASTM standard and plotted the resultant modulus as a straight line shifted from the curve. The height of this modulus line is the failure stress. These plots and summary data for each test have been published elsewhere. Summaries of the results for each condition are provided in Table 3-9 and Table 3-10.

Table 3-9 Hygrothermal BMI Composite Flexure Data - 62% Vf

Condition	Flex Strength (MPa)	Std. Dev.	Flex Modulus (MPa)	Std. Dev.	Fail Strain (%)	Std. Dev.
Dry Low Cure	1000	31.3	87666	1633	1.214	0.054
Dry High Cure	765	19.1	87511	1595	0.891	0.011
Wet Low Cure	900	29.9	90763	1989	1.050	0.041
Wet High Cure	777	52.0	87801	176	0.920	0.072

Table 3-10 Hygrothermal BMI Composite Flexure Data - 35% Vf

Condition	Flex Strength (MPa)	Std. Dev.	Flex Modulus (MPa)	Std. Dev.	Fail Strain (%)	Std. Dev.
Dry Low Cure	698.2	91.9	53864	1084	1.329	0.172
Dry High Cure	460.0	26.7	49543	1385	1.070	0.072
Wet Low Cure	692.2	25.4	53359	501	1.336	0.035
Wet High Cure	512.4	49.8	48929	1433	1.150	0.128

These specimens failed in a few different manners; either a shear mode at the composite mid-plane, or shear through the thickness under the load nose as shown in Figure 3-13. These are not desired failure modes, and this fact alone provides a good deal of information about the system. The mid-plane shear failure mode is similar to that of a short beam shear test which is considered a good measurement of interlaminar shear properties.

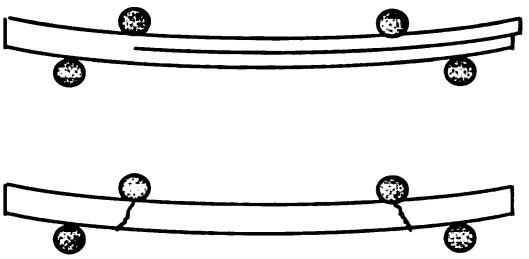

Figure 3-13 Mid-Plane Shear and Load Nose Shear Failures for Flexure Tests

The failure mode of these flex tests was generally either shear in the mid-plane, or shear through the thickness under the load nose. Some compressive failure on the upper surface due to the load noses was also seen, but was not the major failure mode. The failure mode shifted toward load nose failure for the partially cured specimens, but many partially cured specimens showed mid-plane shear failures, or a combined failure, and some fully cured specimens showed load nose failures. No trends were noted between the wet and dry specimens.

The ESEM was used to analyze the failure surface of the specimens which showed mid-plane shear. The mid-plane shear failure generally traversed from one load nose completely across the specimen to the opposite side, leaving the specimen intact. To view the failed surface, it was necessary to complete the failure. This was accomplished by simply pulling the specimen apart. The section which was failed during the actual test was marked to ensure that the "opened" section was not analyzed.

No differences between the 62% and 35% volume fraction specimens were seen on the microscopic level. Similarly, there were no differences between the dry and wet specimens.

The partially cured specimens generally showed a failure surface which consisted of both adhesive failure of the fiber/matrix interface, and hackled regions where the failure deviated into the resin as seen in Figure 3-14. The hackles are the small vertical lines while the horizontal lines represent adhesive failures where fibers used to be. The fully cured specimens showed only the adhesive failure as seen in Figure 3-15. The large vertical lines in both figures are the transverse microcracks discussed in Chapter 3. The adhesive failure seen here is epitomized by the failure shown in Figure 3-16. The fiber runs horizontally across the center of the image and is devoid of adhering resin.

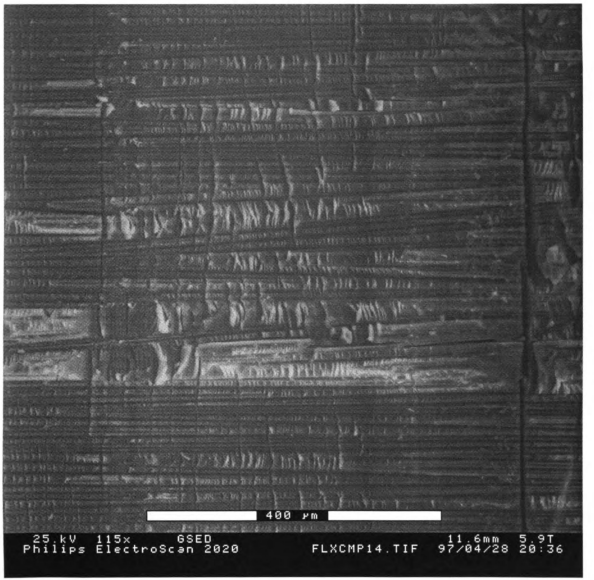

Figure 3-14 ESEM Micrograph of a Partially Cured Dry Specimen Showing "Hackles"

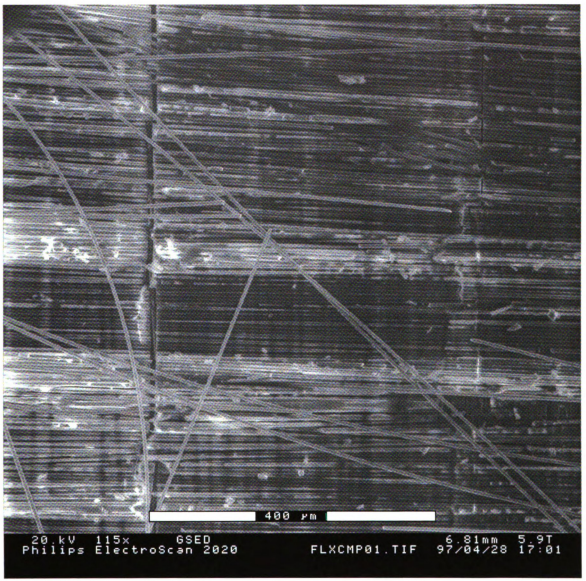

Figure 3-15 ESEM Micrograph of a Fully Cured Dry Specimen Showing No "Hackles"

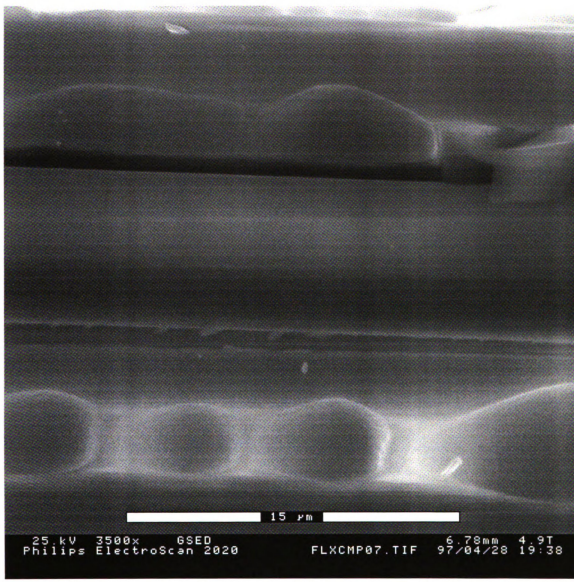

Figure 3-16 Adhesive Failure of a Fully Cured Dry Specimen

3.3.4 Isothermal DMA Testing

Isothermal DMA tests of BMI resin and BMI/IM7 composites were performed at 30°C to determine the change in properties due to moisture saturation, extent of cure, and fiber volume fraction.

Specimens were cut from composite panels H, J, and W which had fiber volume fractions of 62%, 55%, and 47% respectively. All panels had a configuration of $[0°/90°]_S$. The fabrication and conditioning of these specimens is detailed in Sections 3.1.2 and 3.3.1. BMI resin specimens were prepared and conditioned identically to those used in the resin flexure testing.

Testing was performed using the Rheometrics Mark III DMTA in an unclamped three point bend mode with the large frame. Liquid nitrogen was used to maintain a constant temperature of 30°C. A strain of 16 um was used and data was taken at many frequencies (100, 50, 30, 20, 10, 5, 3, 2, 1, 0.3, 0.2, and 0.1 Hz).

Time, temperature, tan delta, and the log of the storage modulus were exported from the DMA and summarized using Excel macros. Plots of tan delta and the log of the storage and loss moduli vs. frequency for each specimen have been published elsewhere. A typical curve is shown in Figure 3-17 for a dry, 47% specimen. Table 3-11 and Table 3-12 summarize the 1 Hz data for the composite and resin specimens.

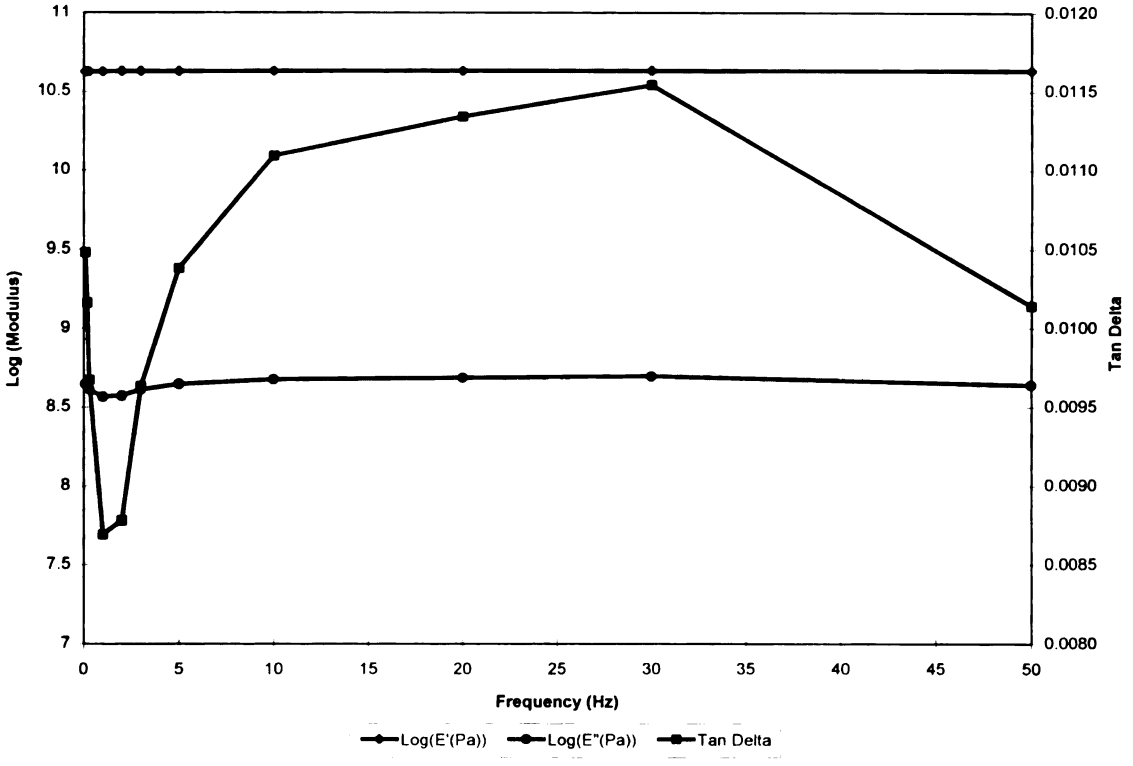

Figure 3-17 Isothermal DMA Curve for Fully Cured 47% Vf Specimen

Table 3-11 - Hygrothermal BMI Composite DMA Data - 1 Hz

Condition	Bending Storage Modulus (MPa)	Std. Dev. (MPa)	Bending Loss Modulus (MPa)	Std. Dev. (MPa)	Tan Delta ($x10^3$)	Std. Dev. ($x10^3$)
62% Vf, Low Cure, Dry	77684	9703	334	39	4.370	0.953
62% Vf, High Cure, Dry	96014	3199	475	73	4.970	0.616
62% Vf, Low Cure, Wet	69130	13530	508	93	7.703	2.904
62% Vf, High Cure, Wet	91201	6131	603	130	6.703	1.372
55% Vf, Low Cure, Dry	66527	12345	555	166	8.583	2.535
55% Vf, High Cure, Dry	67143	2244	341	31	5.083	0.376
55% Vf, Low Cure, Wet	66732	7548	516	351	8.307	4.066
55% Vf, High Cure, Wet	87364	10171	517	59	5.967	0.939
47% Vf, Low Cure, Dry	45116	7792	342	20	7.737	1.895
47% Vf, High Cure, Dry	40241	3955	382	49	9.660	2.165
47% Vf, Low Cure, Wet	49621	6359	386	11	7.797	0.777
47% Vf, High Cure, Wet	45082	4578	435	81	9.680	0.847

Table 3-12 Hygrothermal BMI Resin DMA Data - 1 Hz

Condition	Bending Storage Modulus (MPa)	Std. Dev. (MPa)	Bending Loss Modulus (MPa)	Std. Dev. (MPa)	Tan Delta ($x10^3$)	Std. Dev. ($x10^3$)
BMI Resin, Standard Cure, Dry	2241	69	80	4	35.777	0.917
BMI Resin, Standard Cure, Wet	2040	55	63	11	31.453	6.014

3.3.5 Interfacial Adhesion Testing

Interfacial testing of adhesion (ITS) of BMI/IM7 composites was performed to determine the change in adhesion levels due to moisture saturation, extent of cure, and fiber volume fraction.

3.3.5.1 Hygrothermal Materials & Conditioning

Specimens were cut from composite panels H, J, and W which had fiber volume fractions of 62%, 55%, and 47% respectively. All panels had a configuration of $[0°/90°]_S$. The fabrication and conditioning of these specimens is detailed in Sections 3.1.2 and 3.3.1. The specimens were mounted in epoxy and polished using standard wet polishing techniques. The "Dry" specimens were then dried in a vacuum oven at 80°C and stored in nitrogen purged bags until tested. The "Wet" specimens were placed in the hygrothermal chamber with the other "Wet" samples.

3.3.5.2 Specimen Testing

Specimens were tested using the CMSC's ITS system using a new controlling computer and new software which retains all load-displacement curves and stores images of each loading cycle. The ITS system measures the adhesion in real composite specimens by loading the polished faces of fibers with a hemispherical diamond indentor as depicted in Figure 3-18.

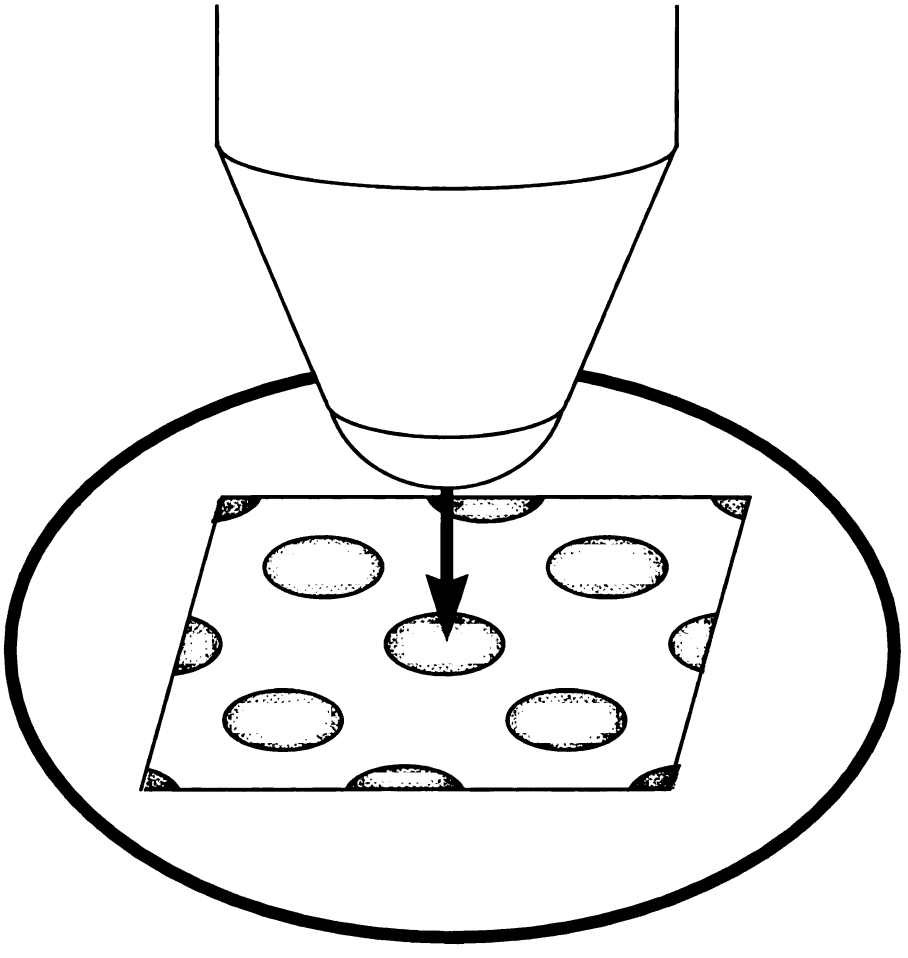

Figure 3-18 The Loading of Fiber in the ITS Test

During the test, the specimen is moved toward the tip using stepper motors in 0.04 μm increments. The applied load is measured using a Sartorius balance interfaced with the controlling computer. The balance has a resolution of 0.01g. The debonding load is determined by using incremental loading steps and visually checking for a debond between each loading using an attached light microscope at magnifications of up to 2000x. A debond appears as a black ring around the fiber, and for these tests, a failure was defined as a debond of at least 120° around the fiber. Twelve fibers were tested for each condition, and the high and low values were rejected before data analysis.

For the "Wet" specimens, a plastic bag was placed around the sample holder and coupled to the indentor/optic collar. A small quantity of water was placed in the bottom of the sample holder, and the bag was sealed. This caused a saturated atmosphere around the specimens. Because the bag was now coupling the balance to the indentor, the ITS program was altered so that the loading cycle could be stopped at various times during the test initialization to re-tare the balance and thus get a test with little contribution from the coupling effect. This method was very successful.

3.3.5.3 Data Reduction

The interfacial shear strength (IFSS) is calculated within the ITS software using a formula obtained from a finite element analysis of this loading condition. The formula takes into account the distance between the tested fiber and it's nearest neighbor as well as the tensile modulus of the fiber, shear modulus of the matrix, and failure load. The formula is shown in Eqn. 3-1.

$$IFSS(psi) = 1811000\left(\frac{L}{d^2}\right)^{\frac{1}{2}}\left[0.875696\left(\frac{E_m}{E_f}\right)^{\frac{1}{2}} - 0.018626\,Log\left(\frac{D}{d}\right) - 0.026496\right]$$

Eqn. 3-1

where:

L = max load in (g)
d = fiber diameter in (μm)
E_m = matrix shear modulus (psi)
E_f = fiber tensile modulus (psi)
D = interfiber distance (μm)

The IFSS results for the hygrothermal testing are provided in tabular format in Table 3-13. The results from the improvement attempts are provided in Table 3-14.

Table 3-13 ITS Results for Hygrothermal Testing

	DRY						WET		
	47% Partial	55% Partial	62% Partial	47% Full	55% Full	62% Full	47% Partial	55% Partial	62% Partial
IFSS (psi)	653	911	834	686	809	743	446	453	562
Std. Dev.	55	129	172	139	102	115	33	96	123

Table 3-14 ITS Results for Improvement Attempts

	DRY						
	RTV Sized	PES Sized	PEI Sized	5218 Sized	Air Plasma	Control	400% ST
IFSS (psi)	804	1314	867	986	1117	955	1324
Std. Dev.	230	203	164	231	207	247	260

3.3.6 The Effect of Cure Progression on the Physical Properties of BMI Resin

Complex thermoset resins like this BMI system have properties which are highly dependent upon their full thermal history, not just their extent of cure. To gain insight into this, resin specimens were made with varied thermal histories and their macroscopic tensile and flexure properties were determined along with their T_g, as measured using modulated DSC.

Neat resin specimens were made using the procedure outlined in Section 3.1.1. All resin plaques were initially cured at 177°C for 1 hour. The subsequent post-cure cycles used are shown in Table 3-15.

Table 3-15 Neat Resin Post-Cure Cycles

Post-Cure Description	**Post-Cure Cycle** (Initial Cure: 177°C/1 hr)
Low Cure Short	200°C/1 hr
Low Cure Long	200°C/3 hrs
Standard Cure Short	200°C/2 hrs, 250°C/1 hr
Standard Cure Long	200°C/2 hrs, 250°C/6 hrs
High Cure Short	200°C/2 hrs, 250°C/6 hrs, 300°C/1 hr
High Cure Long	200°C/2 hrs, 250°C/6 hrs, 300°C/6 hrs

Specimens were machined from the post-cured resin plaques using a diamond saw with a water-based coolant. Since the outer layer of the specimens was contaminated with a release agent, approximately 0.5 mm of material was removed using wet polishing techniques. After polishing, the specimens were dried in a vacuum oven at 80°C for one week to ensure they were equally dry before testing.

Three point flexure testing was performed using a 50 mm span and a test speed of 1.3 mm/min. Specimens were nominally 75 mm x 10 mm x 3.5 mm. Tensile tests were performed using a 'dog bone' specimen with a gauge length of 65 mm and a cross-section of nominally 10mm. Tests were performed at a cross-head speed of 5 mm/min. A representative stress-strain curve is shown in Figure 3-19 for a tensile test. The flexure samples were similarly brittle.

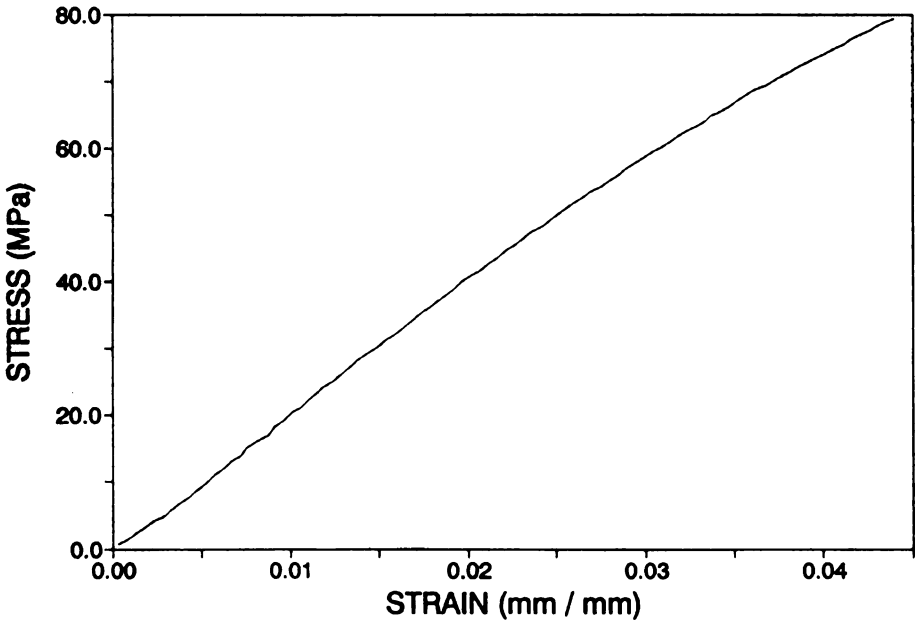

Figure 3-19 Stress - Strain Curve for a Typical Resin Tensile Test

T_g was measured using a modulated DSC with an overall ramp rate of 5°C/min and a one cycle/min modulation of ±1°C. A typical DSC curve is shown in Figure 3-20. T_g was taken to be the point at which there was a step change in the reversible heat loss. A step change in the heat capacity, C_p, was also seen at this temperature as expected. While

some curing could have occurred during the actual test, artificially raising the T_g, the shift should be minimal, and the interest here is in the trends, not specific values.

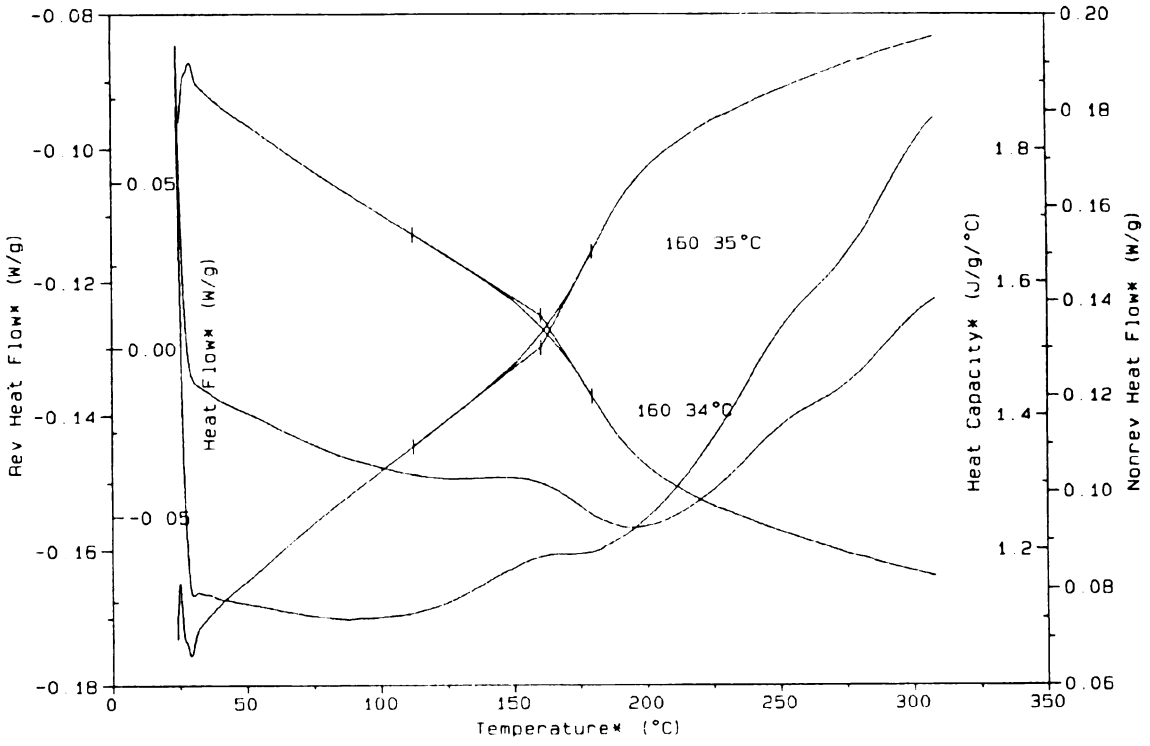

Figure 3-20 Modulated DSC Curve Showing T_g Determination

Data reduction for these flexure, tensile, and DSC tests was performed at The Advanced Materials Engineering Experiment Station (AMEES) in Midland, MI by colleagues. Tabular results for all testing conditions are provided in Appendix A.

3.3.7 Moisture Diffusion Study

A major objective of this research has been to understand the effect of moisture on the properties of the BMI and K3B composites. To effectively utilize the information obtained from the physical property testing, the moisture absorption behavior of these systems must be understood. To this end, moisture absorption studies were performed to determine the ultimate moisture content and diffusion coefficients for BMI and K3B resins and their composites. The effect of extent of resin cure, fiber presence, and microcracking was determined for the BMI/IM7 system. Two temperatures were used so that the diffusivity constants, D_0 and Q, can be calculated allowing knowledge of the actual diffusivity, D.

The methods used to create the resin and composite panels used in this study are detailed in Section 3.1. Specimens were cut to a nominal size of 2" x 1" except for the K3B resin which was nominally 2" x 2/5". All composite and neat resin specimens were dried in a vacuum oven at 80°C under 29.5 in. Hg vacuum for approximately 340 hours, except for K3B cross-ply composites, which were dried at the same conditions for approximately 240 hours.

Specimens were saturated in a pressure cooker at the desired temperature (100°C or 70°C) on glass racks above the water level. The chamber was open to the atmosphere through the open pressure release valve, assuring a pressure of one atmosphere. Weight measurements were made by opening the chamber, quenching the rack and specimens in

a large bath of room temperature deionized water, drying the specimens with paper towels, and weighing them on a Sartorius balance (+/- 0.0001g). The specimens were then returned to the chamber. Measurement time was removed from calculated exposure time.

All composite data is provided both as is, and corrected for fiber volume fraction assuming the fibers to play no role in the diffusion. Absolute weight gain data was converted to percent weight gain vs. time. This data was then fit to a Fickian diffusion model suggested by Shen and Springer [19]. The model assumes two dimensional diffusion through the major faces of a thin sheet and is mathematically represented by Eqn. 3-2. A correction for "thick" specimens was used which adds the area of the edges to that of the faces. The model assumes that initially there is no interaction between the absorption from the edges and faces. Thus, the diffusivity is calculated during the initial linear region of the curve, and the ultimate moisture content is approached asymptotically at long times. A plot of the moisture gain of one specimen showing the Fickian nature of these materials is provided in Chapter 5. The plot also shows a region where the diffusion becomes non-Fickian due to the onset of microcracking.

$$\frac{M_t}{M_\infty} = 1 - e^{\left[-7.3\left(\frac{Dt}{h^2}\right)\right]^{0.75}} \qquad \textbf{Eqn. 3-2}$$

Where:

M_t = The moisture content at time t
M_∞ = the ultimate moisture content (t =∞)

t = time in seconds
D = the diffusion coefficient
h = specimen thickness
C = an adjustable parameter

The data was fit to this equation using a regression analysis with three adjustable parameters: M_t, M_∞, and C. The resultant fit was generally very good with r^2 values ranging from 0.996 to 0.999.

Since experiments were performed at two temperatures, the diffusion coefficient can be calculated as a function of temperature according to Eqn. 3-3. Q is calculated from the slope of the ln(D) vs. 1/T plot, and ln(D_0) is the ordinal intercept.

$$D = D_0 e^{\frac{-Q}{RT}} \qquad \textbf{Eqn. 3-3}$$

Table 3-16 summarizes the whole moisture absorption study. Values of the adjustable parameter, "C", and R^2 are provided in Appendix B. Plots of the original data and curve fit for each specimen and condition have been published elsewhere [18].

Table 3-16 Summary Data for Moisture Absorption Study

Condition	Maximum Moisture % 70°C	Maximum Moisture % 100°C	% Change 70°C-100°C	Diffusivity (mm^2/sec) 70C	Diffusivity (mm^2/sec) 100C	Q (J/molK)	D_0 (mm^2/sec)
BMI Resin Partial Cure	3.31%	3.78%	12.61%	2.369E-08	9.014E-08	47380	3.893E-01
BMI Resin Full Cure	5.14%	5.00%	-2.70%	5.196E-08	1.166E-07	28658	1.203E-03
BMI X-ply	1.55%	1.57%	1.34%	1.879E-06	1.222E-06	-15255	8.927E-09
BMI Unidirectional	2.49%	2.32%	-7.09%	3.206E-08	4.258E-08	10060	1.092E-06
K3B Resin	1.53%	1.62%	5.02%	9.998E-07	2.322E-06	29876	3.547E-02
K3B-IM7 X-ply	0.55%	0.54%	-1.86%	3.383E-08	9.427E-08	36336	1.156E-02
100% Resin Equivalent for Composite Data							
K3B-IM7 X-ply VfCor	1.08%	1.06%	-1.86%				
BMI X-ply VfCor	4.21%	4.27%	1.34%				
BMI Unidirectional	5.10%	4.96%	-2.72%				

3.4 Combined Hygrothermal and Thermal Spike Experiments

Iosipescu shear testing and transient DMA testing for the hygrothermal and thermal spike studies were performed together. The methods used are presented here.

3.4.1 Iosipescu Shear Testing

Iosipescu shear tests were performed on cross-ply composites to determine the change in shear properties due to hygrothermal and thermal spike conditioning.

3.4.1.1 Specimen Details

Hygrothermal specimens were cut from composite panels I and V. Panel I was 62% Vf while V was 35% Vf. All panels had a $[0°/90°]_{1S}$ configuration. The panel fabrication and conditioning of these specimens is detailed in Sections 3.1.2 and 3.3.1.

Upon removal from the hygrothermal chamber, the "wet" specimens were quenched into deionized water and kept saturated between moist towels until +45°/-45° strain gauges were attached to both sides. For these wet specimens, soldering of the leads was done away from of the specimen to prevent specimen drying. Tests were performed immediately after application of the gauges for the wet specimens, but the "dry" specimens were gauged ahead of time and stored under vacuum until tested.

The average weight gain for the wet specimens (by weight measurement) was 1.9 wt% for low cure 62% Vf specimens, 2.4% Vf for the high cure 62% Vf specimens, 2.3 wt% for low cure 35% Vf specimens, and 3.8 wt% for the high cure 35% Vf specimens. The dry specimens showed no weight change.

Thermal Spike BMI/IM7 composite specimens were cut from composite panel Y which had a configuration of $[0°/90°]_{4S}$ and a 47% vf. K3B/IM7 composite specimens were cut from panel 488 which was also $[0°/90°]_{4S}$.

3.4.1.2 Testing and Analysis

All specimens were 3" x ¾". Square shear notches were 0.15" deep with a root radius of 0.050". Testing was performed using a hydraulic MTS testing stand and a modified Wyoming fixture. The test speed was 0.05 in/min and data was stored by the controlling computer at 10 Hz. Strain gauges were set up using one of two methods: either four quarter bridges, or two quarter bridges and one half bridge.

The data was analyzed using a variety of Excel macros. Ultimately, plots of shear stress vs. shear strain were produced for each strain gauge. The macro calculated a shear modulus using the elastic region between 0.2% and 0.6% strain. A failure shear stress was calculated using a 0.2% strain offset criteria. This was also calculated using a macro, and the resultant offset curve was plotted on the shear stress vs. shear strain curve.

To get accurate shear moduli and strengths, interpretation of the curves was necessary because not all of the gauges worked on all specimens. Visual inspection of the curves was performed, and final values were averages from the gauges which performed satisfactorily. The calculation used for each test is provided in the summary above the curves for each specimen. These curves and summaries have been published elsewhere [18]. The shear moduli, strengths, and failure strains for each hygrothermal condition are summarized Table 3-17 and Table 3-18. The results for the thermal spike tests are provided in Table 3-19 and Table 3-20.

Table 3-17 Hygrothermal BMI Composite Shear Data - 62% Vf

Condition	Shear Strength (MPa)	Std. Dev.	Shear Modulus (MPa)	Std. Dev.	Fail Strain (%)	Std. Dev.
Low Cure Dry	56.20	2.37	5360	163	1.230	0.020
High Cure Dry	45.97	1.07	4470	66	1.198	0.014
Low Cure Wet	38.93	21.82	5273	158	1.155	0.104
High Cure Wet	41.63	2.18	4381	264	1.117	0.033

Table 3-18 Hygrothermal BMI Composite Shear Data - 35% Vf

Condition	Shear Strength (MPa)	Std. Dev.	Shear Modulus (MPa)	Std. Dev.	Fail Strain (%)	Std. Dev.
Low Cure Dry	51.08	3.64	3484	14	1.667	0.105
High Cure Dry	35.89	1.41	2878	152	1.462	0.005
Low Cure Wet	45.85	1.80	3782	40	1.384	0.060
High Cure Wet	33.81	0.77	2733	259	1.450	0.083

Table 3-19 Thermal Spiked BMI Composite Shear Data

Condition	Shear Strength (MPa)	Std. Dev.	Shear Modulus (MPa)	Std. Dev.	Fail Strain (%)	Std. Dev.
Dry Control	46.36	0.98	4230	120	1.279	0.022
Wet Control	46.04	0.57	4206	111	1.272	0.022
Dry Cycled	43.63	0.42	3979	351	1.281	0.100
Wet Cycled	46.38	2.78	4272	365	1.266	0.051

Table 3-20 Thermal Spiked K3B Composite Shear Data

Condition	Shear Strength (MPa)	Std. Dev.	Shear Modulus (MPa)	Std. Dev.	Fail Strain (%)	Std. Dev.
Dry Control	47.94	0.33	4873	102	1.155	0.019
Wet Control	48.02	2.49	5025	167	1.141	0.030
Dry Cycled	48.22	1.70	4726	214	1.209	0.118
Wet Cycled	*Blistered*					

3.4.2 Transient DMA Testing

Transient (temperature sweep) DMA tests of both resins and composites were performed to determine the change in T_g due to both hygrothermal and thermal spike conditioning.

The hygrothermal specimens used here were the same ones used for the isothermal tests in Section 3.3.4. After isothermal testing, the specimens were cut to fit the clamped single cantilever fixture using a Dremel tool with an abrasive blade for the dry specimens, and a wet saw with a diamond impregnated blade for the wet specimens. The wet specimens were kept saturated between moist towels until tested.

The thermal spike BMI/IM7 composite specimens were cut from composite panel X which was $[0°/90°]_{4S}$ and 47% Vf. Sixteen 3 in x ½ in specimens were machined with the Bennett saw and dried in a vacuum oven. BMI resin specimens were cut from two separate panels: TSR and 2TSR. The fabrication and post-cure of these panels is described in Section 3.1.1. K3B/IM7 composite specimens were cut from panel 488 using the Bennett saw. The K3B resin was cut from the plaque created at MSU. After conditioning, the thermal spike specimens were cut to fit the DMA's clamped single cantilever fixture using a Dremel tool with an abrasive blade. No cooling water was used, and the amount of heat evolved during cutting was negligible.

Testing was performed using the Rheometrics Mark III DMTA in a clamped single cantilever mode with the large frame. An air atmosphere was used with a strain of 32um

and a 1 Hz frequency. The temperature was ramped at 5°C/min from 100°C to above T_g (between 300°C and 400°C).

NOTE: The temperature measured by this machine is significantly inaccurate. The measured temperatures differ from part temperature by as much as 30°C due to thermal lag. An experiment was performed with three thermocouples taped onto a resin specimen, and this very significant thermal gradient was seen. Fortunately, the readings are very precise, if not accurate, so the repeatability of the tests is very good, and the data is acceptable for comparative studies.

Time, temperature, tan delta, and the log of the storage modulus were exported from the DMA and summarized using Excel macros. Plots of tan delta and the log of the storage and loss moduli vs. temperature have been provided elsewhere. A representative curve is provided in Figure 3-21 for a dry 47% Vf specimen. Table 3-21 and Table 3-22 summarize the T_g values and moduli at 155°C for the hygrothermal specimens. Table 3-23 through Table 3-26 summarize the thermal spike results. The T_g values were measured by the peak of the tan delta curve (calculated by the macro), and from the extrapolated onset of property loss (calculated using the DMA software).

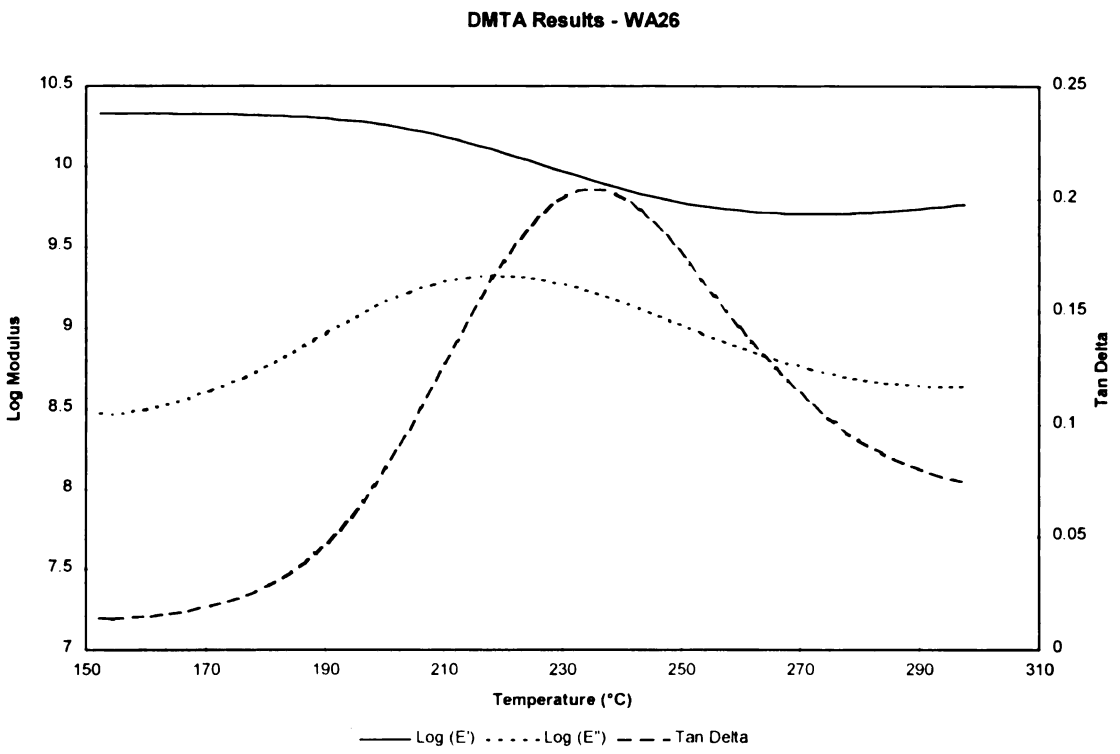

Figure 3-21 Transient DMA Curve for Partially Cured 47% Vf Specimen

Table 3-21 Hygrothermal BMI Composite DMA Data - Transient

Condition	155°C Bending Storage Modulus (MPa)	155°C Bending Loss Modulus (MPa)	Tan Delta ($x10^3$)	Tg (Peak of Tan Delta) (°C)	Tg (Onset of Loss of E') (°C)
62% Vf, Low Cure, Dry	41591	387	9.300	242	203
62% Vf, High Cure, Dry	36898	317	8.580	399	356
62% Vf, Low Cure, Wet	27574	994	39.300	243	160
62% Vf, High Cure, Wet	42855	519	12.100	374	337
55% Vf, Low Cure, Dry	36141	352	9.750	226	195
55% Vf, High Cure, Dry	34995	325	9.290	358	334
47% Vf, Low Cure, Dry	21330	292	13.700	235	200
47% Vf, High Cure, Dry	23496	301	12.800	366	351
47% Vf, Low Cure, Wet	21752	1354	63.125	206	???
47% Vf, High Cure, Wet	15031	354	23.530	365	347

Table 3-22 Hygrothermal BMI Resin DMA Data - Transient

Condition	155°C Bending Storage Modulus (MPa)	155°C Bending Loss Modulus (MPa)	Tan Delta ($x10^3$)	Tg (Peak of Tan Delta) (°C)	Tg (Onset of Loss of E') (°C)
Dry - Average	1473	25.8	17.527	333	299
Dry - Std. Dev.	35.0	0.7	0.104	0.6	2.1
Wet - Average	1312	38.9	29.673	328	
Wet - Std. Dev.	36.5	1.5	1.845	3.9	

Table 3-23 Thermal Spike K3B/IM7 DMA Data - Transient

Condition		155°C Bending Storage Modulus (MPa)	155°C Bending Loss Modulus (MPa)	Tan Delta (x103)	Tg (Peak of Tan Delta) (°C)	Tg (Onset of Loss of E') (°C)
Dry Control	Average	8731	91.50	10.50	251.9	237.9
	Std. Dev.	471	2.75	0.63	3.1	1.9
Wet Control	Average	8931	89.81	10.06	253.9	236.8
	Std. Dev.	154	4.21	0.42	0.7	0.3
Dry Cycled	Average	9090	94.97	10.47	253.8	237.1
	Std. Dev.	1108	16.37	0.80	0.7	0.7
Wet Cycled		***Blistered***				

Table 3-24 Thermal Spike BMI/IM7 DMA Data - Transient

Condition		155°C Bending Storage Modulus (MPa)	155°C Bending Loss Modulus (MPa)	Tan Delta (x103)	Tg (Peak of Tan Delta) (°C)	Tg (Onset of Loss of E') (°C)
Dry Control	Average	6026	78.30	13.32	327.0	291.7
	Std. Dev.	1547	6.37	3.60	3.6	4.5
Wet Control	Average	6613	82.99	12.59	328.9	289.7
	Std. Dev.	899	6.17	1.16	2.3	2.9
Dry Cycled	Average	7277	70.76	9.75	339.2	306.7
	Std. Dev.	828	13.06	0.78	1.1	0.8
Wet Cycled	Average	5918	70.03	11.88	335.9	301.9
	Std. Dev.	961	8.37	1.15	5.3	5.9

Table 3-25 Thermal Spike K3B Resin DMA Data - Transient

Condition		155°C Bending Storage Modulus (MPa)	155°C Bending Loss Modulus (MPa)	Tan Delta (x103)	Tg (Peak of Tan Delta) (°C)	Tg (Onset of Loss of E') (°C)
Dry Control	Average	2260	44.53	19.72	271.4	244.1
	Std. Dev.	225	3.01	0.97	8.4	1.3
Wet Control	Average	2443	43.65	17.87	266.9	243.2
	Std. Dev.	39	0.33	0.42	2.3	0.6
Dry Cycled	Average	2302	50.08	21.76	267.4	243.0
	Std. Dev.	110	1.62	0.33	0.1	1.5
Wet Cycled	Average	2135	53.91	25.28	269.3	243.2
	Std. Dev.	254	3.29	1.45	4.5	1.6

Table 3-26 Thermal Spike BMI Resin DMA Data - Transient

Condition		155°C Bending Storage Modulus (MPa)	155°C Bending Loss Modulus (MPa)	Tan Delta (x103)	Tg (Peak of Tan Delta) (°C)	Tg (Onset of Loss of E') (°C)
Dry Control	Average	1059	24.89	23.54	324.6	191.1
	Std. Dev.	56	0.77	1.74	1.1	165.5
Wet Control	Average	1066	23.91	22.46	325.8	278.9
	Std. Dev.	130	1.10	1.70	0.4	5.6
Dry Cycled	Average	1412	32.75	23.49	330.5	197.1
	Std. Dev.	133	3.22	4.71	9.3	170.8
Wet Cycled	Average	1475	40.36	27.50	332.0	290.2
	Std. Dev.	22	5.16	3.92	9.0	0.5

3.5 Thermal Spike Experiments

The objectives of the thermal spike experiments were to identify any permanent damage due to moisture exposure and thermal cycling. The properties of interest were modulus, strength, failure strain, and retention of composite toughness. The test scheme used is shown in Table 3-27.

Table 3-27 Thermal Spike Testing Scheme

Test Performed	Materials Studied	Properties Reported
Tensile	BMI Resin	Modulus, Strength, Failure Strain
Flexure	BMI Resin (Three Point)	Flexure Modulus
	BMI/IM7 (Four Point)	Flexure Strength
	K3B/IM7 (Four Point)	Flexure Failure Strain
Open Hole Compression	BMI/IM7	Initial Stiffness
	K3B/IM7	Strength
Iosipescu Shear	BMI/IM7	Shear Modulus
	K3B/IM7	Shear Strength
		Shear Failure Strain
Dynamic Mechanical	BMI Resin	155°C Storage Modulus
	K3B Resin	155°C Loss Modulus
	BMI/IM7	155°C Tan Delta
	K3B/IM7	Tg

This testing was organized with a 2^2 factorial design [20] to show both the main effects of moisture exposure and thermal spikes, as well as their interaction effects. The test procedures, including data reduction and results, are presented here, and a discussion of these results including the main and interaction effects is presented in Chapter 6.

3.5.1 Thermal Spike Conditioning

Both neat resin and composites of BMI and K3B were used. Their fabrication was presented in Section 3.1.1 and 3.1.2. Four conditions were used: "Dry Control", "Wet Control", "Dry Cycled", and "Wet Cycled." The Dry Control specimens were kept under vacuum during conditioning. Wet Control specimens, similarly, were kept saturated with moisture at 30°C during conditioning. Dry Cycled specimens were kept under vacuum except during thermal cycling, and Wet Cycled specimens were kept saturated except during thermal cycling.

Thermal cycling was performed by putting the specimens in an oven at 260°C for 15 minutes and then quenching them to room temperature in air. This was performed 11 times for the cycled specimens. A fifteen minute exposure was chosen because an experiment with embedded thermocouples showed that the specimen center reaches the desired temperature (250°C) after 15 minutes of exposure as shown in Figure 3-22. Moisture profiles of the various specimen types through the conditioning cycle are provided in Figure 3-23.

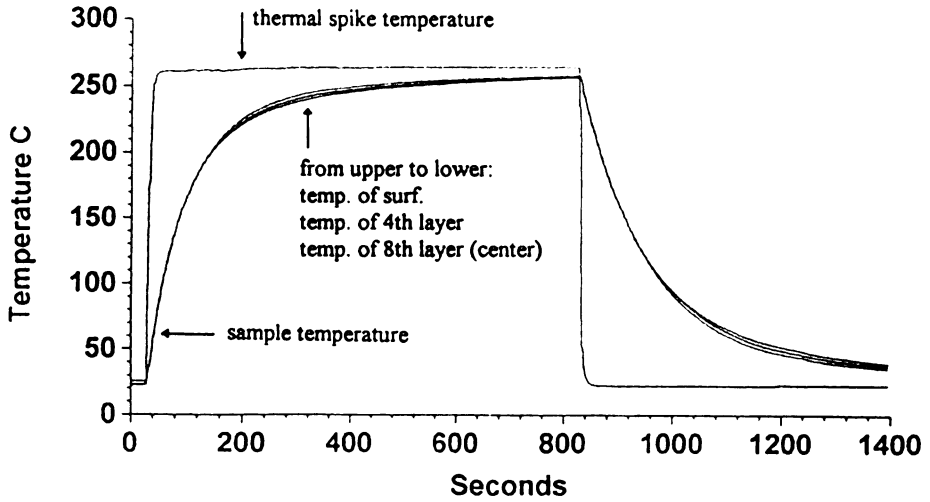

Figure 3-22 Temperature Profile for a Thermal Spiked BMI Composite

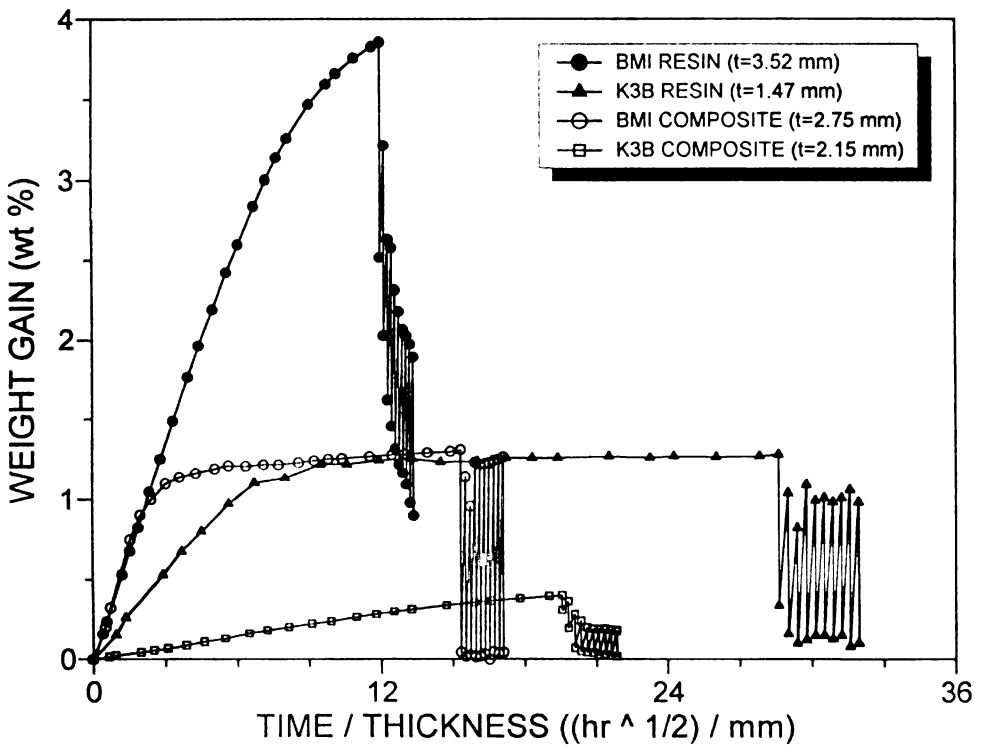

Figure 3-23 Moisture Profiles for All Specimen Types during Thermal Spike Testing

3.5.2 Resin Flexure Testing

Three point flexure tests of neat resin BMI specimens were performed to determine the change in neat resin properties due to moisture exposure and thermal cycling. Tests were not performed on K3B because the resin plaque was not of sufficient size.

Specimens measuring 3" x 2/5" were cut from resin plaque TSR and 2TSR. The fabrication of this plaque was detailed Chapter 4, and conditioning of these specimens was detailed in section 3.5.1 above.

Three point flexure testing was performed at AMEES using a 50 mm span and a test speed of 1.3 mm/min according to ASTM standard D790. Specimens were nominally 75 mm x 10 mm x 3.5 mm. The stress-strain curve for these flex specimens showed a brittle failure in a manner similar to the resin tensile curve. The data reduction was completed at AMEES according to the calculations in the standard. Table 3-28 summarizes the results of this testing.

Table 3-28 Thermal Spike Resin Flexure Results

Condition	Flexure Strength (MPa)	Std. Dev.	Flexure Modulus (MPa)	Std. Dev.	Fail Strain (%)	Std. Dev.
Dry Control	162	10	3244	59	5.19	0.46
Wet Control	153	22	3270	86	4.87	0.95
Dry Cycled	141	11	3255	35	4.41	0.45
Wet Cycled	125	14	3312	23	3.75	0.42

3.5.3 Resin Tensile Testing

Tensile tests of BMI neat resin specimens were performed to determine the change in neat resin properties due to moisture exposure and thermal cycling. Again, tests were not performed on K3B because the resin plaque was not of sufficient size.

The specimens were made from the same panels and conditioned in the same manner as the resin flexure specimens. Tensile tests were performed using a 'dog bone' specimen with a gauge length of 65 mm and a cross-section of nominally 10mm. Tests were performed at a cross-head speed of 5 mm/min according to ASTM standard D638. A representative stress-strain curve is shown in Figure 3-24 showing a brittle failure. Strain was measured using the crosshead motion, so the failure strains are artificially high, and modulus values are thus artificially low. The data reduction was completed at AMEES according to the calculations in the ASTM standard. Table 3-29 summarizes the results of this testing.

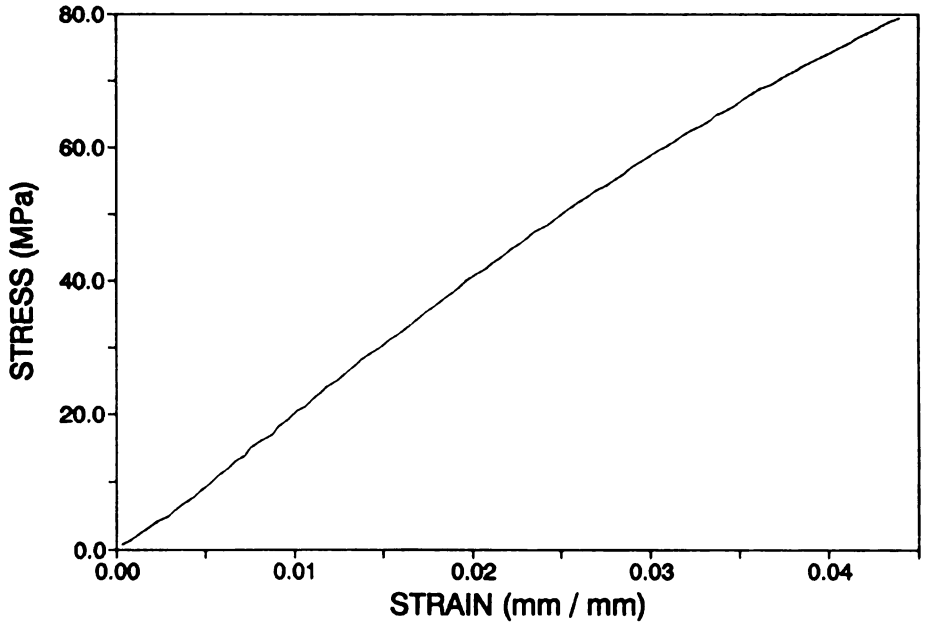

Figure 3-24 A Tensile Stress-Strain Curve for BMI Resin Showing a Brittle Behavior

Table 3-29 Thermal Spike Resin Tensile Results

Condition	Tensile Strength (MPa)	Std. Dev.	Tensile Modulus (MPa)	Std. Dev.	Fail Strain (%)	Std. Dev.
Dry Control	75	9	1762	143	5.2	1
Wet Control	82	7	1779	204	5.6	0.9
Dry Cycled	74	7	1901	68	4.6	0.4
Wet Cycled	81	10	1901	28	5.2	0.7

3.5.4 Thermal Spike Composite Flexure Testing

Four point flexure tests of BMI/IM7 and K3B/IM7 composite specimens were performed to determine the change in composite properties due to moisture exposure and thermal spikes.

BMI/IM7 specimens were cut from composite panel X, and K3B/IM7 specimens were cut from panel 488. Panel X was 47% Vf and both panels were $[0°/90°]_{4S}$. Four inch by one inch specimens were cut from these panels using the Bennett 5000 Plate Saw. The fabrication of the BMI/IM7 panel was described in Chapter 4. Conditioning of these specimens was described in section 3.5.1. Testing was performed according to ASTM standard D790 for four point flexure testing. The test speed was 0.15 in/min. Third-point loading was used with a span of 3 inches. The data reduction was completed at AMEES according to the calculations in the ASTM standard. The BMI specimens showed a compressive failure between the upper load noses. The K3B specimens showed a bending failure under both load noses. While these failure modes are not strictly desirable, they provide some insight into the materials and are discussed later. Table 3-30 and Table 3-31 summarize the composite flexure results.

Table 3-30 Thermal Spike BMI Composite Flexure Data

Condition	Flex Strength (MPa)	Std. Dev.	Flex Modulus (MPa)	Std. Dev.	Fail Strain (%)	Std. Dev.
Dry Control	100	4	1054	31	1.06	0.07
Wet Control	101	6	1069	59	1.09	0.03
Dry Cycled	99	2	1064	23	1.31	0.24
Wet Cycled	96	4	1058	37	1.32	0.27

Table 3-31 Thermal Spike K3B Composite Flexure Data

Condition	Flex Strength (MPa)	Std. Dev.	Flex Modulus (MPa)	Std. Dev.	Fail Strain (%)	Std. Dev.
Dry Control	100	6	1103	52	1.21	0.06
Wet Control	102	2	1161	44	1.28	0.1
Dry Cycled	100	3	1113	32	1.19	0.05
Wet Cycled	***Blistered***					

3.5.5 Open-Hole Compression Testing

Open hole compression tests of BMI/IM7 and K3B/IM7 composite specimens were performed to determine the change in composite toughness properties due to moisture exposure and thermal spikes. BMI/IM7 specimens were cut from composite panel Y, and K3B/IM7 specimens were cut from panel 486. Panel X was 47% vf and both panels were $[0°/90°]_{4S}$. The fabrication of these panels was described in Chapter 4. Three inch by one inch specimens were cut from these panels using the Bennett 5000 Plate Saw. A quarter inch hole was cut in the center of the specimen using a special drill bit for composites. Conditioning of these specimens was described in section 3.5.1. Testing was performed at AMEES and results were provided in tabular form. The exact test conditions are available. Table 3-32 and Table 3-33 summarize the composite flexure results.

Table 3-32 Thermal Spike BMI Open-Hole Compression Data

Condition	Strength (MPa)	Std. Dev.	Modulus (MPa)	Std. Dev.
Dry Control	295	30	528	40
Wet Control	307	26	530	35
Dry Cycled	288	17	560	50
Wet Cycled	290	7	481	46

Table 3-33 Thermal Spike K3B Open-Hole Compression Data

Condition	Strength (MPa)	Std. Dev.	Modulus (MPa)	Std. Dev.
Dry Control	322	16	656	17
Wet Control	343	13	611	48
Dry Cycled	351	5	630	80
Wet Cycled	***Blistered***			

Chapter 4

MICROCRACKING OF CROSS-PLY BMI/IM7 COMPOSITES

4.1 Introduction

Current BMI cure cycles cause significant transverse microcracking which has been shown to greatly increase the moisture diffusion rate as seen in Chapter 2. A reduction in properties has also been observed [1]. This chapter presents a description of the microcracking phenomenon using basic mechanistic principles, and then provides results from both modeling and experimental studies in support of the theory. Finally, the model was used to evaluate various methods for reducing the microcracking in these models. Methods investigated centered around the addition of an appropriate interphase between the fiber and matrix. The ideal properties and size of the interphase were determined.

4.2 Cure Induced Microcracking

Microcracking of continuous fiber composites has been observed in a variety of fiber/matrix systems. There is an irrefutable body of evidence that this microcracking results from thermal expansion mismatch strains induced during cooling from cure temperatures. These thermal strains are proportional to the temperature difference

between the "Stress-Free Temperature" (SFT) and the final part temperature (room temperature). The SFT is the temperature at which residual thermal stresses go to zero in the final laminate. To predict the effect of various cure cycles on the composite's microcracking, this "Stress-Free Temperature" must be known. Simple tests were performed to directly determine the SFT as a function of cure cycle.

There are two causes for the thermal stresses which generate microcracking. One is microscopic and derives from a mismatch between the thermal expansion of the matrix and the transverse thermal expansion of the fiber. The other is based upon the macroscopic thermal expansion mismatch between plies in a cross-ply laminate. Thus, the stress which actually causes microcracking is due to the sum of stresses caused by both mechanisms. To fully understand this cure induced microcracking, both mechanisms must be accounted for.

4.2.1 Review of the Microscopic Microcracking Mechanism

Adams [21] has performed a micromechanical two dimensional finite element analysis of three different carbon fiber/polymer systems. He found that, for an AS4/BMI system, complete yielding of the matrix was possible during cool down from a 204°C cure temperature. He also found that the addition of one weight percent moisture could subsequently cancel almost all of the cure induced stresses.

4.2.2 Review of the Macroscopic Microcracking Mechanism

Cross-ply laminates are subjected to more induced stresses than unidirectional laminates due to the large anisotropy in the thermal expansion of the plies [22]. The 0° plies act as constraints to the 90° plies causing significant thermal residual stresses in the 90° plies. Jones, Mulheron, and Bailey [23] have shown the strain in the 90° ply induced by this mechanism during cooling to be approximated by Equation

Eqn. 4-1.

$$\varepsilon = \frac{E_l(\alpha_t - \alpha_l)\Delta T}{E_l + E_t} \qquad \textbf{Eqn. 4-1}$$

where all properties are in terms of the composite, *l*=longitudinal, and *t*=transverse. Composite property data can be calculated from the constituent materials' properties using formulas from Whitney et al [24], and stresses can be determined using Hooke's law.

4.3 Finite Element Modeling

4.3.1 Introduction

Initially, a finite element model was used to determine the microscopic stresses caused by the mismatch between the transverse thermal expansion of the fiber, and that of the matrix. Ultimately, however, a more accurate and versatile model was used for the

majority of the analyses here, but the FEM solution shows the stress distribution nicely and is thus presented here.

The model assumes a perfectly square packed unidirectional composite under thermal loading. While the packing (square or hexagonal) and fiber spacing are known to have an effect on these stresses [25, 26], calculations based on the square array have been shown to provide good results for this type of analysis [21]. The model used here assumes a completely stress free condition at the SFT, and predicts the stresses generated upon cooling to room temperature. To perform this analysis properly, it was necessary to know both the constituent materials properties and the actual SFT associated with the various cure cycles under investigation.

Figure 4-1 shows the geometry and resultant stresses of this model. A tensile stress is generated along the diagonal between fibers, and tangentially between them while a compressive stress is formed radially between the fibers.

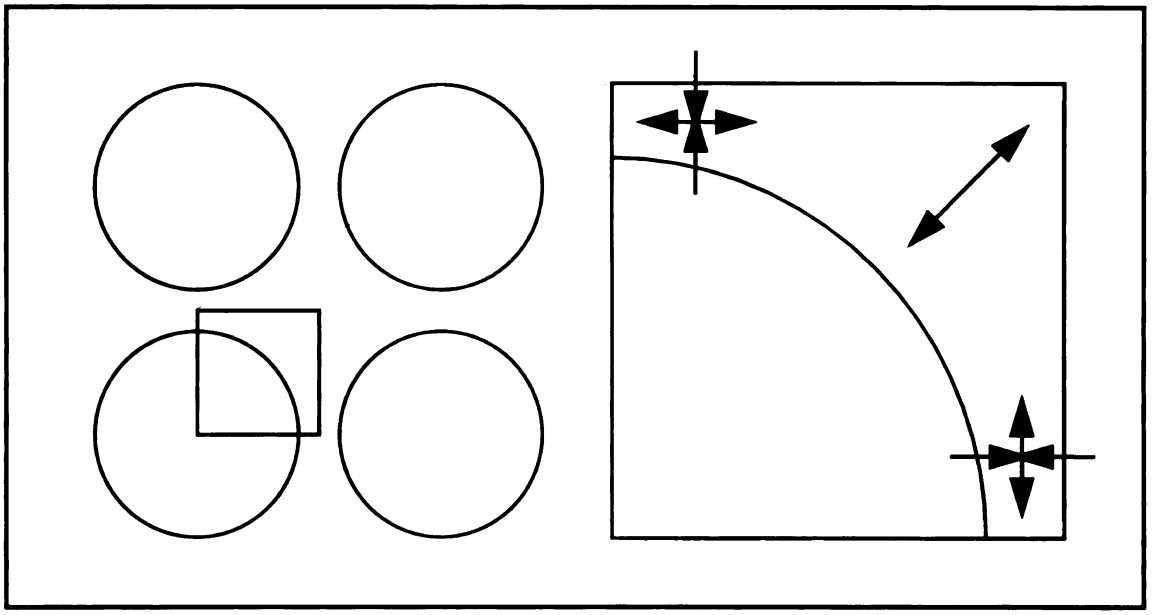

Figure 4-1 Geometry of the Finite Element Model Showing Resultant Stresses

4.3.1.1 Assumptions

The following assumptions are inherent to this analysis:

1. Fibers are arranged in a perfectly square array.
2. The section under consideration is "far" from the laminate edges.
3. Perfect bonding exists between the fiber and matrix.
4. The matrix material is homogenous.
5. The fiber is cylindrically orthotropic.

4.3.1.2 Model Particulars

The Marc finite element package was used for this analysis. The mesh was generated using three noded linear elements and is shown in Figure 4-2. The boundary conditions

are also shown in this figure. The boundary conditions arise from the fact that in a unidirectional composite, there are no external constraints. The only requirements are that the unit cell remain square. Thus, the origin must remain at (0,0), all points along the "X" and "Y" axes must remain on the axes. Lines 2-3 and 3-4 must remain linear such that a square mesh is retained. This is accomplished by tying the "X" values for line 2-3, and the "Y" values for line 3-4.

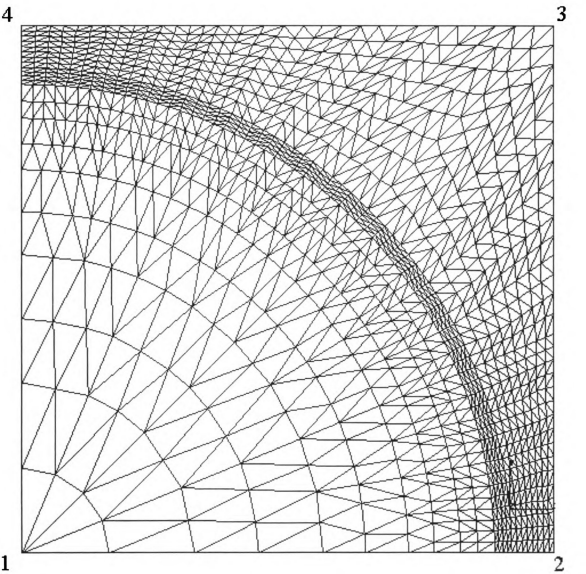

Figure 4-2 The Marc Finite Element Mesh

In the unidirectional case, there is a line of symmetry along 1-3. The material properties used in the FEM calculations are provided in Table 4-1. The matrix properties were obtained from the Ciba-Geigy literature, and the fiber properties are from the Hercules data sheets.

Table 4-1 Material Properties Used in the Marc FEM Calculations

	Constituent Properties	
	IM7 Fiber	Matrimid 5292 BMI
Tensile Strength	5,518 MPa	82.1 MPa
Modulus		4.276 GPa
Longitudinal, E_l	303 GPa	
Transverse, E_t	14 GPa	
In-Plane Poisson's Ratio, ν_n	.20	.34
Coefficient of Thermal Expansion		41.9 x 10^{-6} /°C
Longitudinal, α_l	-0.36 x 10^{-6} /°C	
Transverse, α_t	14.0 x 10^{-6} /°C	

4.3.2 Results

The model was run using a fiber volume fraction of 62%, and various SFTs (130, 177, 200, 250, 300). A typical residual stress diagram for the component of stress in the x direction is provided as Figure 4-3. It can be seen that the maximum compressive stress in the x direction occurs along the x axis between fibers. A tensile stress of a similar magnitude exists between this fiber and the one above it in the y direction. A maximum shear stress occurs just within the matrix at an angle of 45° to the origin. The effect of the SFT on the maximum stress is shown in Figure 4-4. Thus, for a sufficiently high SFT, failure would be expected across the diagonal between fibers. Fortunately, the calculations show that the residual stresses for a perfect unidirectional composite are insufficient to cause failure.

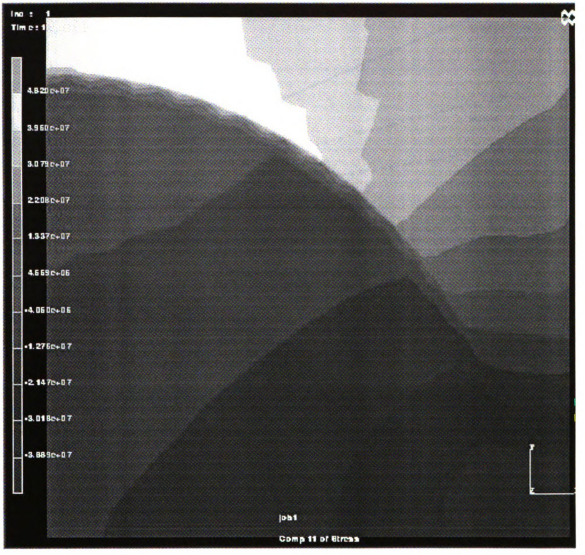

Figure 4-3 Residual Stresses from Marc FEM Model (Vf = 62%, SFT = 200C)

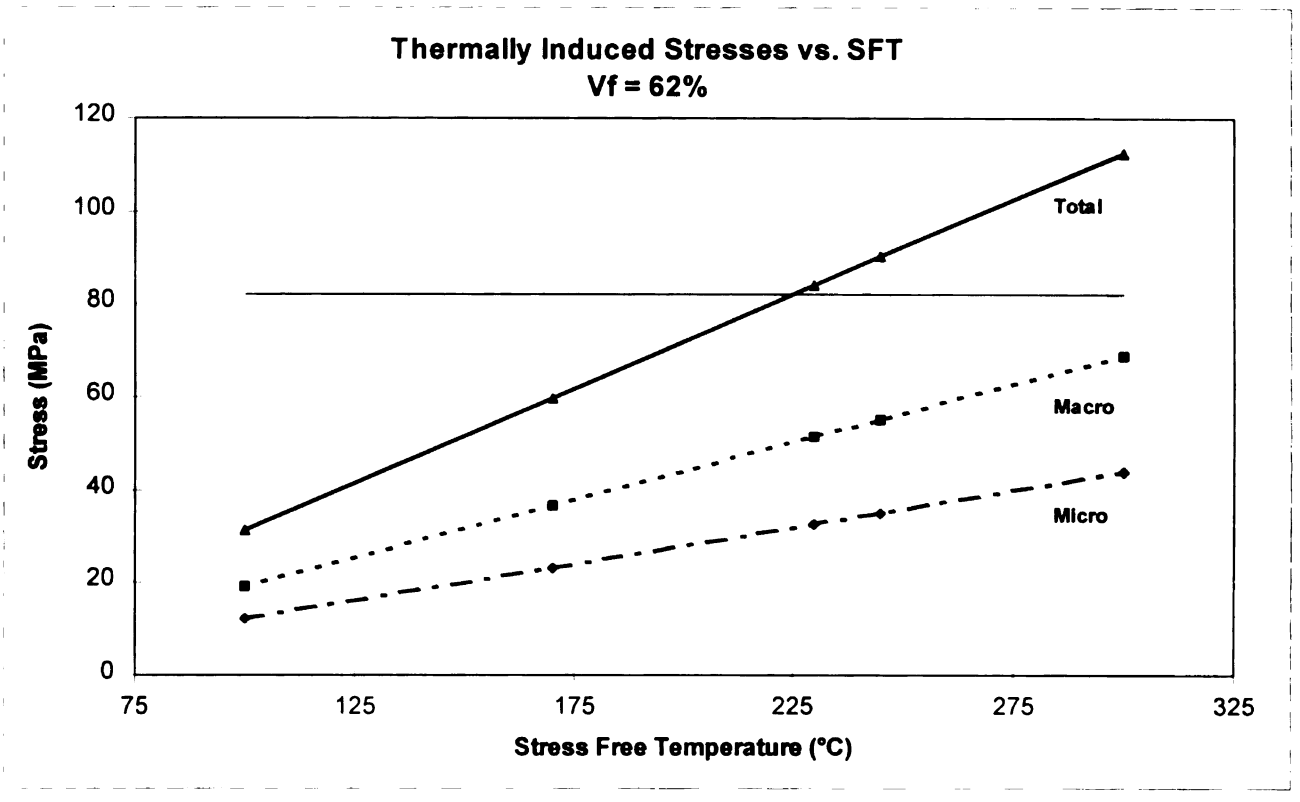

Figure 4-4 Effect of SFT on the Maximum Residual Stress

The fiber volume fraction in this model is the ratio of the fiber area ($\pi d^2/4$) to the total area ($side^2$). To change the volume fraction, or add an interphase of varied thickness, a new mesh is required. Analysis of a cross-ply composite could be done by applying a specified strain to the boundaries at 2-3 and 3-4, but this would require reworking the boundary elements for each SFT. Because constructing new meshes is time consuming, an analytical model was used for further analysis.

4.4 Analytical Modeling using "MicMec"

4.4.1 Introduction to Micmec

MicMec is a Fortran code created by Averill. It provides an elasticity solution to the micromechanical stress state in a composite comprised of a periodic array of fibers in a matrix. The fibers can have any number of interphases with varied properties and thicknesses. The model allows for thermal and moisture loadings. The material properties contain temperature and moisture dependent terms. A more complete description of the model including a derivation of the elasticity solution has been published [27].

4.4.1.1 MicMec Assumptions

The model uses a diamond shaped periodic element as shown in Figure 4-5 and Figure 4-6. The basic assumptions of this analytical model as presented in the paper are:

(i) The fibers are continuous and have infinite length in the η_1-direction.

(ii) The fibers have a circular cross-section that is constant along the length of the fiber.

(iii) The fibers are straight, perfectly aligned with the η_1 axis, and arranged in a periodic diamond array.

(iv) Fiber coatings or interphases may be represented by concentric circular cylinders around the fiber.

materials are homogenous and linearly elastic with temperature- and moisture-endent properties.

material comprising the outermost phase (matrix) is transversely isotropic. All er phases (fiber and interphases) are cylindrically orthotropic.

acent constituents (phases) are perfectly bonded.

chanical loads are applied at infinity. Hygro-thermal effects are uniform within n phase of the composite, but may vary from phase to phase.

ds and material properties do not vary along the η_1-direction.

Model Geometry

mptions made above allow a composite material to be modeled using a tive volume element (RVE). The RVE used in this analysis is shown in Figure location of this element within the model composite is shown in Figure 4-6.

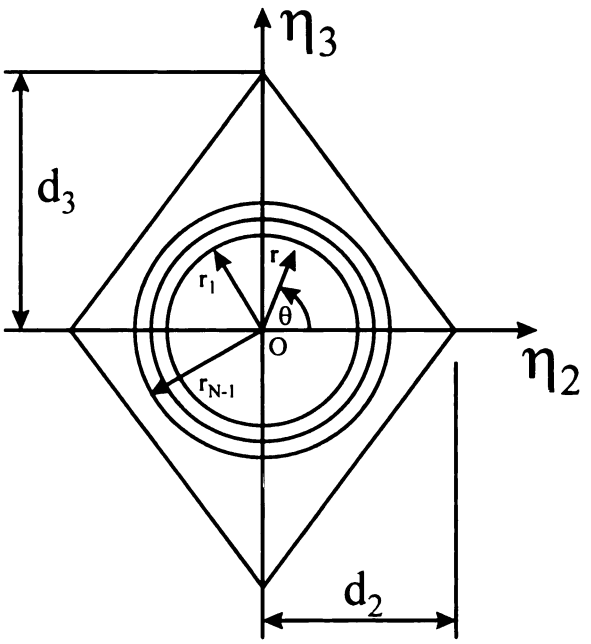

Figure 4-5 The Diamond RVE Used in the MicMec Analysis

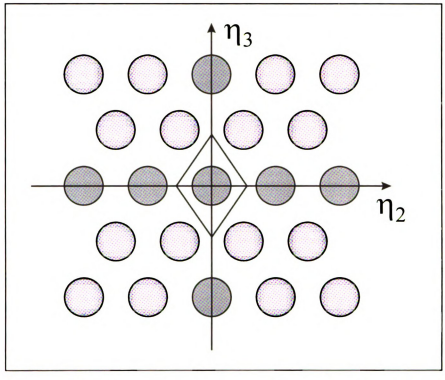

Figure 4-6 Location of the RVE in the Model Composite

The shape of the element is controlled by the adjustable parameters d_2 and d_3. For square packing, $d_2/d_3 = 1$, and for a hexagonally close packed system (HCP), the ratio $d_3/d_2 = \sqrt{3}$. In Figure 4-5, r_1 represents the radius of the fiber, and subsequent radii ($r_2 \ldots r_n$) define the various interphase thicknesses. Multiple interphases with different properties are possible. Thus, a diffused interphase with properties which vary from that of the sizing material, to that of the matrix can be easily approximated.

4.4.1.3 Generation of a Graphical User Interface for MicMec

The MicMec code reads a text file which contains the geometric and property data for the model along with the positions for which solutions are desired. Output can include stresses, strains, displacements, and macroscopic composite properties. The output is provided in various logically organized text files.

Because this can become cumbersome, a Graphical User Interface (GUI) was created in Microsoft Access. The objective of the GUI was to automate the data collection and storage so that a large analysis domain could be covered quickly and accurately. The data generated is stored in tables, and results can be graphed simply by selecting the property of interest, and values for the parameters to be held constant. The GUI interacts with the original code as any user would, by simply creating the input data files, and then importing the output files and storing the data in a logical fashion.

4.4.1.4 The Addition of Laminate Calculations in the GUI

The capability of MicMec was slightly enhanced by allowing the user to choose a layup geometry of either unidirectional, or cross-ply. The choice of a cross-ply laminate requires that external strains be applied to the RVE. These strains are applied by simply stating them in the original MicMec's input file. The magnitude of the applied strains is a function of the thermal expansion mismatch between the 0° and 90° plies, and the SFT. These strains were calculated using Classical Lamination Theory (CLT).

CLT assumes that composite laminate's properties can be calculated from the properties of the individual laminae which make up the laminate. Various assumptions are required for this to be possible.

(i) The lamina must be homogenous and orthotropic.

(ii) All lamina must be perfectly bonded.

(iii) The stress transfer between laminae is perfect.

(iv) No damage occurs.

(v) In this case, it is also assumed that macroscopic stress distribution across each lamina is uniform.

4.4.1.5 Derivation of CLT Equations Used

To calculate the thermal strains during cure in a cross-ply laminate, the following methodology was used.

(i) Obtain the lamina level properties. These were obtained by running MicMec with each specified geometry and material combination.

(ii) Calculate the lamina stiffness matrix [Q] using these lamina properties. The equations used were obtained from Whitney [24].

(iii) Calculate the laminate stiffness matrix for use in the governing equation, Eqn. 4-2.

$$\begin{Bmatrix} \overline{N} \\ \overline{M} \end{Bmatrix} = \begin{bmatrix} AB \\ BD \end{bmatrix} \begin{Bmatrix} \varepsilon^0 \\ \kappa \end{Bmatrix} \qquad \textbf{Eqn. 4-2}$$

Where A, B, and D are the extensional, coupling, and bending stiffnesses, respectively. $\overline{N}$ and $\overline{M}$ are the forces and moments applied, and ε^0 and κ are the strains and curvatures. Due to the symmetry of a cross-ply laminate, there are no coupling stiffnesses (B_{ij}=0). The ABD matrix was calculated using equations from Jones [28].

Given the geometric parameters n, M, F, and t below, the components of the ABD matrix are provided in Equations 4-3 through 4-6.

n = the total number of layers (n = 3).

M = the ratio of the total thickness of odd layers to that of the even layers (M = 1).

F = the ratio of the principle lamina stiffnesses (F= Q_{22}/Q_{11}).

$$A_{11} = \frac{1}{1+M}(M+F)tQ_{11}$$

$$A_{12} = tQ_{12}$$

$$A_{22} = \frac{1}{1+M}(1+MF)tQ_{11}$$ **Eqn. 4-3**

$$A_{16} = A_{16} = 0$$

$$A_{66} = tQ_{66}$$

$$B_{ij} = 0$$ **Eqn. 4-4**

$$D_{11} = \frac{[(F-1)P+1]Q_{11}t^3}{12}$$

$$D_{12} = \frac{Q_{12}t^3}{12}$$

$$D_{22} = \frac{[(1-F)P+F]Q_{11}t^3}{12}$$ **Eqn. 4-5**

$$D_{16} = D_{26} = 0$$

$$D_{66} = \frac{Q_{66}t^3}{12}$$

where

$$P = \frac{1}{(1+M)^3} + \frac{M(n-3)[M(n-1)+2(n+1)]}{(n^2-1)(1+M)^3}$$ **Eqn. 4-6**

(iv) Calculate the thermal forces ($\overline{N}$) and moments ($\overline{M}$). Again, due to symmetry, the moments are zero. The thermal forces calculated here are not actual forces, but are

representations of the forces which would exist if the laminate were fully constrained (which it is not).

In terms of global laminate coordinates, these 'thermal forces' are:

$$\begin{Bmatrix} N_x^T \\ N_y^T \\ N_{xy}^T \end{Bmatrix} = \int \begin{bmatrix} \overline{Q}_{11} & \overline{Q}_{12} & \overline{Q}_{16} \\ \overline{Q}_{12} & \overline{Q}_{22} & \overline{Q}_{26} \\ \overline{Q}_{16} & \overline{Q}_{26} & \overline{Q}_{66} \end{bmatrix}_k \begin{Bmatrix} \alpha_x \\ \alpha_y \\ \alpha_{xy} \end{Bmatrix}_k \Delta T dz \qquad \textbf{Eqn. 4-7}$$

where k represents each layer, and dz denotes integration through the thickness. [28].

In terms of local lamina coordinates, this is equivalent to:

$$N_x^T = \left[\left(Q_{11}\alpha_1 + Q_{12}\alpha_2 \right) 2t_0 + \left(Q_{22}\alpha_2 + Q_{12}\alpha_1 \right) 2t_{90} \right] \Delta T$$

$$N_y^T = \left[\left(Q_{12}\alpha_1 + Q_{22}\alpha_2 \right) 2t_0 + \left(Q_{12}\alpha_2 + Q_{11}\alpha_1 \right) 2t_{90} \right] \Delta T \qquad \textbf{Eqn. 4-8}$$

$$N_{xy}^T = Q_{66}\alpha_{12}\left(2t_0 + 2t_{90} \right) \Delta T = 0$$

where symmetry provides that $Q_{12} = Q_{21}$, $Q_{26} = Q_{16} = 0$, and $\alpha_{12} = 0$.

If there are no applied forces or moments, these fictitious thermal forces can be substituted for $\overline{N}$ in Eqn. 4-2.

(i) Invert the AD matrix and solve for the strains, ε^0. Because of the symmetry, κ will be zero.

(ii) Impose these strains upon the RVE and run MicMec.

4.4.2 MicMec Modeling Test Plan

As with any research, specific objectives must exist, and a logical approach must be used to meet these objectives. The objectives and approach for this modeling study are presented here.

4.4.2.1 Objectives of Modeling Work

Microscopic models such as MicMec or FEM are very useful for understanding the local stress states, but real composites generally violate the modeling assumptions. In particular, the fibers are never truly periodic and the bond between the fiber and matrix is not perfect. The true value of models like this lies in their ability to predict the system's response to geometric or material changes. With this in mind, the objectives for this modeling work are:

(i) Determine the residual stress state and it's response to the SFT, fiber volume fraction, interphase properties, and interphase thickness in cross-ply laminates of BMI/IM7.

(ii) Find the most effective interphase material in terms of material properties and thickness.

(iii) Identify the most practical method for relief of the residual stresses.

The array of test conditions used to accomplish this is given in Table 4-2, and the material properties for the various phases are given in Table 4-3.

Table 4-2 MicMec Test Conditions

Volume Fraction (%)	Stress Free Temperature (°C)	Sizing Thickness (um)	Sizing Tensile Modulus (MPa)
35	100	0	2895
55	200	0.01	182.8
62	300	0.1	18.28
		1.0	2.29

Table 4-3 Material Properties Used in MicMec Analysis

	Hercules IM7 Fiber[a]	Matrimid 5292 BMI	Matrimid 5218	Sizing "A"	Sizing "B"	GE RTV-31
E_1 (MPa)	303,000	1828[d]	2895[b]	182.8	18.28	2.29[d]
$E_{2,3}$ (MPa)	14,000					
G (MPa)	11,000	674[c]	1069[c]	67.4[c]	6.74[c]	0.845[c]
ν_{23}	0.25					
$\nu_{12,13}$	0.20	0.35	0.35	0.35	0.35	0.35
CTE_1	-0.36×10^{-6}/°C	42×10^{-6}/°C[d]	28×10^{-6}/°C[b]	42×10^{-5}/°C	42×10^{-4}/°C	200×10^{-6}/°C[b]
$CTE_{2,3}$	14×10^{-6}/°C					

a From a combination of product literature, AS4 data, and oriented graphite data.
b Product literature values
c Estimated based upon tensile modulus
d Experimentally measured

It is important to note that this model does not provide information about the adhesion level, or failure mode in the system. Failure must be inferred using appropriate failure criteria such as exceeding the material's tensile or shear strength.

4.4.2.2 Analysis Approach

To gauge the system's response to the various parameters, the appropriate response must be measured. The responses of interest here are the location and magnitude of the maximum radial, hoop, and shear stresses. To show these, the radial positions at which they occur was first determined as shown in Section 4.4.3.1, then results for the ensuing analyses were calculated for an array of angles along these radial values. The general location of the analysis points is shown in Figure 4-7. Since the size of the RVE varies with volume fraction, the outer array of points was kept at the maximum possible.

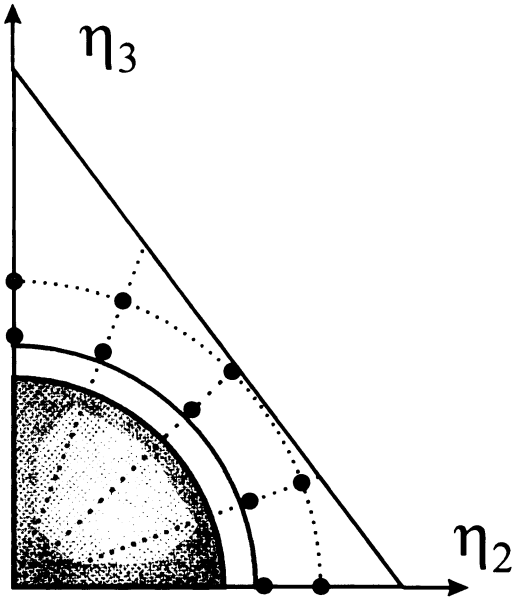

Figure 4-7 Location of Analysis Points Used in the MicMec Model

The results are provided using a cylindrical coordinate system as suggested by the geometry of the analysis. To help clarify the results, a quick review of the three major resultant stresses is provided here. The stresses are the radial (σ_R), theta (hoop, σ_H), and shear stresses (σ_S). These are shown schematically in Figure 4-8. Tensile radial and hoop stresses are depicted. It is important to note that the shear stress acts on the outer surface of the cylinder (the radial plane) in the theta direction and is NOT on the z plane.

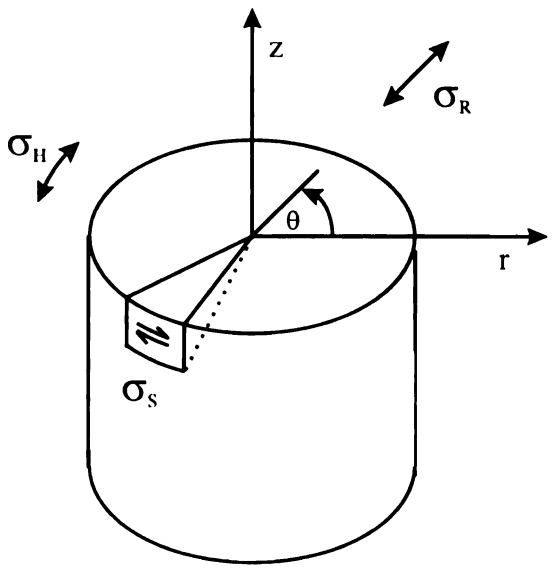

Figure 4-8 Schematic Representation of the Resultant Stresses

4.4.3 Micromechanical Results

The results provide some very interesting information which will help steer research into the use of controlled interphases for relief of residual stresses and are provided in the following sections in terms of the objectives stated in Section 4.4.2.1. First, the distribution of stresses and strains in the radial and theta directions are discussed and the logic used in determining the location of analysis points for the remaining analyses is provided.

The effects caused by changes in fiber volume fraction, stress free temperature, interphase thickness, and interphase modulus are then explained. Finally, the effects of volume fraction, interphase thickness, and interphase modulus on the macroscopic, lamina level, properties is discussed.

4.4.3.1 Determination of Radial Stress Distribution

To determine the position of the maximum stresses and strains, the model was run using an array of radial values along each of five angles. The resultant stresses and strains are shown in Figure 4-9 and Figure 4-10. It can be seen that:

For the stresses,

- The maximum radial stress (44 MPa for this condition) occurs in the bulk matrix as far from the fiber as possible.
- The maximum hoop stress (100 MPa) and shear stress (3.2 MPa) occur in the bulk resin at the interface between the fiber and interphase.

For the strains,

- The radial strain is a maximum at the interface of the fiber and interphase and is near zero in the bulk matrix. The magnitude of these strains is very large (90%) showing that the majority of the strain in the system is absorbed in the interphase.
- The hoop strain is a maximum (3.3%) at the interface between the bulk and the interphase and diminishes with increasing radius.
- The shear strain is nearly zero except in the interphase where it reaches a maximum of almost 18%.

For an interphase with a modulus two orders of magnitude lower than the bulk matrixes modulus, the interphase material's failure strain must be very high in order to avoid

failure in the interphase. Fortunately, materials do exist which have failure strains of this magnitude. Finding the appropriate combination of low modulus, high failure strain, and temperature stability is challenging as discussed in Chapter 7.

Based upon the stress distributions seen here, it was decided to analyze hoop and shear stresses on the bulk side of the interface between the interphase and bulk matrix. Radial stresses were analyzed at the farthest point from the fiber where a complete circle could be used as depicted in Figure 4-7.

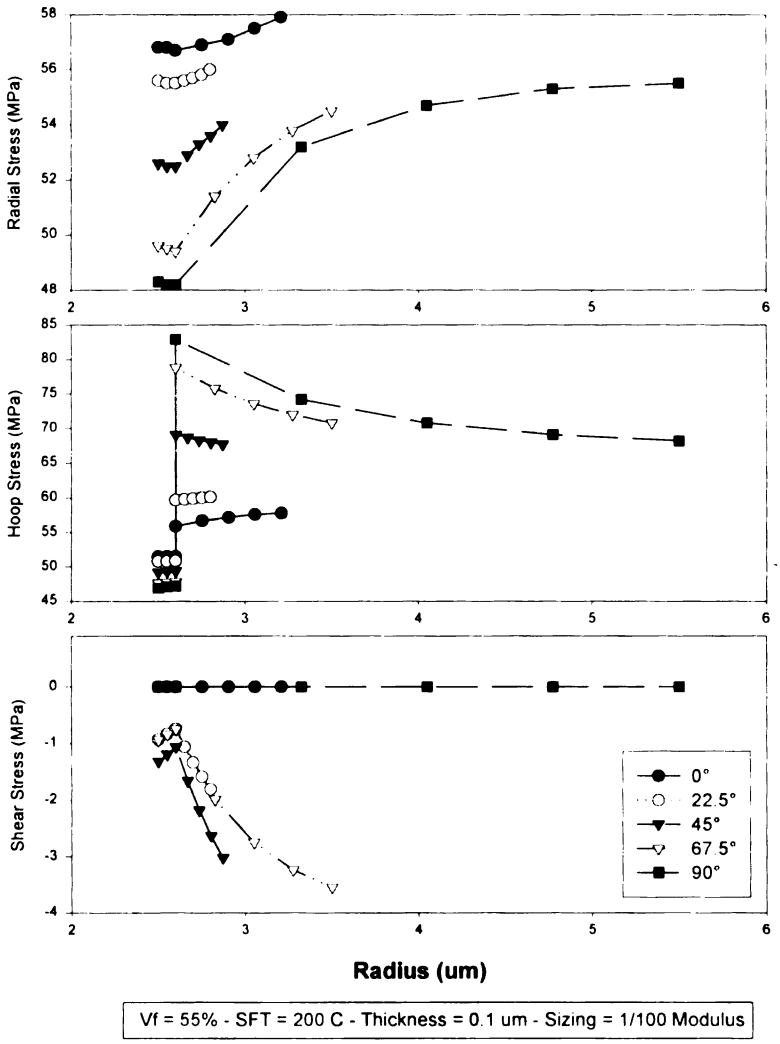

Figure 4-9 Radial Stress Distribution

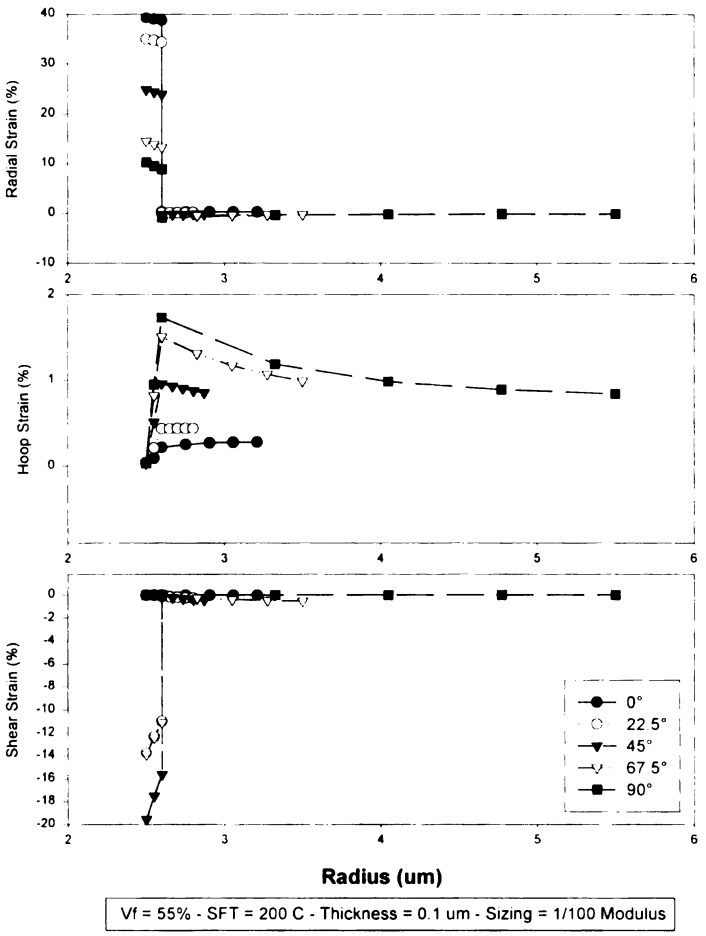

Figure 4-10 Radial Strain Distribution Showing Large Strains in the Interphase

4.4.3.2 The Effect of Fiber Volume Fraction on Residual Stresses and Strains

As shown in Figure 4-11 and Figure 4-12, the stresses are inversely related to the fiber volume fraction. Higher volume fractions show lower residual stresses than the lower volume fractions. This is due to the fact that as the resin content increases, the mismatch in properties between the 0° and 90° plies increases correspondingly. Similar trends are seen for the strains.

Based upon this, composites should be made with a high fiber content in order to reduce the residual stresses. Fortunately, the materials being discussed here are used for high performance applications where high fiber content composites are desired for their high modulus and strength properties.

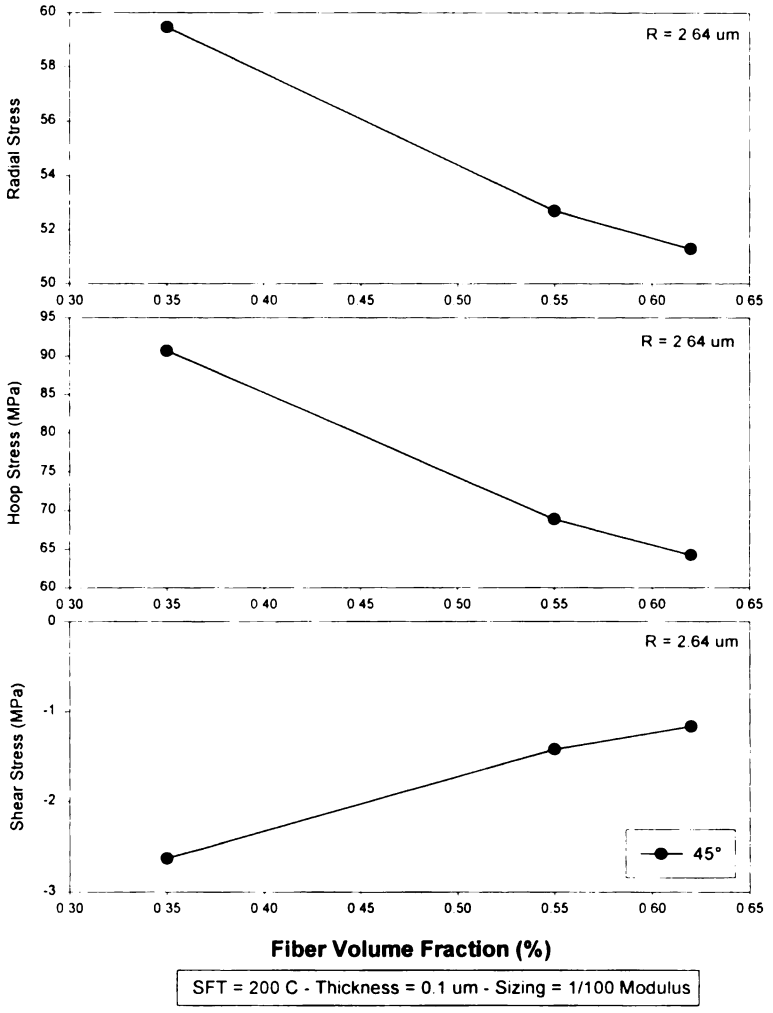

Figure 4-11 Effect of Volume Fraction on Local Stresses

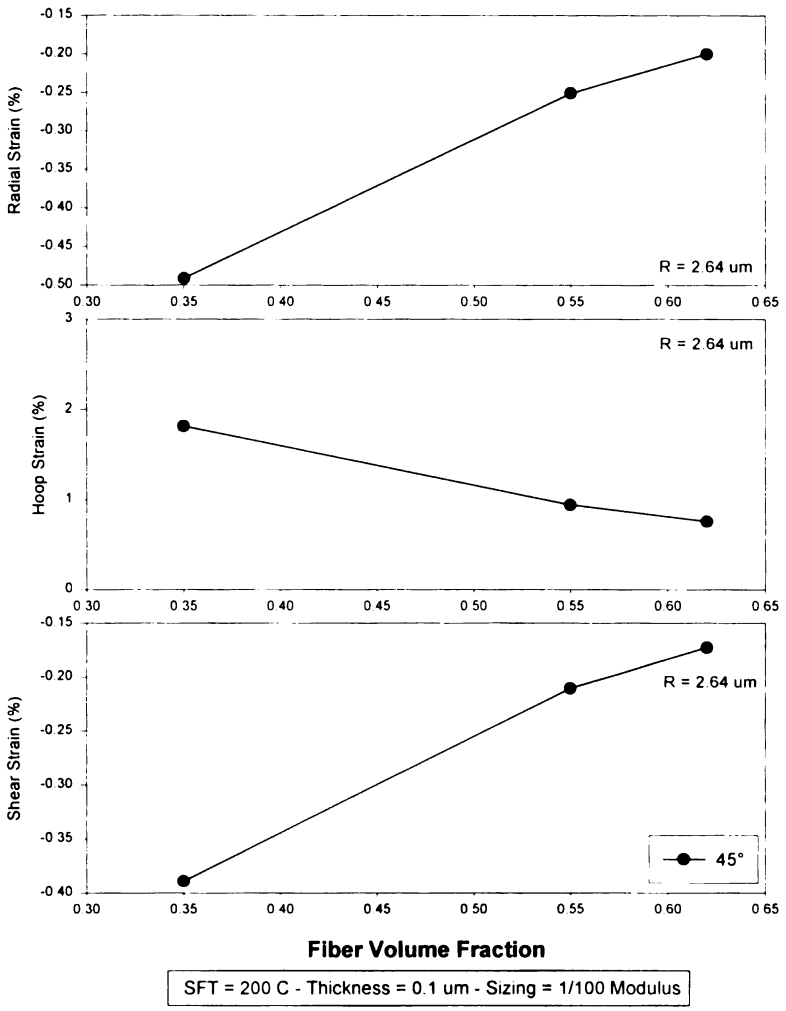

Figure 4-12 Effect of Volume Fraction on Local Strains

4.4.3.3 The Effect of Stress Free Temperature on Residual Stresses and Strains

As can be seen in Figure 4-13 and Figure 4-14, the stress free temperature has a direct, linear relationship with the residual stresses and strains. Higher stress free temperatures cause higher stresses and strains, and thus lower stress free temperatures are desired. Several methods for reducing the stress free temperature of these materials are discussed later in this chapter.

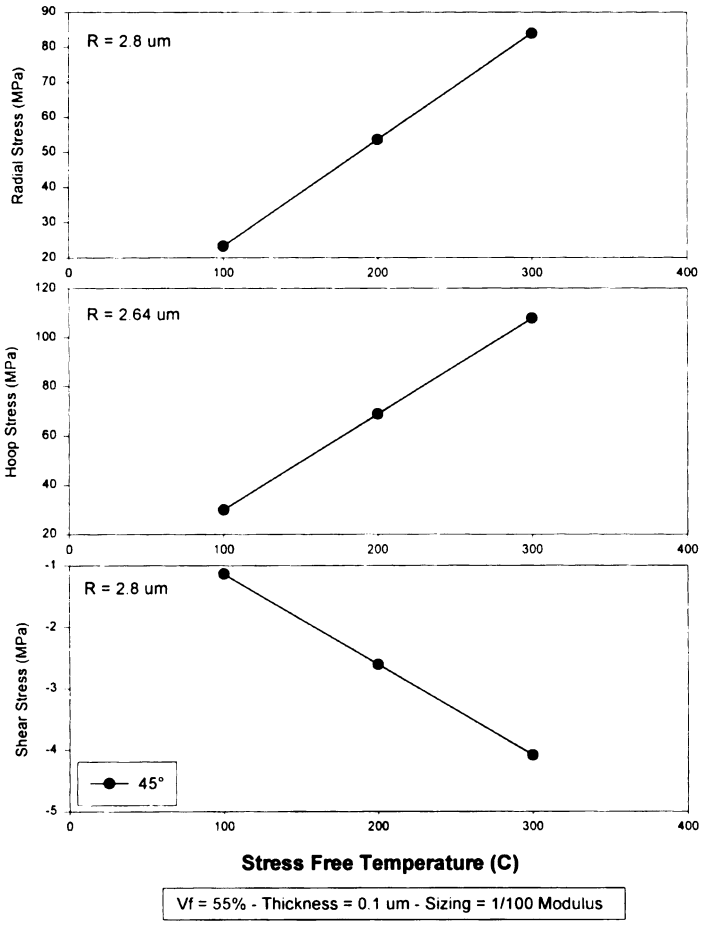

Figure 4-13 Effect of Stress Free Temperature on Local Stresses

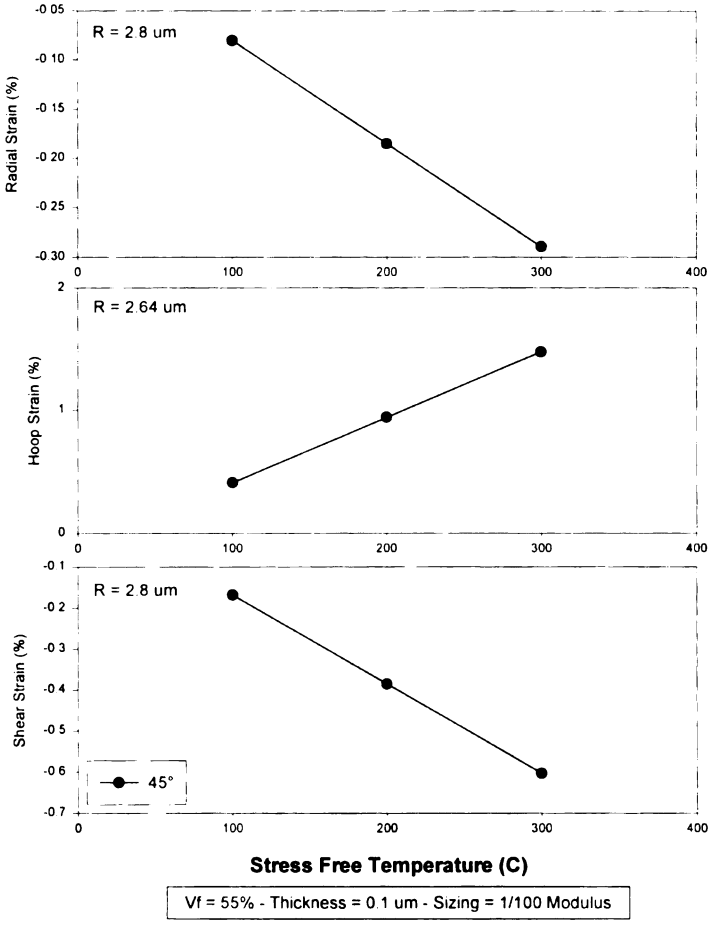

Figure 4-14 Effect of Stress Free Temperature on Local Strains

4.4.3.4 The Effect of Interphase Thickness on Residual Stresses and Strains

As can be seen in Figure 4-15 and Figure 4-16, the thickness has a mixed effect on the stresses and strains shown. The hoop stresses and strains show trends opposite to those of the radial and shear stresses and strains. The hoop stresses increase with increased interphase thickness while the radial and shear stresses decrease. All responses are non-linear with respect to interphase thickness.

To understand this, it is important to remember that very large strains exist in the interphase for this choice of materials. If we consider that the interphase material can act in a manner similar to an incompressible fluid in that it can provide high strains, but volume must be conserved, the results become much more logical. The stresses in the bulk resin are formed due to its larger shrinkage than that of the fiber. As the thickness of the interphase becomes very small compared to the fiber radius, the resin's stresses are directly opposed by the stresses in the fiber. The interphase is incapable of straining sufficiently to fully relieve any of the stresses.

When the thickness of this compliant interphase approaches the magnitude of the fiber radius, the interphase is basically capable of deforming sufficiently to relieve the radial and shear stresses which exist. Again, considering the interphase material to be incompressible, the shrinking resin will continue to have hoop stresses because of the conservation of volume.

This presents a very interesting possibility. The use of a sufficiently thick compliant sizing could redistribute the undesirable tensile and shear stresses into hoop stresses which can help with mechanical bonding which is likely to be responsible for the majority of the adhesion in systems such as are being investigated here. The use of a sizing material with a lower CTE than that of the resin would increase the value of this hoop stress even more. Care must be taken, however, not to generate too large a hoop stress, as this could cause undesirable microcracking.

The most appropriate interphase thickness appears to be one which is capable of redistributing the radial and shear stresses. This appears to require an interphase on the order of 10% of the fiber radius. While this is thicker than commercial sizings are generally applied, it should not present a problem from a processing viewpoint. An interphase of this thickness will represent a full third of the resin content in a 62% volume fraction composite. Because of this, it is very important to consider the effect of the sizing on the thermal capability and chemical resistance of the composite in addition to it's mechanical properties.

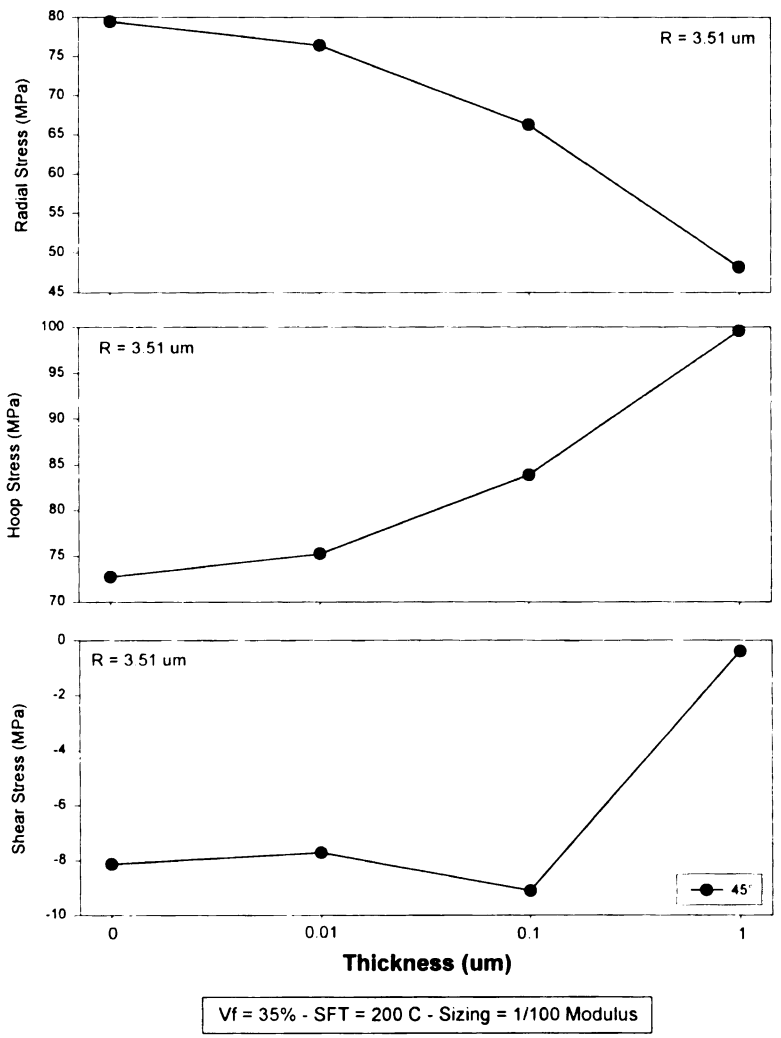

Figure 4-15 Effect of Thickness on Local Stresses

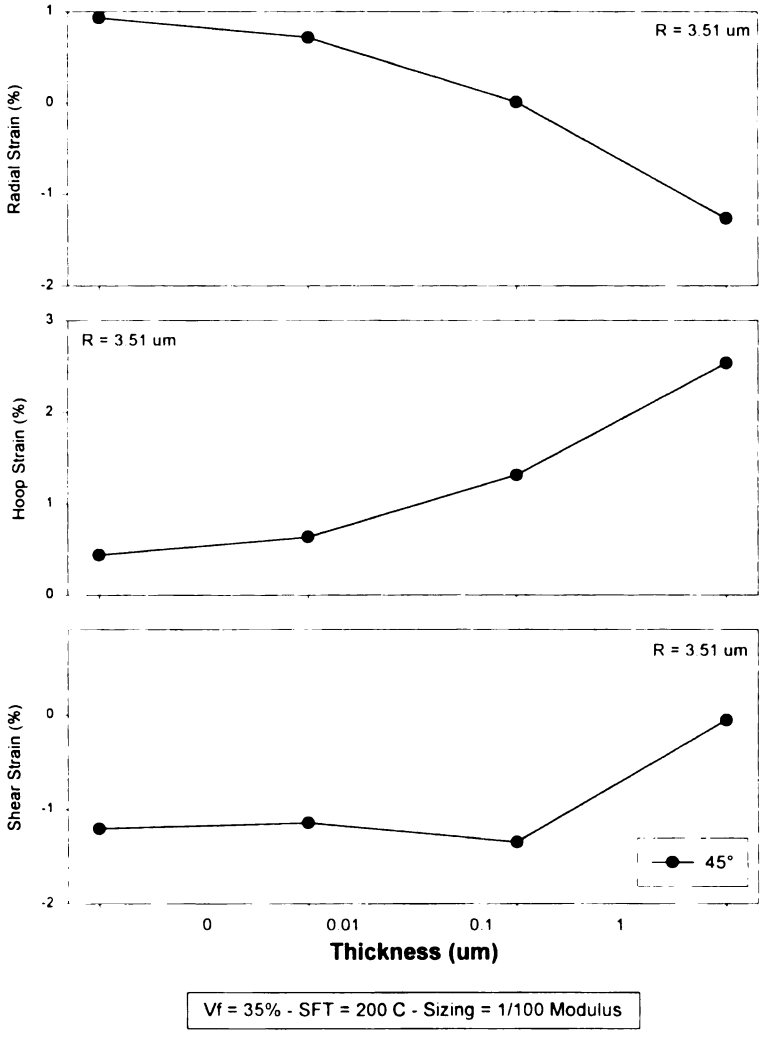

Figure 4-16 Effect of Interphase Thickness on Local Strains

4.4.3.5 The Effect of Interphase Modulus on Residual Stresses and Strains

Figure 4-17 and Figure 4-18 summarize the effect of the modulus on the stresses and strains. To understand the effect the interphase modulus is having, it must be considered in a manner similar to that used in the interpretation of the thickness effect. Interphases with a sufficiently low modulus are capable of relieving the radial and shear stresses while the higher modulus interphases cannot. This is again manifested in a corresponding change in the hoop stress.

To most effectively reduce residual stresses, it is apparent that the use of a lower modulus interphase material is desired. A modulus of 1-10% of the matrix modulus seems to present the best balance between radial and hoop stresses.

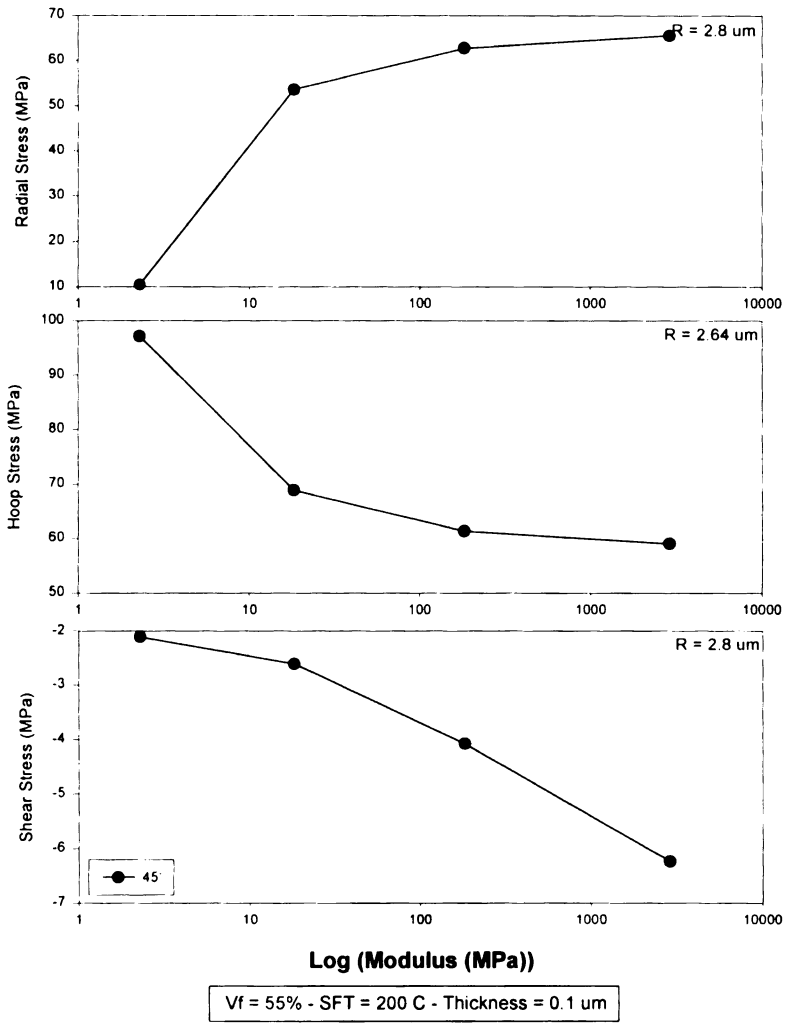

Figure 4-17 Effect of Interphase Modulus on Local Stresses

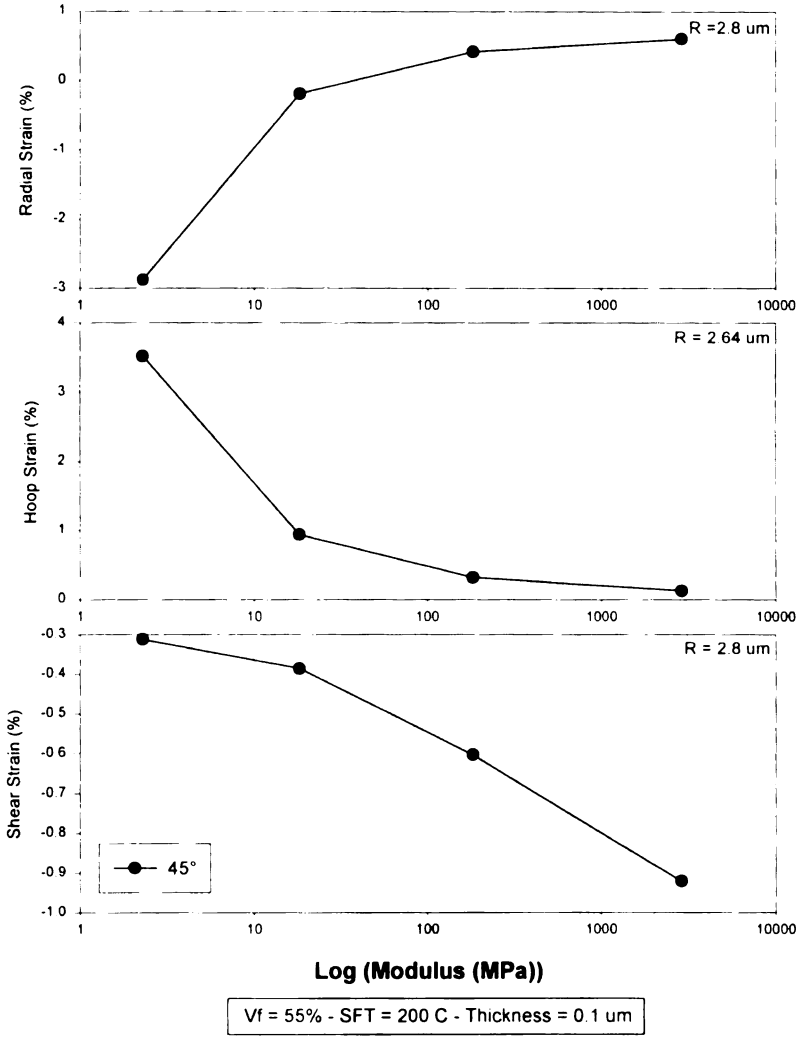

Figure 4-18 Effect of Interphase Modulus on Local Strains

4.4.4 Discussion of the Macroscopic Modeling Results

Since there appear to be some benefits to using a compliant interphase to reduce residual stresses, it is very important to understand how such an interphase will affect the macroscopic properties of the composite. This is investigated here.

The effect of volume fraction is relatively obvious and is shown in Figure 4-19. Increased fiber content causes a dramatic increase in the longitudinal modulus, but has a relatively weak effect on the transverse modulus. Thus, for mechanically loaded parts, it is generally advantageous to have a high fiber content.

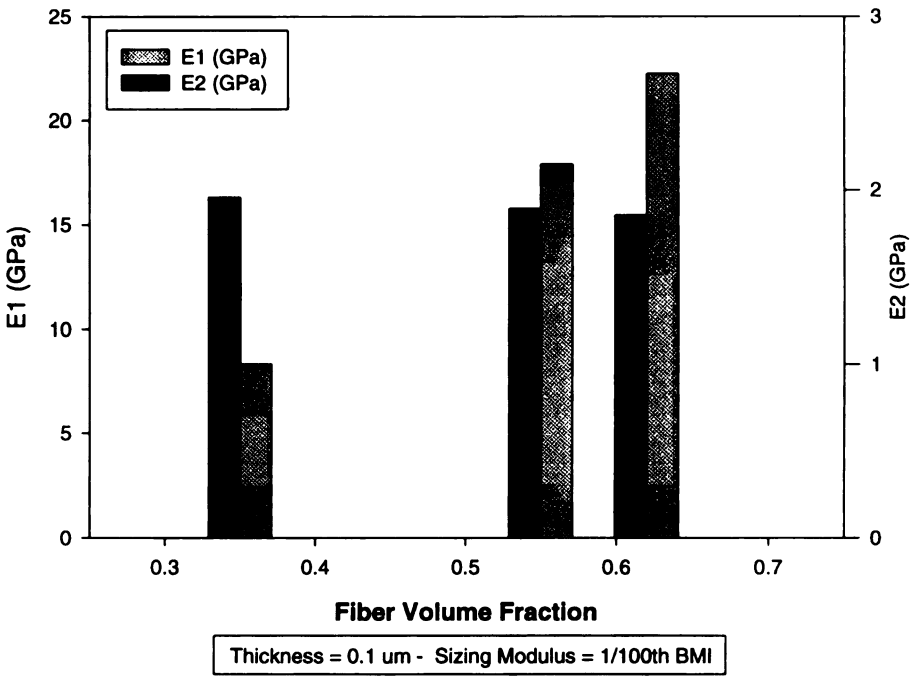

Figure 4-19 The Effect of Fiber Volume Fraction on Lamina Properties

As commonly expected, the sizing has little effect on the longitudinal modulus as seen in Figure 4-20. A sizing with a lower modulus than the matrix can, however, reduce the transverse modulus by as much as 13%. This reduction in off axis modulus may be acceptable in some applications, but commonly cross-ply or quasi-isotropic laminates are utilized, and in these cases, the reduction in modulus would affect the overall composites performance significantly.

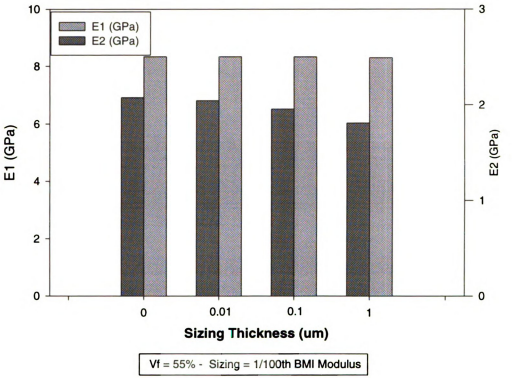

Figure 4-20 The Effect of Sizing Thickness on Lamina Properties

As with the thickness, the modulus of the interphase has little effect on the longitudinal modulus of the lamina as shown in Figure 4-21. It does, however, reduce the transverse modulus by as much as 20%. It should be noted that a sizing having 10% of the matrix modulus is much more likely, and would cause a reduction of less than 4%, which would be quite acceptable in most cases.

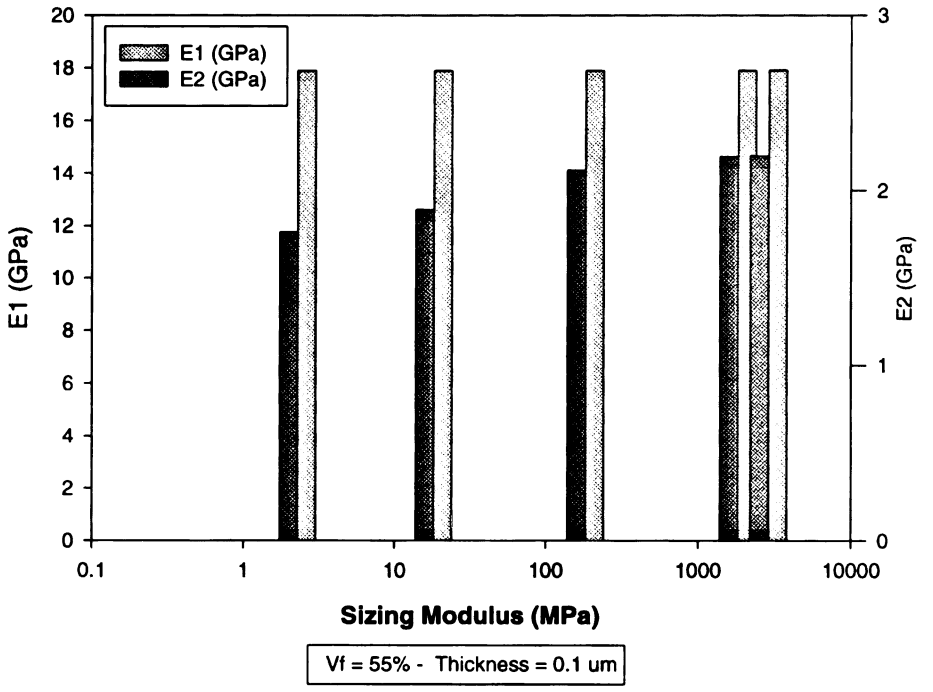

Figure 4-21 The Effect of Sizing Modulus on Lamina Properties

4.4.5 MicMec Modeling Conclusions

The modeling analysis here provides considerable insight into the appropriate methods for relieving cure induced residual stresses. The most obvious method would be to reduce the stress free temperature through methods such as reducing the cure temperature, or utilizing stepped post-cures. A sufficient reduction in the cure temperature is not acceptable because this would leave the resin partially cured, and subject to property

Fortunately, high volume fraction composites have been shown to have the least residual stresses. These materials are generally used in high performance applications where this is required.

The use of a sizing as an interphase material to reduce the residual stresses shows good promise. The results here show that to be most effective, the sizing should be sufficiently thick, and have a low enough modulus to relieve the shear and radial stresses formed during the cure cycle. This thickness appears to be on the order of 10% of the fiber diameter which is considerably larger than sizings are usually applied. The interphase modulus should be between one and two orders of magnitude smaller than that of the matrix to achieve this.

The results also show that the addition of such a sizing will cause a reduction in the transverse modulus of the lamina by on the order of 10%. This would appear to be acceptable if the sizing were able to relieve the residual stresses, and still transfer the load between the fiber and matrix. An additional benefit from the addition of a compliant sizing is that it will increase the toughness of the composite which is generally a very desirable trait.

4.5 Experimental Verification

Various experiments were performed which support the modeling work. In particular, 1) the SFT was determined for various cure cycles; 2) unidirectional composites were examined to see if the microscopic mechanism alone is capable of causing matrix failure; and 3) the crack density and width were determined for various SFTs and volume fractions.

4.5.1 Determination of the Stress Free Temperature

The SFT is caused by a combination of the thermal expansion mismatches from both the microscopic and macroscopic mechanisms described in the modeling section, and also by residual stresses due to the shrinkage of the resin. Thus, the SFT itself cannot be simply predicted, or measured by such properties as T_g. To accurately determine an appropriate value for the SFT, unsymmetric laminates were created with the various post-cures. They were then subjected to a thermal ramp and the temperature at which their deflection returned to zero was determined and deemed the stress free state.

The SFTs associated with various post-cure cycles investigated are provided in Table 4-4. These temperatures provide insight into the possibility of using a stepped post-cure to reduce the stresses which cause microcracking, and provided values for use in the modeling studies.

Table 4-4 Stress Free Temperatures of Various Cure & Post-Cure Cycles

Cure & Post-Cure Cycle	% Cure	Stress Free Temperature
177°C/90 min	.57	100°C
177°C/90 min + 200°C/2hr	.76	170°C
177°C/90 min + 250°C/2hr	.84	230°C
177°C/90 min + 300°C/2hr	.86	245°C
177°C/90 min + 200°C/2hr + 250°C/2hr	.84	210°C
177°C/90 min + 200°C/2hr + 250°C/2hr + 300°C/2hr	.90	240°C

This investigation has shown that the SFT is significantly lower than the cure temperature, which is often used for modeling work. This greatly affects the magnitude of the stress calculated by any model based upon thermal expansion mismatch. This has also shown that while stepped post-cures offer some reduction in SFT, the reduction is relatively small, and would not be sufficient to eliminate microcracking.

4.5.2 Determination of Microscopic (Fiber Level) Cracking

To determine if the microscopic stresses were sufficient to cause microcracking, unidirectional specimens were created with varied post-cures. These were then sectioned, and polished. Both optical microscopy and ESEM analysis were performed and showed that no cracking existed due to this mechanism.

Table 4-5 Post-Cure Cycles Used for Microscopic Cracking Experiment

Cure & Post-Cure Cycle
177°C/90 min
177°C/90 min + 200°C/2hr
177°C/90 min + 250°C/2hr
177°C/90 min + 300°C/2hr
177°C/90 min + 200°C/2hr + 250°C/2hr + 300°C/2hr

To determine if there were any microcracks caused by the fiber level expansion mismatch, polished sections of the $[0_4]_T$ panel with varied post-cures were examined. The CMSC's Environmental Scanning Electron Microscope (ESEM) was used to view the specimens at magnifications of up to 10,000x. No microcracking was evident in any of the samples, and thus the thermal stresses induced by the microscopic mechanism curing cure of these composites are insufficient to cause failure.

4.5.3 Determination of Crack Density and Crack Width

Two separate experiments were performed to measure crack densities and widths. The first was designed to determine the effect of post-cure temperature and stepped post-cures. Stepped post-cures include post-curing at initially lower temperatures and then increasing the temperature as required to defeat the hindrances caused by the glassy state as the T_g of the curing material rises. The second was designed to show the effect of fiber volume fraction (47, 55, and 62% Vf) and cure cycle (Low and High).

4.5.3.1 The Effect of Vf and Post-Cures on Microcracks using Optical Microscopy

Initially, panels were created with varied volume fractions and cure cycles. Crack densities and widths were measured using optical microscopy.

Table 4-6 Post-Cure Cycles Used for the Microscopic Cracking Experiment

Cure & Post-Cure Cycle
177°C/90 min
177°C/90 min + 200°C/2hr
177°C/90 min + 250°C/2hr
177°C/90 min + 300°C/2hr
177°C/90 min + 200°C/2hr + 250°C/2hr
177°C/90 min + 200°C/2hr + 250°C/2hr + 300°C/2hr

The effect of post-cure temperature on crack density, and crack width are shown in Figure 4-22 and Figure 4-23, respectively. The effect of stepped post-cures is shown in Figure 4-24 and Figure 4-25. Here the stepped post-cures match the last two cycles in Table 4-6 and are compared to post-cures with the same final temperature.

The results seen here are not completely self-consistent, and there are a variety of reasons for this. First, a single set of experiments was performed, and thus the numbers reflect single values, not averages. This means that any single data point may be inaccurate and should not be the basis for any strong conclusions. The emergence of trends does, however, suggest that the data is revealing the nature of the system.

Second, the initiation of cracks in any material is very subject to the presence and distribution of flaws. By nature, composites are quite inhomogenous materials. A reasonably thick and varied interply resin rich region is always present. Within each layer, resin rich regions exist at the outside of the tows, and in other regions due to the processing method. These resin rich regions can easily act as stress concentrators, or even cause failure locally due to thermal expansion mismatch or resin shrinkage during cure.

Finally, the measurement of crack widths is subject to the definition of the crack width. Crack width was measured using areas where cracks propagated through resin-rich regions, because these were easily measurable, and seemed the least affected by damage from local fibers. Measurements were made as close as possible to the mid-plane of the ply because crack width decreases near the outer 0° plies due to their constraining effect.

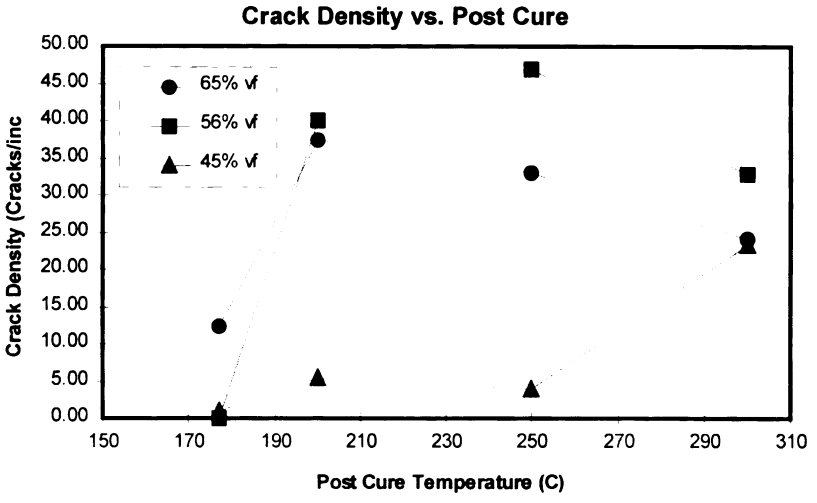

Figure 4-22 Effect of Post Cure Temperature on Crack Density

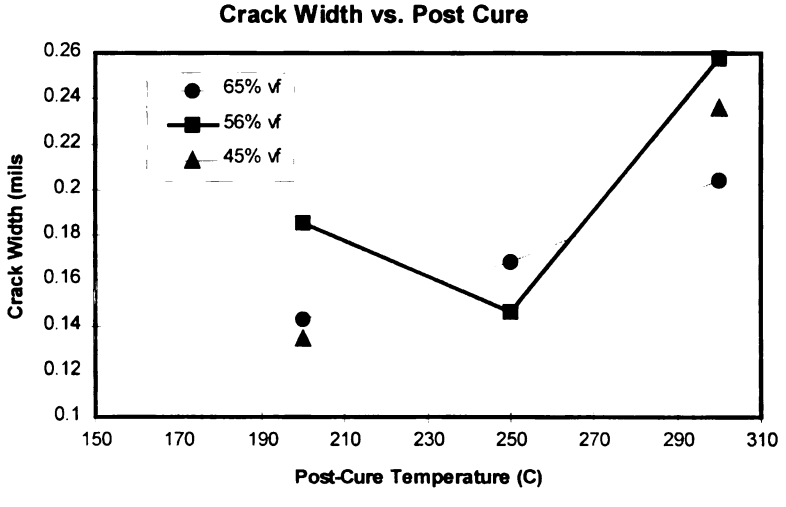

Figure 4-23 Effect of Post Cure Temperature on Crack Density

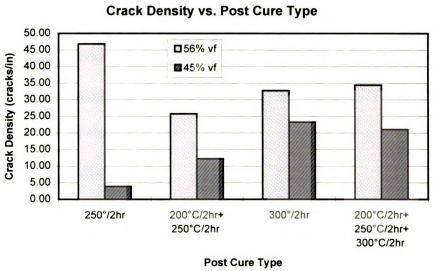

Figure 4-24 Effect of Stepped Post-Cure on Crack Density

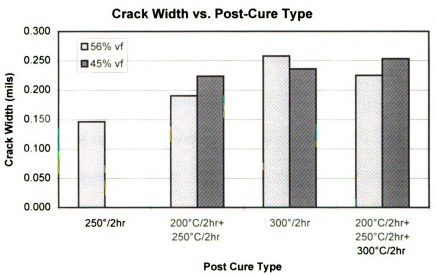

Figure 4-25 Effect of Stepped Post-Cures on Crack Width

4.5.3.1.1 Conclusions

Despite the scatter in the data, it can be stated that:

- Standard volume fraction (64%) composites are microcracked after the 177°C cure.
- Post-cures at any of the 200°, 250°, and 300°C temperatures result in significantly increased crack densities.
- Higher post-cure temperatures *may* result in a lower crack density, but the data is inconclusive.
- The effect of stepped post-cures on crack density varied, but the data supports the previous sections conclusion that stepped post-cures do not reduce the SFT sufficiently to prevent or significantly reduce microcracking.

4.5.3.2 Effect of Vf and Post-Cure on Microcracks using the Environmental SEM

Since the previous experiments contained a fairly wide scatter, new specimens were made, and the analysis of crack widths was performed in the CMSC's Environmental Scanning Electron Microscope (ESEM). Optical microscopy was still used for the crack density measurements.

Panels H, J, and W were used in this experiment. Their fabrication was discussed in Chapter 4. The "High" post-cure was 280°C for 6 hours. "Low" post-cure was 200°C for 2 hours. The specimens were 4 cm x 1 cm and were polished without mounting, or the use of any solvent.

The effects of volume fraction and post-cure on crack density are seen in Figure 4-26 and Figure 4-27. Their effects on crack width are plotted in Figure 4-28, and Figure 4-29. It is more convincingly illustrated by the ESEM images shown in Figure 4-30 and Figure 4-31

After fabrication, the 55 vol% panel (MSW-J) was visually different than the other panels, thus it is felt that the absolute values for crack density and width obtained from it are not meaningful, but the trends appear valid.

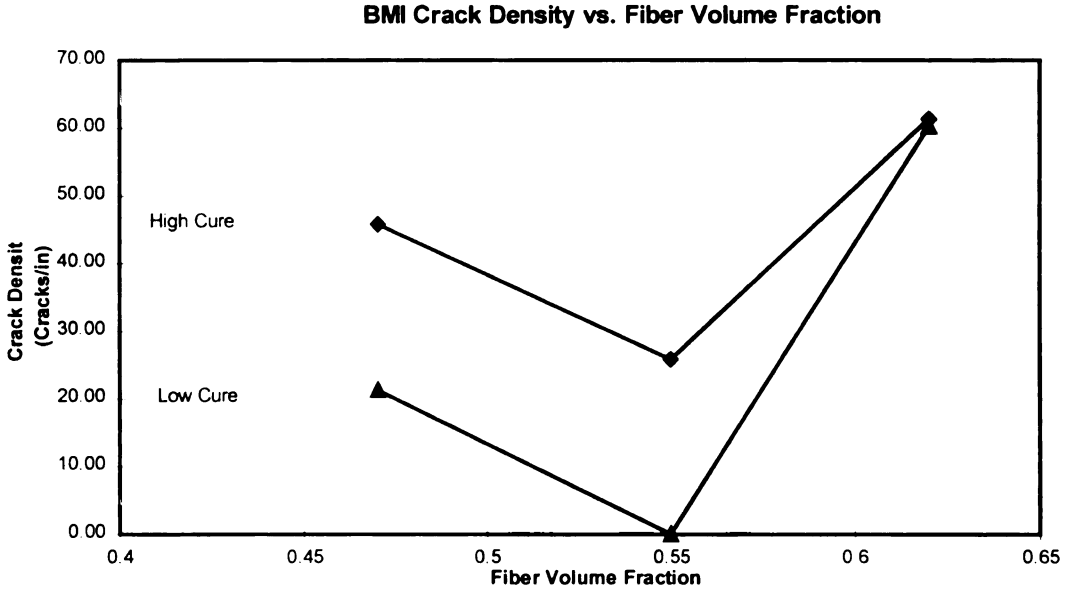

Figure 4-26 Effect of Vf on Crack Density

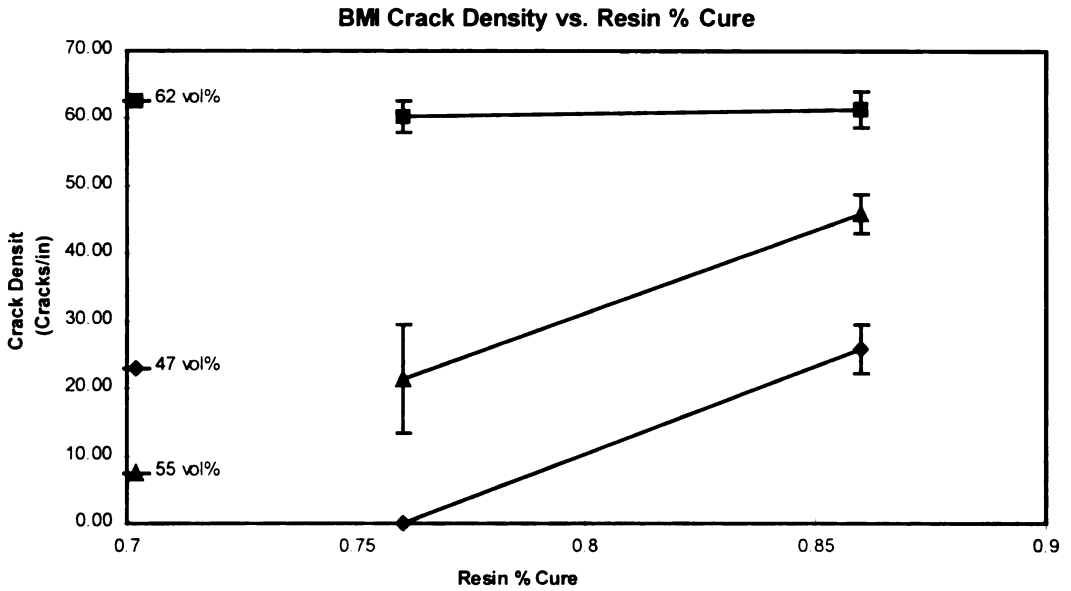

Figure 4-27 Effect of Post-Cure on Crack Density

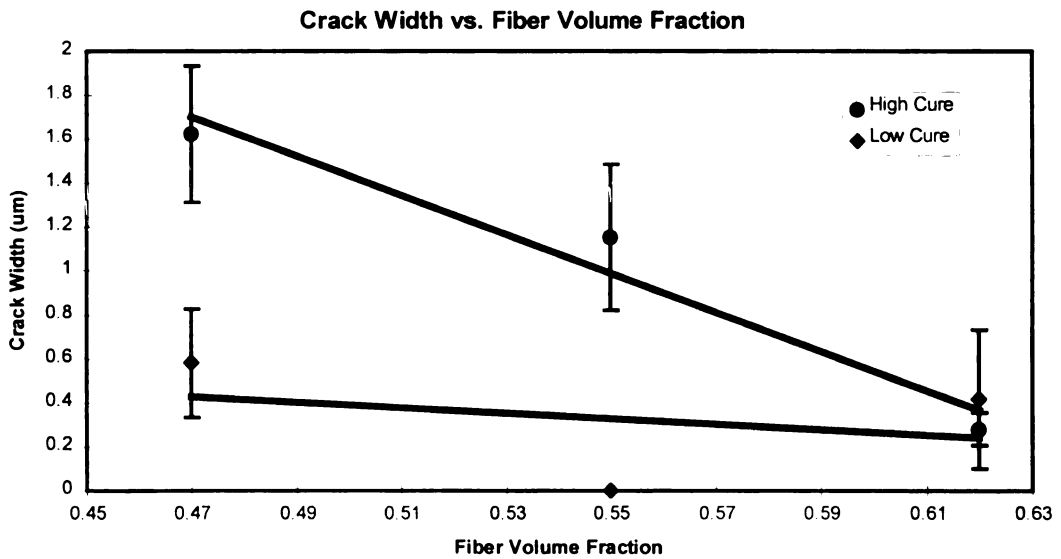

Figure 4-28 Effect of Vf on Crack Width

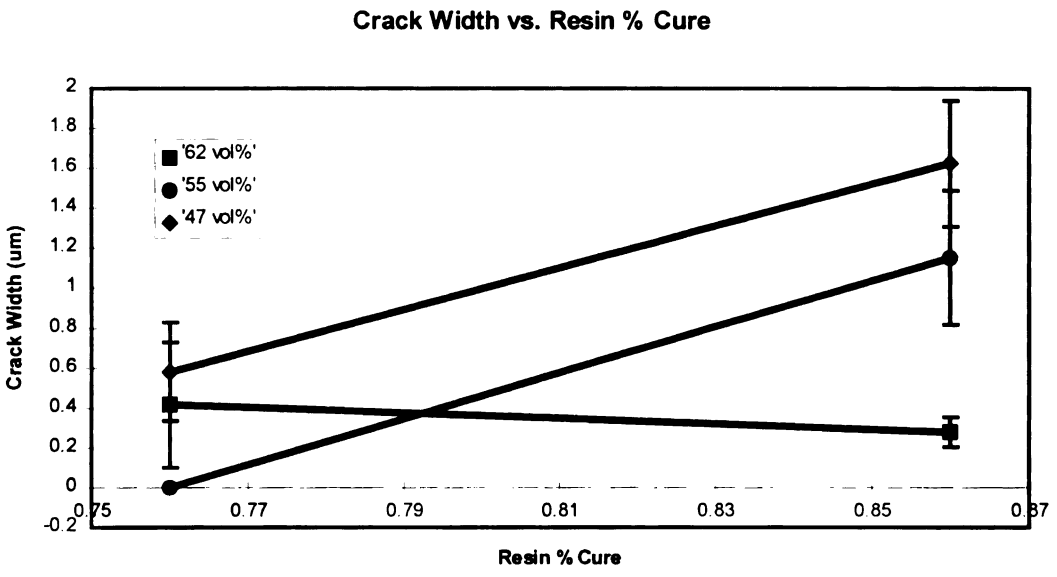

Figure 4-29 Effect of Post-Cure on Crack Width

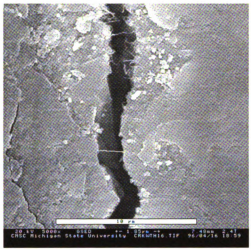

WB17
47 Vol% Fiber
High Post Cure
5000X

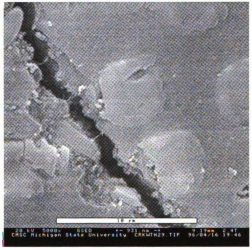

Specimen JB17
55 vol% Fiber
High Post Cure
5000x

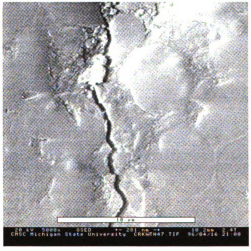

Specimen HB17
62 vol% Fiber
High Post Cure
5000x

Figure 4-30 ESEM Micrographs of BMI/IM7 composites showing the increase in crack width with decreasing fiber content.

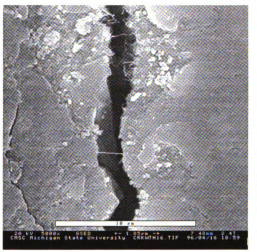

WB17
47 Vol% Fiber
High Post Cure
5000X

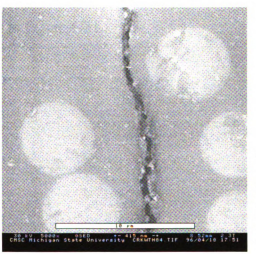

WA17
47 vol% Fiber
Low Post Cure
5000x

Figure 4-31 ESEM Micrographs of BMI/IM7 composites showing the increase in crack width with increased post-cure.

4.5.3.2.1 Conclusions

- Crack density increases with increasing fiber volume fraction as shown in Figure 4-26.
- Crack density increases with increasing post-cure as shown in Figure 4-27
- Both crack width and density were insensitive to post-cure cycle for the 62 vol% composites (see Figure 4-27 and Figure 4-29). This is undoubtedly due to the fact that the contribution from the resin diminishes drastically as the fiber packing becomes nearly perfect, and while 62% is not yet perfect, the inhomogenous nature of the laminate causes a majority of the fibers to be nearly perfectly packed by 62 vol%.
- Crack width increases with decreasing fiber volume fraction as seen in Figure 4-28 and shown graphically in Figure 4-30.
- Crack width increases with increased post-cure as seen in Figure 4-29 and shown graphically in Figure 4-31.

4.6 General ESEM Crack Observations:

A variety of observations were made using the ESEM which support the microcracking theory presented here, or provide further insight into the nature of this system. They are:

- Cracks form in a tensile mode at the ply mid-plane (Figure 4-32) or in a shear mode near the ply interface (Figure 4-33). This supports the theory that stresses are caused by the mismatch between the properties of the 0° ply and the 90° ply. Stresses which are formed in this manner would be transferred between the plies through shear and would result in a tensile load in the center of the constrained ply.
- The crack failure mode is interfacial for both tensile and shear cracks (Figure 4-34). This suggests that an improvement in the overall composite system could be achieved by designing an interphase region between the fiber and matrix which is capable of better adhesion and/or increased strain relief. Another method which has been attempted for this system is to add a tough interleave between the plies to relieve the residual stresses by allowing shear strain at the ply interface [2].

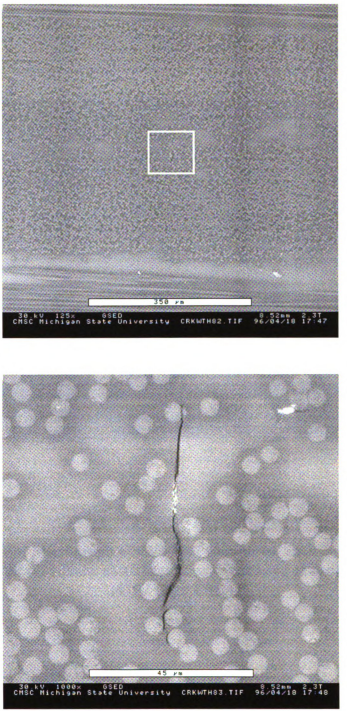

Figure 4-32 ESEM Micrographs of BMI/IM7 Composites Showing that Cracks Form in a Tensile Mode at the Mid-Plane (47% vf, Low Cure)

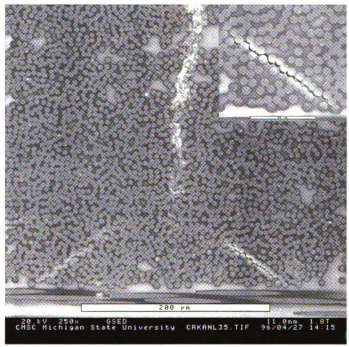

Figure 4-33 ESEM Micrograph of BMI/IM7 Composite Showing Tensile Cracks Forming in the Mid-Plane and Shear Cracks Forming at the Ply Interface (47%, High Cure)

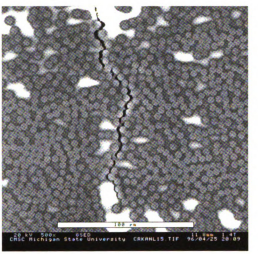

47% vf, Low Cure

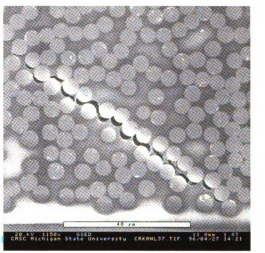

47% vf, High Cure

Figure 4-34 ESEM Micrographs of BMI/IM7 Composites Showing that the Failure Mode is Interfacial for Both Tensile and Shear Cracks

4.7 Identification of Microcrack Initiation During the Standard Cure Cycle

Because microcracking in BMI/IM7 cross-ply laminates occurs during the initial 177°C cure, it is difficult to determine the point of crack initiation, and correspondingly difficult to measure improvements aimed at preventing this initiation. Thus, a method for monitoring the crack initiation throughout the cure cycle was desired.

To accomplish this, one needs to be able to detect crack formation during the cure cycle. This requires the ability to observe the formation of cracks at the cure and post-cure

temperatures of up to 300°C. A method for detecting these cracks has been devised, and the required hardware has been manufactured and tested.

The method consists of laying up a small cross-ply laminate (3/4" x 1/2") and placing it in a vertical heating stage which can be controlled within the ESEM. The ESEM can then be used to monitor the edge of the laminate for cracks while the laminate is subjected to a controlled thermal cycle. This can be used to determine what changes to the cure cycle may reduce the severity of the microcracking. Changes which can be investigated include different cure temperatures/times, varied ramp rates, or the addition of a lower temperature dwell either before or after the main dwell, to name the obvious.

The Vertical Heating Stage with a chill plate was designed and manufactured as seen in Figure 4-35 and Figure 4-36 to achieve thermal cycles with specified ramp rates and hold times. Heating rates in excess of 50°C/min and cooling rates of over 30°C/min have been achieved within the temperatures of interest using 25°C cooling water. A cooling rate of 2.5°C/min was achieved between 50°C to 30°C. Cooling rates are achieved through the use of the water cooled base plate, thus faster cooling rates could be achieved by chilling the water with the attached water chiller.

To ensure accurate part temperature, a thermocouple mounted directly to the specimen is used to control the thermal cycle. The system is controlled by a remote computer which records real time specimen temperatures which will certify that the desired thermal cycle

was actually achieved. In addition, a video record of the experiment can be kept via a direct cable connection to the ESEM.

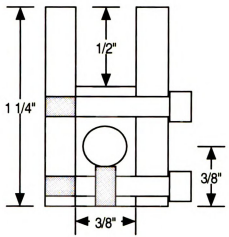

Side View

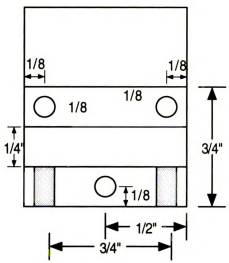

Front View

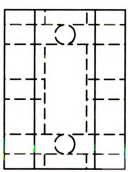

Top View

NOTE: All Threads are 4/40
Unless otherwise noted.

Image of Assembled Vertical Heater Stage
(with Chill Plate)

Figure 4-35 ESEM Vertical Heating Stage Drawings

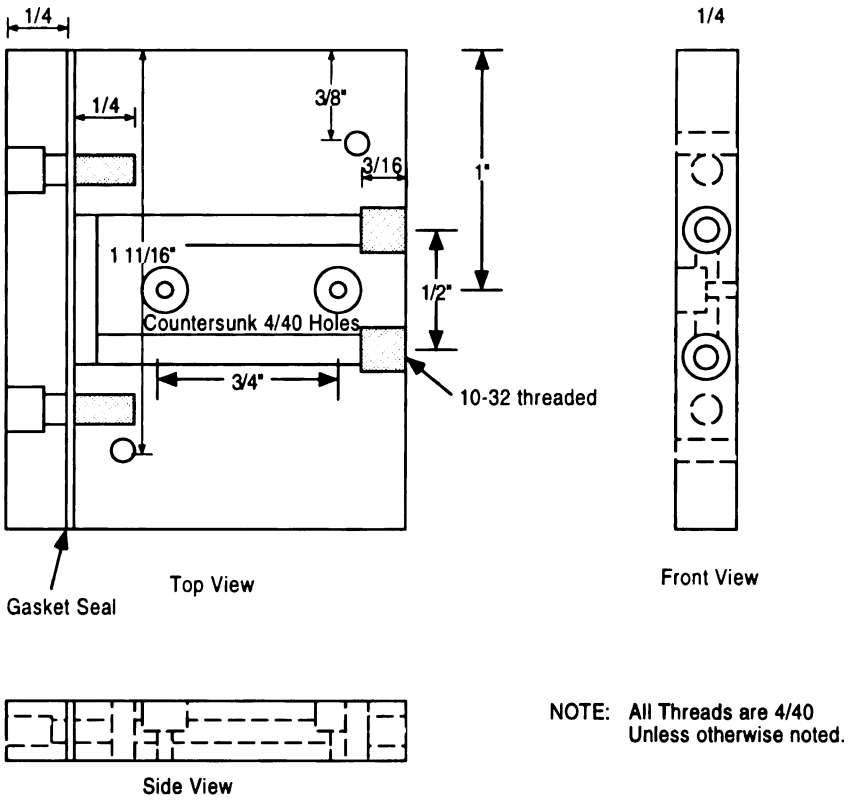

Figure 4-36 ESEM Vertical Heating Stage Chill Plate Drawings

4.8 Identification of the Effect of Laminate Features on Crack Propagation

To improve the BMI/IM7 system's toughness, the propagation behavior of cracks must be understood. To determine this, unidirectional composite specimens were incrementally fractured in the ESEM while being monitored.

It was observed that resin rich regions appear to act as crack deflectors/stoppers. This is demonstrated by the progression of the crack in Figure 4-37. Initially, the crack initiates at the right edge of the specimen and propagates to the left until it hits the resin region shown in (A). With additional load, the crack widens, but does not propagate as seen in (B) and (C). Finally, with sufficient applied load, the crack deflects to a region above the

current crack (D) and continues (E). This behavior suggests that the use of a tough interleave between plies may help to slow crack formation, and thus increase the overall toughness of the composite.

4.9 Failure Analysis of a Mechanically Fractured K3B/IM7 Specimen

A tensile test of a K3B/IM7 composite ($[0°/90°]_{4S}$) was performed to determine the locus of failure in this system. A specimen was cut from K3B/IM7 panel 488. It was approximately 6.5 cm x 1 cm and one edge of the specimen was polished for analysis while the other was notched to promote cracking away from the grips. The specimen was loaded in a tensile frame until both a significant load drop and audible cracking were observed.

Failure analysis was performed in the ESEM and a few interesting observations were made. The resin has a high strain to failure (Figure 4-38) which causes bridging of the interfacial cracks which formed. It is known that the resin has a failure strain of between 8% and 12%, fitting the failure mode seen here. It is also obvious that there is poor adhesion between the fiber and matrix (Figure 4-39).

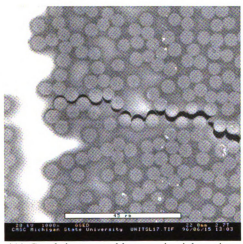

(A) Crack is stopped by a resin rich region.

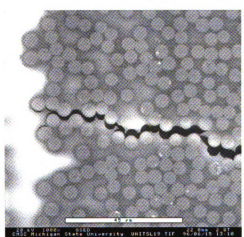

(B) Crack widens with additional load, but does not progress.

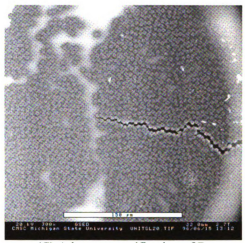

(C) A lower magnification of B.

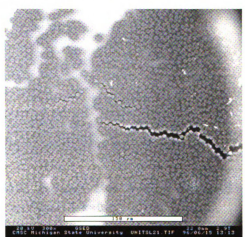

(D) Crack is deflected with additional load.

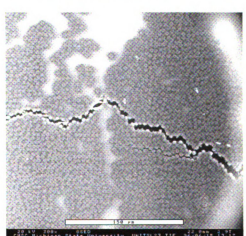

(E) Deflected crack widens and propagates with additional load.

Figure 4-37 Micrographs Showing That Resin Rich Regions Deflect Cracks

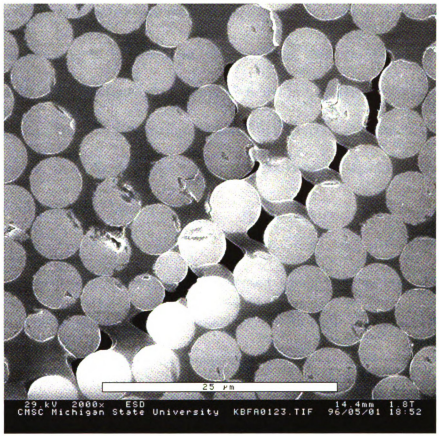

Figure 4-38 ESEM Micrograph Showing That K3B Resin Has A High Strain To Failure Which Causes Bridging Of The Interfacial Cracks Which Form.

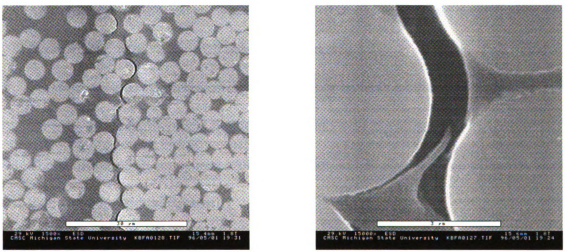

Figure 4-39 ESEM Micrographs Showing Poor Adhesion Between IM7 and K3B.

4.10 General Microcracking Conclusions

Two models were utilized to provide insight into the microcracking mechanism, and to determine if an appropriate interphase could be found to help relieve the residual curing stresses. Experiments were then performed to verify the results of the model, and provide some information about the formation of microcracks in real composites. The following conclusions were drawn:

- A mechanism for microcracking was proposed which includes contributions from both microscopic and a ply-level mechanisms due to thermal expansional mismatch strains during cool-down from cure temperatures.
- Finite Element Analysis using a square packed array of fibers suggests that the stresses from either the microscopic or macroscopic mechanisms alone are insufficient to cause microcracks, but the combination of stresses will cause microcracking in any sufficiently cured composite.
- Analytical modeling using MicMec shows that the stress free temperature has a direct, linear relationship with the residual stresses.
- The fiber volume fraction was shown to have an inverse relationship with the residual stresses, thus a high volume fraction is desired.
- The addition of an interphase around the fiber was shown to be an effective method for relieving residual stresses.
- The appropriate interphase thickness was found to be on the order of 10% of the fiber diameter, and the modulus should be a fraction of that of the bulk matrix. Such an

interphase was shown to cause approximately a 10% reduction in the transverse modulus of the lamina, but shows little effect on the longitudinal properties.

- Stress free temperatures were experimentally found to be over 200°C for a sufficiently cured system.
- Microcracking due to the microscopic mechanism was not found as would be expected from the modeling.
- Cross-ply composites are microcracked after the initial cure, and subsequent post-cures cause an increase in both crack density and width.
- Stepped post-cures are at best marginally successful at limiting crack formation.
- Higher cures were shown to produce larger crack densities and widths.
- Higher fiber volume fractions were shown to produce smaller crack widths.
- High volume fraction composites were shown to be insensitive to changes in the cure.
- Tensile cracks form at the mid-plane of the transverse plies, and shear cracks form near the ply interface.
- A vertical heating stage for the ESEM was created to allow detection of the point of crack initiation during the cure cycle.
- Resin rich regions were shown to act as crack deflectors.
- Failure in both the BMI/IM7 and K3B/IM7 systems were shown to be interfacial suggesting poor adhesion.

Chapter 5

HYGROTHERMAL PROPERTY TESTING

5.1 Introduction

The mechanical and thermal properties of BMI and K3B composites are the final judge of their utility as high performance materials. The applications for these materials require temperatures of up to 190°C with moist environments. Thus, their response to heat and moisture must be understood. During use at elevated temperatures, BMI composites may undergo further curing and/or degradation. Either of these can adversely affect performance, so the cure mechanisms were studied and presented in Chapter 2, and the effect of extent of cure and moisture on material properties have been tested and are presented here.

Composite properties are a strong function of the fiber volume fraction both globally, and locally. To help understand the effect of local volume fraction fluctuations and to magnify the effects caused by matrix changes, composites with varied volume fractions were studied.

The current state of knowledge concerning the effects of moisture and cure advancement for various systems are reviewed in the following sections both in a general sense, and then specifically for the systems of interest here.

5.1.1 Moisture Degradation

The moisture degradation of polymer matrix composites is of great concern because most of these materials are used in humid environments. The effect of moisture on composite properties is complex and varies dramatically from system to system. In the following sections, the general effect of moisture on composites will be presented, and then specific knowledge associated with the degradation of BMIs and K3B will be reviewed.

5.1.1.1 General Moisture Degradation

When exposed to a humid enviroment, thermoset polymers absorb moisture on the order of 1-3% by weight [29, 30]. This moisture can have a variety of effects on the polymer's properties which will cause very significant effects on the properties of their reinforced composites.

The rate of diffusion and equilibrium moisture content in these systems is a function of temperature and environment. While attempts have been made to describe moisture diffusion in epoxies throught the use of Fickian diffusional laws, this method is incomplete, and thus potentially inaccurate in that it ignores the possibility of damage

accumulation which may significantly alter the diffusion of moisture [1]. Absorbed moisture will plasticize resins causing a drop in any matrix controlled composite properties [30], a lowering of it's T_g, an increase in impact properties above T_g [31], swelling stresses, and a change in the deformation and failure modes [1]. It weakens the fiber/matrix interface in graphite/epoxy systems [32]. Moisture has no measurable effect on the thermal expansion coefficients for epoxies [33,34], but an effect is seen in polyesters which can cause larger thermal residual stresses [34].

5.1.1.2 BMI Moisture Degradation

Composites made from Hexcel's F655 BMI reinforced with T650-35 carbon fibers have been shown to attain an equilibrium moisture content of 1.1-1.5% by weight after 30 days which resulted in a reduction in Tg of approximately 80°C [35]. Varma, Needles, Kourtides, and Fish [36] studied the effect of moisture and found that the moisture had little effect on the ILSS, and even found an increase in some cases. Very few other studies of the effect of moisture content on the properties of BMI/carbon fiber composites have been published.

5.1.1.3 K3B Moisture Degradation

Composites made from Avimid® K3B attain an equilibrium moisture content of 0.4% by weight after approximately 20 days with an associated reduction in T_g of only 20°C [35]. A recent study has found that the T_g of saturated K3B/IM7 composites can be as much as

15°C lower than the dry baseline, but that the T_g is recovered after drying [37]. The same study showed the intralaminar fracture toughness, G_{Ic}, to be essentially unaffected by moisture.

5.1.2 BMI Cure Advancement Effects

BMI composites do not reach full cure during their standard cure and post-cure cycles as shown in Chapter 2. Completely cured BMI exhibits a T_g of ~350°C while the standard post-cure (200°C/2 hr; 250°C/6 hr) has a T_g of only ~325°C. The cure reaction shifts from being kinetically controlled to being diffusionally controlled as the T_g of the resin increases past the cure temperature. To complete the cure, the addition of a 300°C/2 hr cycle is necessary [2]. Unfortunately, these high post-cure temperatures cause the inherent, cure-induced, microcracks to widen to a point where they are visible without the aid of either a microscope or penetrant [2, 3].

The increase in cure associated with the T_g increase from ~325°C to ~350°C did not cause a decrease in G_{Ic} toughness values of Matrimid 5292 BMI/AS4 composite specimens. This fact is thought to be due to a toughening of the resin due to a more fully cured and "defect-free" crosslinked network where unreacted chain sites are considered defects [2]. This suggests that increasing T_g to 350°C by performing the additional post cure at 300°C will not directly reduce the room temperature physical properties of the composite. Unfortunately, this investigation did not determine the moisture sensitivity, or thermal aging effect of the increased T_g.

A reduction in interlaminar shear strength with increase in T_g or moisture content has been reported for the Hexcel F665/T650-35 carbon fiber system [35]. There is no measurable effect of T_g on IITRI compression strengths, but moisture is shown to cause a significant decrease. Other investigations (using *O,O'*-dicyanobisphenol A, BMI) have shown a notable reduction in impact strength after thermal aging at 190°C. All specimens in this study failed in shear due to the small span-to-depth ratio (12:1) and the aging times were sufficient (1000 hours) to cause a significant rise in T_g [13]. All of these investigations show the importance of performing a detailed study of combined hygrothermal exposures.

A careful study of the relationship between crosslinking and composite properties for the PMR-PI/Celion 6000 system was recently performed [4]. The study has shown that the T_g, initial weight loss and density, and elevated temperature interlaminar shear strength increase linearly with increases in crosslink density. Elevated temperature flexural strength and modulus were found to increase in a non-linear manner with an increase in crosslink density. Initial moisture absorption and coefficient of thermal expansion were found to decrease linearly with an increase in crosslink density.

It is suggested that a similar set of relations for bismaleimide resins could be used to predict the effect of crosslink density on properties [4]. Another paper, relating to a high T_g amine/epoxy system, also states that there is a direct, one-to-one relation between T_g and percent conversion, independent of cure temperature [38]. A relationship between T_g

and percent conversion has already been determined for the BMPM-DABPA BMI system [15].

5.2 Test Design

The objectives of this hygrothermal study were to identify any effect due to post-cure cycle, moisture, or fiber volume fraction. These factors were chosen for a variety of reasons. Cure may change over the life of the part, and has been shown to reduce mechanical properties over time. Moisture has been shown to be both beneficial and detrimental to composite properties. Volume fraction was chosen because most laminates contain local regions of very high resin content which can have a great effect on composite performance. The properties of these regions can be determined by testing low volume fraction composites.

The majority of the hygrothermal testing performed was organized into a designed experiment. The list of tests used in this experiment is provided in Table 5-1. In addition to the testing shown here, a more complete set of resin tests was performed which included flexure tests, tensile tests, and Tg determination for a wide variety of cure histories. A study of the moisture absorption behavior of these materials was also conducted.

Table 5-1 Hygrothermal Testing Scheme

Test Performed	Materials Studied	Properties Reported
Tensile	BMI Resin	Modulus, Strength, Failure Strain
Flexure	BMI Resin (Three Point. Moisture) BMI Resin (Three Point. Cure Progression) BMI/IM7 (Four Point)	Flexure Modulus Flexure Strength Flexure Failure Strain
Iosipescu Shear	BMI/IM7	Shear Modulus Shear Strength Shear Failure Strain
Isothermal Dynamic Mechanical - Three Point Bend	BMI Resin BMI/IM7	30°C Storage Modulus 30°C Loss Modulus 30°C Tan Delta Tg
Transient Dynamic Mechanical - Single Cantilever	BMI Resin BMI/IM7	155°C Storage Modulus 155°C Loss Modulus 155°C Tan Delta Tg

This testing was organized with a 2^3 factorial design to show both the main effects of cure, moisture, and volume fraction, as well as their interaction effects. The test procedures including data reduction and tabular results are presented in Chapter 3. The discussion of these results including the main and interaction effects are presented in separately in Section 4.6. Here the data is presented with respect to changes in the properties of interest, encompassing the data from all pertinent tests. First, a detailed study of the effect of cure history on the physical and thermal properties of the BMI system is presented, and then an investigation into the moisture absorption behavior of the system is provided.

5.3 Neat BMI Resin Testing

The results of the tensile, flexure, and DSC tests are provided in Figure 5-1. It can be seen that there is a distinct relationship between T_g and the cure time and temperature as expected. It is also apparent that the ultimate T_g for this system is slightly over 350°C.

The results of these studies have been interpreted in terms of the changes brought about by longer cures at the same temperature, and increased cure temperatures. A summary of the findings is in Table 5-2.

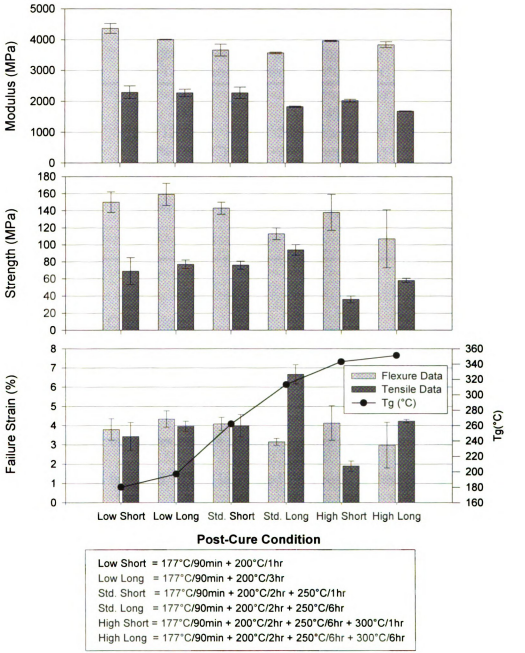

Figure 5-1 Flexure, Tensile, and Tg Data for BMI Resin with Various Post-Cure

Table 5-2 Summary of Resin Testing Results

	Longer Cures at Same Temperature	Increasing Temp from 200°C-250°C	Increasing Temp from 250°C-300°C
Tensile Modulus	-20%	-20% (long cures)	mixed
Flexural Modulus	-8%	-14%	+9%
Tensile Strength	+12-61%	-29% (long cures)	-38-62%
Flexural Strength	-21% (250°C)	-29% (long cures)	~0
Tensile Failure Strain	+15-120%	+80% (long cures)	-36-72%
Flexural Failure Strain	-23% (250°C)	-23% (long cures)	~0

5.3.1 Resin Testing Conclusions

Generally, low temperature post-cured specimens show the best combination of properties. A reduction in most properties is seen as the post-cure temperature is increased, and longer exposures at each temperature seem to decrease the modulus while the effect on strength is mixed. Thus, low cured BMI resin is desired due to it's superior properties, but continued cure during component use is likely, and will cause a change in the material's properties. This change must be understood and minimized, so that proper design criteria can be utilized.

5.4 Moisture Diffusion Study

A major objective of this research has been to understand the effect of moisture on the properties of the BMI and K3B composites. To effectively utilize the information

obtained from the physical property testing, the moisture absorption behavior of these systems must be understood. To this end, moisture absorption studies were performed to determine the ultimate moisture content and diffusion coefficients for BMI and K3B resins and their composites. The effect of extent of resin cure, fiber presence, and microcracking was determined for the BMI/IM7 system. Two temperatures were used so that the diffusivity constants, D_0 and Q, can be calculated allowing knowledge of the actual diffusivity, D. The results of these experiments are provided in Table 5-3 and discussions follow.

Table 5-3 Summary Data for Moisture Absorption Study

Condition	Maximum Moisture % 70°C	Maximum Moisture % 100°C	% Change 70°C-100°C	Diffusivity (mm^2/sec) 70C	Diffusivity (mm^2/sec) 100C	Q (J/molK)	D_0 (mm^2/sec)
BMI Resin Partial Cure	3.31%	3.78%	12.61%	2.369E-08	9.014E-08	47380	3.893E-01
BMI Resin Full Cure	5.14%	5.00%	-2.70%	5.196E-08	1.166E-07	28658	1.203E-03
BMI X-ply	1.55%	1.57%	1.34%	1.879E-06	1.222E-06	-15255	8.927E-09
BMI Unidirectional	2.49%	2.32%	-7.09%	3.206E-08	4.258E-08	10060	1.092E-06
K3B Resin	1.53%	1.62%	5.02%	9.998E-07	2.322E-06	29876	3.547E-02
K3B-IM7 X-ply	0.55%	0.54%	-1.86%	3.383E-08	9.427E-08	36336	1.156E-02
100% Resin Equivalent for Composite Data							
K3B-IM7 X-ply VfCor	1.08%	1.06%	-1.86%				
BMI X-ply VfCor	4.21%	4.27%	1.34%				
BMI Unidirectional	5.10%	4.96%	-2.72%				

5.4.1 The Effect of the Extent of Cure on *D* and M_∞ for BMI Resin

BMI resin with a full cure showed an increase in ultimate moisture content, M_∞, by an average of 44% over the partially cured resin. Unfortunately, there was a significant difference between the partially cured values for the two experiments. It is unlikely that this was caused by an increase in cure of the resin, because the exposure at 100°C is fully

100°C below the post-cure temperature for the partially cured system. An interaction due to both the temperature and water is also unlikely as this would have been evident in the thermal spike data shown in Chapter 6.

The increase in cure also caused a very significant increase in the moisture diffusivity. For the 70°C experiment, the diffusivity increased by 119%, while the 100°C experiment showed an increase of only 29%. Despite the anomaly in the data, it is obvious that resin with a higher extent of cure will absorb moisture faster and to a higher ultimate content.

5.4.2 The Effect of Microcracking on the Diffusivity of BMI Composites

By comparing the cross-ply and unidirectional specimens, it is easily seen that the presence of microcracks increases the moisture diffusivity by over 50x (5700%). This is expected because the microcracks allow the moisture access to a tremendously larger surface area, thus requiring the moisture to diffuse over a much smaller distance to achieve saturation.

It should be noted that the diffusivity calculated here is not a valid material property, even for the microcracked composite. The model used here assumes two dimensional Fickian diffusion with negligible diffusion through the exposed edges (due to their smaller surface area). It is obvious that this is not the case for these materials because the microcracking is most prevalent in the central plies, and thus the increased diffusion is through the microcracks in the edges.

5.4.3 Effect of Microcracks on the Ultimate Moisture Content of BMI Composites

The ultimate moisture content, M_{∞}, of the resin in microcracked composite specimens is an average of 16% lower than that of the fully cured neat resin. This difference is believed to be due to the incredible speed with which moisture can diffuse into and out of this specimen. It is known that this specimen lost weight during the measurement process despite efforts to avoid this.

Another contributing factor may be that this composite panel was created with the "old" batch of resin which has been shown to have a lower reaction rate. Thus this may be less cured resin which should show a lower M_{∞}.

5.4.4 Effect of Fibers on the Ultimate Moisture Content of BMI Resin

The ultimate moisture content of the resin in the unidirectional composite specimens matches the M_{∞} of the fully cured resin to within 2% error. This suggests that the resin in the composite has a similar morphology to that of the neat resin. Thus, there is no evidence of a difference in the resin cure due to the presence of the fibers.

5.4.5 Microcrack Formation in Composite Specimens During Saturation

Careful examination of the absorption profiles of the unidirectional BMI/IM7 and cross-ply K3B/IM7 specimens shows a shift in the diffusivity and apparent ultimate content after 225 hours of exposure as seen in Figure 5-2 for a unidirectional BMI/IM7 sample.

Failure analysis of the saturated specimens in the ESEM at magnifications of up to 2000x after polishing did not showed the presence of microcracks in either the K3B/IM7 or the unidirectional BMI/IM7, but a recent study of the K3B/IM7 system has shown that ply-level microcracking is observed after approximately 400 hours of immersion at 80° [37]. This suggests that microcracking of these specimens may have initiated, but that the width of the microcracks was still extremely small due to the short duration of the test.

Zhou and Lucas [39, 40] have seen a similar crack formation in a T300/934 graphite/epoxy system after 4300 hours in water at temperatures of 75°C and 90°C. Crack initiation was detected in the absorption curve as early as 800 hours which is essentially at the end of the Fickian region.

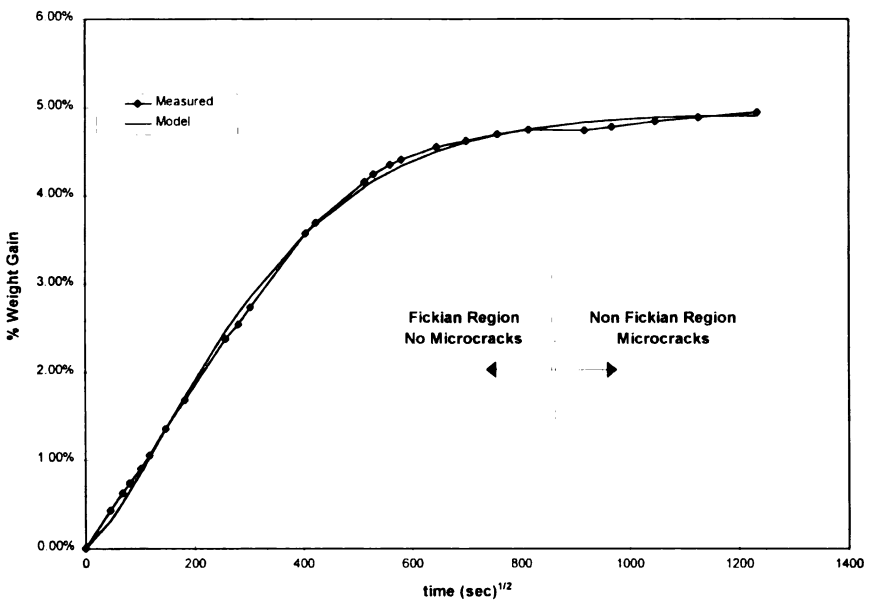

Figure 5-2 Absorption Curve for Unidirectional BMI/IM7 Showing a Good Fit to the Fickian Model, and Non-Fickian Behavior Due to Microcrack Formation

5.4.6 K3B Resin and Composite Data

As previously mentioned, the resin used in these studies was fabricated using a significantly different processing cycle than the composites received, and thus is very likely to have significantly different properties. The diffusivity and ultimate moisture content of the resin and composite are obviously different, and this is undoubtedly due largely to the difference in their manufacture. It is possible, however, that there are other factors contributing to the differences, such as a steric interaction between the fiber and the polymerizing resin. These factors cannot be ruled out from this experiment, but it is felt that they are unlikely.

5.5 Interfacial Adhesion Testing

Interfacial testing of adhesion (ITS) of BMI/IM7 composites was performed to determine the change in adhesion levels due to moisture saturation, extent of cure, and fiber volume fraction. The IFSS results are shown in Figure 5-3.

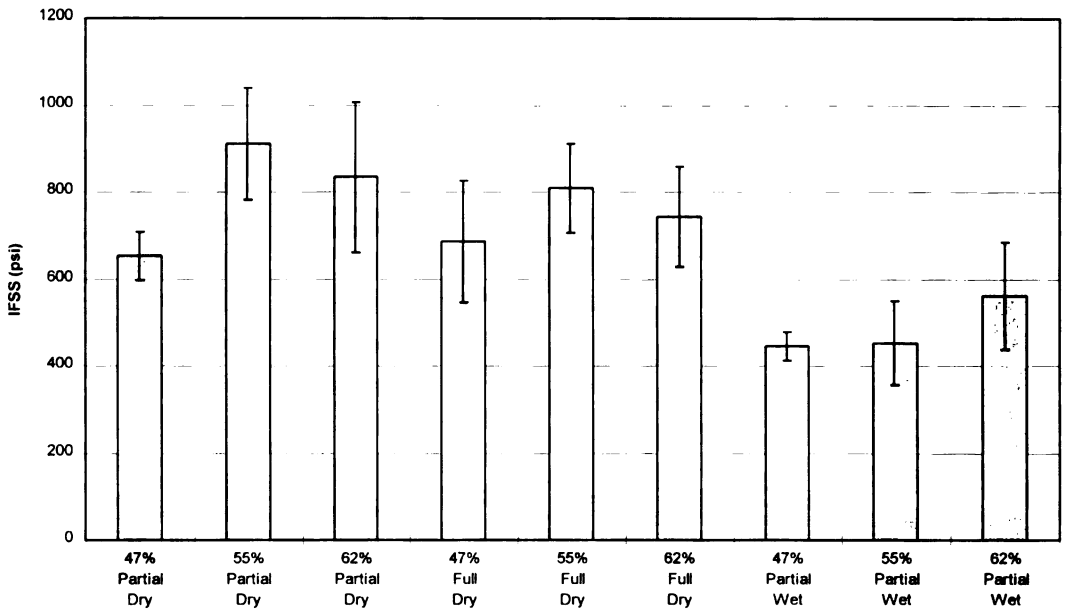

Figure 5-3 Hygrothermal IFSS Results

The failure loads for this system were generally between 0.2 and 0.6 grams. Failure loads this low are approaching the limit of accurate testing with this machine, and have undoubtedly caused an increase in the scatter seen here. Despite this, a number of things are apparent. First and foremost is the fact that the adhesion in this system is very low. IFSS values for a carbon/epoxy system are generally on the order of 10,000 psi while the results here are less than 1,000 psi.

There appears to be little variation due to fiber volume fraction, as would be expected because the testing here is performed by choosing fibers within a specific local volume fraction range. No change is apparent due to the increase in cure from partial to full.

Saturation with moisture appears to reduce the IFSS. The magnitude of this effect is rather uncertain considering the low adhesion of the system in general, and the difficulties in the test method. The reduction in IFSS due to moisture is supported by the fact that the fully cured specimens were debonded after saturation without the addition of any load. A fiber from a saturated, fully cured specimen showing this debonding is shown in Figure 5-4.

5.6 Mechanical Test Results and Discussion

All of the testing was performed to determine the effect which advancing cure, moisture, and fiber content have on the physical properties of the BMI/IM7 system. All tests provided a measure of the modulus of the system, and some provided failure strengths and strains. Because we are interested in these properties of the system regardless of the test method, all mechanical test methods will be examined together. The dynamic mechanical tests will be discussed separately due to the functionally different nature of their result. As mentioned at the beginning of the chapter, the testing was designed using a statistical design so that interaction effects could be studied. To ensure clarity in this presentation of results, the statistical design is first reviewed with a sample set of calculations, and the method utilized for data presentation is provided, but first the complete set of data is plotted without manipulation in Figure 5-5.

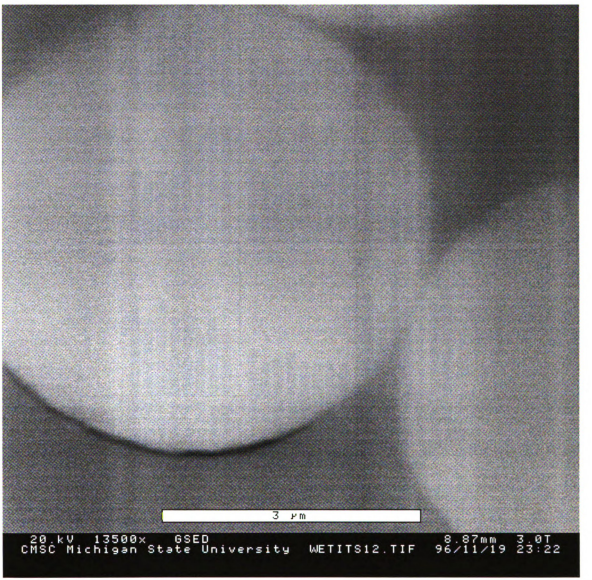

Figure 5-4 A Fully Cured and Saturated Specimen Showing Fiber Debonding Without Applied Load

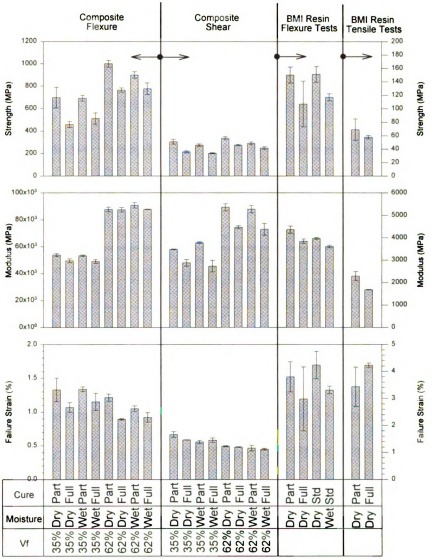

Figure 5-5 Plot of All Hygrothermally Conditioned Mechanical Test Data

5.6.1 Review of the Experimental Design

This testing was performed using a 2^3 factorial design with extent of cure, moisture, and volume fraction as the factors. This was a two level design, so "low" and "high" levels of each factor were chosen. These levels are presented in Table 5-4.

Table 5-4 Factor Levels Used in Hygrothermal Testing

	Factor Level	
Factor	Low	High
Extent of Cure	Partially Cured 177°C/90 min; 200°C/2 hr	Fully Cured 177°C/90 min; 200°C/2 hr; 280°C/10 hr
Moisture	Dry	Wet
Volume Fraction	35% or 47%	62%

An easy way of viewing this type of statistical design is to consider that each factor represents one side of a cube as depicted in Figure 5-6. Viewing the data in this manner makes it easy to see that there are four sets of data which provide a measure of the effect of the extent of cure. This change is represented by the change in response from the left side of the cube to the right side. Since interaction effects are present in this analysis, the data for each change is provided instead of presenting just the average change from face to face.

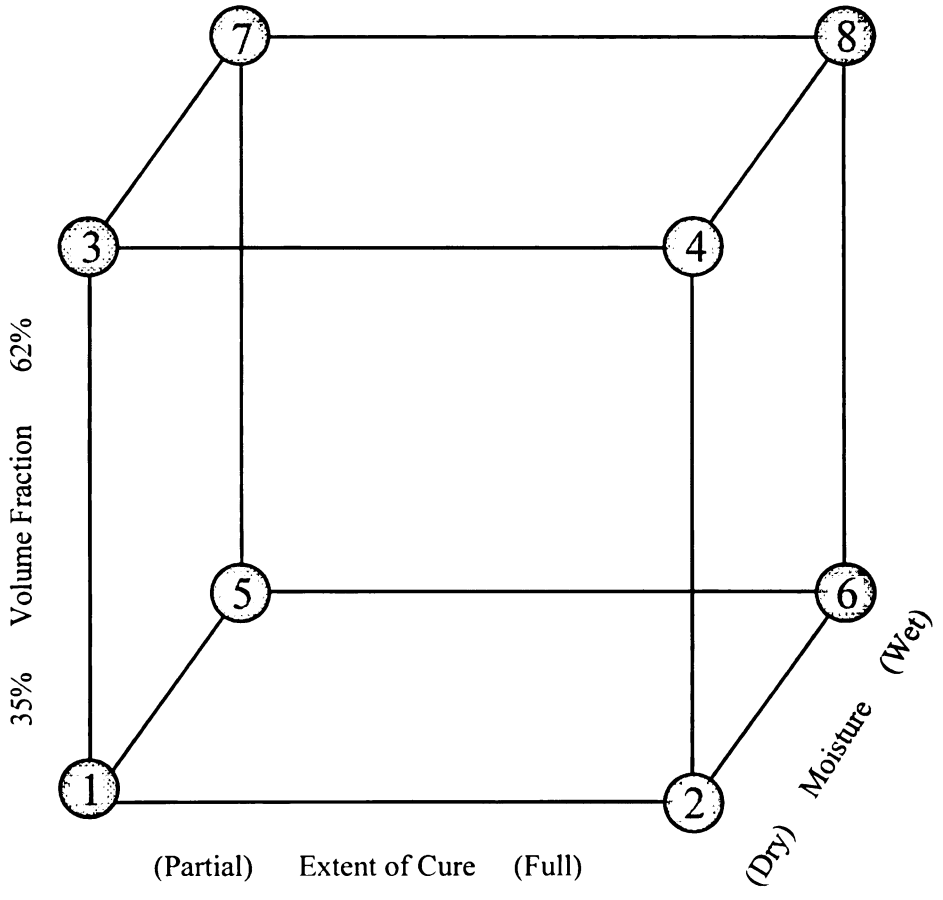

Figure 5-6 A Cubic Representation of the Experimental Design

From the original data, the percentage change in response for each edge (like condition 1 to condition 2 on the cube) was calculated as the difference in the two values divided by the overall average of all of the data (the grand mean). In this testing, each condition (corner of the cube) is represented by between 3 and 5 tests. Thus, each condition has a standard deviation of it's own. A derivation of the proper standard deviation for the percent changes is provided in Appendix C. These standard deviations represent the

actual deviation in the percent change value, not just the average of the standard deviation of the two conditions.

All data has been analyzed in this manner, and will be presented in terms of the change in physical properties caused by the change in each factor. The transient DMA test is the only test which provides the T_g of the system, and thus is the only test present in the discussion of the thermal response to each factor. Interaction effects will be discussed whenever they are present.

5.6.2 Sample Results Calculation

An example of the calculations use to generate the plots found in the following sections is provided here. The calculations for the percent change in flexural strength which results from increasing the cure from partial (177°C/90min + 200°C/2hr) to full (177°C/90min + 200°C/2hr + 280°C/10hr) are reviewed. All other calculations were performed in a similar manner.

First, the original data from Tables 3-9 and 3-10 is plotted on the eight corners of the cube as seen in Figure 5-7. The overall (grand) average is 726 for this case. Using this, the change in strength as the cure increases is calculated for each combination of volume fraction and moisture. These calculations are shown in Equation 5-1. Finally, the results for all related testing are plotted in one figure allowing quick, easy visualization of the meaning of the test results. These results are plotted in Figure 5-8 and it is easily seen

that all test methods show a reduction in strength due to an increase from partial to full cure (because all 'percent change' values are negative).

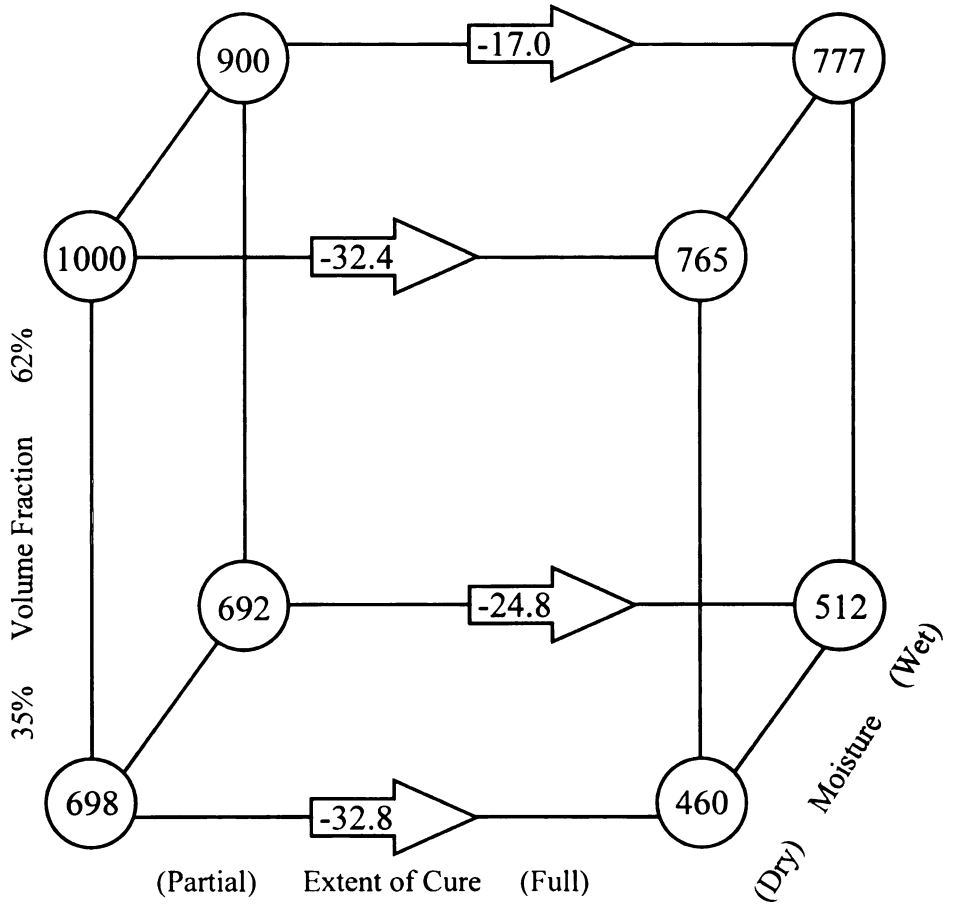

Figure 5-7 Graphic Representing the Change in Flexural Strength Due to Cure

$$Dry, LowVf = \left(\frac{460-698}{726}\right)100 = -32.8$$

$$Dry, HighVf = \left(\frac{765-1000}{726}\right)100 = -32.4$$

$$Wet, LowVf = \left(\frac{512-692}{726}\right)100 = -27.6$$

$$Wet, LowVf = \left(\frac{777-900}{726}\right)100 = -17.0$$

Eqn. 5-1

5.6.3 Mechanical Testing Results

Both flexure and Iosipescu shear tests were performed on composite specimens for all conditions. Flexure testing on resin specimens was performed to show the effect of cure and moisture. Tensile tests of resin specimens with varied cures were performed to show the effect of cure as discussed in Chapter 2 and will be used here as well to support these results.

5.6.3.1 The Effect of Cure on BMI/IM7 Properties

The results of the physical testing in terms of the change from partial cure to full cure is presented in Figure 5-8. Increasing cure can be seen to decrease the modulus of both the resin and composite samples by between 5 and 30% with the flexure properties being the least sensitive. Their is an interaction effect in the flexure data which shows that the lower volume fraction composites show the effect of cure more than the high volume fraction composites.

The fully cured resin shows a lower strength for all tests by between 15 and 35%. As with the flexure modulus response, the Iosipescu shear strength changes more for the low volume fraction specimens than the high volume fraction specimens. The flexure response in terms of volume fraction is clouded by an effect from the moisture. For both the flexure and Iosipescu shear tests, the strength of the dry specimens is reduced by a larger amount than the wet specimens. It will become apparent that this is due to a reduction in the partially cured wet specimens strength due to the moisture.

Finally, the failure strain data is quite scattered, but the flexure specimens show a loss of approximately 15% while the Iosipescu shear specimens are generally unaffected. The tensile and flexure resin tests show rather large changes in the failure strain, but also have very large scatter, so the meaning of the data is uncertain. More information concerning the effect of cure on the resin's response is available in Chapter 2. The interactions seen for the failure strain are basically the same as those seen for the strength.

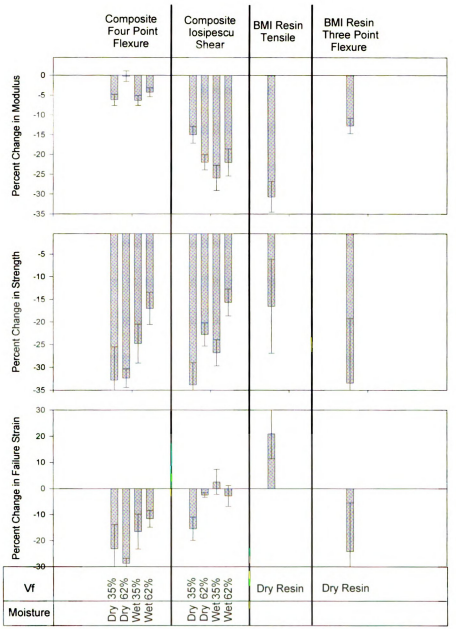

Plots showing the percent change in strength, modulus, and failure strain values of BMI resin and composites as the cure varies from a partially cured to a fully cured condition.

Part Cure = 177°C/90min + 200°C/2hr
Full Cure = 177°C/90min + 200°C/2hr + 280°C/10hr

Figure 5-8 The Effect of Increased Cure on the Physical Properties of BMI/IM7

5.6.3.2 The Effect of Moisture on BMI/IM7 Properties

The results of the physical testing in terms of the change from partial cure to full cure is presented in Figure 5-9. The resin flexure data shows a loss in modulus of almost 10%, but the composite data is quite insensitive to the presence of moisture. The high volume fraction flexure and low volume fraction shear specimens even show an increase in modulus of approximately 5%. The fact that the resin modulus falls while the composite's modulus is either insensitive to moisture, or shows a slight increase suggests that another mechanism is active in the composites. It is likely that the swelling of the resin due to moisture presence has caused an increase in modulus which completely counters the loss in resin modulus. The resin strength shows a drop of approximately 25% with the addition of moisture. The flexure strength was generally insensitive to the presence of moisture with the exception of the partially cured high volume fraction specimens which showed a decrease of approximately 10%, as did the Iosipescu shear specimens in general.

There were a few actual interaction effects present in the Iosipescu shear strength data. The high volume fraction specimens were more affected by moisture than the low volume fraction specimens, and the partially cured specimens were more affected than the fully cured specimens. The resin specimens showed a 25% loss in failure strain while the flexure data was generally insensitive, and the Iosipescu shear specimens showed only a slight loss.

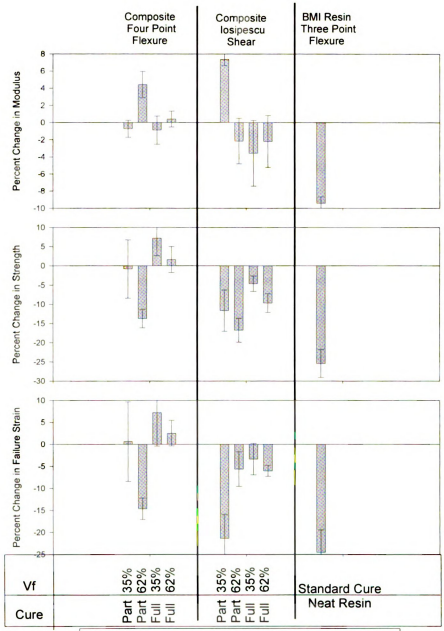

Plots showing the percent change in strength, modulus, and failure strain values of BMI composites associated with a change from dry to moisture saturated specimens.

Part Cure = 177°C/90min + 200°C/2hr
Full Cure = 177°C/90min + 200°C/2hr + 280°C/10hr
Standard Cure = 177°C/90min + 200°C/2hr + 250°C/6hr

Figure 5-9 The Effect of Moisture Presence on the Physical Properties of BMI/IM7

5.6.3.3 The Effect of Volume Fraction on BMI/IM7 Properties

The results of the physical testing in terms of the change from low to high volume fractions is presented in Figure 5-10.

Increasing the fiber content of composites is known to have a very strong affect on the mechanical properties of the system. The results seen here are no different. The modulus values are increased by between 40 and 50%. The strength values increase by 10 to 30%, and the failure strain shows a decrease on the order of 15%. One interaction effect is apparent in these results. The fully cured Iosipescu shear specimens appear to show a greater increase in strength than the partially cured specimens when the volume fraction is increased.

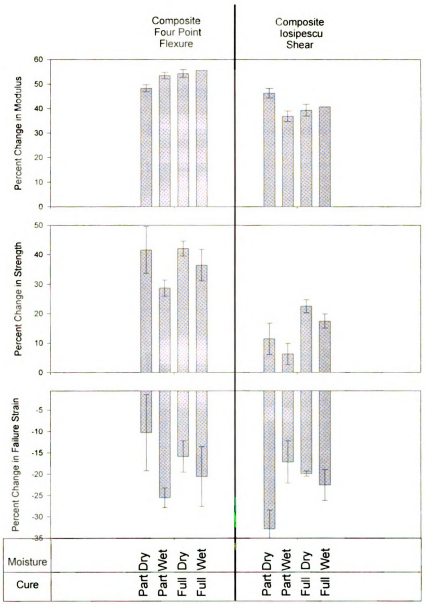

Figure 5-10 The Effect of Increased Volume Fraction on the Properties of BMI/IM7

5.6.4 Dynamic Mechanical Testing Results

Dynamic mechanical tests were performed to show the system's rheological response to the factors. In addition to the information about the rheological response of the system, T_g has been determined. The results of the dynamic mechanical testing is shown in standard form in Figure 5-11.

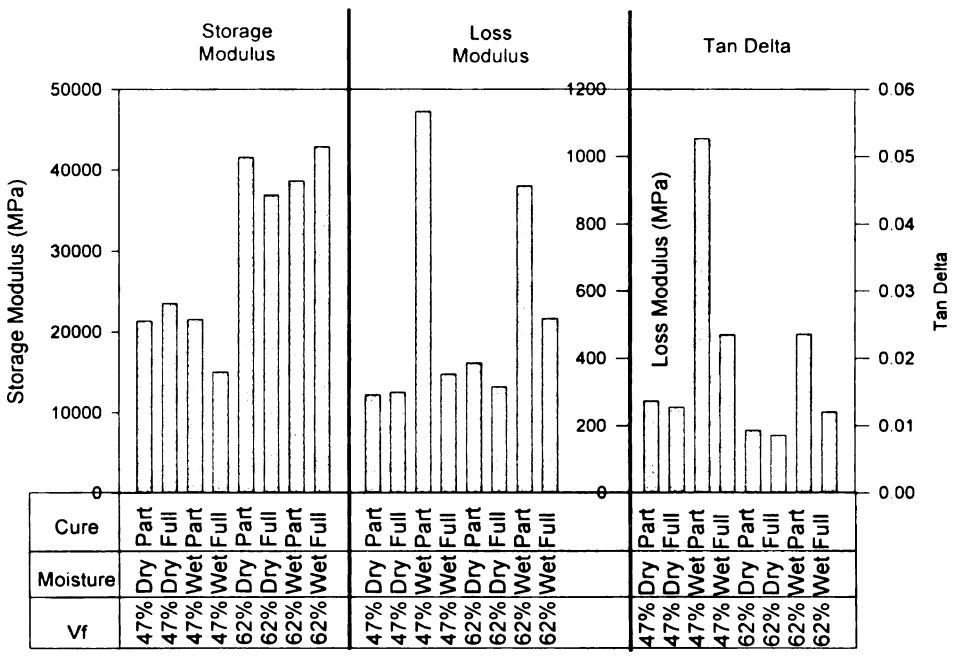

Figure 5-11 Hygrothermal DMA Test Results

5.6.4.1 The Effect of Cure on BMI/IM7 Rheological Properties

The results of the dynamic mechanical testing in terms of the change from partial cure to full cure is presented in Figure 5-12.

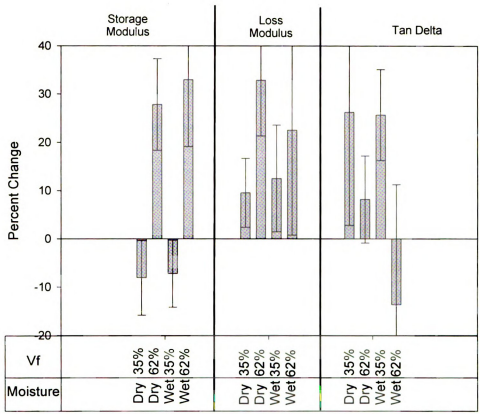

Figure 5-12 The Effect of Increased Cure on the Rheological Properties of BMI/IM7

The isothermal DMA test results show an increase in both the storage and loss moduli. The value of tan delta which is the ratio of the loss modulus to the storage modulus (E"/E') shows a slight increase with increased cure. This suggests that the damping

characteristics of the fully cured resin may be slightly higher than that of the partially cured resin.

The effect of increased cure on the T_g of this system as measured by transient DMA testing is shown in Figure 5-13. As would be expected, increased cure causes a significant increase in the T_g of the system.

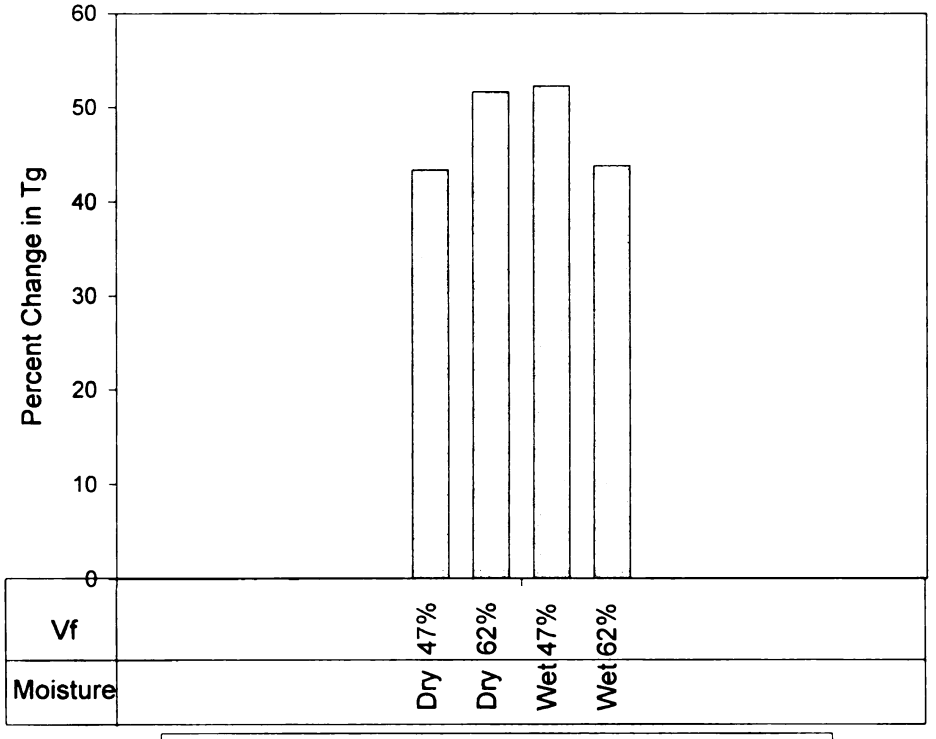

Figure 5-13 The Effect of Increased Cure on the T_g of BMI/IM7

5.6.4.2 The Effect of Moisture on BMI/IM7 Properties

The results of the physical testing in terms of the change from partial cure to full cure is presented in Figure 5-14.

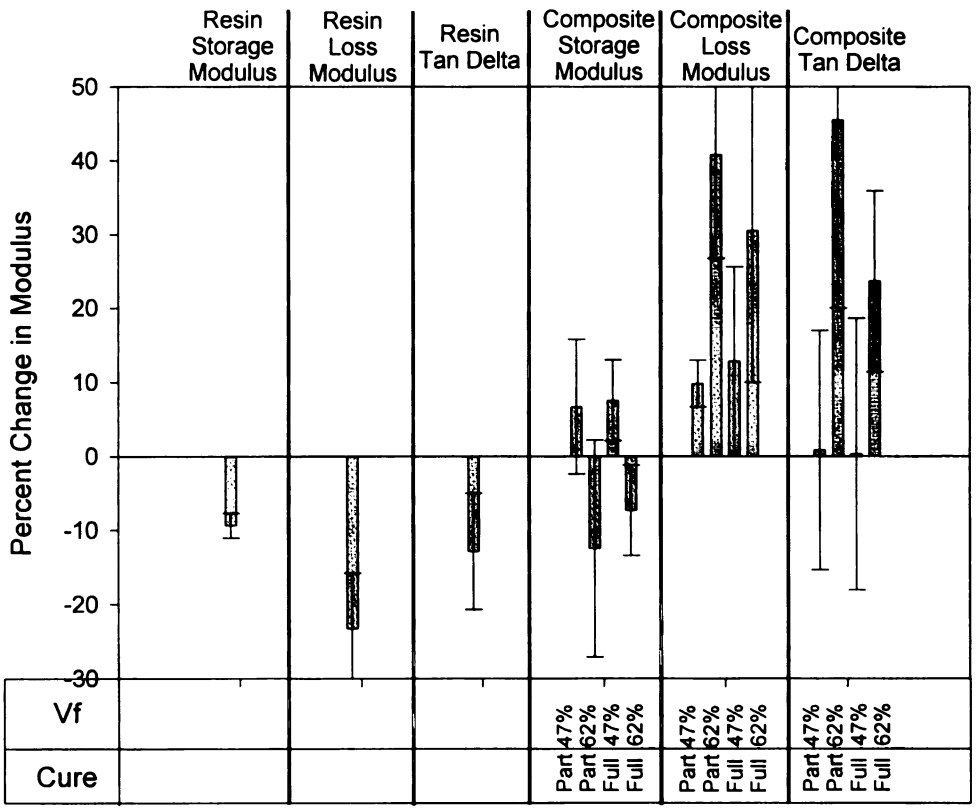

Plots showing the percent change in the rheological properties of BMI composites associated with an increase in moisture content from dry to wet.

Part Cure = 177°C/90min + 200°C/2hr
Full Cure = 177°C/90min + 200°C/2hr + 280°C/10hr

Figure 5-14 The Effect of Moisture Presence on the Rheological Properties of BMI Resin and Composites

The resin specimens show a decrease in both the storage and loss moduli as well as the value of tan delta with increased moisture content. This suggests that the resin becomes less viscous and more elastic in nature and would have lower damping capability. The composite data shows little change in the modulus values for the low volume fraction specimens. The high volume fraction specimens, however, show some decrease in the storage modulus and some increase in the loss modulus. These changes cause the tan delta values to rise suggesting that the composite system is becoming more viscous in nature with the addition of moisture.

The fact that the high fiber content specimens show this change more than the low fiber content specimens, and the resin specimens actually show the opposite effect suggests that the increase in the damping characteristic (viscous nature) of the composite is caused by an interaction between the fibers and resin. This is likely to be due to a change in the adhesion level as has been seen with the ITS tests.

The effect of moisture presence on the T_g of this system as measured by transient DMA testing is shown in Figure 5-15. There is an interaction effect present here between the moisture and extent of cure, and mentioned previously. The partially cured system is subject to changes in T_g due to the presence of moisture, while the fully cured system appears insensitive to the presence of moisture.

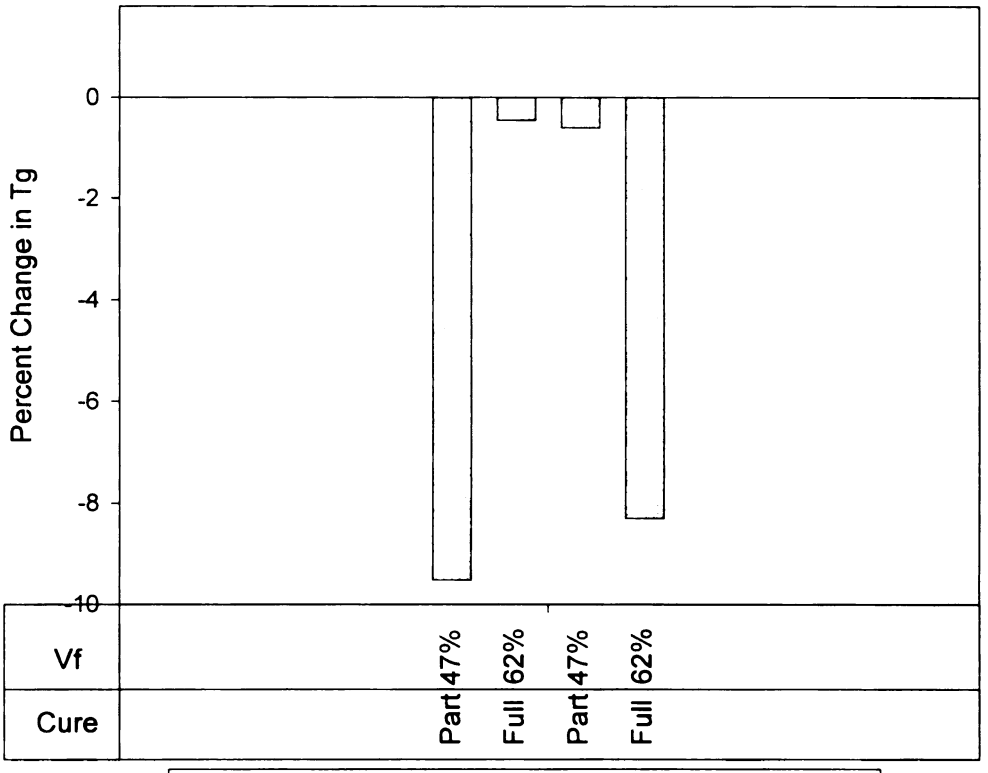

Plot showing the percent change in the glass transition temperature of BMI composites associated with an increase in moisture content from dry to wet.

Part Cure = 177°C/90min + 200°C/2hr
Full Cure = 177°C/90min + 200°C/2hr + 280°C/10hr

Figure 5-15 The Effect of Moisture Presence on the T_g of BMI/IM7

5.6.4.3 The Effect of Volume Fraction on BMI/IM7 Properties

The results of the physical testing in terms of the change from low to high volume fractions is presented in Figure 5-10.

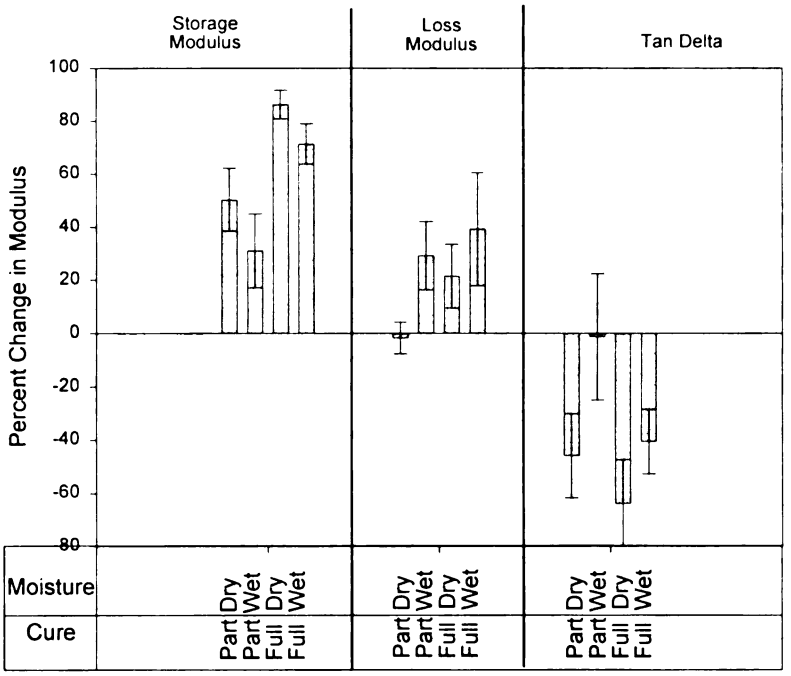

Plots showing the percent change in the rheological properties of BMI composites associated with an increase in volume fraction from 47% to 62%.

Part Cure = 177°C/90min + 200°C/2hr
Full Cure = 177°C/90min + 200°C/2hr + 280°C/10hr

Figure 5-16 The Effect of Increased Volume Fraction on the Rheological Properties of BMI/IM7 Composites

Increasing the volume fraction of BMI/IM7 composites produces an increase in both the storage and loss moduli. This is manifested in a loss in the value of tan delta and suggests that the presence of more fibers makes the specimen more elastic in nature as would be expected.

The effect of increased volume fraction on the T_g of this system as measured by transient DMA testing is shown in Figure 5-17. No specific trends can be seen in terms of interaction effects. A general increase in the value of T_g is seen here, but is believed to be due to an experimental effect. The lower fiber content specimens will lag the actual test temperature by a larger amount than the higher content specimens because of their lower thermal conductivity. Thus, the effect is believed to be an artifact of the test method.

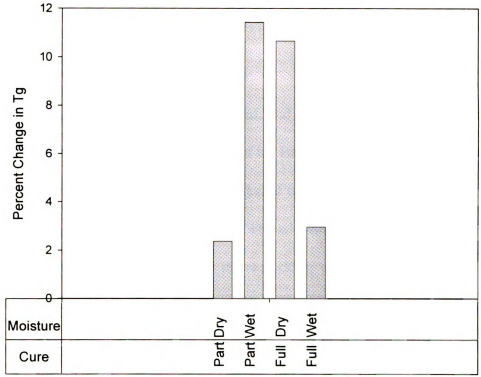

Plot showing the percent change in the glass transition temperature of BMI composites associated with an increase in volume fraction from 47% to 62%.

Part Cure = 177°C/90min + 200°C/2hr
Full Cure = 177°C/90min + 200°C/2hr + 280°C/10hr

Figure 5-17 The Effect of Increased Volume Fraction on the T_g of BMI/IM7

5.7 Hygrothermal Conclusions

The hygrothermal response of the BMI resin and BMI/IM7 composite systems have been characterized using a wide variety of tests. A number of general conclusions can be drawn in terms of the effect of extent of cure, moisture presence, and increased volume

fraction. They are presented here organized in terms of these factors after a summary of the conclusions from the moisture absorption study

5.7.1 Moisture Absorption Behavior

A moisture absorption study was performed, and the diffusivity and ultimate moisture content for both the resins and composites of the BMI and K3B systems were determined. It was found that for the BMI system, increased cure causes a higher ultimate moisture content as well as a higher diffusion rate. The addition of fibers to the BMI resin does not appear to affect the cure, but the microcracking caused by the cross-ply laminate caused a tremendous increase in the diffusion rate as expected. The diffusion was generally seen to be Fickian in nature, but a deviation from this was seen for the unidirectional BMI/IM7 and cross-ply K3B/IM7 composites after approximately 225 hours. This has been attributed to the formation of microcracks after this amount of exposure as has been seen by other researchers on this and similar systems.

5.7.2 The Effect of Increased Cure

Increasing the cure of BMI has been shown to decrease both the modulus and strength for both composite and resin specimens. Generally, the lower volume fraction specimens showed this effect more than the higher volume fraction specimens because of the increased contribution of the resin.

A detailed study of the progression of BMI resin properties with advancing cure was presented, and it was found that lower cure temperatures produce the best combination of properties, but with partially cured resins, cure will continue during service life, causing a reduction in part performance. Thus, this progression must be understood and accounted for when designing with this system.

Increased cure was seen to have little effect on adhesion as measured by the ITS test, but failure analysis of the failed flexure specimens showed the fully cured system to have lower adhesion. Finally, increasing the cure was seen to cause a very significant increase in Tg.

5.7.3 The Effect of Moisture Presence

Moisture has been shown to decrease the resin's modulus, but the composite's modulus is insensitive to moisture presence. It is suggested that this effect is most likely due to a resin swelling mechanism in the composites.

Moisture decreases the strength of resin specimens, and the composite specimens show a decrease as well, although the effect is much smaller. A general trend showing that moisture causes a larger decrease in the properties of the partially cured resin than the fully cured resin is seen. This suggests that the unreacted chain sites in the resin may interact with moisture causing a reduction in strength.

Both ITS and DMA testing have shown that the adhesion is decreased by the presence of moisture. Moisture has also been shown to decrease the Tg of the system as has been seen in many other systems.

5.7.4 The Effect of Increased Fiber Volume Fraction

Increasing the fiber content of these composites causes the expected increases in strength and modulus as well as the associated drop in failure strain. The use of low volume fraction specimens has proven very useful in differentiating the effects of resin property changes from the composite property changes.

No effect of volume fraction was seen on the ITS adhesion values and increased fiber content was shown via DMA testing to cause the composite materials to become more elastic in nature. An apparent change in the Tg due to changing volume fraction has been attributed to an artifact of the experimental method.

Chapter 6

THERMAL SPIKE RESPONSE OF BMI AND K3B RESINS AND COMPOSITES

6.1 Introduction

Thermal excursions were known to increase the equilibrium moisture content of many resin systems as early as the mid 1970s [41]. This has been attributed to a variety of causes ranging from chemical changes in the resin to physical damage. Recently, there has been interest in the effect of more rapid temperature changes because high temperature composite systems are being used for components which see a larger range of temperatures, and are subjected to very rapid excursions between the temperature extremes. The BMI and K3B resin systems are used for aerospace applications where components are often moist due to outdoor storage and then called upon to reach the extremes of their design envelope within extremely small time periods. Previous work on the BMI/IM7 system has shown only a small effect when specimens are cycled [42].

6.2 Experimental Summaries

6.2.1 Test Design

The objectives of this study were to identify any permanent damage due to moisture exposure and thermal cycling. The properties of interest were modulus, strength, failure strain, and retention of composite toughness. The test scheme used to study these is shown in Table 6-1.

Table 6-1 Thermal Spike Testing Scheme

Test Performed	Materials Studied	Properties Reported
Tensile	BMI Resin	Modulus, Strength, Failure Strain
Flexure	BMI Resin (Three Point)	Flexure Modulus
	BMI/IM7 (Four Point)	Flexure Strength
	K3B/IM7 (Four Point)	Flexure Failure Strain
Open Hole Compression	BMI/IM7	Initial Stiffness
	K3B/IM7	Strength
Iosipescu Shear	BMI/IM7	Shear Modulus
	K3B/IM7	Shear Strength
		Shear Failure Strain
Dynamic Mechanical	BMI Resin	155°C Storage Modulus
	K3B Resin	155°C Loss Modulus
	BMI/IM7	155°C Tan Delta
	K3B/IM7	Tg

This testing was organized with a 2^2 factorial design to show both the main effects of moisture exposure and thermal spikes, as well as their interaction effects. The test procedures, including data reduction and results, are presented in Chapter 3. A discussion of these results including the main and interaction effects is presented in Section 6.3.

These sections will focus on the properties of interest, encompassing the data from all pertinent tests.

6.2.1.1 Post-Conditioning Observations

To determine the effect of the thermal spikes on the morphology of the specimens, the ESEM was utilized to analyze the specimens after conditioning. After thermal spiking, the wet K3B composites were visually blistered to the point that the thickness had doubled. The BMI specimens showed no effect due to the thermal cycling. Figure 6-1 shows the blisters present in a moist, thermally spikes K3B resin specimen. The specimen was approximately 1 cm^3 and has been sectioned in half for analysis. Note that no blisters occur near the edges where moisture is able to escape during the early stages of the exposure. Figure 6-2 provides a higher magnification showing the general morphology of the blisters in the resin specimen.

Figure 6-3 shows a blister in the K3B/IM7 composite. Figure 6-4 shows the viscous nature of the failure in this specimen which suggests that the failure occurred above the resin's T_g. This suggests that the T_g of wet K3B should be accurately determined and any applications in the presence of moisture should utilize a design which remains well below this value.

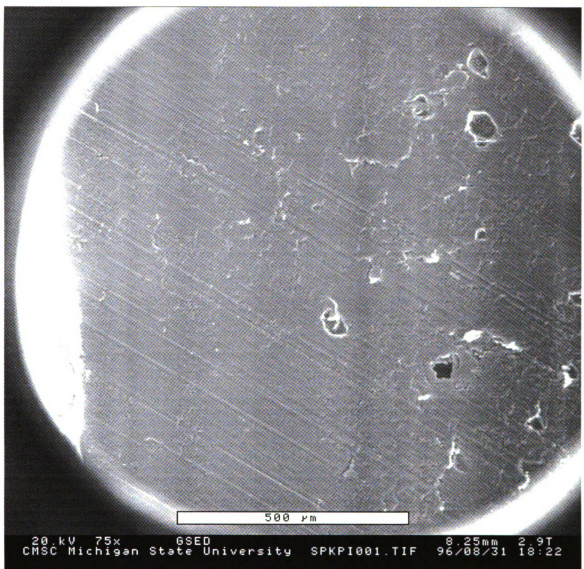

Figure 6-1 Thermally Spiked K3B Resin Showing Blistering

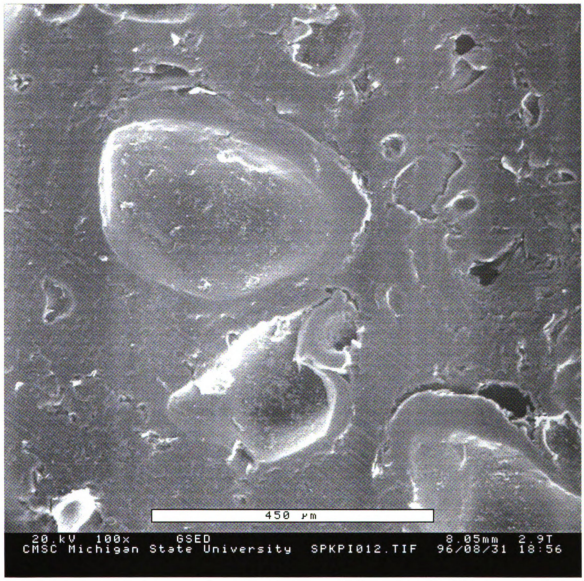

Figure 6-2 Close-up of a Blister in a Moist, Thermally Spiked K3B Resin Sample

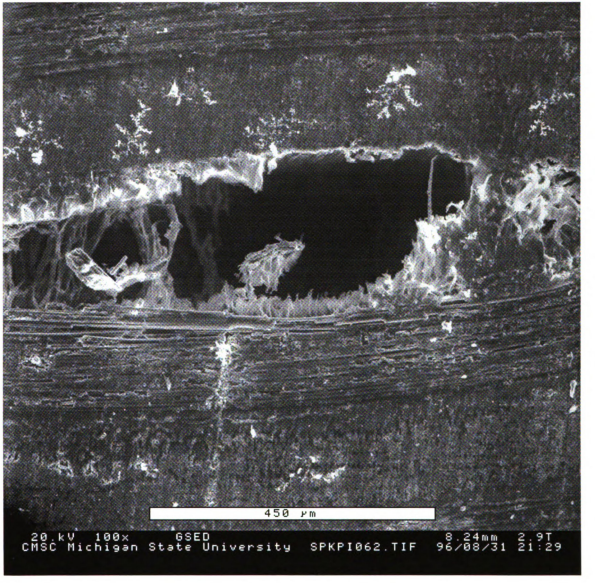

Figure 6-3 A Blister in a Moist, Thermally Spiked K3B/IM7 Composite

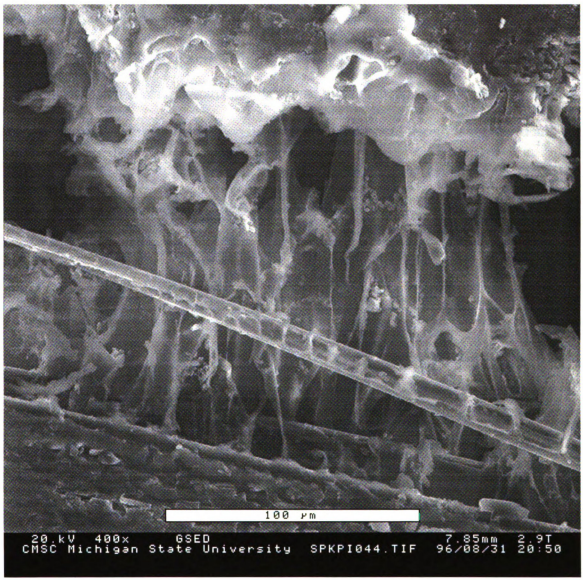

Figure 6-4 A Close-Up of a Moist, Thermally Spiked K3B/IM7 Composite Showing the Viscous Nature of the Failure

6.3 Combined Results and Discussion

All of the testing was performed to determine the effect moisture exposure and thermal spiking have on the physical and thermal properties of the BMI and K3B resin and composite systems. All tests provided a measure of the modulus of the system, and some provided failure strengths and strains. As mentioned at the beginning of the chapter, the testing was designed using a statistical design so that interaction effects could be studied. To ensure clarity in this presentation of results, the statistical design is reviewed and the method utilized for data presentation is provided, but first the complete set of data is plotted without manipulation in Figure 6-5 and 6-6.

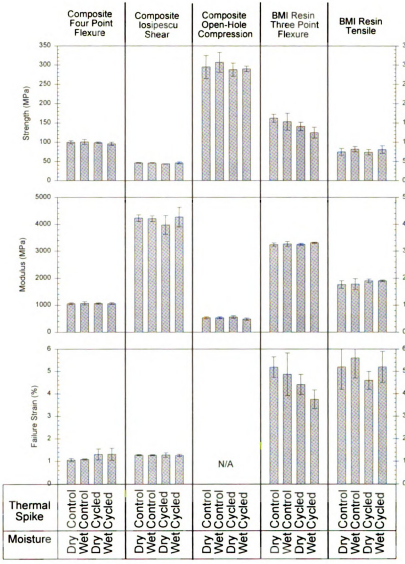

Figure 6-5 All Thermal Cycling Test Data for BMI/IM7 Composites

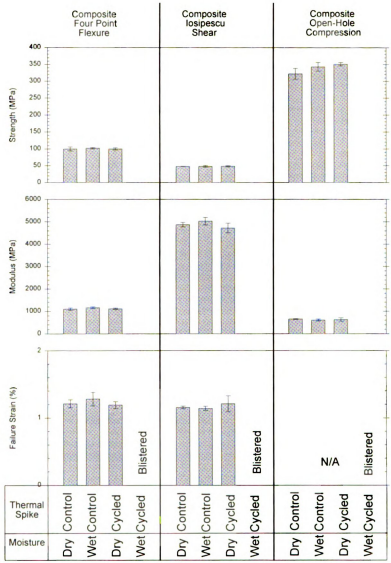

Figure 6-6 All Thermal Cycling Test Data for K3B/IM7 Composites

6.3.1 Review of Experimental Design

This testing was performed using a 2^2 factorial design with moisture exposure and thermal spiking as the factors. This was a two level design, so "low" and "high" levels of each factor were chosen. These levels are presented in Table 6-2.

Table 6-2 Factor Levels Used in Thermal Spike Testing

	Factor Level	
Factor	Low	High
Moisture Exposure	Dry	Wet
Thermal Spiking	Control	Cycled

An easy way of viewing this type of statistical design is to consider each factor to represent one side of a square as depicted in Figure 6-7. Viewing the data in this manner makes it easy to see that there are two sets of data which provide a measure of the effect of the thermal spiking. This change is represented by the change in response from the left side of the square to the right side.

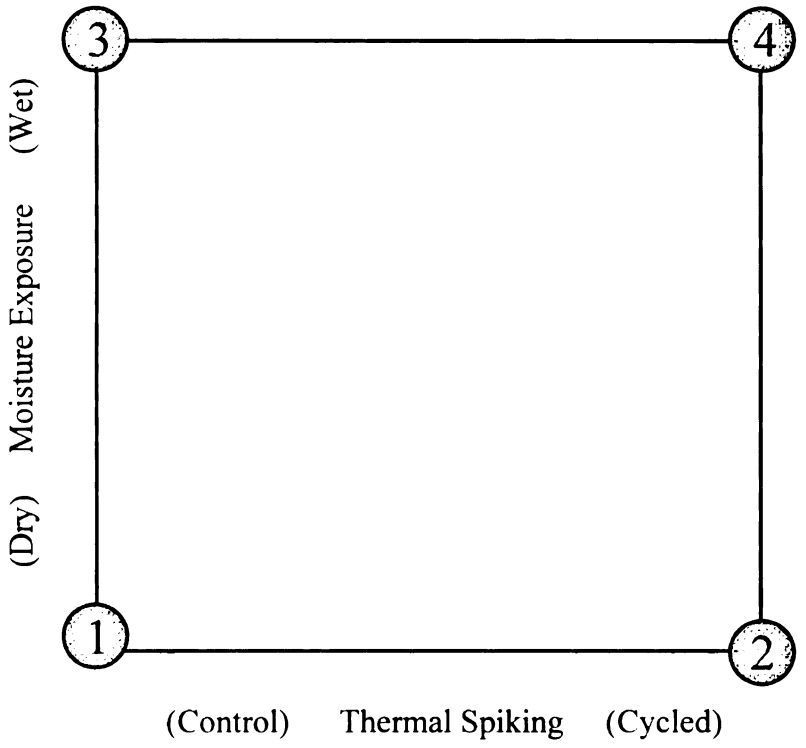

Figure 6-7 A Square Representation of the Experimental Design

From the original data, the percentage change in response for each edge (like condition 1 to condition 2 on the square) was calculated as the difference in the two values divided by the overall average of all of the data (the grand mean). In this testing, each condition (corner of the square) is represented by between three and five tests. Thus, each condition has a standard deviation of it's own. A derivation of the proper standard deviation for the percent changes is provided in Appendix C. These standard deviations represent the actual deviation in the percent change value, not just the average of the standard deviation of the two conditions.

All data has been analyzed in this manner, and will be presented in terms of the change in physical properties caused by the change in each factor. The transient DMA test is the

only test which provides the T_g of the system, and thus is the only test present in the discussion of the thermal response to each factor. Interaction effects will be discussed whenever they are present.

6.4 Effect of Moisture Exposure on Final Properties

It is very important to keep in mind that all testing was performed on dry specimens. The moisture saturated specimens were fully dried before testing, and thus any effects due to moisture are due to irreversible changes resulting from the exposure to moisture, not simply its presence.

The effect of saturating the specimens with moisture during the experimentation for BMI resin and composites is shown in Figure 6-8. A slight increase in the shear modulus and shear strength for the cycled specimens is seen and there are some effects evident in the resin tensile and flexure results. The change in properties in the flexure and tensile resin results show opposite trends and contain a high amount of scatter, so it is felt that there is little or no real effect here. There is also a loss in modulus of approximately 15% for the wet, cycled open-hole compression specimens. This result is discussed further in the thermal spiking section.

The T_g was measured using transient tests in the DMA, and the results are provided in Figure 6-9. No effects of trends of significance can be seen.

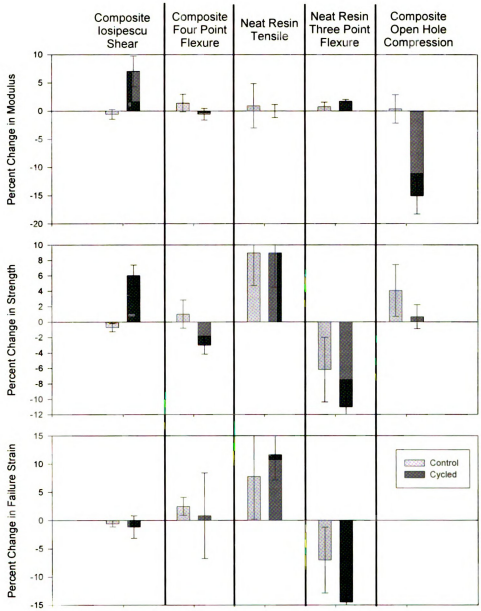

Plots showing the percent change in strength, modulus, and failure strain values of BMI resin and composites associated with the change from a control specimen to a moisture saturuated specimen.

Figure 6-8 The Effect of Exposure to Moisture on the Properties of BMI Resin and Composites

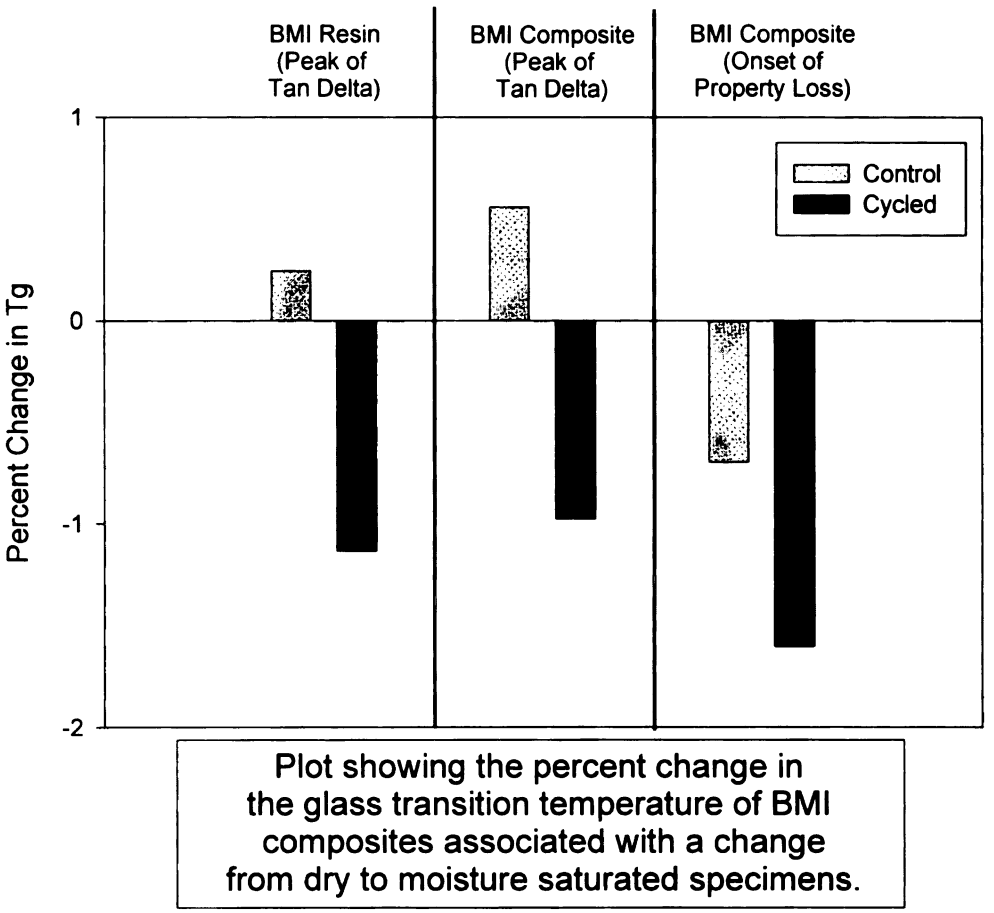

Figure 6-9 The Effect of Moisture Exposure on T_g for BMI Resin and Composites

The effect of saturating the specimens with moisture during the experimentation for K3B resin and composites is shown in Figure 6-10. No significant effects are seen for the control specimens, but the wet, cycled K3B specimens show a very large loss in properties. This is due to the blistering effect which has been discussed in Section 6.2.1.1. No effect on T_g was seen for either the resin or composites as shown in Figure 6-11.

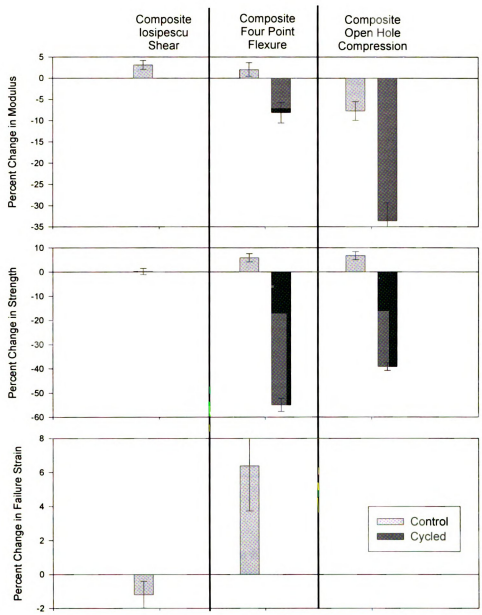

Figure 6-10 The Effect of Exposure to Moisture on the Properties of K3B Resin and Composites

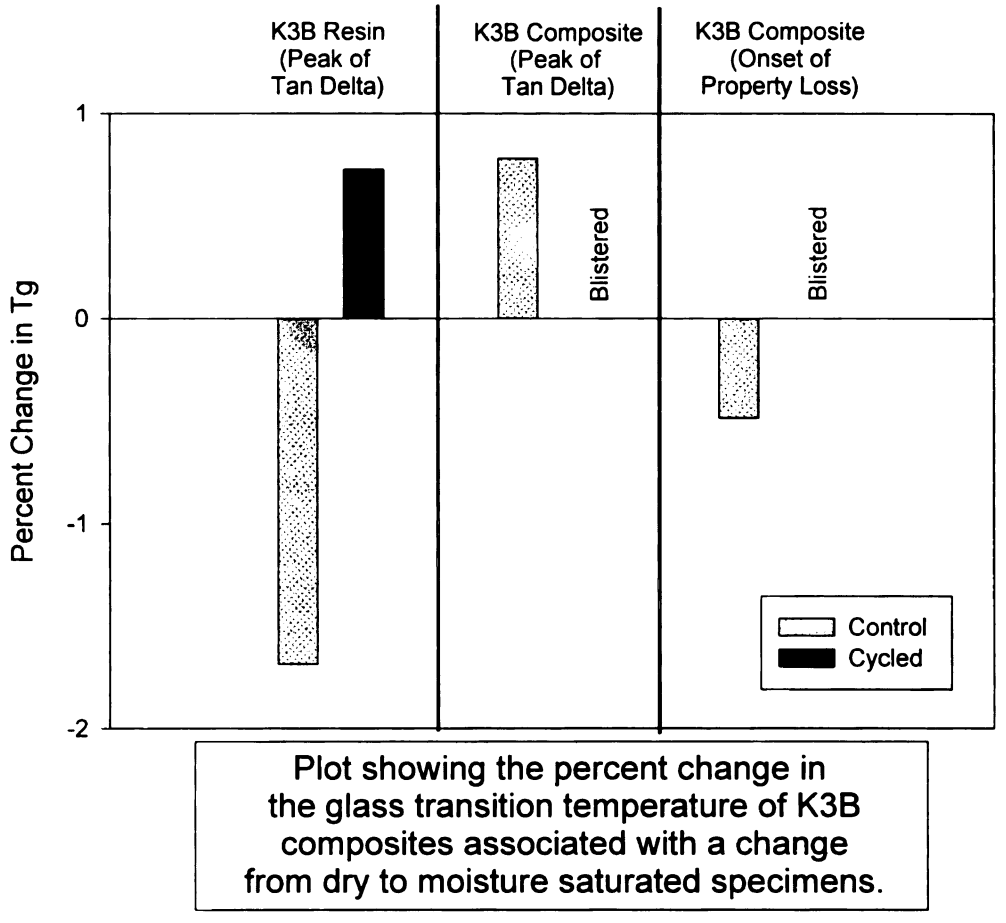

Figure 6-11 The Effect of Moisture Exposure on the T_g of K3B Resin and Composites

6.5 Effect of Thermal Spikes on Final Properties

The effect of thermally spiking specimens in a 250°C oven for 15 minutes for BMI resin and composites is shown in Figure 6-12. While some individual effects are apparent within the various tests, no overall conclusions for the properties of the system can be drawn.

The only effect which appears to be real is the loss in modulus for the wet, cycled open-hole compression specimens. It is felt that this may be due to the formation of a permanently damaged region around the hole due to the combination of moisture and cycling. Since the hole will magnify the effects of any edge damage, it is a better indicator of this than the other tests performed.

A small increase in the T_g of the system is seen in Figure 6-13 and is easily attributed to increased cure of the resin.

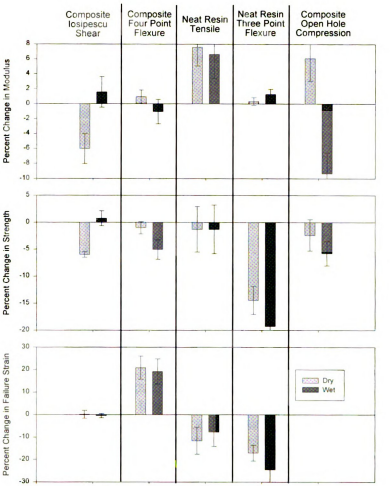

Plots showing the percent change in strength, modulus, and failure strain values of BMI resin and composites associated with the change from a control specimen to a thermally cycled specimen.

Figure 6-12 The Effect of Thermal Spiking on the Properties of BMI Resin and Composites

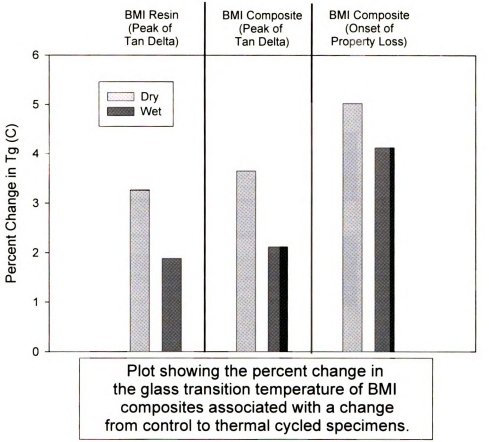

Figure 6-13 The Effect of Thermal Spikes on the T_g of BMI Resin and Composites

The effect of thermally spiking specimens in a 250°C oven for 15 minutes for K3B resin and composites is shown in Figure 6-14. No effect is seen for the dry specimens, but the wet cycled specimens showed a catastrophic failure during conditioning as shown and discussed in Section 6.2.1.1. No effect on the T_g of K3B was seen as shown in Figure 6-15.

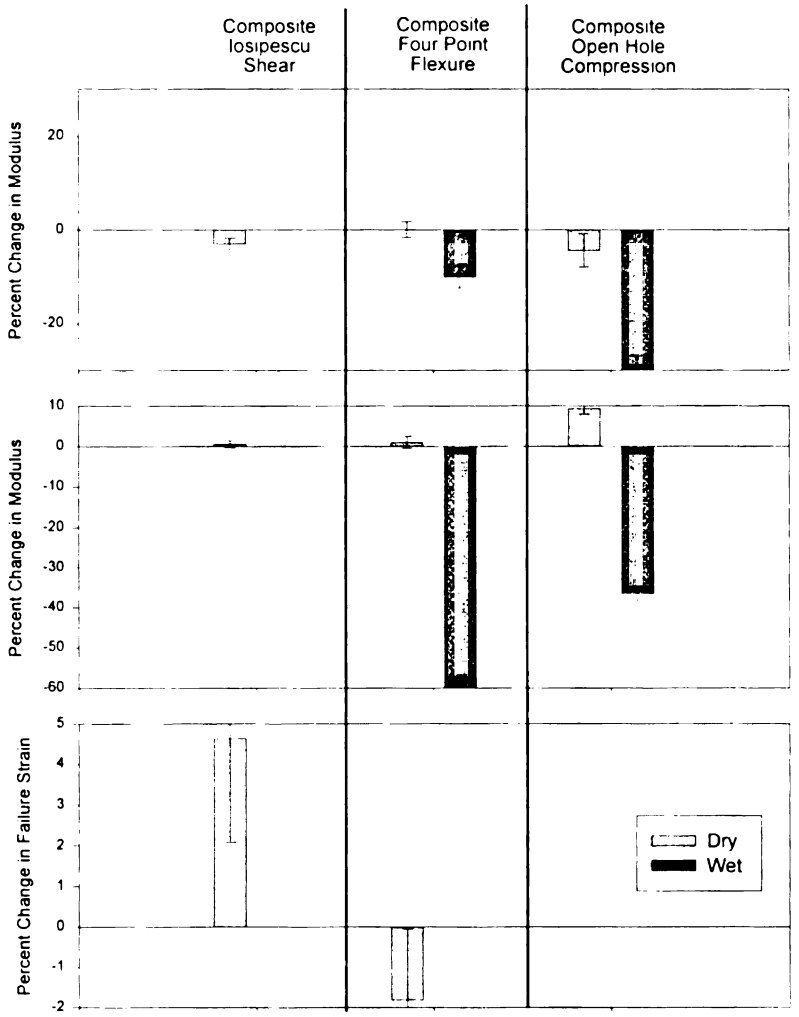

Plots showing the percent change in strength, modulus, and failure strain values of K3B composites associated with the change from a control specimen to a thermally cycled specimen.

Figure 6-14 The Effect of Thermal Spiking on the Properties of K3B Resin and Composites

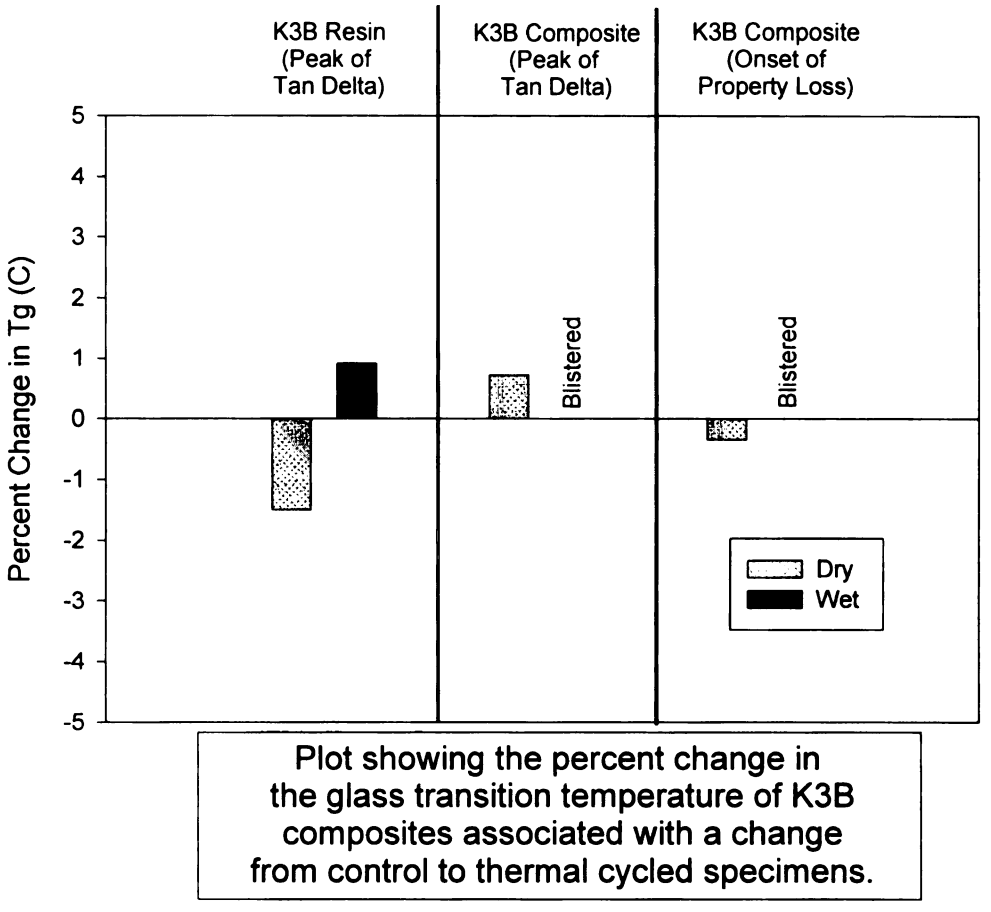

Figure 6-15 The Effect of Thermal Spikes on the T_g of K3B Resin and Composites

6.6 Thermal Spike Conclusions

The thermal spike testing performed here was designed to determine the effect of exposure to moisture, and thermal cycling as is likely to occur during the life cycles of these materials. All tests were performed in a dry condition because the effect of the

presence of moisture has been studied in Chapter 4. The following conclusions are apparent from the testing:

- Exposure to moisture and subsequent drying of the specimens has very little discernable effect on T_g or the mechanical properties of BMI specimens, or dry K3B specimens.

- Thermal spiking causes a small increase in the Tg of the BMI specimens. This would be expected because an exposure to a temperature of 250°C represents enough of a thermal event to increase the cure of these specimens. Thermal spiking has no effect on the T_g of K3B resin or composites.

- The wet, cycled BMI open-hole compression samples showed a modulus loss of approximately 15% suggesting that a large damaged region around the hole may be formed during this exposure.

- Finally, wet, cycled K3B specimens showed a catastrophic blistering failure during the thermal spike conditioning. The specimens showed blisters which caused the composite specimen to double in thickness. Since the 250°C exposure is above the T_g of this resin, it is very apparent that the wet T_g needs to be known, and all designs using this material must remain well below this temperature.

Chapter 7

IMPROVEMENT OF BMI/IM7 PROPERTIES

7.1 Introduction

The cure cycle of BMI/IM7 composites has been shown to cause tensile stresses in the transverse direction of cross-ply laminates. Calculations (FEM and Analytical) show in some cases, these stresses are insufficient to cause cracking in the plies, but cracking does exist suggesting that the presence of the weak interfacial bond between fiber and resin is partially to blame for the microcracking. Relief of cracking could, therefore, be accomplished through either increased adhesion, or a strain absorbing mechanism.

The adhesion in the BMI/IM7 system has been measured using a variety of techniques. Direct evidence of poor adhesion was obtained by ESEM imaging of Mode I crack opening failure surfaces. The revealed fibers were completely devoid of resin which is seen in adhesive failures. Images of both thermally and mechanically induced cracks also show a completely adhesive failure. Four point flex testing of composites revealed very poor interlaminar shear strength as evidenced by the mid-plane shear failure of flexure samples with a 28:1 span to depth ratio. IFSS values measured using the Interfacial

Testing System (ITS) were less than 10% of the values for standard epoxy/carbon fiber systems.

All of these observations verify the need for increased adhesion in this system. The following section describes the factors which affect the IFSS and reviews work performed on various related systems. This forms the basis for the testing approach taken here.

7.1.1 Factors Affecting the Interfacial Shear Strength (IFSS)

Since this effort concentrates on the adhesion in these systems, it is important to understand all of the factors which can effect the IFSS. Rao and Drzal used extensive single fiber fragmentation testing of epoxy/AS4 to show that the IFSS decreases with decreasing matrix modulus [43], and decreases as temperature rises with a large decrease as the Tg of the matrix is approached [44].

Similarly, Varma, Needles, Kourtides, and Fish [36] showed a decrease in interlaminar shear strength (ILSS) with increased temperature and attributed it to a reduction in IFSS. Pegoraro and Landro [45] used single fiber fragmentation to show a decrease in adhesion with increased temperature for the PEI/carbon fiber system. They attributed this to a reduction in the residual compressive stress formed during cure. Unfortunately, their analysis did not include the effect of nearest neighbor fibers or ply level interactions which will severely change the resultant stress magnitudes and patterns [46].

Carman and Averill [46, 27] have shown that an optimum interphase can be designed to increase the transverse strain to failure by a factor between three and six. The interphase is optimized in terms of modulus and thickness.

7.1.2 Adhesion Improvement In BMI/IM7 And Related Systems

There has been much interest in the adhesion of BMI to carbon fibers. While the focus and results of the available literature vary, it is generally acknowledged that the adhesion is poor. Due to this a variety of approaches have been employed to improve the system's performance. These fall into four major categories: (I) changes in fiber surface energy, (II) changes in functional group concentration, (III) resin chemistry changes (toughening), and (IV) fiber sizing.

7.1.2.1 Surface Energy Changes

Fiber wetting is a requirement for most composite manufacture. Without it composites generally have poor adhesion and porosity. The wetting between two materials can be predicted using thermodynamic surface energy concepts. Generally liquids will wet solids if the liquid's surface energy is lower than that of the solid. A relatively weak but functionally important bond can be formed between surfaces due to dipole-dipole, dispersive, or acid-base interactions.

Krekel, Huttinger, and Hoffman [47] calculated the work of adhesion for fibers with varied surface treatments and correlated these directly to the concentration of carboxylic acid groups as measured by thermal desorption of CO_2 species. They suggest that the work of adhesion resulting from carboxylic acid groups is a better predictor of adhesion to thermoplastics than CO_2 desorption losses because CO_2 can be produced by other surface species.

In a series of articles, Nardin et al characterized the reversible work of adhesion (W) as the sum of the dispersive and acid-base components of PEEK and carbon fibers of various surface treatments [48]. They then found a linear correlation between W and the interfacial shear strength as measured with the single fiber fragmentation test [49]. Finally [50], they related W to the transverse tensile strength of composites. Here they found a weak correlation because the fractures were cohesive through the resin, not adhesive in nature. The correlation which was seen was explained as an effect of the improved surface bond on the nature of the resin in the failure region.

Bucher and Hinkley [51] related transverse flexural strength to wetting angles in carbon fiber/PEKK composites. They found that the G30-500 fiber exhibited the lowest contact angle of fibers tested, and thus best transverse strength.

Jangchud et al [52] found that the ILSS of PMR-15/carbon fiber composites correlated well with the polar nature (% weighted dipole moment) of the various fibers tested. They

suggest that increased bonding can be achieved by increasing the polar components in the resin.

Heisey et al [53] attributed an increase in the adhesion of bismaleimide resin (Matrimid 5292®) and a phosphorus containing BMI) to treated AS4 and AU4 carbon fibers to surface energy increases of the fibers. Unfortunately, the microbond single fiber pull-out technique used to measure the adhesion caused fiber failure more often than not, and the results were too scattered for any conclusive observations.

7.1.2.2 Surface Morphology Changes

Many surface treatments also change the morphology of the fiber surface as seen by SEM, AFM, STM, and surface area analysis (Kr adsorption). Increased surface area has been proposed to aid in adhesion by promoting mechanical interlocking of the resin and fiber surface.

O'Kell and Jones [54] found that air and nitrogen plasma both roughen the surface on the nanometer level. Jangchud et al [52] were not able to correlate surface morphology as measured by AFM to ILSS for PMR-15/carbon fiber systems. They suggest that correlations might exist with dimensional scales below 25nm.

Dzenis et al [55] performed AFM analysis of Kevlar®, graphite, and polyimide fibers and determined that the surface roughness is fractal in nature, and thus the interphase should

be fractal in nature. They propose that studying this fractal nature will aid in the understanding of stress transfer between fibers and resins and ultimately help in the design of appropriate topographies for efficient stress transfer.

7.1.2.3 Surface Chemistry Changes

Surface treatments have been used widely to increase the adhesion between carbon fibers and matrices. There are generally four types of surface treatment: gas phase, liquid phase, electrochemical, and plasma treatment. Donnet [56] provides a review of these methods and their effect on fiber and composite properties. The most characterized change is in the concentrations of surface functional groups, which has been readily correlated to adhesion in many systems.

It is well known that nitric acid treatment of carbon fibers increases the concentration of acidic surface functional groups, decreases the fiber tensile strength, and causes fiber weight loss [57]. This change in surface chemistry has been readily correlated with increased adhesion in many composite systems [6].

Testing of BMI/IM7 fiber composites with electrolytic anodization in ammonium bicarbonate treatment varying from 50% to 400% showed no significant affect on adhesion as shown by the purely adhesive failure of Mode I fractured composites (internal work). This suggests that an increase in the surface functionality is insufficient to cause significant property improvement.

Plasma treatment of carbon fibers has been performed with a variety of gasses, including air [7, 53, 58, 59], Argon [7, 60], Nitrogen [7], Ammonia [53, 60], and oxygen [53, 60]. The results generally conclude that plasma treatment increases the functionality and/or energy of the fiber surface. These increases have been correlated with adhesion improvements in many cases [7, 53, 58, 60]. O'Kell and Jones [54] determined that nitrogen plasma can only chemically interact with edge sites of graphite, but may activate the basal planes, allowing oxygen adsorption when exposed to air.

Oxygen and air appear to be the most effective at increasing the oxygen containing functionalities which are generally considered to be responsible for increases in adhesion. It has also been noted, however, that oxygen plasma tends to etch the fiber surface more dramatically, and thus reduce fiber tensile strength[60].

Chang [60] proposed that Ammonia/Argon plasma to be the most effective in increasing adhesion between carbon fibers (AU4) and BMI (Matrimid 5292) without decreasing fiber strength. His data, however, shows higher transverse tensile strength for oxygen treated fibers with only a 20% reduction in fiber tensile strength after a full 20 minutes of treatment. While the plasma treatments here may have been effective, 20 minutes of plasma treatment is not commercially viable, and others suggest that most active sites are oxidized after just 60 seconds.

He suggested that the effectiveness of the Ammonia/Argon plasma is due to a Michael Addition reaction between the amines formed on the surface, and the maleimide groups in

the BMI. It should be noted that this study was performed using type AU4 fibers, and Drzal has shown [6] that AU4 fibers have a weak boundary layer which limits apparent adhesive strength. The removal of this layer by long time oxygen plasma may account for the increase in transverse tensile strength seen here.

Heisey et al [53] found that 15 seconds of air plasma treatment caused a twofold increase in the surface oxygen content of the fibers (9.3% to 19.8%) with only a 7% loss in fiber strength. A one minute NH_3 plasma treatment caused an almost twofold increase in nitrogen content (2.7% to 5.2%) with no significant loss of fiber strength. The air plasma treatment caused an increase in Na content from 0.0026% to 0.084% after five minutes suggesting an etching of the surface. Both treatments caused a significant increase in the overall surface free energy which was manifested in the polar component. SEM images at 50,000x showed that the air plasma treatment had roughened the surface, but the NH_3 had not. Unfortunately, the adhesion measurements to the BMI resin were inconclusive due to experimental difficulties.

7.1.2.4 Resin Chemistry Changes

As noted previously, changing the modulus of the matrix material can have a very significant effect on the IFSS which can, in turn, have a major effect on macroscopic composite properties. Many people have studied methods for improving the toughness of high temperature resins.

Lin and Chen [61] mixed BMI with TGDDM and DDS (as a curing agent) and found an almost 3x increase in resin fracture toughness due to a simultaneous interpenetrating network, but sacrificed thermal stability.

Morgan et al [2] added PEI and Kevlar® 49 whiskers to the Matrimid 5292® BMI/IM7 carbon fiber system and found that the PEI formed a 1 μm diameter second phase within the BMI which caused an ~30% increase in G_{Ic} due to crack bridging. The Kevlar® fibers caused an increase in G_{Ic}, but with a lower crack initiation stress. The increased toughness is due to a more torturous crack path while the lower initiation stress is most likely due to a lack of adhesion between the Kevlar® and resin.

Cartwright et al [62] added maleimide terminated polysulfone to the Matrimid 5292® system and studied the cure using FTIR. They cite literature which suggests that the size and morphology of a second phase is due to competition between the thermodynamic driving force for phase separation and kinetic inhibition due to cure advance. They also cite work which has used microwave processing to produce novel morphologies.

The BMI system being used in this study (Ciba-Geigy's Matrimid 5292®) is a two part system consisting of 4,4' bismaleimidodiphenyl methane (BMI) and O,O' diallyl bisphenol A (DABPA). Guozheng, Aijuan, and Liwen [63] showed that the addition of four different allyl compounds (including DABPA) improve the processability and toughness of BMI while retaining thermal capability and wet performance. Continuing

work at MSU has shown that simply varying the ratio of the BMI and DABPA monomers can have a significant effect on final neat resin properties.

Wilkinson, Ward, and McGrath [64] mixed five thermoplastics into the Matrimid 5292 system and reported the thermal, mechanical, and morphological changes for both neat resins and composites. They found that the Tg of the modifier controls the onset of decline in storage modulus of the cured resin and thus should be considered carefully when choosing a modifier. Higher molecular weight modifiers showed further increased fracture toughness (K_{Ic}). A phase-inverted morphology was noted for all modifiers, but was not shown to be required for the increased toughness seen. Resin toughness translated into composite toughness well, and the addition of modifiers to the melt did not impede the use of standard composite prepreg and cure methods.

7.1.2.5 Fiber Sizing

Since the probability of significantly increasing adhesion in this system via fiber surface treatment appears low, an alternate method is required. The addition of an interphase has great potential because its composition and properties can be tailored to provide adhesion to the fiber, miscibility with the resin, and overall composite property improvement. The property improvements can come about through an adhesion improvement and/or a strain absorption mechanism.

Jenkins et al [65] showed that the use of a thermoplastic sizing on carbon fibers reduced the transverse microcrack density, increased the transflexural strength, and improved the thermo-oxidative stability of PMR-15 composites. The thermoplastics used were polyisoimide, polyarylsulphone, and an imidised polyarylsulphone.

Since one of the requirements for a good interphase material is bonding to the fiber, the work on adhesion between thermoplastic matrices and carbon fibers provides a wealth of useful information.

Denault [66] found that the interfacial strength between thermoplastics and carbon fibers was primarily due to a chemisorption mechanism. This was supported by the fact that polypropylene did not form a good bond until degraded, while polyamide-12 readily formed a good bond. Polypropylene has many fewer reactive groups than polyamid-12. It was also supported by the large loss in short beam shear strength of PA-12 composites after cure cycles above 350°C where a large number of the carbon fiber surface functional groups have thermally evolved from the surface. Unfortunately, degradation of the resin may have contributed to this result in addition to the evolution of the surface functionalities.

A large amount of work has been focused on understanding the way interphases affect composite properties, and what the optimum interphase should be. For epoxy sizes in epoxy matrices, it was seen that a low molecular weight sizing led to the highest

interfacial shear strength [67]. This was attributed to the ability of the sizing to diffuse into the resin.

Carman and Averill [46] showed that the modulus of the interphase plays a large roll in its ability to increase the composites ability to absorb strain. This would strongly suggest a molecular weight dependence. Unfortunately, it is also known that for high molecular weight materials chemical bonding with the surface is unlikely. Pittman et al [68] also showed that low modulus interphase materials provide the greatest increase in impact strength (toughness) and that interphase thicknesses show a maximum effect on impact strength in the range of 1000-1500 angstroms [69].

Raghavendron and Drzal [70] have shown that lower molecular weight materials have a thermodynamic tendency toward the fiber surface, and thus graduated interphase properties may be readily achievable.

Rajagopalan et al [71] showed that the amount of diffusion of polysulfone into epoxy had a strong effect on adhesive properties. A wider diffusion zone was achieved with higher initial processing temperatures and increased the fracture toughness of the joint by 35%. The size of the diffusion zone and thus toughness of the joint can be seen to be a function of the miscibility of the two polymers. Carman and Averill's work showed that the size of a distinct interphase must be tailored to provide a maximum strain to failure for transversely loaded composites.

7.2 Treatment of IM7 Fibers for Increased Adhesion

With all of this background available, attempts were made to increase adhesion through both fiber surface treatments, and the addition of various sizings.

7.2.1 Fiber Surface Treatment

To determine the effect of changing the fiber surface chemistry and/or morphology, two different surface treatments were studied. IM7 fibers with varied levels of commercial treatment were provided by Hercules, Inc. Air plasma treatment of the unsized IM7 fiber was performed and evaluated due to the promising results seen in the literature. Before discussing these treatment methods, it is imperative to discuss a few experiments on the thermal and chemical stability of the surface functional groups which are formed by these processes.

7.2.1.1 Chemical Bonding of K3B monomers During Processing

A study has been performed in which monofunctional counterparts of the K3B constituent materials were reacted with the fiber surface to determine the type and extent of chemical reactions between K3B and IM7 [72]. These model compounds were phthalic anhydride, pyromellitic dianhydride, APB-133, and 2-phenyl-APB-144. Fiber bundles were sealed in containers with a solution of each component and n-methyl pyrrolidone (NMP, a solvent used in the processing of K3B). The containers were then subjected to the 350°C thermal cycle used in the processing of K3B. The fiber bundles

were then washed in hot NMP to remove all physisorbed species, leaving only those bonded to the surface.

No evidence of the model compounds was found after processing, and it was also found that in all cases, the amount of oxygen containing species (which would account for the majority of the chemical bonding in this system) decreased by 50%. The fact that this occurred in the control specimens (NMP only) suggests that the combination of NMP and a 350°C thermal cycle will reduce the number of active bonding sites. NMP without the 350°C thermal cycle was shown to have little effect.

7.2.1.2 TPD showing chemical species Desorption

Since the previous study showed that a temperature of 350°C and an NMP environment strips surface functionalities from the IM7 fiber, a temperature programmed desorption (TPD) was performed to determine whether this was due to the temperature alone, or if both the temperature and the NMP were required. The fiber used for this study was 400% surface treated IM7. The resultant desorption profile is provided in Figure 7-1.

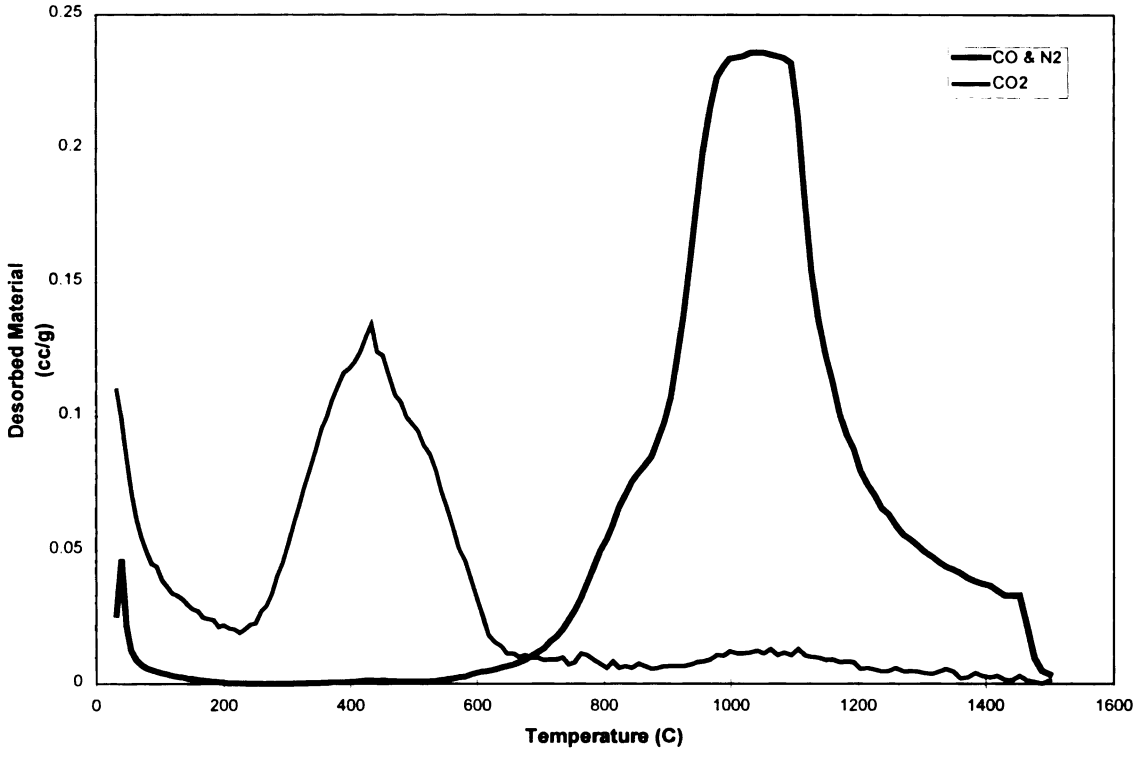

Figure 7-1 - TPD Profile for 400% Surface Treated IM7 Fibers

The TPD was performed by Zhigang Zhang in the Chemical Engineering Department of MSU. Experimentally, a section of fiber was placed in a ceramic tube in a tube furnace. The tube was attached to a mass spectrometer which analyzed the gasses which evolved from the surface as a function of furnace temperature. The gasses detected were CO, CO_2, and N_2. The CO_2 is generally attributed to the decomposition of carboxylic groups while the CO is attributed to carbonyl and hydroxyl groups. It is generally believed that the carboxylic species are more active and thus have a greater contribution to adhesion. In this case, it is shown that temperatures of 300°C will cause a loss of less than 10% of these groups, and at 350°C, less than 20% are gone, but the species lost at lower temperatures are likely to be the more chemically active species.

This may suggest that the combination of temperature and NMP removes more surface functionality from the carbon fiber surface then the temperature alone. TPD results for similar fibers [56] also show that the amount of functionality lost solely due to thermal desorption is lower than found in the NMP solvent results.

7.2.1.3 Commercial Treatment

Carbon fibers are generally provided with a surface treatment which alters it's surface in a variety of ways. It has been shown that the treatment removes an outer "skin" or weak boundary layer, and increases the surface functionality of the fibers. The IM7 fibers used here were received from Hercules with treatment levels of 100% and 400%. These levels refer to a percentage of the standard commercial treatment which is an anodic electrolization in an ammonium bicarbonate bath. The amperage was varied to produce the different levels. Unfortunately, this surface treatment process is proprietary, and further information is unavailable.

The effect of treatment series like this has been studied previously for a different resin system. Waterbury showed that the concentration of oxygen containing species increases linearly with the amount of treatment after an initial jump. This trend was also seen in the polar surface free energy. There was a direct correlation between these factors and the adhesion between the fiber and matrix as measured by the single fiber fragmentation test. Thus, once the initial treatment is performed, large changes in adhesion are not seen.

7.2.1.4 Air Plasma Treatment

As shown at the beginning of this chapter, some success has been reported for increasing the adhesion of high temperature resins to carbon fibers through the use of air plasma treatments. Unfortunately, the adhesion data is consistently suspect, and the plasma treatments used generally cause a significant reduction in fiber tensile strength. The high energies and long treatment times used in these studies should not be necessary to cause very significant increases in surface oxygen containing species.

A Plasma Sciences plasma chamber was used. The unit was run under experimental conditions for approximately five minutes before treatment of these fibers to clean the chamber of any possible contaminates, and check for irregularities in the plasma field. Fiber tows of approximately 8" in length with aluminum foil holding the ends together were laid in the chamber between glass bars which held the tows off the chamber floor. The parameters used for the plasma run are shown in Table 7-1.

Table 7-1 Plasma Chamber Experimental Parameters

Parameter	Level
Power	55 Watts
Process Time	30 seconds
Base Pressure	0.05 torr
Gas Flow Rate	100 cc/min
Temperature	26°C
Purge	Slow Purge to Air over 40 minutes
Vent Time	3 min maximum

After processing, the fiber tows were removed and placed in clean aluminum foil until analyzed with the XPS, and manufactured into a unidirectional composite for adhesion measurements.

7.2.1.5 XPS Analysis of Treated Fiber Chemistries

To quantify the difference in the surface chemical nature of the fibers used here, XPS was performed on a baseline fiber tow, as well as the air plasma and 400% commercially treated fibers. The XPS experiment was carried out using a Physical Electronics 5400 ESCA spectrometer. The instrument was equipped with a monochromatic Al x-ray source (15kV, 40 mA, 600W). Signal collection utilized a 180° hemispherical analyzer operating in the fixed analyzer transmission mode at a pass energy of 89.45 eV for survey scans and 35.75 eV for high resolution scans, and a position-sensitive detector for signal detection. The signal was digitized and processed using the Physical Electronics V4.0 ESCA software. Spectra were collected over an analysis area of 1.5 mm x 5 mm with the sample surface oriented at 65° relative to the analyzer lens (sampling depth of the order of 70A). The samples were oriented parallel to the x-ray source and analyzer aperture.

The instrument was calibrated using Mg K_α x-ray radiation where the Ag $3d_{5/2}$ peak had a binding energy of 368.2 ± 0.1 eV with a full width at half maximum (FWHM) of 1.06 eV at 35.75 eV pass energy and 515,856 counts per second, with a rectangular analysis area of 1.5 x 5 mm in the small-area, large solid angle aperture. The difference between the Cu $2p_{3/2}$ and Cu $3p_{3/2}$ was 857.75 eV at 17.9 eV pass energy. The binding energy of Au 4f

was 84.0 eV. Using the monochromated Al K_α x-radiation, the FWHM of sputtered Ag $3d_{5/2}$ was 1.06 eV at 35.75 eV pass energy and 1.5 x 5 mm analysis area, with a count rate of 45,476 counts per second.

Surface atomic concentrations were used to calculate the surface composition and thus, the surface oxygen/surface carbon ratios. The results of the XPS testing for the 100%, 400%, and plasma treated samples are provided in Table 7-2. It can be seen that the 400% commercially treated fibers had the highest surface oxygen content, and the air plasma treatment provided only a small increase in the functionality.

Table 7-2 Surface Composition for All Treated Fibers

	Carbon	Oxygen	Nitrogen	Sodium
100% Baseline	83.0	11.6	4.8	0.5
400% Commercial	73.1	20.2	3.5	0.3
30 sec Air Plasma	79.7	16.2	3.6	0.5

7.2.1.6 Surface Treatment Conclusions

Both the higher levels of commercial treatment, and the plasma treatment have been shown to increase the amount of oxygen containing surface groups. The thermal stability of these species has been demonstrated by thermally programmed desorption. The ability of this increased functionality to increase the adhesion in the BMI/IM7 system was

investigated using the Interfacial Testing System, and Mode I failure analysis as discussed in Section 7.4.

7.3 Sizing of Carbon Fibers

A thermally stable, compliant, adhesion promoting sizing has been sought with the goals of improved adhesion, reduced microcracking, and thermal stability. Unfortunately this combination of properties is rather self-limiting in that thermal stability of polymeric carbon chains is generally directly related to their modulus and the available high temperature resins generally show very little adhesion to carbon fibers. Several high temperature thermoplastic polymers and a silicone resin have been investigated as sizings here. The specific reasons for their investigation are provided below.

7.3.1 Use of Thermoplastic Sizings

As discussed in Chapter 2, the microcracking stresses can be relieved through the addition of a compliant sizing. The thickness of this sizing was shown to be most effective when on the order of 0.5 microns for this system. It was also shown that the effect of sizings which have approximately the same moduli as the bulk matrix are relatively insensitive to thickness. The ability of the thermoplastic sizings to bond with both the fiber and matrix is of much greater importance.

7.3.1.1 Sizing Chemistries and Properties

Three thermoplastic materials were chosen as candidates for sizings in this system. They are polyetherimide (PEI), polyethersulphone, and Matrimid® 5218, a thermoplastic polyimide. All materials were chosen due to their ability to meet the service and processing temperature requirements. The properties of these resins are provided in Table 7-3.

Table 7-3 Physical Properties of Sizing Materials

	Matrimid 5292 BMI	Matrimid 5218	Ultem 1000 PEI	Victrex PES	GE RTV-31
E (MPa)	1828[d]	2895[b]	3000[b]	2410[b]	2.29[d]
ν	0.35	0.35	0.44[b]	0.35[c]	
CTE_1	$42x10^{-6}$/°C[d]	$28x10^{-6}$/°C[b]	$56x10^{-6}$/°C[b]	$55x10^{-6}$/°C	$200x10^{-6}$/°C[b]
Tensile Strength[b]	94.1 MPa	86 MPa	105 MPa	70.3 MPa	6 MPa
Elongation @ Break[b]	6.66%	48.6%	60%	75%	170%
Tg	350°C[d]	326°C[d]	226°C[d]	229°C[d]	
MW	-			5200	-

b Product literature values
c Estimated based upon tensile modulus
d Experimentally measured

The chemistries of the PEI and PES polymers are provided in Figure 7-2. The general chemical structure of thermoplastic polyimides such as Matrimid® 5218 and the backbone chemistry of PDMSO are provided in Figure 7-3.

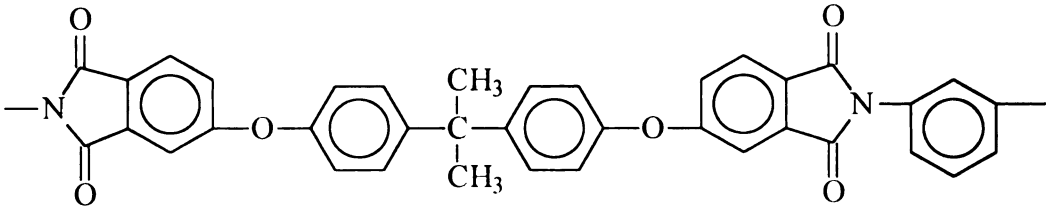

polyether-imide chemical structure

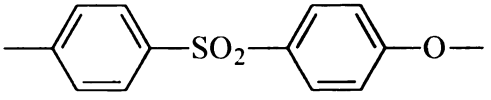

polyethersulfone chemical structure

Figure 7-2 The Chemistries of PEI and PES

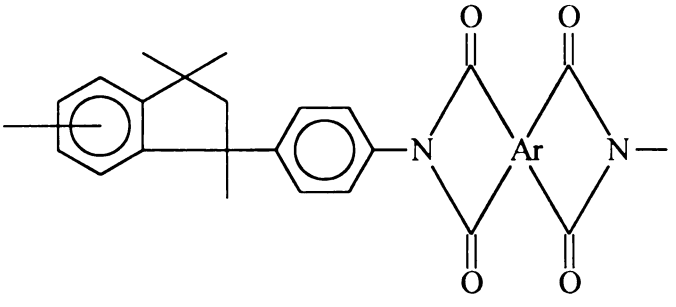

thermoplastic polyimide chemical structure

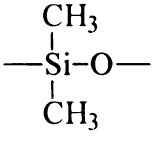

polydimethylsiloxane chemical structure

Figure 7-3 The Chemistries of PDMS and Thermoplastic Polyimides

7.3.1.2 Sizing Method

The thermoplastic sizings were applied to the carbon fiber tow using a solution chemistry method. First, solutions of 1% polymer in dichloromethane were prepared. Approximately one yard of carbon fiber tow was wrapped around a glass rack and kept in place with nickel wire. The sizing solution was poured into a clean polypropylene basin and the rack was immediately immersed in the solution. The rack was removed after one minute and slowly spun in air to dry the tows. All three sizing solutions showed a very good ability to spread the fiber tow and impregnation was not an issue. After drying in air for fifteen minutes, the sized fibers were placed in an air oven at 60°C for one hour to ensure removal of the solvent.

The thickness of the sizing was approximated using geometric calculations based on the weight gain of the fibers, density of the resin, density and radius of the fiber. This estimate showed that sizing thicknesses were on the order of 0.1 μm.

7.3.1.3 Sizing Results

The sized fibers were analyzed for morphology using the ESEM. Each sizing had a skin on the outer surface of the tow as shown for the PEI sizing in Figure 7-4. The sizing penetrated the tow and coated the fibers as shown in Figure 7-5, again for the PEI sizing. Figure 7-6 shows a case where the sizing formed a bridge between fibers, and still coated the whole fiber. A similar image for the Matrimid 5218 sizing shows the presence of the sizing on the fiber surface (Figure 7-7) while it can also be seen when looking at the edge

of a fractured fiber (Figure 7-8). The conclusion to be drawn from the sizing morphologies is that the sizing method was sufficiently successful at coating the fibers for this analysis, but better process is achievable and should be used if these methods are found to be of interest.

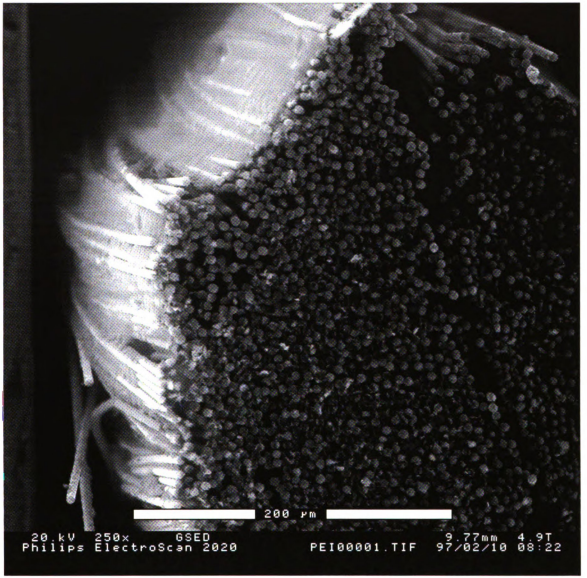

Figure 7-4 Outer Skin of PEI Sized IM7 Tow

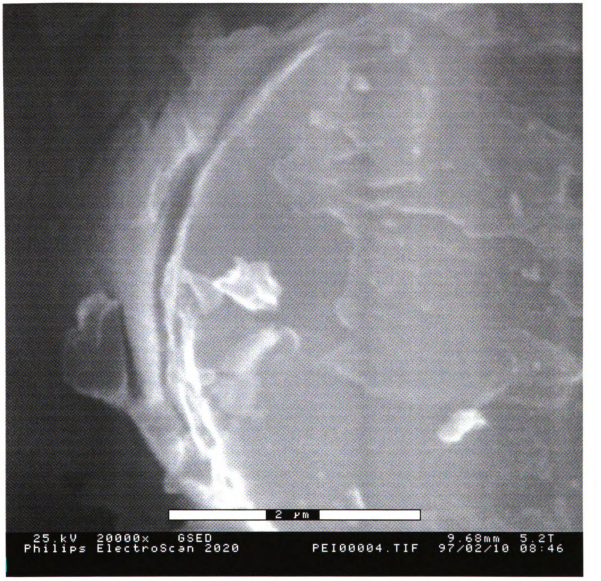

Figure 7-5 PEI Sizing on an IM7 Fiber

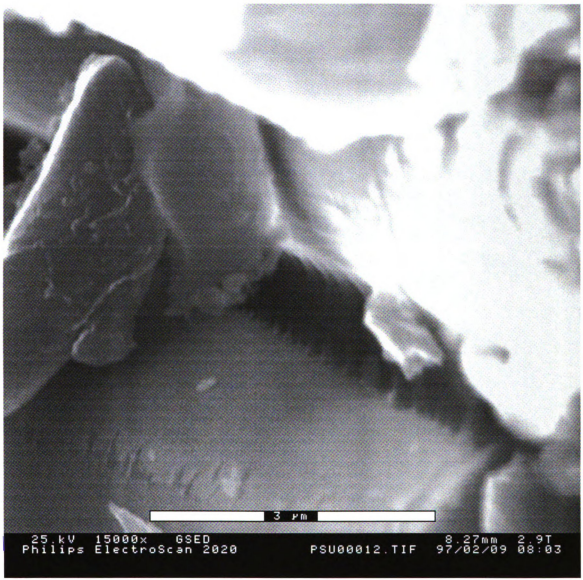

Figure 7-6 PES Sizing on an IM7 Fiber

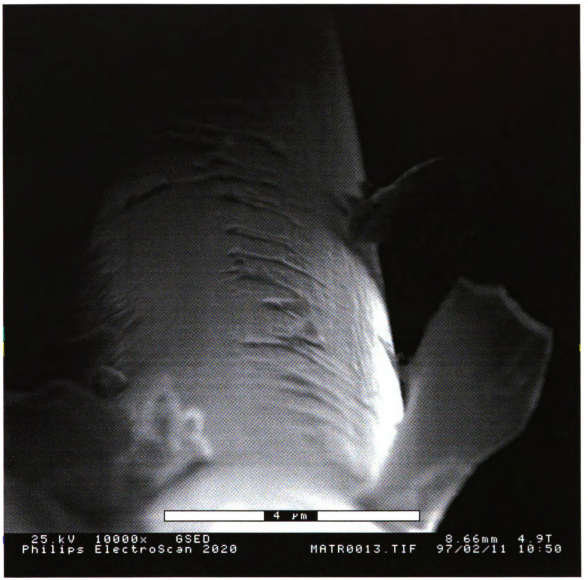

Figure 7-7 Matrimid® 5218 Sizing on an IM7 Fiber Surface

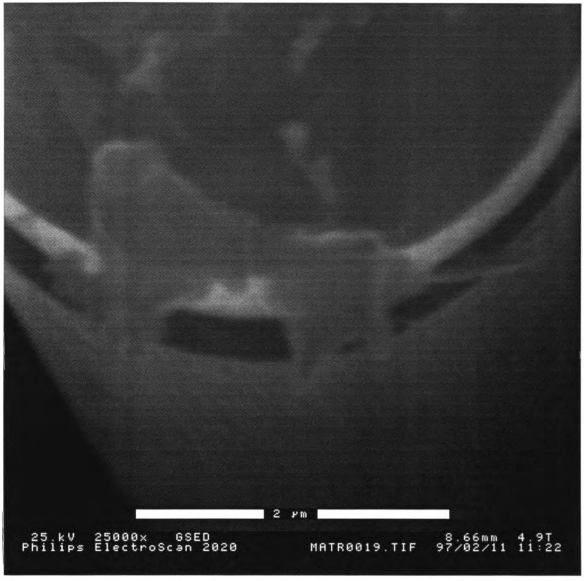

Figure 7-8 Matrimid® 5218 Sizing on an IM7 Fiber Edge

7.3.2 Use of a Compliant Sizing

A compliant material which was capable of withstanding the use temperatures of 200°C was desired. The only materials found which meet this description are high temperature silicones based on the polydimethylsiloxane (PDMSO) backbone shown in Figure 7-3. A sample of General Electric's RTV-31 was obtained from GE. The exact contents of this material are unknown, but it's general contents are given as 30-60 wt% PDMSO, 10-30 wt% diatomaceous earth, 1-5 wt% ethyl silicate, and 30-60 wt% red iron oxide. The material is crosslinked with the aid of a dibutyl tin dilaurate (DBT) curing agent. This is a moisture activated catalyst.

7.3.2.1 Sizing Method

Initially, the "base compound" of silicone is a thick red viscous liquid. The DBT curing agent is a liquid which is provided in a small tube. To get the RTV onto the fibers and then cured into a lightly cross-linked network, the base compound was put into a 1.25 wt% solution with toluene as the solvent. Three drops of the DBT was added to the solution. This is the appropriate amount of DBT for the amount of base compound in solution. The solution was immediately poured into the clean polypropylene beaker and fibers were pulled through the solution as quickly as possible and hung to dry. The fibers were handled only using the nickel wire which was used to tie the ends. After drying for eighteen hours in air, the fiber tows were subjected to a thermal cycle of 150°C for 1 hour and 200°C for 1 hour because there is an evolution of formaldehyde reported at 150°C

and the evolution of volatiles during composite processing causes voids and generally poor laminate quality. A maximum weight loss of 1.3% was seen.

A macroscopic piece of RTV was created at the same time the sized fibers were made to help ensure that the silicone became crosslinked, and to allow the determination of a modulus value. This was made by mixing the compound and curing agent in the same ratio as used for the sizing. After this mixing, 40% by weight of the sizing solution was added to the mixture. This was done to simulate the effect of the solvent on the processing of the sizing. The specimen was dried in air until solid. The specimen was fully solid and the crosslinking reaction was successful.

Small strips of this piece of silicone rubber were cut and tested on a tensile testing machine to provide accurate modulus values for use in the modeling conducted in Chapter 2. Three specimens were tested, and the average modulus value was 2.29 MPa. Specimens were not tested to failure, so strength and elongation at break values were not obtained.

7.3.2.2 RTV Sizing Results

Small sections of the sized fiber were analyzed in the ESEM and the resultant sizing morphology was determined. It was found that in general, the RTV did not provide a uniform coating on the fiber, but adhered to the fiber in small patches as shown in Figure 7-9 and Figure 7-10. While this is not the ideal coating desired to determine the

effectiveness of a compliant sizing at reducing strain in composites, the use of a silicone sizing has already broken one of the assumption of the analysis used in Chapter 2. Silcones are well known for providing very poor adhesion to surfaces, and thus failure would be expected at either the fiber/sizing interface, or at the sizing/matrix interface.

Figure 7-9 RTV Sizing Between Two IM7 Fibers

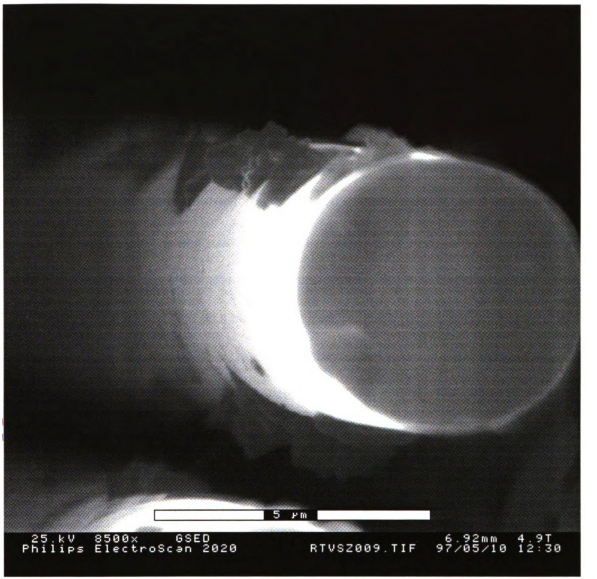

Figure 7-10 RTV Sizing Patches on IM7 Fibers

7.3.2.3 Composite Preparation

A cross-ply composite was made from the RTV sized fibers to determine if the sizing was capable of reducing the strains either through it's compliant nature, it's poor adhesion, or a combination of the two. The morphology of the sizing was not known at the time. Since only a small amount of sized fiber had been created, a small (¾ in^2) cross ply laminate

was fabricated. To ensure that any changes in the microcracking behavior were not due to the processing method, a control laminate was also fabricated using the unsized IM7 fiber.

Both the sized and unsized fibers were "prepregged" by being pulled through a bath of BMI resin and laid on telflon release film. The unsized fiber showed good wet-out of the tow, while the RTV sized fiber showed very poor wet-out. The cross-ply was fabricated by cutting ¾ in lengths of tow and placing them together to form a unidirectional sheet. This was done on release film on a hot plate so that the resulting ¾ in^2 prepreg sheet could be removed. Four sheets were made and they were then stacked in a $[0°/90°]_S$ configuration. The sized fiber tows were spread out on the hot plate to promote impregnation of the resin.

The two laminates were then vacuum bagged in the same manner as presented in Chapter 2 for the macroscopic panels. This vacuum bag was then placed in the programmable Nitrogen purged oven and a vacuum was pulled on the specimens for the same cycle as used in the creation of the macroscopic panels. The only difference in the processing of these laminates is that the 100 psi of pressure was not applied. The cure cycle was 5°C/min to 177°C for 90 minutes and 5°C/min to room temperature. The standard post-cure cycle of 200°C for 2 hours and 250°C for 6 hours was performed in a Nitrogen atmosphere after the specimens were removed from the vacuum bag.

The RTV panel quality was poor in terms of high performance composites, but more than sufficient for the objectives here. A section of this panel was mounted in epoxy and polished for analysis of panel quality and ITS testing. The remainder of the specimen was kept for Mode I failure analysis.

7.3.2.4 Composite Morphology

The polished section of RTV sized cross-ply composite was examined both using an optical microscope and in the ESEM. Optically, it was apparent that the laminate contained a fairly large number of voids and some regions where the matrix resin did not impregnate the tow. The laminate did show good bonding between the layers, and had some evidence of both resin shrinkage stresses, and ply level expansion mismatch stresses.

ESEM analysis of this specimen was difficult, but images of the pertinent features were obtained. A region showing a resin rich region where the resin has pulled away from the surrounding fibers is shown in Figure 7-11. Another region shows the formation of a ply-level microcrack (Figure 7-12). This was one of the two such cracks found on the whole ½" length.

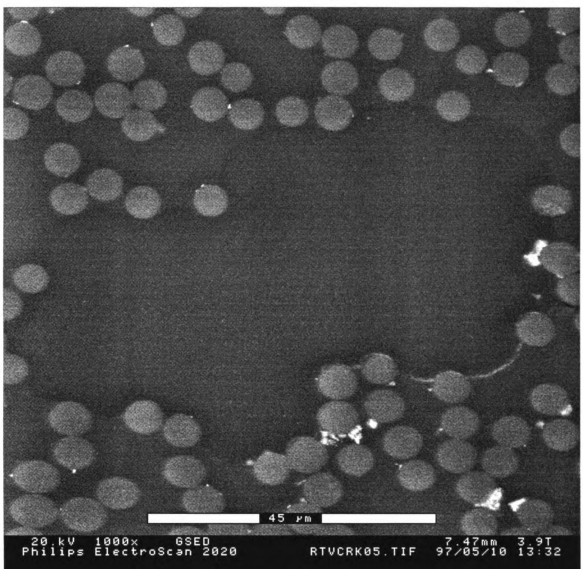

Figure 7-11 Cracking of RTV Sized Composite Caused by Resin Shrinkage

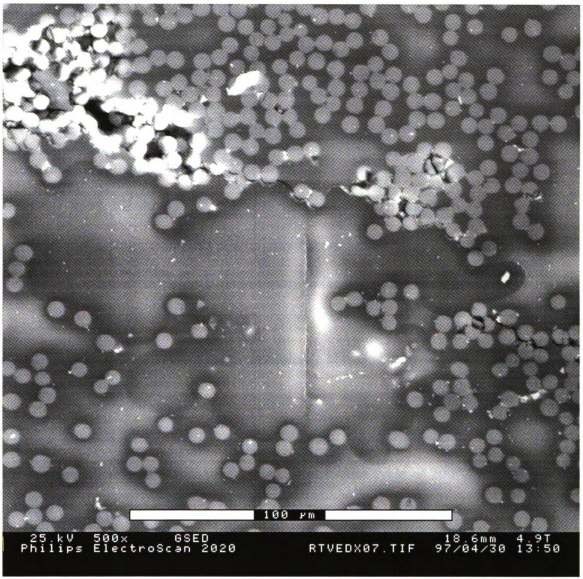

Figure 7-12 A Microcrack Within the RTV Sized Cross-Ply Composite
(The outer plies run in the direction of the 100 micron bar)

7.4 Measurement of Adhesion Levels for Treated and Sized Fiber Composites

The effect of increased levels of commercial surface treatment was measured by use of the interfacial testing system (ITS), and by ESEM analysis of a Mode I crack opening failure.

7.4.1 Unidirectional Specimen Manufacture

Unidirectional specimens were made using the three types of thermoplastic sized fiber, the 400% treated fiber, and the air plasma treated fiber, as well as the baseline 100% treated and unsized fiber. The specimens were made by placing three inch lengths of the fiber tows in a silicone mold. The mold had previously been post-cured at 200°C and thus was stable for the 177°C cure used here. BMI resin was then heated to 130°C, degassed in a vacuum oven, and poured over the pre-heated molds. The molds were then placed in the vacuum oven and degassed more to facilitate wetting of the fibers.

The molds were then placed in the programmable Nitrogen purged oven an subjected to a 177°C cure for 90 minutes. The thermal cycle was verified using a thermocouple attached to a data logging computer. After this cycled, the specimens were removed from the molds and were subjected to the standard post-cure cycle of 200°C for 2 hours and 250°C for 6 hours. All ramp rates were 5°C/min. Finally, the specimens were removed and ½" pieces were cut for analysis. One piece of each was mounted in epoxy for ITS testing, while a similar piece was set aside for Mode I fracture and analysis.

7.4.2 ITS Testing

The ITS testing method was identical to that presented in Chapter 4. The results are provided in Table 7-4 and are plotted in Figure 7-13.

Table 7-4 ITS Results for Improvement Attempts

	DRY						
	RTV Sized	PES Sized	PEI Sized	5218 Sized	Air Plasma	Control	400% ST
IFSS (psi)	804	1314	867	986	1117	955	1324
Std. Dev.	230	203	164	231	207	247	260

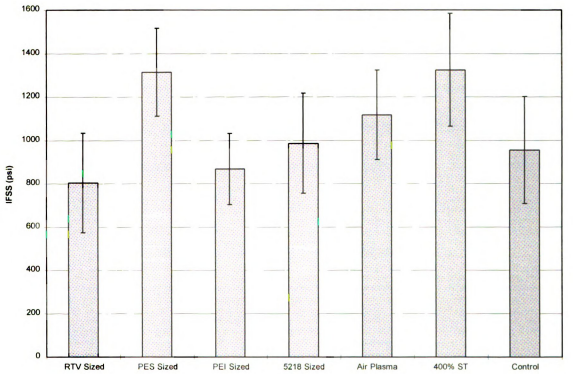

Figure 7-13 Plot of ITS Results for Treated and Sized Specimens

It can be seen that the adhesion levels are still very poor. The data scatter prevents any definite conclusions, but it is apparent that the PES sized fibers and the 400% treated fibers aided in the adhesion of the IM7 fiber to the BMI resin. The increase seen for the

400% treated fibers is attributed to an increase in the surface roughness because no chemical bonding is expected in this system as discussed earlier. The air plasma showed a slight increase which appears to track with the slight increase in oxygen content, but also can be explained as a surface roughness phenomenon. Air plasma treatment of carbon fibers is known to etch the fibers significantly.

Finally, the RTV sized specimens showed a small drop in the adhesion. This is expected because of the poor bonding generally experienced with silicones.

7.4.3 Mode I Failure Analysis

Small pieces of the unidirectional specimens were used for this analysis. Specimens were failed in a Mode I, crack-opening manner by initiating the crack with a razor blade and then forcing the specimen apart. This was performed by hand, so no mechanical data are available. One fractured surface was then analyzed in the ESEM. No surface coating or preparation was performed.

The objectives of the analysis were to determine the locus of failure around the fibers and note any differences in failure morphology which may provide information about the level of adhesion in the system. The conclusions of this study are provided in tabular form in , and then images supporting the conclusions are provided.

Table 7-5 Sizing Improvement Summary

	Adhesion Level	Failure Locus	Interdiffusion?
100% Unsized	Poor	Fiber/Matrix	---
400% Unsized	Improved	Fiber/Matrix	---
Air Plasma	Poor	Fiber/Matrix	---
Matrimid 5218	Poor	Fiber/Sizing	Yes
Ultem PEI	Poor	Sizing/Matrix	???
Victrex PES	Improved	Sizing/Matrix	Yes
GE RTV-31	Poor	Fiber/Sizing	No?

The failure of all of specimens, both sized and unsized, showed the same general appearance at relatively low magnifications as seen in Figure 7-14 and Figure 7-15. The

poor adhesion of the 100%, unsized control specimen and the air plasma treated specimen is shown in Figure 7-16. Figure 7-17 shows two images of 400% commercially treated fibers which exhibit better adhesion, although the adhesion is still generally poor.

The adhesion levels for the sized specimens are shown in Figure 7-17. It can be seen that there is poor adhesion in the Matrimid® 5218, PEI, and RTV sized systems. The PES system, however, exhibits evidence of better bonding. It is important to understand whether the failure was between the fiber/sizing interface, or the fiber/matrix interface, and to what level interdiffusion of the sizing occurred.

Regions in which the sizing existed as a second phase were found for the PES and Matrimid® 5218 systems. Close examination revealed good adhesion between the sizing materials and the BMI matrix as shown in Figure 7-18. The ductile failure mode of these materials is also obvious from the images.

To determine locus of failure of the sizing, beam etching was used. The beam was focused on the seemingly bare fibers at 80,000x, and allowed to heat the surface for approximately five minutes, or until damage was seen. Images of this for the various systems are provided in Figures 7-19 and 7-20. In Figure 7-19, it can be seen that the etched fiber showed no evidence of the presence of any polymer on it's surface. A region from which a fiber had been removed was etched next, showing a viscous flow of the polymer due to the beam. This suggests that the failure was between the fiber and sizing because the BMI resin itself will not flow, it will only thermally degrade.

In Figure 7-20, images of the regions before etching have been provided as part of Figure 7-17. It is seen that the PES sizing has adhered to the fiber, and there is some viscous nature to the matrix surrounding the fiber, suggesting interdiffusion of the polymers. The RTV sized specimen shows a region believed to be only sizing. No evidence of polymer on the fiber surface was seen after etching. When the sized region was etched, it exhibited shrinkage characteristics normally attributed to rubbers, and kept it's shape like a lightly cross-linked material would.

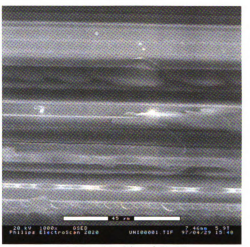

100%, UnSized IM7

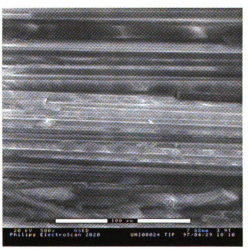

400% Commercial Treated IM7

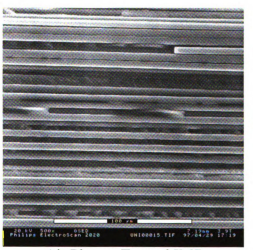

Air Plasma Treated IM7

Figure 7-14 General Images of Control, 400% and Air Plasma Treated Failure Modes

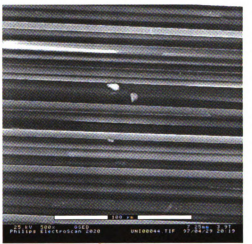

Matrimid® 5218 Sized IM7

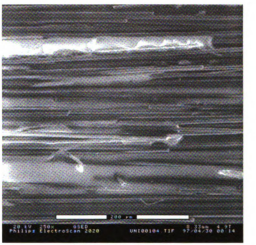

PES Sized IM7

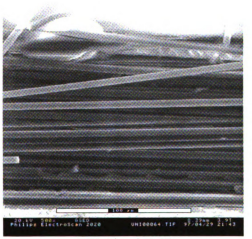

PEI Sized IM7

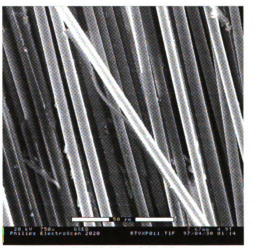

RTV Sized IM7

Figure 7-15 General Images of Sized Composite Failure Modes

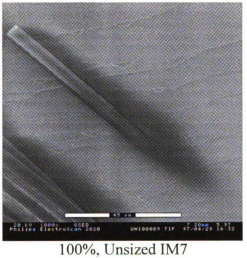

100%, Unsized IM7

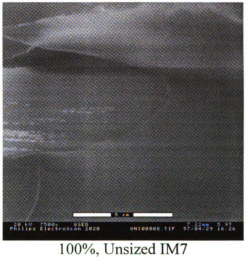

100%, Unsized IM7

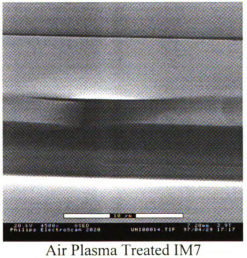

Air Plasma Treated IM7

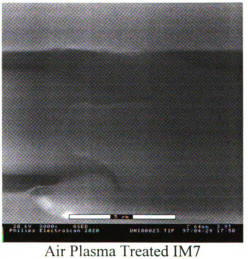

Air Plasma Treated IM7

Figure 7-16 100%, Unsized and Air Plasma Treated Mode I Failure Modes Showing Poor Adhesion Levels

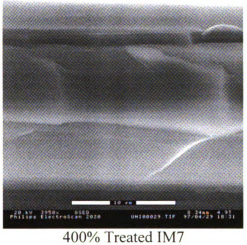

400% Treated IM7

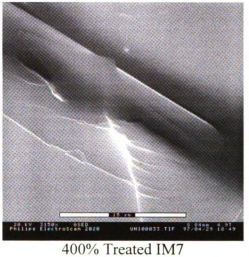

400% Treated IM7

Figure 7-17 400% Treated IM7 Mode I Failure Mode Showing Increased Adhesion

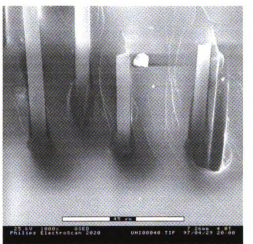

Matrimid® 5218 Sized Failure Mode

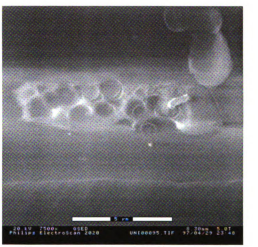

Victrex PES Sized Failure Mode

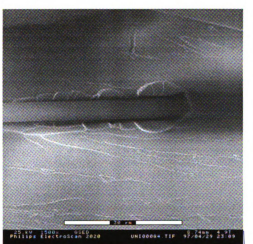

Ultem® PEI Sized Failure Mode

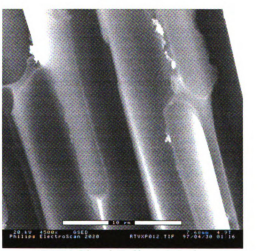

RTV Sized Failure Mode

Figure 7-18 Images Showing the Adhesion of the Sized Samples After Mode I Failure

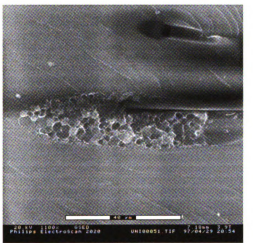

Matrimid® 5218 Sizing Failure

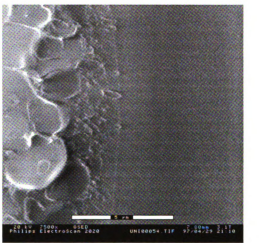

Matrimid® 5218 Sizing Failure

Victrex® PES Sizing Failure

Victrex® PES Sizing Failure

Figure 7-19 Regions Showing the Failure of PEI and 5218 Sizings Showing Adhesion Between the Sizing and BMI Matrix

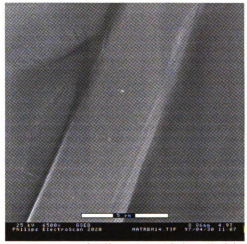

Beam Damaged Fiber (No Sizing Evident)

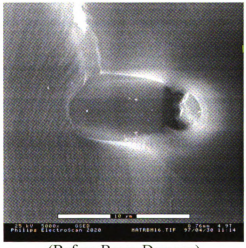

(Before Beam Damage)

Beam Damage Showing 5218 Sizing Adhered to BMI

Figure 7-20 Images Showing that the Failure in 5218 Sized Specimens is Between the Fiber and Sizing

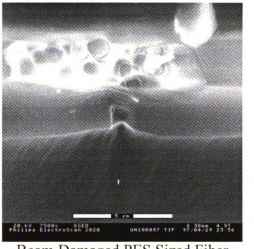

Beam Damaged PES Sized Fiber
Showing Good Adhesion

Beam Damaged RTV Sizing Showing
Rubber-Like Properties

Figure 7-21 Beam Damaged Regions of the PES and RTV Sized Specimens

7.5 Improvement Conclusions

All of the efforts presented in this chapter were designed to help improve the adhesion and reduce the microcracking observed in cross-ply laminates. The nature of the adhesion in the BMI/IM7 system was determined and discussed, and various attempts were made to improve the system. The following conclusions can be drawn.

- There is very little chemical bonding in this system as shown by the K3B model compound study. This is supported by TPD data which shows the evolution of a significant amount of the surface oxygen at processing temperatures.

- IM7 fibers subjected to 400% of the standard commercial treatment showed a very significant increase in surface oxygen content while the air plasma performed here showed only a marginal increase.

- IM7 fibers were successfully sized with PES, PEI, and the thermoplastic polyimide Matrimid® 5218.

- An RTV silicone was sized onto the IM7fibers, but the resulting morphology was poor. A cross-ply laminate made from the RTV sized fibers showed an ability to reduce microcracking, but the mechanism for this is believed to be due to both the presence of the sizing, and the formation of cracks due to resin shrinkage and the extremely poor adhesion in the sample.

- ITS testing showed an increase in adhesion for both the 400% surface treated and the PES sized fibers, while all other improvement attempts showed no significant effect.

- Failure analysis of Mode-I fractured specimens provided evidence supporting the ITS testing results. The failure locus for the PEI and PES was found to be between the sizing and matrix while the failure in the 5218 sized specimens showed failure between the fiber and sizing. Interdiffusion of the PES and 5218 was seen and a ductile failure mode was seen for the sizing material.

Chapter 8

THEORETICAL INTERPHASE DESIGN

8.1 Introduction

The experimental work in the previous four chapters has shown that the interfacial properties of composites has a dramatic effect on it's performance. It has been shown that the addition of an interphase in the form of a fiber sizing has great potential for improving both the adhesion of the system, and relieving thermally induced stresses. The ideal interphase will vary depending upon the fiber and matrix material being used, and the service environment for the final component. The interphase should be able to bond with the fiber and the matrix in addition to having specific physical properties. The choice of a sizing material which meets all of these requirements is a challenge for even the most experienced scientist. Thus, a systematic approach for designing these interphases is needed and has been created here and implemented within an artificial intelligence framework. The purpose of this work has been to illustrate the relationships involved in the engineering of an interphase and to introduce a methodology which can be utilized. The methodology is not meant to provide a prediction of interphase properties or performance. The purpose is not to review or comment on the artificial intelligence technique.

The original artificial intelligence framework was created as a tool for the design of basic composite materials based on service requirements. This intelligent decision support system, termed COMADE (Composite Material Designer), uses a combination of theoretical calculations and heuristic knowledge to select composite systems which meet the essential performance requirements. These resulting systems are defined by a Matrix Material, Chemical Agent, Fiber Type and Fiber Length [73]. While COMADE provides theoretically viable systems, there is no insurance that the chosen matrix material/chemical agent combination and fiber are sufficiently compatible to form a composite with acceptable properties.

In an effort to bridge the gap between the theoretical material combinations provided by COMADE and actual materials which meet the specified requirements, an Interphase Designer has been created to design the interfacial region (interphase) between the chosen fiber and matrix combination. With the proper specification of the interphase, a complete composite material system is defined. This specification can be used to point to actual commercial systems, or to steer research activity toward promising material combinations.

8.2 Definitions

There is a large amount of ambiguity in the terminology used to describe composite interphases. The following definitions are presented to clarify the exact meanings used here.

Binder - a material applied to the fiber directly after the manufacturing process. It can contain such things as starch, oils, polyvinyl alcohol or acetate, wetting agents, dispersing agents, cationic softeners, etc. Its purpose is to aid handling in subsequent operations, and to improve the wetting between the matrix and fiber.

Chemical Coupling Agent - any chemical substance designed to chemically react with both the fiber and matrix. For the purposes of this report, it is defined as a combination of three elements: the fiber functional group, the matrix functional group, and the connecting polymeric chain. Figure 8-1 shows the function of the chemical coupling agent. Note that the chemical coupling agent is one part of a sizing which will also contain a binder to promote wetting on the fiber, and various other components. The chemical coupling agent usually represents about 3-5% by weight of the sizing.

Finish - a finish commonly refers to the coating applied to *carbon* fibers at the time of manufacture. It is a film former whose purpose is to bind the fibers together, protect them during future operations, and promote wetting. In this report, the *overall* coating applied to carbon fibers will be called a sizing. The binder portion of the sizing represents what is commonly referred to as a finish.

Functional group - any chemically reactive species. It may be attached to either an organic chain (polymer), or a fiber surface.

Interphase - the material between the bulk fiber and bulk matrix. It has a different composition than the matrix, and thus different properties. It usually measures anywhere from 3 - 1000Å in thickness. By tailoring the properties of the interphase, the properties of the overall composite can be changed dramatically.

Sizing - a material applied to fibers during the final stages of manufacture. It contains a variety of components which are often proprietary. The most important of these components are: lubricants, antistatic agents, binders, and chemical coupling agents. The binder and chemical coupling agent are of greatest importance for this project. A sizing usually refers to the coating applied to *glass* fibers. For this report, a sizing will be defined as the combination of binder, chemical coupling agent, lubricant, and antistatic agents used on *any* fiber. Sizings are usually applied to fibers to about 1% of the fiber weight.

8.3 Theoretical Approach - Interphase Design

The interphase in a composite material is defined as the material which exists between the fiber surface and bulk matrix. The role of this interphase in composite materials has been well documented by various authors [6, 8-11, 43, 49, 74-77] It may be a sizing which has been applied to the fiber, or just an extension of the bulk matrix material which has varied properties due to it's proximity to the fiber. The Interphase Designer builds a definition of a specific interphase material by providing a set of characteristics which should cause

it to adhere well to both the fiber and matrix suggested by COMADE. The interphase designed here is based upon the model shown in Figure 8-1.

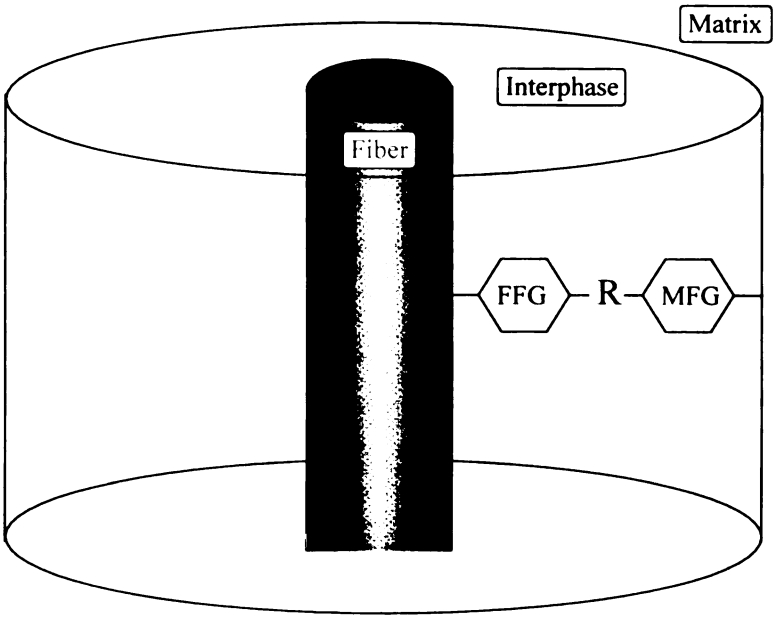

FFG = Fiber Functional Group
MFG = Matrix Functional Group
R = A Polymeric Chain

Figure 8-1 Function of the Chemical Coupling Agent

The interphase consists of three major components which are the binder, the coupling agent, and a surface treatment for the fiber. The role of the binder is to transport the functional groups of the coupling agent to both the fiber surface and the matrix material. It also provides any mechanical properties required of the interphase. The coupling agent is responsible for chemically adhering to the fiber surface and matrix material. Surface treatment is required in many cases to alter the concentration and types of functional

groups on the fiber surface. The importance of utilizing appropriate surface treatments was shown in Chapter 7.

Since the most challenging part of defining an interphase is determining what combination of binder, coupling agent, and surface treatment will adhere to both the fiber and matrix, the adhesion between polymers and fiber surfaces is reviewed as well as the adhesion between two polymers.

8.3.1 Polymer/Fiber Adhesion

The adhesion of a polymer to a fiber is governed by both chemical and physical interactions. The chemical interaction is brought about by either the chemical bonding of the polymer to functional groups present on the fiber surface, or secondary interactions between the two species. Both covalent and ionic chemical bonds are extremely strong (39-111 kcal/mol). Secondary interactions are much weaker (2-6 kcal/mol), but can play a significant role[78]. These interactions include non-polar dispersive forces (van der Waals forces) and polar dipole interactions. In the Interphase Designer created here, functional group reactions are predicted by using references to cases where the reactions have been seen to occur. A degree of confidence is assigned to each reaction based upon how closely it fits the kinetic and thermodynamic environment of it's intended use. More detail of this approach is provided in Section 8.3.1.

The physical interaction is the anchoring of the polymer into the topographical features of the fiber surface. When the fiber surface is rough, the polymer can surround asperities on it's surface. When the composite is stressed, load is transferred to the fiber by the mechanical interlocking of the asperities and the polymer. In order for either the chemical, or the mechanical interactions to take place, the fiber and sizing must be in intimate contact.

The degree of intimacy between two surfaces can be gauged using the degree of wetting, which is a measure of the thermodynamic compatibility between the two surfaces and is a described using the surface free energies (γ) of the two materials. The surface free energy is a measurable quantity which can be broken into various components. A few different sets of components have been suggested. The most common components used are the polar (γ_p) and the dispersive (γ_d); where $\gamma_{tot} = \gamma_p + \gamma_d$. Other researchers have added a third component to the system, the hydrogen bonding component γ_H. Yet other researchers suggest that the surface energy should be measured in terms of it's Lewis acid-base character. While all methods have their benefits this knowledge based system requires data to be available on a large variety of materials, and since the majority of the available data is for the polar and dispersive components, they have been utilized here.

Once the two components of the surface energy are known, a specific set of logic must be applied to try to ensure the wetting of the two components. For the best wetting in a fiber/matrix system, the total surface free energy of the fiber should be greater than that

of the matrix ($\gamma_{tot,\ fiber} > \gamma_{tot,\ matrix}$), and the ratio γ_p/γ_d for the two materials should be as nearly equivalent as possible [79].

8.3.2 Polymer/Polymer Adhesion

The adhesion of two polymers also involves both chemical and mechanical interactions. The chemical interactions are similar to those described above and are dominant in the bonding of thermosetting polymers. physical interactions arise from the entanglement of the polymeric chains and are the dominant mechanism in the adhesion of thermoplastics. To properly define the adhesion between two polymers, one must define both the reactive functional groups, and the capability of the polymers' chains to entangle.

The intermingling of two polymers can be described by their miscibility. Two polymers which are highly miscible will have well entangled chains, and thus have a high degree of mechanical integrity. The miscibility of polymers can be estimated using the concept of a miscibility parameter. The concept of such a parameter, and the solubility parameters used to calculate it has been reviewed by David and Sincock [80].

Solubility parameters of a polymers can be estimated using various methods [80]. These method can be used to calculate a solubility parameter for a polymer by using a group contribution theory which assumes additivity of the molar attractive forces of the various groups which make up the polymer structure. Because this contribution theory does not allow for the steric effects which occur when the groups are bonded to one another, it is

important to calculate the polymer solubility parameter based upon the largest contributing groups for which data exists.

The general relationship for determining the solubility parameter of a compound is given in Equation 8-1 where F_i is the molar attraction constant of group i, and V is the molar volume.

$$\delta = \sum \frac{F_i}{V} \qquad \textbf{Eqn. 8-1}$$

The solubility parameter may have contributions from various components, in a manner similar to the various surface free energy components. These components are combined according to Equation 8-2, giving a solubility parameter for the polymer as a whole.

$$\delta_t^2 = \delta_d^2 + \delta_p^2 + \delta_h^2 \qquad \textbf{Eqn. 8-2}$$

where d, p, and h represent the dispersive, polar, and hydrogen bonding components of the solubility parameter.

Once the solubility parameters for two materials are known, the enthalpy of mixing per unit volume is calculated according to Equation 8-3.

$$\Delta H_m = \phi_1 \phi_2 \left(\delta_1 - \delta_2\right)^2 \qquad \textbf{Eqn. 8-3}$$

where ϕ_1 and ϕ_2 are the volume fractions of components 1 and 2, and δ_1 and δ_2 are their solubility parameters. The Gibbs free energy of mixing is given by Equation 8-4, and when negative is indicative of a spontaneous event.

$$\Delta G_m = \Delta H_m - T\Delta S_m \qquad \textbf{Eqn. 8-4}$$

where T is temperature and ΔS_m is the entropy of mixing. Since the mixing of two components increases the entropy of the system as a whole, ΔS_m is positive and there is an entropic driving force for mixing. Thus, if ΔH_m is sufficiently small, mixing will be thermodynamically favored, and given no kinetic hindrances, will occur.

The concept of a miscibility parameter based upon the enthalpy of mixing is therefore utilized, as shown in Equation 8-5.

$$MP = \left(\delta_1 - \delta_2\right)^2 \qquad \textbf{Eqn. 8-5}$$

For mixing to occur, MP must be as small as possible [80].

8.4 Implementation

The Interphase Designer uses a hierarchical knowledge structure based upon matching tables. The logic used to translate the knowledge from the individual materials into the

definition of an appropriate sizing is reviewed here. A schematic of the variable dependencies used in COMADE and the Interphase Designer is provided in Figure 8-2.

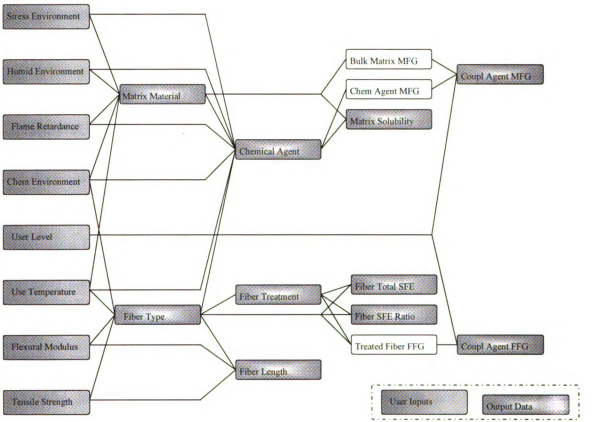

Figure 8-2 COMADE and Interphase Designer Variable Dependencies

The matching tables used for the addition of the Interphase Designer were created using data found in reference books and published literature for the surface energetics, miscibility parameters, and functional group reactions discussed in the previous section. Since the data available in the literature is often lacking, or only partially applicable to the system of interest, a method was introduced which takes into count the confidence of the data desired by the user.

8.4.1 Functional Group Reactions

The reaction between the functional groups of the coupling agent, and the functional groups present on the fiber, or in the resin are accounted for using a set of confidence levels based upon the similarity between known reactions and the desired reaction in terms of chemical and physical environment. Four confidence levels were chosen: Commercial, High, Medium, and Low. Commercial confidence will provide the user with results based upon reactions which are known to exist commercially, with available references cited. The High confidence level will provide the user with systems which are based upon reactions between the two species in the form of interest (solid surface or polymer) and in environments very similar to those used in the processing of the composite. Thus, extrapolation to the composite system of interest should be safe. The Medium confidence level allows for data in which the reactions have been shown to be successful in the form of interest, but the environment was not the same as the environment of interest. For example a reaction could be known to occur at a temperature of 200°C, but the composite fabrication is formed at only 120°C, so the viability of the reaction is uncertain.

The Low confidence level allows data for which the reactions have been shown to occur in solution chemistry, or under very different conditions. In this case the composite processing conditions would be quite different, and there is a good chance that the reaction would not occur.

8.4.2 Miscibility Data

The miscibility data is used to design an interphase by determining the solubility parameter for the matrix material and requiring the solubility parameter of the binder to be as close to this as possible. This results in the smallest miscibility parameter, and thus the best intermingling of polymer chains.

8.4.3 Fiber Surface Treatments

The fiber surface treatments are implemented within the framework by the thermodynamic description of their surface energies, and the functional groups which are present upon the surface after treatment. The surface energies ultimately provide a range for the total surface energy of the binder. The fiber functional groups are used to suggest coupling agent functional groups which will react with the species on the fiber.

8.4.4 Data Contained Within the Tables.

The matching tables used within the program of COMADE were generated using data for gathered for reactions between the utilized functional groups. Miscibility parameters were gathered for the polymers, and information concerning the functional groups present after the various surface treatments was found. The functional groups used within this study are provided in Table 8-1 which also presents the references upon which these were based.

Table 8-2 shows the solubility parameters for the various resins as calculated using group contribution theory. Finally, the surface free energies for the various functional groups is provided in Table 8-3.

Table 8-1 Functional Group Reactions Used in COMADE

	Amine	Vinyl	Carboxylic Acid	Mercaptan	Chloroalkyl
Amine	N				
Vinyl	Y [86,p689]	Y			
Carboxylic Acid	Y [83, p92]	N	N		
Mercaptan	N	N [86, p687]	?	Y	
Chloroalkyl	Y [83, p104]	N	N [86, p353]	Y [86, p362]	N
Alcohol	N 7[87, p11] A	N	Y [81, p6]	N [86, p361]	Y [82, p258;281]
Nitrile	N [86, p803] B	N	Y [86, p870]	Y	Y [86, p872]
Isocyanate	Y	N	Y [84, p125]	?	?
Epoxy	Y [83, p134]	N	Y [88, p47]	Y [89, 86 p360]	Y [89, 88 p37]
BMI	Y [83, p161]	Y [84, p255]			
Keytone	Y [87, p11]				

	Alcohol	Nitrile	Isocyanate	Epoxy	BMI
Amine					
Vinyl					
Carboxylic Acid					
Mercaptan					
Chloroalkyl					
Alcohol	N				
Nitrile	Y	N			
Isocyanate	Y [83, p136]	N	N		
Epoxy	Y [85, p438]	?	Y [89, 88 p48]	Y 9	
BMI					Y
Keytone	Y [83, p3]				

Table 8-2 Resin Solubility Parameters Used in COMADE

RESINS				CHEMICAL AGENTS	
Semi-Crystalline Thermoplastics		**Thermoset Epoxies**		**For Thermoset Epoxies**	
PBT	10.83	DGEBA	8.32	DEAPA	10.06
PA66	10.28	EpoxPhenNov		Dicyandiamide	
PET	11.72	TGMDA	9.06	MPDA	10.44
PPO	8.59	TGETPE	8.42	Chlorendic Anhydride	
PPS	10.60			DDS/BF3-MEA	10.74
PEEK	10.39				
		Phenolics		**For Phenolics**	
Amorphous Thermoplastics		Novolac		HMTA	17.64
ABS		Resole			
PC	9.39				
PSU	9.53	**Polyesters**		**For Polyesters**	
PAS		Orthophthalic		DAP	9.88
PEI	11.45	Isophthalic		Vinyl Toluene	8.56
PAI		Vinyl Ester		Styrene	8.47
		BPA Fumarate			
Blend Thermoplastics		Chlorendic			
ABS/PBT					
PC/PBT	10.11	**Bismaleimides**		**For Bismaleimides**	
PC/ABS		44MDA BMI	13.19	Dicyanate BPA	21.03
				00DiallylBPA	9.70
				MABA	12.86
				1,4Tolyl BMI	14.18
		Polyimides		**For Polyimides**	
		PMR15	10.70	MeOH	16.17
		Thermid 600	10.26	EtOH	13.68

All values expressed in $cal^{1/2}cm^{3/2}/mol$

Table 8-3 Functional Group Surface Free Energies

Temperature (°K)	298			Temperature (°K)	398		
	dH	dS	dG		dH	dS	dG
Alcohol	-41.56	1.28	-45.3744	Alcohol	-41.56	1.28	-46.6544
Amines				Amines			
Primary	2.82	2.71	-5.2558	Primary	2.82	2.71	-7.9658
Secondary	12.93	3.16	3.5132	Secondary	12.93	3.16	0.3532
Tertiary	19.46	3.82	8.0764	Tertiary	19.46	3.82	4.2564
Carboxylic Acid	-98.39	2.86	-106.9128	Carboxylic Acid	-98.39	2.86	-109.7728
Chloroalkyl	-8.25	0	-8.25	Chloroalkyl	-8.25	0	-8.25
Epoxy	12.86	-0.63	14.7374	Epoxy	12.86	-0.63	15.3674
Mercaptan	-10.68	1.07	-13.8686	Mercaptan	-10.68	1.07	-14.9386
Nitrile	30.75	-0.72	32.8956	Nitrile	30.75	-0.72	33.6156
Vinyl (H_2C=CH-)	13.737	1.655	8.8051	Vinyl (H_2C=CH-)	13.737	1.655	7.1501
Water	-58.076	1.154	-61.51492	Water	-58.076	1.154	-62.66892
Ester	-92.62	2.1	-98.878	Ester	-92.62	2.1	-100.978
Ammonia	-11.606	2.556	-19.22288	Ammonia	-11.606	2.556	-21.77888
Methane	-18.948	2.225	-25.5785	Methane	-18.948	2.225	-27.8035
Methyl	-10.943	2.215	-17.5437	Methyl	-10.943	2.215	-19.7587
Ether	-15.79	-0.85	-13.257	Ether	-15.79	-0.85	-12.407
Aldehyde	-29.28	0.77	-31.5746	Aldehyde	-29.28	0.77	-32.3446
Ketone	-28.08	0.91	-30.7918	Ketone	-28.08	0.91	-31.7018
Carboxylic Acid	-87.66	2.473	-95.02954	Carboxylic Acid	-87.66	2.473	-97.50254

All values in dyn/cm

8.5 Future work

The presentation of specific materials which meet the users requirements has been alluded to a number of times in this discussion. The implementation of this requires the addition of essentially two more logical modules to the system as it exists. The function of the modules would be to match the description of the sizing to actual sizings, and having done this, to match the fiber type, fiber length, matrix, chemical agent, and sizing to commercially available composite materials. The two modules would be programmatically quite different than the Interphase Designer in that they would essentially be an interface to a large database using a SQL (Structured Query Language)

request for records matching the criteria. It is envisioned that ultimately, a very large, encompassing database will exist, and that this type of information will be readily available.

These two modules have been termed the "Interphase Critique" and "Composite Critique." Logic flows for them are provided in Figures 8-3 and 8-4.

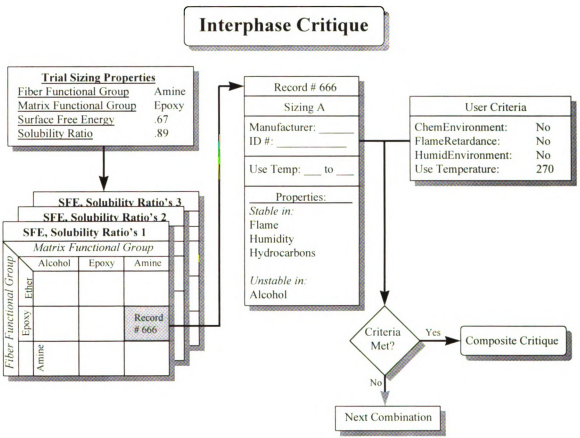

Figure 8-3 Logic Flow for the Interphase Critique

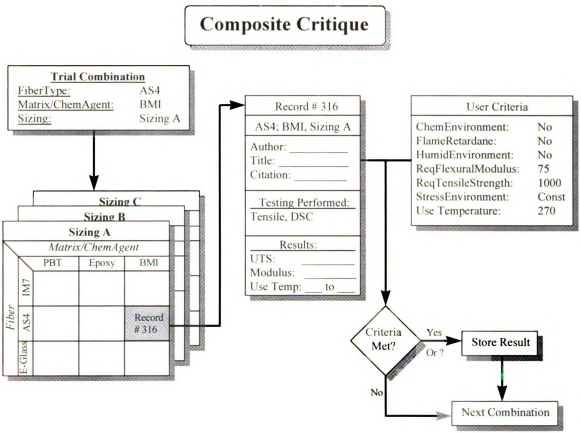

Figure 8-4 Logic Flow for the Composite Critique

8.6 An Example and Conclusions

With the understanding of the interphase's adhesion mechanisms with both the bulk matrix and fiber provide here, it follows that an appropriate interphase is sufficiently defined by surface energetics (γ_{tot}, γ_p/γ_d), a solubility parameter, and a chemical coupling agent containing a fiber functional group to react with the fiber and a matrix functional group to react with the matrix.

A diagram showing the information flow for a simple example is shown in Figure 8-5. In this figure, the Interphase Critique, and Composite Critique have been lumped into a black box called the Current Material Database. The user needs a material which has a minimum tensile strength of 1000 MPa, a minimum flexural modulus of 200 GPa, at a maximum temperature of 80°C in a constant stress environment. Amongst other combinations, COMADE suggests an epoxy matrix of DGEBA (diglycidylether of bisphenol A) with a DEAPA (diethylaminopropylamine) chemical agent and continuous AS4 carbon fiber.

One of a multitude of the interphase options suggested by the Interphase Designer is specified as having no fiber surface treatment, γ_{tot} >56 dyn/cm, $\gamma_p/\gamma_d \cong 1.154$, $\delta \cong 8.32$ $cal^{1/2}cm^{3/2}$, and a coupling agent consisting of carboxylic acid and amine functional groups. This information will then be used to probe a material database for commercially available systems shown to actually meet the original requirements. The interested researcher will be able to find the material combinations which have not been researched.

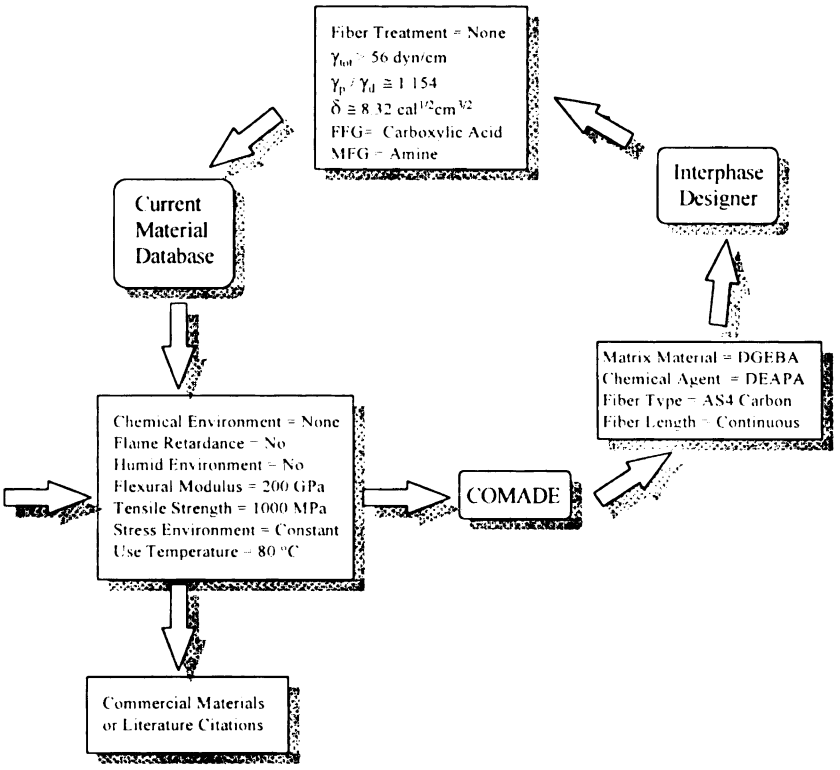

Figure 8-5 Information Flow for COMADE and the Interphase Designer

The COMADE and Interphase Designer system is currently operational for most of the common composite fibers and matrices. Data for some of the less common materials still needs to be researched. A future expansion will utilize the current results to provide industrial users with commercially available materials which meet their requirements. Academic or industrial researchers will be provided with literature citations related to the specific composite systems suggested, and will be able to quickly determine if there is a need for further research.

Chapter 9

CONCLUSIONS AND FUTURE RECOMMENDATIONS

This research has provided a great deal of insight into the hygrothermal properties of the Matrimid® 5292 BMI system. This chapter will attempt to present the conclusions to be drawn from the research as a whole. Conclusions concerning specific details of the studies were presented at the end of each chapter, and are not necessarily repeated here.

9.1 Microcracking Conclusions

At the macroscopic level, it was seen that advancing cure in the BMI system causes a general reduction in properties and partially cured resin will continue to cure at anticipated use temperatures. The increase in cure was also shown to cause an increase in the moisture diffusion rate and ultimate moisture content.

A mechanism for the cure induced microcracking was presented. It is shown that microcracking is due to a combination of two mechanisms. One results from a ply level thermal expansion mismatch between the 0° and 90° ply orientations in a cross-ply laminate. Other stresses are caused by a thermal expansion mismatch between the transverse expansion of the fiber, and the expansion of the matrix. Two models were

utilized to show that a reduction in the residual stresses induced by the cure cycle can be obtained by a variety of methods. These methods include a reduction in the stress free temperature; use of high volume fraction composites; and the addition of a compliant interphase. The addition of an interphase has the added potential of increasing the adhesion of the system which was shown to be inherently very poor.

9.2 Physical Property Conclusions

Both increased cure and the presence of moisture were shown to be detrimental to the performance of BMI resin. In addition, it was seen that the moisture had a more detrimental effect on the performance of partially cured resin specimens. The decreases in performance of the resins due to the presence of moisture were also found to be fully recoverable. Composites, on the other hand, were insensitive to the presence of moisture.

Thermal spiking of both wet and dry BMI specimens between room temperature and 250°C was shown to have very little effect on properties, at least for short term tests involving a relatively small number of cycles. Dry K3B resin and composites showed the same lack of sensitivity to thermal spiking, but wet K3B specimens cycled to 250°C were shown to fail a catastrophically. This is attributed to stresses caused by the escaping moisture. Since this temperature is above T_g for K3B, the stresses were easily able to deform the material causing excessive damage. It is felt that this should not occur below the wet T_g of the resin.

9.3 Interfacial/Adhesion Conclusions

The interfacial adhesion in the BMI/IM7 system was seen to be very poor both in failure analysis of flexure and Mode I fractured specimens and through direct testing of the interfacial properties via ITS. The presence of moisture showed a detrimental effect on adhesion both through a reduction in the measured interfacial shear strength of partially cured resin specimens, and by causing interfacial failure in unstressed samples for fully cured and saturated specimens. The adhesion that does exist in this system is believed to be due to mechanical interactions between the fiber surface and matrix, not because of chemical bonding.

Attempts at improving the adhesion of the BMI/IM7 system were made by both fiber surface treatment and the addition of sizings. Fibers treated with 400% of the commercial treatment and those sized with PES were shown to cause an improvement in adhesion. The improvement due to the commercial treatment is attributed to an increase in fiber surface roughness which aids in the mechanical bonding of the system.

9.4 Recommendations for Future Studies

This research is part of an ongoing study of these materials, so the efforts begun here will be very useful for steering this continuing effort.

First, the microcracking in this system was seen to be a strong function of the stress free temperature, and stepped post-cures were seen to be at least moderately successful at reducing it. It is felt that significant reductions in the SFT may be achieved by using stepped cure cycles. By creating a gelled network at a lower temperature, the stresses caused during the subsequent, necessary, post-cures may be reduced. The vertical heating stage which was manufactured will allow the efficient investigation of this.

The thermal spiking here showed very little effect, but the number of cycles was very small so longer term testing is required. The open-hole compression tests showed some response to wet cycling for the BMI system suggesting cumulative damage at the edge of these composites. More testing should be performed in which the holes are cut into the composite both before and after conditioning. This will reveal whether the loss in properties is an edge effect.

Since the K3B specimens failed during the tests above T_g, testing should be performed below T_g to determine if this catastrophic failure is possible for wet specimens below the resin's wet T_g (in the region of component service).

The dynamic mechanical tests on wet BMI/IM7 specimens showed an increase in the viscoelastic nature of the system while the resin alone showed a decrease in its viscoelastic nature. This suggests either a mechanical constraint caused by the fibers and expansion of the resin, or a change in the adhesion of the system. This should be

investigated because this may be a useful method for characterizing composite interfacial bonding.

The 400% surface treated and PES sized fibers showed an increase in the adhesion of the system and should be investigated further. A more controlled sizing method should be used and should not be difficult to achieve. A sizing using a lower molecular weight of PES should be investigated. This may allow increased interdiffusion with the BMI resin which should further increase the adhesion. A combination of the 400% fiber treatment and the PES sizing should also be attempted.

Finally, the knowledge base for the expanded COMADE system should be filled further, and the concepts of the Interphase Critique and Composite Critique should be implemented. The methodology presented within this study should be investigated further, and expansions should be made to include such appropriate things as fiber morphology, processing temperatures/environments, and many of the other things known to affect the adhesion at the interphase.

APPENDICES

APPENDIX A

Appendix A

TABULAR BMI RESIN TEST DATA

Table A-1 Three Point Flexural Data for BMI Resin

Cure Cycle	Flexural Strength	Std. Dev.	Flexural Modulus	Std. Dev.	Flexural Failure Strain (%)	Std. Dev.	Tg From Peak of Tan Delta
Low Short	150	12	4368	159	3.8	0.558	180
Low Long	159	13	4009	11	4.34	0.424	197
Std. Short	143	7	3665	193	4.09	0.342	262
Std. Long	113	7	3573	28	3.15	0.181	313
High Short	138	21	3965	23	4.13	0.902	343
High Long	107	34	3846	97	2.98	1.188	351

Table A-2 Tensile Data for BMI Resin

Cure Cycle	Tensile Strength	Std. Dev.	Tensile Modulus	Std. Dev.	Tensile Failure Strain (%)	Std. Dev.
Low Short	69	15.8	2293	201	3.43	0.732
Low Long	77	5	2274	120	3.96	0.269
Std. Short	76	4.7	2275	185	3.99	0.587
Std. Long	94	6.1	1828	23.6	6.66	0.5
High Short	36	3.8	2024	46.6	1.893	0.258
High Long	58	2.6	1683	12.7	4.23	0.085

Where:
Low Short = 177°C/90min + 200°C/1hr
Low Long = 177°C/90min + 200°C/3hr
Std. Short = 177°C/90min + 200°C/2hr + 250°C/1hr
Std. Long = 177°C/90min + 200°C/2hr + 250°C/6hr
High Short = 177°C/90min + 200°C/2hr + 250°C/6hr + 300°C/1hr
High Long = 177°C/90min + 200°C/2hr + 250°C/6hr + 300°C/6hr

APPENDIX B

Appendix B

MOISTURE ABSORPTION STUDY DATA

Table B-1 Summary Data from 100°C Moisture Absorption Experiment

Summary of 100C Moisture Absorption Experiment								
Condition	Maximum Moisture %	Std. Dev.	Diffusivity	Std. Dev.	C	Std. Dev.	Rsquared	Std. Dev.
100C BMI Resin Low Cure	3.783%	0.006%	9.014E-08	5.08E-09	0.677	0.002	0.9990	0.0001
100C BMI Resin High Cure	5.003%	0.021%	1.166E-07	1.35E-08	0.712	0.004	0.9990	0.0001
100C BMI X-ply	1.573%	0.009%	1.222E-06	2.39E-07	0.331	0.021	0.9961	0.0004
100C BMI Undirectional	2.324%	0.133%	4.258E-08	1.80E-08	0.580	0.103	0.9984	0.0003
100C K3B Resin	1.615%	0.026%	2.322E-06	2.39E-07	0.701	0.012	0.9985	0.0003
100C K3B-IM7 X-ply	0.538%	0.011%	9.427E-08	8.95E-09	0.667	0.025	0.9975	0.0009
100% Resin Equivalent for Composite Data								
100C K3B-IM7 X-ply	1.063%	0.025%	9.430E-08	8.93E-09	0.667	0.025	0.9975	0.0009
100C BMI X-ply	4.266%	0.024%	1.220E-06	2.42E-07	0.330	0.021	0.9961	0.0004
100C BMI Undirectional	4.964%	0.068%	4.258E-08	1.80E-08	0.580	0.103	0.9984	0.0003

Table B-2 Summary Data from 70°C Moisture Absorption Experiment

Summary of 70C Moisture Absorption Experiment								
Condition	Maximum Moisture %	Std. Dev.	Diffusivity	Std. Dev.	C	Std. Dev.	Rsquared	Std. Dev.
70C BMI Resin Low Cure	3.306%	0.031%	2.369E-08	1.725E-09	0.653	0.004	0.9995	0.0000
70C BMI Resin High Cure	5.138%	0.027%	5.196E-08	2.743E-09	0.721	0.000	0.9989	0.0000
70C BMI X-ply	1.552%	0.019%	1.879E-06	1.200E-07	0.612	0.006	0.9933	0.0009
70C BMI Unidirectional	2.488%	0.062%	3.206E-08	5.275E-10	0.656	0.056	0.9984	0.0008
70C K3B-IM7 X-ply	0.548%	0.003%	3.383E-08	1.731E-09	0.672	0.003	0.9988	0.0002
70C K3B Resin	1.534%	0.011%	9.998E-07	3.688E-07	0.707	0.006	0.9986	0.0003
100% Resin Equivalent for Composite Data								
70C K3B-IM7 X-ply VfCor	1.084%	0.007%	3.383E-08	1.732E-09	0.672	0.003	0.9988	0.0002
70C BMI X-ply VfCor	4.210%	0.007%	1.879E-06	1.178E-07	0.612	0.006	0.9933	0.0009
70C BMI Unidirectional	5.099%	0.030%	3.206E-08	5.275E-10	0.656	0.056	0.9984	0.0008

APPENDIX C

Appendix C

DERIVATION FOR THE ERROR IN PERCENT CHANGE VALUES

The calculation of appropriate measures of the error associated with the percent difference in properties associated with the results of the Hygrothermal and Thermal Spike designed experiments is not simply the average of the two condition's standard deviations. A proper calculation of the error in this measure is provided here. In all cases, x represents a property such as the modulus, strength, or failure strain.

For the Hygrothermal study, the designations for the different conditions are shown in Table C-1, where all x_i are assumed to be independent.

Table C-1 Factor Level Designations for the Hygrothermal Experiments

Designation	Moisture	Volume Fraction	Extent of Cure
x_1	Dry	Low Vf	Partial Cure
x_2	Dry	Low Vf	Full Cure
x_3	Dry	High Vf	Partial Cure
x_4	Dry	High Vf	Full Cure
x_5	Wet	Low Vf	Partial Cure
x_6	Wet	Low Vf	Full Cure
x_7	Wet	High Vf	Partial Cure
x_8	Wet	High Vf	Full Cure

For the Hygrothermal experiment, the percent differences are calculated using Equation C-1.

$$f(x_1,\ldots,x_8) = \frac{x_1 - x_2}{\frac{1}{8}\sum_{i=1}^{8} x_i} \qquad \textbf{Eqn C-1}$$

To approximate the appropriate error associated with this, a Taylor series expansion (Equation C-2) is used. The series is truncated at the linear term for mathematical simplicity, but higher order terms should be negligible.

$$f(x_1,\ldots,x_8) \cong f(x_{10},\ldots,x_{80}) + \sum_{i=1}^{8}(x_i - x_{i0})\frac{\partial f}{\partial x_i}(x_{10},\ldots,x_{80}) + \ldots \qquad \textbf{Eqn C-2}$$

The derivative terms from Equation C-1 are:

$$\frac{\partial f(x_1,\ldots,x_8)}{\partial x_1} = 8\frac{2x_2 + \sum_{i=3}^{8} x_i}{\left(\sum_{i=1}^{8} x_i\right)^2} = 8\frac{\sum_{i=1}^{8} x_i + x_2 - x_1}{\left(\sum_{i=1}^{8} x_i\right)^2} \qquad \textbf{Eqn C-3}$$

$$\frac{\partial f(x_1,\ldots,x_8)}{\partial x_2} = -8\frac{2x_1 + \sum_{i=3}^{8} x_i}{\left(\sum_{i=1}^{8} x_i\right)^2} = -8\frac{\sum_{i=1}^{8} x_i + x_1 - x_2}{\left(\sum_{i=1}^{8} x_i\right)^2} \qquad \textbf{Eqn C-4}$$

$$\frac{\partial f(x_1,\ldots,x_8)}{\partial x_j} = 8\frac{x_2 - x_1}{\left(\sum_{i=1}^{8} x_i\right)^2} \quad \text{for } 3 \le j \le 8 \qquad \textbf{Eqn C-5}$$

Using the designations in Table C-1, the percent change in property by moving from Partial to Full Cure for the Dry, Low Vf specimens is represented by

$$\%Change = \frac{\bar{x}_1 - \bar{x}_2}{\frac{1}{8}\sum_{i=1}^{8} \bar{x}_i}, \qquad \textbf{Eqn. C-6}$$

and the variance of this is given by

$$Var\left[\frac{(\bar{x}_1 - \bar{x}_2)}{\frac{1}{8}\sum_{i=1}^{8} \bar{x}_i}\right] = \frac{64}{\left(\sum_{i=1}^{8} \bar{x}_i\right)^4}\left[\frac{s_1^2}{n_1}\left(\sum_{i=1}^{8} \bar{x}_i + \bar{x}_2 - \bar{x}_1\right)^2 + \frac{s_2^2}{n_2}\left(\sum_{i=1}^{8} \bar{x}_i + \bar{x}_1 - \bar{x}_2\right)^2 + (\bar{x}_1 - \bar{x}_2)^2 \sum_{j=3}^{8} \frac{s_j^2}{n_j}\right]$$

Eqn. C-7

where s_i and n_i are the sample deviation and size for condition i, respectively. $\frac{s_i^2}{n_i}$ is the variance. The errors shown for the percentage changes reported in this study all represent the square root of this variance which is approximation of it's standard deviation.

This same analysis can be easily adapted for the Thermal Spike experiments. For this case, instead of a three factor designed experiment, a two factor designed experiment was used. Equation C-8 results from a derivation very similar to that shown above. Again, the square root of this variance is used as an approximation of the standard deviation of the percent change.

$$Var\left[\frac{(\bar{x}_1-\bar{x}_2)}{\frac{1}{4}\sum_{i=1}^{4}\bar{x}_i}\right]=\frac{16}{\left(\sum_{i=1}^{4}\bar{x}_i\right)^4}\left[\frac{s_1^2}{n_1}\left(\sum_{i=1}^{4}\bar{x}_i+\bar{x}_2-\bar{x}_1\right)^2+\frac{s_2^2}{n_2}\left(\sum_{i=1}^{4}\bar{x}_i+\bar{x}_1-\bar{x}_2\right)^2+(\bar{x}_1-\bar{x}_2)^2\sum_{j=3}^{4}\frac{s_j^2}{n_j}\right]$$

Eqn. C-8

The designations for the different factors in the Thermal Spike experiments are shown in Table C-2.

Table C-2 Factor Level Designations for the Thermal Spike Experiments

Designation	Moisture	Cycling
x_1	Dry	Control
x_2	Dry	Cycled
x_3	Wet	Control
x_4	Wet	Cycled

LIST OF REFERENCES

LIST OF REFERENCES

1. Roger J. Morgan, James E. O'Neal, and Dale L. Fanter, "The Effect Of Moisture On The Physical And Mechanical Integrity Of Epoxies," *Journal of Materials Science,* **15** (1980), pp. 751-764.

2. Roger J. Morgan, Robert J. Jurek; Anna Yen; and Tom Donnellan, "Toughening Procedures, Processing And Performance Of Bismaleimide-Carbon Fibre Composites," *Polymer*, **34 (4)** (1993), pp. 835-842.

3. H.H. Man, R.J. Morgan; and P.J. Hogg, "The Effects of Impact and Moisture Content on the Flexural Properties of Bismaleimide-Carbon Fiber Composites," *Advanced Composite Materials: New Developments and Applications Conference Proceedings,* Detroit, MI, Sept. 30-Oct. 3, 1991.

4. R. H. Pater, K. Whitley; C. Morgan and A. Chang, "Crosslinking-Property Relationships in PMR Polyimide Composites. Part I," *Polymer Composites,* **12 (2)** (1991), pp. 126-132.

5. Dick Cornelia, "Hygrothermal Performance Of Polyimides," *39th International SAMPE Symposium*, April 11-14, 1994, pp. 917-929.

6. Lawrence T. Drzal, "Adhesion of Carbon Fibers to Epoxy Matrices," Treatise on Adhesion and Adhesives Volume 6, ed. Robert L. Patrick, Marcel Dekker, Inc, 1989, pp. 187-211.

7. Nirmala P. Vaidyanathan, Vinayak N. Kabadi, Ranji Vaidyanathan, and Robert L. Sadler, "Surface Treatment of Carbon Fibers Using Low Temperature Plasma," *Journal of Adhesion,* **48** (1995), pp. 1-24.

8. Madhu S. Madhukar And Lawrence T. Drzal, "Fiber-Matrix Adhesion and Its Effect on Composite Mechanical Properties: I. Inplane and Interlaminar Shear Behavior of Graphite/Epoxy Composites," *Journal of Composite Materials,* **25** (1991), pp. 932-957.

9. Madhu S. Madhukar And Lawrence T. Drzal, " Fiber-Matrix Adhesion and Its Effect on Composite Mechanical Properties: II. Longitudinal (0) and Transverse (90) Tensile and Flexure Behavior of Graphite/Epoxy Composites," *Journal of Composite Materials,* **25** (1991), pp. 958-991.

10. Madhu S. Madhukar And Lawrence T. Drzal, " Fiber-Matrix Adhesion and Its Effect on Composite Mechanical Properties. III. Longitudinal (0) Compressive Properties of Graphite/Epoxy Composites," *Journal of Composite Materials,* **26** (1992), pp. 310-333.

11. Madhu S. Madhukar And Lawrence T. Drzal, "Fiber-Matrix Adhesion and Its Effect on Composite Mechanical Properties: IV. Mode I and Mode II Fracture Toughness of Graphite/Epoxy Composites," *Journal of Composite Materials,* **26 (7)** (1992), pp. 936-968.

12. Dupont Publication, "Properties and Characteristics of Avimid® K Composite Materials."

13. Lin Li, "Thermal Aging Properties Of Graphite Fiber Reinforced Peek And Graphite Fiber Reinforced BMI Composites," *Polym.-Plast. Technol. Eng.*, **29 (5&6)** (1990), pp. 549-562.

14. R.H. Pater, "Thermosetting Polyimides: A Review," *SAMPE Journal,* **30 (5)** (1994), pp. 29-38.

15. Roger J. Morgan, E. Eugene Shin, Boris Rosenberg, and Ann Jurek, "Characterization of the Cure Reactions of Bismaleimide Composite Matrices," *Polymer,* **38 (3)** (1997), pp. 639-645.

16. M. Chaudhari, T. Galvin, and J. King, "Characterization of Bismaleimide System, XU 292," *SAMPE Journal,* July/August 1985.

17. Roger J. Morgan and E. T. Mones, *J. Appl. Polym. Sci.*, **33** (1987), p. 999.

18. Mark S. Wilenski, MSU internal publication, "Test Data in Support of AFOSR Grant No. F49620-95-1-0129", 1997.

19. Chi-Hung Shen and George S. Springer, "Moisture Absorption and Desorption of Composite Materials," in *Environmental Effects on Composites, volume 2*, ed. G. S. Springer, Technomic Publishing Co., **15** (1981).

20. G. E. P Box, W. P. Hunter, and J. S. Hunter, Statistics for Experimenters, John Wiley & Sons, New York, 1978.

21. Donald F. Adams, "A Micromechanics Analysis of the Influence of the Interface on the Performance of Polymer-Matrix Composites," *Journal of Reinforced Plastics and Composites,* **6** (1987), pp. 66-88.

22. P. M. Jacobs, M. Simpson and F R. Jones, "Generation Of Thermal Strains In Carbon Fibre-Reinforced Bismaleimide (PMR-15) Composites: Part 1: The Determination of Residual Thermal Strains in Cross-Ply Laminates," *Composites,* **22 (2)** (1991).

23. F. R. Jones, M. Mulheron, J. E. Bailey, "Generation Of Thermal Strains In GRP Part 2 The Origin Of Thermal Strains In Polyester Cross-Ply Laminates," *Journal of Materials Science,* **18** (1983), pp. 1533-1539.

24. J. M. Whitney, I. M Daniel, and R. B. Pipes, Experimental Mechanics of Fiber Reinforced Composite Materials, Revised Edition, Prentice-Hall, Inc., Englewood Cliffs, New Jersey, 1984.

25. B. Cunningham, J. P. Sargent, K. H. G. Ashbee, "Measurement Of The Stress Field Created Within The Resin Between Fibres In A Composite Material During Cooling From The Cure Temperature," *Journal of Materials Science,* **16** (1981), pp. 620-626.

26. Catherine A. Bigelow, "The Effects of Uneven Fiber Spacing on Thermal Residual Stresses in a Unidirectional SCS-6/Ti-15-3 Laminate," *Journal of Composites Technology and Research,* **14 (4)** (1992), pp. 211-220.

27. R. C Averill. and G. P. Carman, "Analytical Modeling of Micromechanical Stress Variations in Continuous Fiber-Reinforced Composites," *IUTAM Symposium on 'Local Mechanics Concepts for Composite Material Systems,'* (1991), pp. 28-31.

28. R. M. Jones, Mechanics of Composite Materials, Scripta Book Co., Washington, 1975, p176.

29. Alfred C. Loos and George S. Springer, "Effects of Thermal Spiking on Graphite-Epoxy Composites," *Journal of Composite Materials,* **13** (1979), pp. 17-34.

30. E. L. McKague, Jr, J. E. Halkias and J. D. Reynolds, "Moisture in Composites: The Effect of Supersonic Service on Diffusion," *Journal of Composite Materials,* **9** (1975), pp. 2-9.

31. Mark L. Karasek, Larry H. Strait, Maurice F. Amateau and James P. Runt, "Effect of Temperature and Moisture on the Impact Behavior of Graphite/Epoxy Composites: Part I-Impact Energy Absorption," *Journal of Composites Technology and Research,* **17 (1)** (1995), pp. 3-10.

32. T.K. Tsotsis, Y. Weitsman, "Energy Release Rates for Cracks Caused by Moisture Absorption in Graphite/Epoxy Composites," *Journal of Composite Materials,* **24** (1990), pp. 483-496.

33. Q. Zheng and R. J. Morgan, "Synergistic Thermal-Moisture Damage Mechanisms Of Epoxies And Their Carbon Fiber Composites," Submitted to *Journal of Materials Science,* April 28, 1993.

34. F. R. Jones, M. Mulheron, J. E. Bailey, "Generation Of Thermal Strains In GRP Part 1 Effect Of Water On The Expansion Behavior Of Unidirectional Glass Fibre-Reinforced Laminates," *Journal of Materials Science*, **18** (1983), pp. 1522-1532.

35. Dick Cornelia, "BMI Mechanical Properties and Performance," Presented at High Temple Workshop XV.

36. D. S. Varma, H. L. Needles, D. A. Kourtides, and R. H. Fish, "Interlaminar Shear Properties of Graphite Fiber, High-Performance Resin Composites," *Polymer Composites,* **4 (2)** (1983), pp. 98-103.

37. Loyd J. Burcham, Mark R. Vanlandingham, Rushad F. Eduljee, and John W. Gillespie, Jr., "Moisture Effects on the Behavior of Graphite/Polyimide Composites," *Polymer Composites,* **17** (1996), pp. 682-690.

38. G. Wisanrakkit and J.K. Gillham, "The Glass Transition Temperature (Tg) As an Index of Chemical Conversion For a High-Tg Amine/Epoxy System: Chemical and Diffusion Controlled Reaction Kinetics," *Journal of Coatings Technology,* **62 (783)** (1990), pp. 35-50.

39. Jiming Zhou and James P. Lucas, "The Effects of a Water Environment on the Anomalous Absorption Behavior in Graphite/Epoxy Composites," *Composites Science and Technology,* **53** (1995), pp. 57-64.

40. Jiming Zhou and James P. Lucas, "Effects of Water on a Graphite/Epoxy Composite," *Journal of Thermoplastic Composite Materials,* **9** (1996), pp. 316-328.

41. Alfred C. Loos and George S. Springer, "Effects of Thermal Spiking on Graphite-Epoxy Composites," *Journal of Composite Materials,* **13** (1979), pp. 17-34.

42. E. E. Shin and R. J. Morgan, "Effects of Thermal Cycling on Mechanical Properties of High Temperature Bismaleimide (BMI)-Carbon Fiber Composites", ANTEC '93, pp. 1357-1363.

43. Venkatesh Rao And Lawrence T. Drzal, "The Dependence of Interfacial Shear Strength on Matrix and Interphase Properties," *Polymer Composites*, **12 (1)** (1991), pp. 48-56.

44. V. Rao and L. T. Drzal, "The Temperature Dependence of Interfacial Shear Strength for Various Polymeric Matrices Reinforced with Carbon Fibers," *Journal of Adhesion*, **37** (1992), pp. 83-95.

45. M. Pegoraro and L. Di Landro, "Influence of Components and Interface Conditions on Mechanical Properties of Composites and Blends," *Macromol. Symp.*, **70/71** (1993), pp. 193-212.

46. Gregory P. Carman, Ronald C. Averill, Kenneth L. Reifsnider, and J. N. Reddy, "Optimization of Fiber Coatings to Minimize Stress Concentrations in Materials," *Journal of Composite Materials*, **27 (6)** (1993), pp. 589-612.

47. G. Krekel, K. J. Huttinger, W. P. Hoffman, " The Relevance Of The Surface Structure And Surface Chemistry Of Carbon Fibres. In Their Adhesion To High Temperature Thermoplastics Part II Surface Chemistry," *Journal of Materials Science*, **29** (1994), pp. 3461-3468.

48. M. Nardin, E. M. Asloun, and J. Schultz, "Study of the Carbon Fiber-Poly(Ether-Ether-Ketone) (PEEK) Interfaces, 1: Surface Characterization of Fibers and Matrices, and Interfacial Adhesion Energy," *Polymers for Advanced Technologies*, **2** (1991), pp.109-114.

49. M. Nardin, E. M. Asloun and J. Schultz, "Study of the Carbon Fiber-Poly(Ether-Ether -Ketone) (PEEK) Interfaces, 2: Relationship Between Interfacial Shear Strength and Adhesion Energy," *Polymers for Advanced Technologies*, **2** (1991), pp. 115-122.

50. M. Nardin, E. M. Asloun, J. Brandt, H. Richter, and J. Schultz, "Study of the Carbon Fiber-Poly(Ether-Ether-Ketone) (PEEK) Interfaces, 4: Influence of Fiber-Matrix Adhesion on the Mechanical Properties of Unidirectional Composites," *Polymers for Advanced Technologies*, **2** (1991), pp.171-176.

51. R. A. Bucher and J. A. Hinkley, "Fiber/Matrix Adhesion in Graphite/PEKK Composites," *Journal of Thermoplastic Composite Material*, **5** (1992), pp. 2-13.

52. Ittipol Jangchud, R. K. Eby, A. M. Serrano, and M. A. Meador, "Studies of PAN-Based Carbon Fiber Surfaces: Their Influence on Interfacial Bonding with PMR-15 Polymide and Composite Thermo-Oxidative Stability," *Journal of Advanced Materials*, October (1996), pp. 19-25.

53. C. L. Heisey, P. A. Wood, J. E. McGrath, and J. P. Wightman, "Measurement of Adhesion Between Carbon Fibers and Bismaleimide Resins," *Journal of Adhesion,* **53** (1995), pp. 117-147.

54. S. O'Kell, and C. Jones, "A Study Of The Effects Of Low Power Plasma Treatment On Graphite And Highly Orientated Pyrolytic Graphite(HOPG)Surfaces," *Proceedings of the Eighteenth Annual Adhesion Society Meeting*, 1995, pp. 75-76.

55. Yu A. Dzenis, D. H. Reneker, V. V. Tsukruk, and R. Patil, "Fractal Analysis of Surfaces of Advanced Reinforcing Fibers by Atomic Force Microscopy," *Composite Interfaces,* **2 (4)** (1994), pp. 307-319.

56. Jean-Baptiste Donnet, Carbon Fibers, Marcel Dekker, New York, 1990.

57. Zhihong Wu, Charles U. Pittman, Jr., and Steven D. Gardner, "Nitric Acid Oxidation of Carbon Fibers and the Effects of Subsequent Treatment in Refluxing Aqueous NaOH," *Carbon,* **33 (5)** (1995), pp. 1-9.

58. Yue-Zhen Wei, Zhi-Qian Zhang, Yin Li, Zi-Hai Guo, Bai-Ling Zheng, " A Study Of The Interfacial Bonding Between Carbon Fibre And PMR 15 Resin," Controlled Interphases in Composite Materials, Hatsuo Ishida Editor, Elsevier Science Publishing Co., Inc., 1990.

59. K. E. Atkinson, and C. Jones, "A Study of the Interphase Region in Carbon Fibre/Epoxy Composites using Dynamic Mechanical Thermal Analysis," *Journal of Adhesion,* **56** (1996), pp. 247-260.

60. Tao Chou Chang, "The Effects of Fiber Surface Treatments on the Mechanical Properties of Graphite Fiber/Bismaleimide Composites," PhD Dissertation, Auburn University, 1991.

61. King-Fu Lin and Jyh-Chien Chen, "Curing, Compatibility, and Fracture Toughness for Blends of Bismaleimide and a Tetrafunctional Epoxy Resin," *Polymer Engineering and Science,* **36 (2)** (1996), pp. 211-217.

62. J. M. Cartwright, S. P. Wilkinson, J. Hellgeth, T. C. Ward, and D. E. Kranbeuhl, "Toughened Bismaleimide Resins: Kinetics, Morphology and Processing, Part 1," pp. 51-52.

63. L. Guozheng, G. Aijuan, and L. Liwen, "Modification of BMI and Allyl Compounds," *Journal of Advances Materials,* January (1996), pp. 61-64.

64. S. P. Wilkinson, T. C. Ward, and J. E. McGrath, "Effect of Thermoplastic Modifier Variables on Tougheninga Bismaleimide Matrix Resin for High-Performance Composite Materials," *Polymer,* **34 (4)** (1993), pp. 870-884.

65. S. D. Jenkins, G. T. Emmerson, P. T. Mcgrail And R. M. Robinson, "Thermoplastic Sizing of Carbon Fibres in High Temperature Polyimide Composites," *Journal of Adhesion,* **45** (1994), pp. 15-27.

66. J. Denault, "Interfacial Interaction in Carbon Fiber/Thermoplastic Composites," *Composite Interfaces,* **2 (4)** (1994), pp. 275-289.

67. T. H. Cheng, J. Zhang, S. Yumitori, F. R. Jones, and C. W. Anderson, "Sizing Resin Structure and Interphase Formation in Carbon Fiber Composites," *Composites,* **25 (7)** (1994), pp. 661-669.

68. Charles U. Pittman, Jr., Steven D. Gardner, Guoren He, Lichang Wang, Zhihong Wu, C. Singamsetty, Biahua Wu, and Glyn Booth, "Reactions of Defined Oxidized Carbon Fiber Surfaces with Model Compounds and Polyurethane Elastomers." MRS, April 1995.

69. V. Raghavendran, Effects of Molecular Weight of Thermoplastic Matrix and Processing Conditions of Interfacial Adhesion in Carbon Fiber Composites, MS Thesis, Michigan State University, 1994.

70. G. Rajagopalan, K. M. Immordino, S. H. McKnight, and J. W. Gillespie, Jr., "Characterization and Fracture Toughness of Diffuse Adhesive Interphases," *Advances in Polymers and Fibers,* pp. 539-547.

71. C. L. Weitzsacker, and L. T. Drzal, *SPE Conference Proceedings: ANTEC '96,* May 5-10, 1996, pp. 3656-3660.

72. T. Lenz, J. K. McDowell, B. Moy, J. Sticklen, and M. C. Hawley, "Intelligent Decision Support for Polymer Composite Material Design in an Integrated Design Environment," *Proceedings of the American Society for Composites Ninth Technical Conference,* Newark, DE, September 20-22, 1994, pp. 685-691.

73. M. Nardin, E. M. Asloun, F. Muller, and J. Schultz, "Study of the Carbon Fiber-Poly(Ether-Ether-Ketone) (PEEK) Interfaces, 3: Influences and Properties of Interphases," *Polymers for Advanced Technologies,* **2** (1991), pp. 161-169.

74. A. R. Sanadi and R. V. Subramanian, V.S. Manoranjan, "The Interphasial Regions in Interlayer Fiber Composites," *Polymer Composites*, **12 (6)** (1991), pp. 377-383.

75. J. G. Williams, M. E. Donnellan, M. R. James, and W. L. Morris, "Properties of the Interphase in Organic Matrix Composites," *Materials Science and Engineering,* A126 (1990), pp. 305-312.

76. John F. Maguire, Peggy L. Talley, and Mark Lupkowski, "The Interphase in Adhesion: Bridging the Gap," *Journal of Adhesion,* **45** (1994), pp. 269-290.

77. Javad Kalantar, "The Bonding Mechanism of Aramid Fibers to Epoxy Matrices," MS Thesis, Michigan State University, 1988.

78. Ryutoku Yosomiya, Kiyotake Morimoto, Akio Nakajima, Yoshito Ikada, and Toshio Suzuki, Adhesion and Bonding in Composites, Marcel Dekker, Inc., New York, 1990.

79. D. J. David and T. F. Sincock, "Estimation of Miscibility of Polymer Blends Using the Solubility Parameter Concept," *Polymer,* **33 (21)**, 1992, pp. 4505-4514.

80. Sidney H. Goodman, Handbook of Thermoset Plastics, Noyes Publications, Park Ridge, New Jersey, 1986.

81. R. T. Morrison, and R. N. Boyd, Organic Chemistry, Allyn and Bacon, Boston, MA, 1966.

82. George G. Odian, Principles of Polymerization, 3rd Ed., John Wiley & Sons, New York, 1991.

83. Materials Handbook: Plastics

84. F. Rodriguez, Principles of Polymer Systems, Hemisphere Pub. Corp., New York, 1989.

85. J. March, Advanced Organic Chemistry: Reactions, Mechanisms, and Structure, 4th Ed., John Wiley & Sons, New York, 1992.

86. R. Yosomia et al, Adhesion and Bonding in Composites, Marcell Dekker, New York, 1990.

87. E. Plueddeman, Silane Coupling Agents, 2nd Ed., Plenum Press, New York, 1982.

88. Petrarch Systems - Silane Coupling Agent Selector